Investigating the role of rotavirus GS10(NSP4) and GS6(VP6) in reassortment

J Herbert



orcid.org 0000-0002-8437-8574

Dissertation accepted in partial fulfilment of the requirements for the degree *Master of Science* in Biochemistry at the North-West University

Supervisor: Prof. A.A. van Dijk

Co-supervisor: Prof. A.C. Potgieter

Graduation May 2023

28340485

Acknowledgements

I would like to thank the following people, without whom this project would not have been possible.

Prof. Albie van Dijk, who has spent hundreds of hours with me over the past two and a half years, editing drafts of grants, proposals, this dissertation, and my many questions. When she has finished proofreading, it always results in changes that lead to higher quality writing. Her door is always open, and she is always ready for a discussion on problems or approaches. Her support for and championing of her students is unparalleled, and her knowledge of virology immense. Without her insight into rotavirus field reassortment, the research question that led to this project would not have existed. I could not have asked for a better supervisor.

Prof. Christiaan Potgieter, who has also spent many hours with this project. He has taught me everything I know about reverse genetics and transfection. He is always ready for a phone call that usually lasts an hour or more. His breadth of knowledge of basic bench science as well as theory is staggering. Without his input and advice, this project would not have reached the conclusions it did. Also, for all the reagents and cell lines, he provides for our laboratory.

My lab mates, Martin Visser, Pierre le Roux, Khanyisile Hlongwane, and Strauss van Graan. They made every day better and were always available to help with writing questions as well as lab work. Their humour really helped to keep perspective in a very difficult project. Each one of them challenges me to evaluate every assumption I have, and leads to me becoming a more critical scientist.

My fiancée, Chandré Liebenberg, who has listened to every rambling thought I have had on the pSMART reverse genetics system, and listened patiently as I tried to figure things out, out loud. Thank you for your unconditional love and support, for challenging me also not to assume that all is as it seems with the reverse genetics system. Just being there and thinking about small things I need that I forget about has made a total and complete difference. She is my best friend and I cannot imagine life or science without her.

My family, especially my father, Ruan Herbert, my mother, Liesl Herbert, and brother, Thian Herbert. My parents have loved and supported me immensely and completely throughout this project by being there when things did not go as planned, listening when I complained, and caring for my physical health and needs. My brother has had to endure

one-sided discussions about a topic he has no background in and has had to endure my irritation after long and fruitless weeks in the lab.

The North-West University, Poliomyelitis Research Foundation, and Deutsche Forschungsgemeinschaft for providing financial support for both myself and for this project. It goes without saying that research is not possible without funding.

Finally, the Lord our God. Who sent his Son to die for me and has given me the ability and opportunity to do virology. Through this project, He has enabled me to grow in patience, a virtue I have never possessed. I would not have wanted to have had this project any other way, as it shaped me as a Christian.

Abstract

Rotaviruses are dsRNA viruses and are the leading causative agent of severe gastroenteritis. All current licenced rotavirus vaccines contain live-attenuated strains and are capable of reassorting their genome segments with those of co-circulating field strains. This requires elucidation of the determinants of reassortment to produce vaccine seed strains that incorporate novel safety features. Rotavirus GS6(VP6) and GS10(NSP4) are possible candidates. Analyses of circulating field strains have shown that GS6(VP6) and GS10(NSP4) co-reassort and that VP6 subgroup and NSP4 genotype is often associated. Reverse genetics can be used to interrogate the functions of specific amino acids in protein-protein interactions. A NWU SA11-N5 pSMART reverse genetics system was developed previously, but it has not been reproducible due to plasmid instability. To start to elucidate the mechanism of GS6(VP6)/GS10(NSP4) reassortment, the stability of the SA11-N5 pSMART plasmid set needed to be improved.

Previous single plasmid NGS and Sanger sequencing data of the SA11-N5 pSMART plasmid set was reanalysed and showed that the plasmids containing GS7(NSP3) and GS9(VP7) did not contain ribozymes, and could be traced back to the original glycerol stocks. It was decided to reorientate the transcription cassettes to determine whether this improved plasmid stability by avoiding collisions between the transcription and replication machinery. All 11 plasmids were reorientated successfully. Sanger sequencing and NGS showed that they were still stable even when the NGS was repeated a year later from plasmids that were extracted from archived glycerol stocks. Rescue was attempted using the original protocol without success. Rescue was then attempted using seven different transfection reagents, five different transfection and infection cell lines, and an expression plasmid approach. Rescue could not be achieved in any attempt. Eventuallly, PCR testing of our transfection and infection cell lines showed that our MA104 and ST cells were heavily contaminated with mycoplasma. The cell lines were exchanged with uncontaminated ones, but rescue could not be attempted extensively. This resulted in the use of the SA11-L2 pT7 system for the remainder of this project.

Reverse genetics showed that NSP4 amino acids 169 and 174 may be important in determining its receptor interaction with VP6. Random NGS-generated sequences of 36 RVA VP6 and 38 NSP4s from Genbank were analysed. For DS-1-like strains NSP4 amino acids 169K/S and 174A/S were observed. For Wa-like strains, 169I/S and 174S were observed. For VP6 DS-1-like strains (SGI, I2), strains had 172A, 305A, and 306A at their subgroup determining epitopes. Whereas, the Wa-like strains (SGII. I1) had 172M, 306N, and 306A.

VP6s from a Wa-like Moz0060a and Moz308 strain, an SA11 NSP4 with the Moz0060a binding domain, and two SA11 NSP4s, SA11_NSP4_R169I and SA11_NSP4_A174S were tested. Only rSA11_Moz308
_VP6, rSA11_NSP4_0060a_DLP-BD, rSA11_NSP4_R169I were rescued. rSA11_Moz0060a_VP6, rSA11_Moz0060a_VP6_DLP-BD, and rSA11_NSP4_A174S could not be rescued. Growth kinetics showed rSA11_Moz308_VP6 replicated to a titre nearly 2 logs lower than rSA11. A single amino acid difference in the VP6/VP2 contact may destabilise the DLP. Alhough VP4 and VP7 also contact VP6, no significant amino acids changes were seen in the contacts been SA11 and the Moz308 strain. rSA11_NSP4_R169I replicated to a titre similar to rSA11. Non - rescue of rSA11_NSP4_A174S may show that this amino acid is essential to the interaction and that a non-polar/polar 169/174 pair is required in an SA11 background. This result was confirmed by the growth curve of rSA11_NSP4_0060a_DLP-BD, a virus that contains a non-polar/ polar 169/174 NSP4 DLP-BD pair. Taken together this provides new insights into a rotavirus protein-protein interaction that requires further investigation. Also, additional work is required to determine the reasons for non-rescue of the SA11-N5 pSMART reverse genetics system.

Keywords: Rotavirus; Reverse genetics; Rotavirus VP6; Rotavirus NSP4; Reassortment

Contents

List of Figures **ix**

List of Tables **xxii**

1 Introduction and literature review **1**

1.1 Introduction 1

1.2 Rotavirus burden of disease 2

1.3 *Reovirales* overview 3

1.4 Rotavirus discovery 3

1.5 Rotavirus classification 4

1.6 Rotavirus genome structure, coding assignment, and capsid structure 6

1.6.1 Genome structure and coding assignment 6

1.6.2 Capsid structure 9

1.7 Rotavirus replication cycle 12

1.7.1 Attachment and entry 13

1.7.2 Uncoating 14

1.7.3 (+)ssRNA synthesis and translation 14

1.7.4 Viroplasm formation, genome packaging, and DLP assembly 15

1.7.5 DLP Transport 18

1.7.6 Virus particle maturation and release 20

1.8 Rotavirus pathogenesis 21

1.9 Rotavirus Vaccines 23

1.9.1 Live-attenuated vaccines 24

1.9.2 Non-replicating and dead-subunit vaccines 25

1.10 Reassortment in segmented RNA viruses 26

1.10.1 *Orthomyxoviridae* genome reassortment 26

1.10.2 *Cystoviridae* genome reassortment 26

1.10.3 *Reoviridae* genome reassortment 27

1.11 Overview of *Reoviridae* reverse genetics 32

1.11.1 Reovirus reverse genetics 33

1.11.2 Bluetongue and African horsesickness reverse genetics 34

1.11.3 Rotavirus reverse genetics 36

1.11.4 Applications of the rotavirus and orbivirus RG systems 43

1.12 Problem statement 45

1.13 Aims and Objectives 46

2 Troubleshooting the NWU pSMART SA11-N5 reverse genetics system 47

2.1 Introduction 47

2.2 Materials and Methods 48

2.2.1 Design and construction of the pSMART-T7_SA11-N5_inline plasmid set 48

2.2.2 Reverse genetics 58

2.2.3 Rescue verification 63

2.3 Results and Discussion 64

2.3.1 Sequence analysis of the original pSMART SA11-N5 reverse genetics plasmids 64

2.3.2 PCR amplification of pSmart backbone and SA11-N5 transcription cassettes for reorientation 72

2.3.3 Seamless cloning of the SA11-N5 RG transcription cassettes in the same orientation as the origin of replication 76

2.3.4 Endotoxin-free plasmid purification for transfection and sequence verification using Next-Generation sequencing 90

2.3.5 Attempted viral rescue with the SA11-N5 pSMART_inline plasmid set 99

2.3.6 Various modifications applied to facilitate rescue with the SA11-N5_inline pSMART system 101

2.3.7 Mycoplasma contamination in cell lines 105

2.3.8 Summary 107

3 Investigation of GS6(VP6)/GS10(NSP4) co-reassortment using SA11-based reverse genetics 109

3.1 Introduction 109

3.2 Materials and methods 110

3.2.1 Plasmid construction 110

3.2.2 SA11-L2 pT7 reverse genetics protocol 113

3.2.3 Genome segment-specific single-step cDNA synthesis 113

3.2.4 Plaque assay and growth kinetics 114

3.3 Results and Discussion 115

3.3.1 Analysis of selected VP6 and NSP4 amino acid sequences to inform rational construct design 115

3.3.2 Generation of plasmids to evaluate the effect of variations in VP6 and NSP4 on NSP4/DLP binding 121

3.3.3 Assessment of rescue efficiency of different VP6/NSP4 combinations and NSP4 mutants 125

3.3.4 Growth kinetics of rescued viruses and implications for GS6(VP6)/GS10 (NSP4) co-reassortment 131

3.3.5 A possible interplay exists between non-polar 169 and polar 174 . . 134

3.4 Summary 135

4 Concluding summary and future prospects 138

4.1 Improving the stability of the NWU SA11-N5 pSMART reverse genetics plasmid set 138

4.2 Investigating the determinants of rotavirus GS6(VP6)/GS10(NSP4) co-reassortment using rotavirus reverse genetics 140

Bibliography **143**

Appendix **166**

A Plasmid maps of pSMART-T7_RV-SA11_inline reverse genetics plasmid set 167

B GS6(VP6)/GS10(NSP4) plasmid maps 170

C Consensus of NGS of pSMART-T7_RV-SA11_inline plasmid set alignment . 171

D Growth Curve titration raw data 182

E Statistical analysis using 2-way ANOVA and LSD post-hoc of differences between SA11 and rescued viruses 184

F First replicate plaque assays of viruses rescued in Chapter 3 186

G Permissions for figures reproduced in this project 188

List of Figures

1.1 **Rotavirus genome constellations. The three main genetic backbones are illustrated.** Wa-like genotypes are coloured in green, DS-1 in red and AU-1 in orange. Genotypes that do not classify according to these three strains are each coloured separately. Note the multiple reassortments that have occured between genetic backbones. Used with permission Matthijnssens et al. 2008. 6

1.2 **Rotavirus genome segments, coding assignment and capsid structure.** (A) SDS-PAGE gel of the rotavirus dsRNA genome and corresponding genome segment coding assignment. Genome segments are numbered from largest to smallest. The protein products of each genome segment are listed next to its respective genome segment. (B) Rotavirus TLP structure showing the VP4 spike and VP7 trimer. (C) Cut-away of TLP showing VP6, which forms the middle protein layer known as the DLP and the core consisting of the replication complex, VP1 and VP3, and VP2 which forms the core structure. (D) Rotavirus core showing a theoretical genome organisation as well as the VP1/VP3 replication complex. Used with permission Jayaram et al. 2004 7

1.3 **Rotavirus genome segment structure** Note the 5'and 3'-UTRs that are required for genome segment selection, dsRNA genome replication from (+)ssRNA, and (+)ssRNA synthesis from (-)ssRNA during transcription. Each genome segment also contains an ORF encoding one, or in the case of GS11 2 proteins. Used with permission Estes & Greenberg 2013. 9

1.4 **Rotavirus VP6 monomer and trimer structure.** (A) Rotavirus VP6 monomer showing the head (H) and Base (B) domains. Note the loop at the top of the trimer whch contains amino acids 305 and 306 and the β-sheet CHEF on the exterior. (B) Top view and (C) Side view showing rotavirus VP6 trimer structure. Note the Zn^{2+} ion at the centre of the trimer, represented by the green sphere. Used with permission Mathieu 2001 11

1.5 **Rotavirus VP7, VP6, and VP2 position in the TLP.** Cut-away view showing uncleaved VP4 (VP8* and VP5*) with the foot domain. VP7 is attached around the foot domain anchoring it in VP6. VP6 trimers attach to VP2 dimers via each monomer's base domain. Used with permission Settembre et al. 2011 12

1.6 **Rotavirus replication cycle. 1.** Attachment of rotavirus to cell surface via interactions between VP8 and sialic acids. **2.** Interaction of various integrin motifs in VP5 and VP7 with integrins α2β1, αvβ3 and αxβ2 enabling viral attachment and initiation of viral entry via endocytosis. Interaction with hsp70 is also illustrated. **3.** Viral entry via endocytosis and formation of endosome. Uncoating of the outer VP4 and VP7 layer exposing the transcriptionally active DLP to the cytoplasm.**4.** Transcription of the viral genome.**5.** Translation of the viral (+)ssRNA resulting in viral protein synthesis. Formation of the viroplasm. NSP2 and NSP5 are essential to its formation.**6.** Transcription of viral mRNA for incorporation into cores.**7.** Recruitment of lipid droplets for the formation of the viroplasm. VP1, 2, 3 and 6 are also associated with the viroplasm.**8.** Formation of cores during which one of each of the 11 genome segments are encased in the core particle in association with VP1, VP3 and VP2.**9.** Attachment of VP6 to the core, forming the DLP and dsRNA synthesis within the core from VP1.**10.** Transport of DLP to ER for attachment of VP7 and VP4, particle is transiently enveloped.**11.** During initial uncoating and later maturation of the TLP, Ca^{2+} ion concentrations play a critical role in the stabilization of VP7 trimers. Low concentrations of Ca^{2+} (such as those found in the endosome) destabilize VP7 trimers and initiate uncoating. Increased concentrations of Ca^{2+} (facilitated through NSP4 activity) are required for proper coating of the DLP and maturation of the TLP.**12.** Maturation of TLP following the disassociation of the envelope and non-vesicle transport of virions to cell surface for viral egress. This process is independent of the Golgi apparatus and is not fully understood.**13.** Final release of matured viral particles through cell lysis or viral budding. Matured TLPs are now deemed infectious and spread to adjacent cells. Used with permission Desselberger 2014. 13

1.7 **Rotavirus (+)ssRNA synthesis.** (+)ssRNA exit from channels transversing the SLP and DLP. Note (+)ssRNA only exits at the five-fold axes. Used with permission Jayaram et al. 2004 15

1.8 **Current model of BTV genome packaging.** Recruitment cascade of BTV virus (+)ssRNAs of genome segments, showing initial interaction of the small(+)ssRNA of the genome segments with the eventual recruitment of the larger (+)ssRNAs to form the complete set of (+)ssRNAs for packaging. Used with permission Roy 2017 17

1.9 **Model of the possible mechanism of rotavirus (+)ssRNA recruitment.** VP1 binds to the 3'-UTR consensus sequence. NSP2 then binds and remodels the secondary structure. This exposes complementary sequences between the (+)ssRNA, which allows the formation of stable intersegment interactions. The resulting ribonucleoprotein complex may cause the formation of VP2 cores around the complex, after which NSP2 may be evicted prior to (-)ssRNA synthesis. Used with permission Borodavka et al. 2018. . 18

1.10 **Rotavirus A NSP4 N and C-terminals, with various functional domains illustrated.** H1-H3 comprises the hydrophobic domains that contain the membrane destabilising and viroporin domains. The C-terminal is hydrophilic and contains the coiled-coiled and flexible regions. The coiled-coil region contains the Integrin-binding domain, the signal transducing domain, the extracellular matrix protein binding domain, the VP4 binding domain, the caveolin binding domain, the Ca^{2+} binding and enterotoxin domains. The flexible region contains the tubulin binding and DLP domains. Used with permission Hu et al. 2012 19

1.11 **Proposed model of NSP4 transport in COPII vesicles.** Sar1-GDP is phosphorylated to Sar1-GTP. Sar1-GTP interacts with Sec23, with Sec23 inturn interacting with Sec24, allowing binding of NSP4. This forms the inner coat of the vesicle. The Sec31/Sec13 heterotetramer then forms the outer coat around the vesicle. Phosphorylation of Sec31 by CK2 results in transport from the ER. These vesicles are then hijacked by the cellular autophagy machinery, where at some point LC3 interacts with NSP4. It is believed that autophagy isolation membranes then form around viroplasms, which allows transport of DLPs from viroplasms. Used with permission Crawford et al. 2019 20

1.12 **NSP4 viroporin activity proposed mechanism.** The H2 signal domain inserts into the ER membrane, which in turn allows the insertion of the pentalysine domain into the ER membrane followed by the amphipathic helix domain, creating a 3- pass membrane topology. NSP4 tetramerises to forms a functional viroporin. Used with permission Hyser et al. 2010 22

1.13 **Mechanism of pathogenesis in rotaviruses.** Cells are infected, resulting in expression of NSP4. NSP4 disrupts tight junctions of neighbouring cells. The extracellular form of NSP4 can interact with integrins which causes a signal cascade IP3 that causes calcium efflux from the cell. NSP4 also causes chloride ion loss from intestinal crypt cells, which causes water loss, the primary causes of dehydrating diarrhoea seen in rotavirus gastroenteritis. Used with permission Greenberg & Estes 2009 23

1.15 **Insertion of 3 amino acids in RVG 03V0567 as compared to RVA SA11.** This is believed to narrow the template entrance tunnel width, which is linked with the different 3' consensus sequence in clade B. Used with permission Ogden et al. 2012 27

1.14 **Rotavirus VP1 structure showing the template entrance tunnel, the dsRNA/(+)ssRNA exit tunnel, the (+)ssRNA exit tunnel, and the NTP entrance tunnel.** The template entrance tunnel is pictured with an RNA encoding the 3'-consensus sequence bound to the tunnel. The 3'-CS inserts into the template entrance tunnel and is required for transcription to be initiated. Used with permission Steger et al. 2019 28

1.16 **Mingo *et al.* mapping of GS(NSP2) sub-region.** Full length AU-1 GS8(NSP2) could not be reassorted into the SA11 genetic background using reverse genetics. A construct was then used which only contained the ORF for NSP2, which also could not be rescued. Two constructs were then tested where the first 440 bp of the SA11 ORF was used to replace the AU-1 genome segment, which could not be rescued or the second where bp 482 to 1000 of the SA11 genome segment was placed in the AU-1 ORF, which could be rescued. The sub-region was then mapped to position 784-820. Used with permission under a Creative Commons Attribution 4.0 International License. 30

1.17 **NSP4 amino acid sequences clustering into distinct Wa-like and DS-1-like groups designated as NSP4-B and NSP4-A respectively.** The box indicates the DLP binding domain. These genotypes were found to be linked to a specific VP6 subgroup. Used with permission Iturriza-Gomara et al. 2003. 31

1.18 **Reovirus plasmid-based reverse genetics.** (A) cDNAs of each genome segment is flanked by a T7 promoter and a HDV ribozyme. (B) The 10 plasmid set is transfected into L929 cells, and the cells are infected with a vaccinia virus expressing T7 RNA polymerase. (C) Schematic of the reovirus 4 plasmid system showing each cDNA genome segment flanked by a T7 promoter and HDV ribozyme. Used with permission from Kobayashi et al. 2007 and Boehme et al. 2011 34

1.19 **Bluetongue virus plasmid-based reverse genetics.** (A) A transcription cassette, consisting of a BTV genome segment cDNA flanked by a T7 promoter and an HDV ribozyme, is cloned into a pRG15 backbone. (B) The 10 plasmid set is transfected into BSR5-T7 cells and virus is rescued. Used with permission Pretorius et al. 2015. 36

1.20 **AHSV plasmid-based reverse genetics.** (A) pJAD1 has a StuI restriction enzyme site flanking the T7Te terminators, whereas pJAD2 has PmeI sites. (B) A transcription cassette, consisting of an AHSV genome segment cDNA flanked by a T7 promoter and an HDV ribozyme, is cloned into a pRG15 backbone. (C) The 10 plasmid set is transfected into BSR-T7/5 cells and virus is rescued. Used with permission Conradie et al. 2016. . . . 37

1.21 **Komoto et al. helper virus system.** Cos-7 cells are infected with a vaccinia virus expressing T7 RNA polymerase. transfection with a plasmid containing a recombinant genome segment flanked by a T7 promoter and HDV ribozyme. After transfection, the cells are infected with a rotavirus KU helper virus. Used with permission Taniguchi & Komoto 2012 38

1.22 **The Kanai *et al.* plasmid-only reverse genetics system.** The first plasmid-only rotavirus reverse genetics system consisting of 14 plasmids. 11 cDNA plasmids encoding the 11 genome segments, 2 plasmids for the subunits of the vaccinia virus capping enzyme and 1 for the FAST protein. The 14 plasmid set is then transfected into BHK-T7 cells. Used with permission Kanai et al. 2017 39

1.23 **Komoto *et al.* adaptations.** As in the original Kanai *et al.* system, cDNAs of each genome segment is flanked by a T7 polymerase and HDV ribozyme. only the 11 cDNA plasmid set is transfected into BHK-T7 cells, with 3x the amount of the GS8(NSP2) and GS11(NSP5/6). This is followed by co-seeding with CV-1 cells 48 hours after transfection. Viruses are rescued following passage on MA104 cells. Used with permission Komoto et al. 2018 40

1.24 **Rotavirus human strain KU reverse genetics system.** Note exchange of plasmid containing the KU GS4 cDNA replaced with an SA11 GS4. The design is identical to the Komoto *et al.* adaptations published in 2018. Used with permission Komoto et al. 2019. 41

1.25 **SA11-N5 plasmid-based reverse genetics system developed by M.GJ Huyzers.** The 11 SA11-N5 cDNAs are cloned into pSmart. C3P3 and FAST are cloned on phDream. The 13 plasmid set is transfected in an equimolar ration into BSR5-T7 cells, co-seeded with ST cells 48 hours later and incubated until CPE. The whole lysate is passage on ST cells and rescue is confirmed via IFMA. Used with permission Huyzers 2020 . . . 42

1.26 **Schematic showing plasmid replication and transcription.** This shows the possible scenarios arising from the different orientations of the transcription cassette. Replication and transcription can occur either in the same direction, or different directions. Used with permission Hamperl & Cimprich 2016 43

2.1 **Schematic of rationale used to re-orientate transcription cassette, the pSMART_T7 reverse genetics plasmid set.** The pSMART backbone was amplified using primers pSMART-BB-T7p and pSMART-BB-T7t (discussed in Section 2.2.1.1). Primers T7-ins-p and T7-ins-t were used to amplify the complete transcription cassette. The new plasmid set was then constructed using InFusion or NEBuilder seamless cloning. 50

2.2 **Alignment of Sanger Sequencing of pSMART-T7_RV-SA11_NSP3 obtained from plasmid generated by L. Geldenhuys.** The plasmid shows a complete deletion of the HDV ribozyme. The T7 promoter, genome segment, ribozyme location, terminator, and part of the pSMART backbone sequence is indicated. 66

2.3 **Alignment of Sanger Sequencing performed by M.J. Visser of pSMART-T7_RV-SA11_VP7 from plasmid generated by L. Geldenhuys and used by M.GJ Huyzers.** The plasmid show a complete deletion of the HDV ribozyme. The T7 promoter, genome segment, ribozyme location, terminator, and part of the pSMART backbone sequence is indicated. 67

2.4 **Alignments of pSMART-T7_RV-SA11_VP1 and pSMART-T7_RV-SA11_NSP3.** (a) Alignment of *de novo* assembly of sequencing of pSMART-T7_RV-SA11_VP1 using ABySS and HiSAT2. The black box indicates the position where the ribozyme is expected in this plasmid. The assembly confirms that this plasmid does contain a ribozyme. This assembly was performed in order to show that the assembly is occurring correctly, since it has been shown via Sanger sequencing that this plasmid contains a ribozyme and T7 terminator.(b) Alignment of the *de novo* assembly of sequencing of pSMART-T7_RV-SA11_NSP3. The black box indicates the position where the ribozyme is expected in this plasmid. The assembly confirms that this plasmid does not contain a ribozyme or T7 terminator. 69

2.5 **Alignment of the *de novo* assembly of sequencing of pSMART-T7_RV-SA11_VP7.** The black box indicates the ribozyme in this plasmid. The assembly confirms that this plasmid does not contain a ribozyme or T7 terminator. 70

2.6 **1% agarose gel of amplicons from a thermal-gradient PCR of the pSMART backbone and GS1 transcription cassette.** The pSmart backbone amplicon has a size of 1800 bp, the correct size for the backbone without the T7 promoter and T7 terminator. The GS1 amplicon has a size of 3500 bp, equating to a size of 3300 bp for the genome segment and 200 bp for the T7 promoter and T7 terminator. 73

2.7 **1% agarose gel of the thermal-gradient PCR amplicons for the GS2-GS11 transcription cassettes.** Amplicon size: GS2 = 3000 bp, GS3 = 2900 bp, GS4 = 2500 bp, GS5 = 1700 bp. GS11 amplicon size = 800 bp GS10 = 1000 bp, GS6 = 1500 bp, GS7 = 1500 bp, GS8 = 1200 bp, GS9 = 1200 bp. 74

2.8 **1% agarose gel of pSMART backbone, GS7, and GS9 PCR amplicons.** pSMART backbone amplicon size= 2018 bp GS7= and GS9 = GS11 amplicon size = 800 bp. All amplicons have equal amplification efficiency. . 76

2.9 **Schematic showing the orientation of sequencing primers with respect to the transcription cassette.** Note that in the previous orientation, Sanger sequencing from the pSMART_Downstream would have sequenced the T7 terminator and HDV ribozyme. In the new orientation, it sequences across the T7 promoter and 5'-end of the genome segment. The Upstream primer previously sequenced across the T7 promoter, it now sequences across the T7 terminator, HDV ribozyme, and 3'- end of the cDNA genome segment. Selected sequences of each element in the plasmid are shown to illustrate how the sequenced changed with respect to the sequencing primers. 78

2.10 **Sanger sequencing of the pSMART-T7_RV-SA11_GS1(VP1)_inline transcription cassette using the pSMART_Upstream and Downstream primers.** This shows that the orientation of the cassette was successfully changed and that the T7 promoter, cDNA genome segment, HDV ribozyme, and T7 terminator are present. 79

2.11 **Sanger sequencing of the pSMART-T7_RV-SA11_GS2(VP2)_inline transcription cassette using the pSMART_Upstream and Downstream primers.** This shows that the orientation of the cassette was successfully changed and that the T7 promoter, cDNA genome segment, HDV ribozyme, and T7 terminator are present. 80

2.12 **Sanger sequencing of the pSMART-T7_RV-SA11_GS3(VP3)_inline transcription cassette using the pSMART_Upstream and Downstream primers.** This shows that the orientation of the cassette was successfully changed and that the T7 promoter, cDNA genome segment, HDV ribozyme, and T7 terminator are present. 81

2.13 **Sanger sequencing of the pSMART-T7_RV-SA11_GS4(VP4)_inline transcription cassette using the pSMART_Upstream and Downstream primers.** This shows that the orientation of the cassette was successfully changed and that the T7 promoter, cDNA genome segment, HDV ribozyme, and T7 terminator are present. 82

2.14 **Sanger sequencing of the pSMART-T7_RV-SA11_GS5(NSP1)_inline transcription cassette using the pSMART_Upstream and Downstream primers**. This shows that the orientation of the cassette was successfully changed and that the T7 promoter, cDNA genome segment, HDV ribozyme, and T7 terminator are present. 83

2.15 **Sanger sequencing of the pSMART-T7_RV-SA11_GS6(VP6)_inline transcription cassette using the pSMART_Upstream and Downstream primers.** This shows that the orientation of the cassette was successfully changed and that the T7 promoter, cDNA genome segment, HDV ribozyme, and T7 terminator are present. 84

2.16 **Sanger sequencing of the pSMART-T7_RV-SA11_GS7(NSP3)_inline transcription cassette using the pSMART_Upstream and Downstream primers.** This shows that the orientation of the cassette was successfully changed and that the T7 promoter, cDNA genome segment, HDV ribozyme, and T7 terminator are present. 85

2.17 **Sanger sequencing of the pSMART-T7_RV-SA11_GS8(NSP2)_inline transcription cassette using the pSMART_Upstream and Downstream primers.** This shows that the orientation of the cassette was successfully changed and that the T7 promoter, cDNA genome segment, HDV ribozyme, and T7 terminator are present. 86

2.18 **Sanger sequencing of the pSMART-T7_RV-SA11_GS9(VP7)_inline transcription cassette using the pSMART_Upstream and Downstream primers.** This shows that the orientation of the cassette was successfully changed and that the T7 promoter, cDNA genome segment, HDV ribozyme, and T7 terminator are present. 87

2.19 **Sanger sequencing of the pSMART-T7_RV-SA11_GS10(NSP4)_inline transcription cassette using the pSMART_Upstream and Downstream primers**. This shows that the orientation of the cassette was successfully changed and that the T7 promoter, cDNA genome segment, HDV ribozyme, and T7 terminator are present. 88

2.20 **Sanger sequencing of the pSMART-T7_RV-SA11_GS11(NSP5/6)_inline transcription cassette using the pSMART_Upstream and Downstream primers.** This shows that the orientation of the cassette was successfully changed and that the T7 promoter, cDNA genome segment, HDV ribozyme, and T7 terminator is present. Note that the Downstream sequence was generated from the reverse complement of the Upstream sequence, due to a technical error with the Upstream sequencing. 89

2.21 **1% Agarose gel of BsaI restriction enzyme digestion of the pSmart_SA11-N5_inline_ori reverse genetics plasmid set.** This shows correct plasmid size following recloning of the transcription cassettes in the new orientation. U = Undigested. D = Digested. 90

2.22 **(a) *De novo* assembly and alignment of trimmed reads of pSMART-T7_RV-SA11_GS1(VP1)_inline and (b) *de novo* assembly and alignment of pSMART-T7_RV-SA11_GS2(VP2)_inline.** The black box indicates the ribozymes in each plasmid. The alignment confirms that these plasmids do contain a ribozyme. 93

2.23 **(a) *De novo* assembly and alignment of trimmed reads of pSMART-T7_RV-SA11_VP3(GS3)_inline and (b) *de novo* assembly and alignment of pSMART-T7_RV-SA11_GS4(VP4_inline.** The black box indicates the ribozymes in each plasmid. The alignment confirms that these plasmids do contain a ribozyme. 94

2.24 **(a) *De novo* assembly and alignment of trimmed reads of pSMART-T7_RV-SA11_GS5(NSP1)_inline and (b) *de novo* assembly and alignment of pSMART-T7_RV-SA11_GS6(VP6)_inline.** The black box indicates the ribozymes in each plasmid. The alignment confirms that these plasmids do contain a ribozyme. 95

2.25 **(a) *De novo* assembly and alignment of trimmed reads of pSMART-T7_RV-SA11_GS7(NSP3)_inline and (b) *de novo* assembly and alignment of pSMART-T7_RV-SA11_GS8(NSP2)_inline.** The black box indicates the ribozymes in each plasmid. The alignment confirms that these plasmids do contain a ribozyme. 96

2.26 **(a) *De novo* assembly and alignment of trimmed reads of pSMART-T7_RV-SA11_GS9(VP7)_inline and (b) *de novo* assembly and alignment of pSMART-T7_RV-SA11_GS10(NSP4)_inline.** The black box indicates the ribozymes in each plasmid. The alignment confirms that these plasmids do contain a ribozyme. 97

2.27 **Alignment of trimmed reads of pSMART-T7_RV-SA11_GS11(NSP5/6.)** The black box indicates the ribozyme in this plasmid. The alignment confirms that this plasmid does contain a ribozyme. 98

2.28 **Cytopathic effect in ST cells** (a) Cell morphology 24 hours post infections (b) Cell morphology 72 hours post infection. Note that the monolayer progressed from 80 % confluent 24 hours post-infection to 10% confluent 48 hours later, with amorphic patches of cells forming. (c) Infection of transfection negative control (No serum, 0.3 μg/ml trypsin) in ST cells, 72 hours post infection 100

2.29 **Immunofluorecence showing ZsGreen1 and Alexa555 fluorescence in the green and red channels during epifluorescence.** Both green and red fluorescence can be visualised on their respective channels. Overlaying of the channels shows exact overlap between the two signals 101

2.30 **2% Agarose gel of Sigma LookOut Mycoplasma amplicons from BSR-T7/5, MA104 and ST cells.** When compared to the positive control, MA104 and ST cells were heavily contaminated, since the ratio of the amplification efficiency of the internal control band at 480 bp to the positive band at 280 bp determines the amount of contamination. 106

3.1 **Schematic showing the design of the transcription cassettes of GS6(VP6) and GS10(NSP4) constructs used in this project.** pSMART-T7_RV-Moz_308_GS6_VP6, pSMART-T7_RV-Moz-0060a_GS6_VP6, and pSMART-T7_RV-SA11_NSP4_Moz_0060a_NSP4_DLP-BD were ordered from Genscript. pSMART_RV_SA11-N5_NSP4_A174S, and pSMART_RV_SA11-N5_NSP4_R169I were constructed from pSMART_RV_SA11-N5_GS10(NSP4) using site-directed mutagenesis. 112

3.2 **RVA NSP4 DLP binding domain amino acid sequence alignment.** This figure shows E1 and E2 NSP4s. Note the clear segregation of amino acid sequence between E1 and E2 NSP4 genotypes at amino acid 174. . . . 116

3.3 **Alignment of RVA VP6 amino acid sequences obtained from Genbank.** These sequences correspond to the viruses for which the NSP4s were aligned in figure 3.2. The red box indicates amino acid position 172. The blue box indicates amino acids 305 and 306. 118

3.4 **Multiple sequence alignment of the forward and reverse Sanger sequences of the Moz308 and Moz0060a GS6(VP6) transcription cassettes.** This shows that plasmids from each selected colony aligned correctly with their reference sequence. The T7 promoter, 5'-UTR, 3'-UTR, HDV ribozyme, and T7 terminator sequences are indicated. The red box indicates the T7 promoter, the gold boxes the 5' and 3'UTRs, the blue boxes indicate the codons that code for amino acids 172, 305, and 306, the green box the HDV ribozyme, and the light blue box the T7 terminator. . . 123

3.5 **Multiple sequence alignment of the forward and reverse Sanger sequences of the SA11_NSP4_0060a_DLPBD, SA11_NSP4_A174S, and SA11_NSP4_R169I constructs.** The T7 promoter, 5'-UTR, 3'-UTR, HDV ribozyme, T7 terminator, and DLP binding domain sequences are indicated. The red box indicates the T7 promoter, the gold boxes the 5' and 3'UTRs, the purple box the DLP binding domain, the yellow boxes indicate the codons that code for amino acids 169 and 174, the green box the HDV ribozyme, and the light blue box the T7 terminator. 124

3.6 **1.5% agarose gel showing dsRNA of rescued viruses. dsRNA genomes extracted from P0 cell pellets.** Genomes can be seen for rSA11_Moz308_VP6, rSA11_NSP4_0060a_DLP-BD, rSA11_NSP4_R169I, and rSA11. The other combinations did not present CPE and were not used for RNA extraction. 126

3.7 **1% agarose gel showing amplicons from one-Step cDNA synthesis of GS6(VP6) and GS10(NSP4) from the extracted dsRNA genomes.** D=Denatured, U=Undenatured. 127

3.8 **(a) Sanger sequencing of rSA11_Moz308_VP6 cDNA and (b) rSA11_NSP4_0060a_DLP-BD cDNA generated from GS6(VP6) and GS10(NSP4).** Note that sequencing length does not correspond to the actual length of the construct, since InFusion primers were used for sequencing, resulting in an extra 17 bp being incorporated into each cDNA genome segment. Only the sequences that encode the VP6 subgroup and the sequences for the NSP4 DLP-BD are indicated. 129

3.9 **Sanger sequencing of rSA11_NSP4_R169I cDNA generated from GS6(VP6) and GS10(NSP4).** Only the sequences encoding the VP6 subgroup, as well as the sequences for the NSP4 DLP-BD, are indicated. . 130

3.10 **rSA11_Moz308_VP6 growth curve and plaque morphology.** This shows $\log_10$ PFU/ml against time point in hours. At each time point rSA11_Moz308_VP6 replicated slower than rSA11-L2. ** indicates a significace of $p < 0.001$ 131

3.11 **VP2 and VP6 contact surfaces.** This shows the VP6 aa 61-74 contacts in red. The amino acid residues are labelled from residues 61-74. Note the residue 62, which is an asparagine in SA11 as compared to aspartic acid for rotavirus UK shown here. 133

3.12 **rSA11_NSP4_R169I growth curve and plaque morphology.** This virus has differences in replication when compare to rSA11, but reached a comparable final titre. ns = not significant. Plaque morphology was similar to SA11. 134

3.13 **rSA11_NSP4_0060a_DLP-BD growth curve and plaque morphology.** rSA11_NSP4_0060a_DLP-BD reached its maximum titre at 36 hours, as compared to rSA11 at 48 hours. Plaque morphology was similar to rSA11. * Indicates that the growth curves were significantly different, p = 0.042 135

S1 pSMART-T7_RV-SA11_inline GS1(VP1)-GS4(VP4) reverse genetics plasmid maps 167

S2 pSMART-T7_RV-SA11_inline GS5(NSP1)-GS8(NSP2) reverse genetics plasmid maps . . . 168

S3 pSMART-T7_RV-SA11_inline GS9(VP7)-GS11(NSP5/6) reverse genetics plasmid maps . . . 169

S4 pSMART-T7_RV-Moz308_VP6 and pSMART-T7_RV-Moz0060a_VP6 plasmid maps . . . 170

S5 pSMART-T7_RV-SA11_NSP4_Moz0060a_DLP-BD . . . 171

S6 Alignment of consensus sequence generated from pSMART-T7_RV-SA11_GS1_VP1_inline with reference sequence . . . 172

S7 Alignment of consensus sequence generated from pSMART-T7_RV-SA11_GS2_VP2_inline with reference sequence . . . 173

S8 Alignment of consensus sequence generated from pSMART-T7_RV-SA11_GS3_VP3_inline with reference sequence . . . 174

S9 Alignment of consensus sequence generated from pSMART-T7_RV-SA11_GS4_VP4_inline with reference sequence . . . 175

S10 Alignment of consensus sequence generated from pSMART-T7_RV-SA11_GS5_NSP1_inline with reference sequence . . . 176

S11 Alignment of consensus sequence generated from pSMART-T7_RV-SA11_GS6_VP6_inline with reference sequence . . . 177

S12 Alignment of consensus sequence generated from pSMART-T7_RV-SA11_GS7_NSP3_inline with reference sequence . . . 178

S13 Alignment of consensus sequence generated from pSMART-T7_RV-SA11_GS8_NSP2_inline with reference sequence . . . 179

S14 Alignment of consensus sequence generated from pSMART-T7_RV-SA11_GS9_VP7_inline with reference sequence . . . 180

S15 Alignment of consensus sequence generated from pSMART-T7_RV-SA11_GS10_NSP4_inline with reference sequence . . . 181

S16 Alignment of consensus sequence generated from pSMART-T7_RV-SA11_GS11_NSP5/6_inline with reference sequence . . . 182

S17 Tests of normality of the normalised log-transformed growth curve data set. Significance values of $p > 0.05$ indicate that the data set has a normal distribution. . . . 184

S18 Multiple comparison data using a univariate 2-way ANOVA with LSD post-hoc tests. This shows the comaprison of the mean between each virus. . . . 185

S19 Plaque assays of the first replicate of each timepoint for rSA11_Moz308_VP6 186

S20 Plaque assays of the first replicate of each timepoint for rSA11_NSP4_0060a_DLP-BD 187

S21 Plaque assays of the first replicate of each timepoint for rSA11_NSP4_R169I 188

List of Tables

1.1 Rotavirus A genome segment size, protein coding assignment, protein size, location, genotype, and main protein function. Used with permission Desselberger 2014 8

1.2 Globally and locally licensed rotavirus vaccines (adapted from Burke et al. (2019)) 23

1.3 Ogden *et al.* terminal sequences of of RV (+)RNA GS1(VP1)[a]. 28

1.4 GS6 and GS10 genotypes showing reassortments documented in Pakistan. Adapted, used with permission Tamim et al. 2019 32

2.1 In-Fusion HD reaction composition 49

2.2 NEBuilder reaction composition 49

2.3 Primers used for seamless cloning of transcription cassettes. 51

2.4 PCR template designations for seamless cloning 52

2.5 Q5 DNA polymerase PCR master mix components: 52

2.6 Overnight restriction endonuclease digestion composition 53

2.7 Primers used to verify succesful cloning using Sanger sequencing 57

2.8 Expected fragments and size of the SA11-N5 pSMART_inline_ori plasmid set after BsaI digestion 91

2.9 Variations applied to the basic rescue protocol to facilitate rescue with the SA11-N5_inline pSMART reverse genetics system 103

2.10 Use of transcription and expression plasmid co-transfection to facilitate rescue 105

3.1 Primers used for the synthesis of cDNA from GS6 (VP6) and GS10 (NSP4) 114

3.2 SuperScript III RT-PCR reaction compostion 114

3.3 Summary of GS6(VP6) and GS10(NSP4) of strains analysed in this study . 120

3.4 Summary of GS6(VP6) and GS10(NSP4) constructs designed in this study 122

3.5 Plasmids of different combinations of GS6(GS6)/GS10(NSP4) tested for rescue compatibility. 125

S1 PFU/ml raw titration data 183

Table of abbreviations

aa	amino acid
AHSV	African horsesickness virus
ASFV	African swine fever virus
BHK	baby hamster kidney cells
bp	base pairs (nucleic acids)
BTV	bluetongue virus
CAT	chloramphenicol acetyltransferase
C3P3	chimeric cytoplasmic capping-prone phage polymerase
CPE	cytopathic effect
DLP	double-layered particle, also known as the intermediate particle
DLP-BD	double-layered particle binding domain (NSP4)
DMEM	Dulbecco's modified medium
DNA	deoxyribonucleic acid
EDTA	ethylenediamine tetraacetic acid
dNTP	deoxyribonucleotide triphosphate
FAST	fusion-associated small transmembrane protein
GS	genome segment
HDV	hepatitis delta virus
IFMA	immunofluorescence monolayer assay
kDA	kilodalton
LB	Luria broth
LPS	lipopolysaccharides
MCS	mutliple cloning site
MEM	Minimal essential medium
NEAA	non-essential amino acids
NGS	next generation sequencing
NICD	National Institute for Communicable Diseases
NSP	non-structural protein (rotavirus)
NWU	North-West University
ORF	open reading frame
PAGE	polyacrylamide gel electrophoresis
PBS	phosphate-buffered saline
PCR	polymerase chain reaction

RG	reverse genetics
RNA	ribonucleic acid
RV	otavirus
RT-PCR	reverse transcription - polymerase chain reaction
SA11	simian agent 11
SDS	sodium dodecyl sulphate
SG	rotavirus VP6 sub-group
SLP	single-layered particle, also known as the core
(+)ssRNA	positive-sense single-stranded RNA
(-)ssRNA	negative-sense single-stranded RNA
ST	swine testis cells
TAE	tris, acetic acid, EDTA
TBE	tris, boric acid, EDTA
$TCID_{50}$	50% tissue culture infectious dose
TLP	triple-layered particle, also known as mature virion
UTR	untranslated region
VLP	virus-like particle
VP	viral protein (Structural protein)
w/v	weight per volume
WT	wild-type

Chapter 1

Introduction and literature review

1.1 Introduction

The current SARS-CoV-2 pandemic is the clearest example, since the 1918 influenza pandemic, of the worldwide devastation that a pandemic can cause. The SARS-CoV-2 pandemic also highlights the importance of new vaccine development technologies that allow rapid vaccine development during pandemic situations. For SARS-CoV-2, unprecedented development, clinical testing, licensure, and implementation occurred in 18 months. It was achieved by applying mRNA vaccine technology, a technology that had never been seen in an approved viral vaccine prior to the pandemic. This shows the utility of applying alternative vaccine technologies when rapid development of a vaccine is required. Currently, approved COVID-19 vaccines are based either on mRNA, viral vector, subunit, or inactivated vaccine technologies. However, in the future, the availability of fully tractable reverse genetics systems for coronaviruses is anticipated to allow the development of rationally designed live-attenuated vaccines by removing determinants of pathogenesis (Thao et al., 2020; Amarilla et al., 2021).

Existing reverse genetics for influenza virus has already been developed for strains that have either resulted in pandemics or have high pandemic potential (Bridgen, 2012). During the 2009 H1N1 pandemic and the 2005 H5N1 outbreak, seed viruses for vaccine production were generated by plasmid-based reverse genetics (Desheva et al., 2006; Chen Zhongying et al., 2010). This means that viruses with the required HA and NA genes can be generated and isolated directly. This shows the utility of reverse genetics in the generation of reassortants, which is the platform technology of this MSc. Currently, seasonal influenza vaccine seed strains are produced by co-infecting a strain that has a high growth rate in embryonated chicken eggs with a strain that contains the required hemagglutinin and neuraminidase genes for that season to reassort those genes into the high growth background (O'Neill & Donis, 2009). However, the time it takes for passage (up to seven passages, five to six months) and isolating reassortant viruses makes this approach unsuitable for the rapid production of vaccines during a pandemic.

Rotavirus is the causative agent of rotavirus gastroenteritis and was responsible for large-scale epidemics prior to the introduction of vaccines (Tate et al., 2012). Rotaviruses

remain an important area of study due to the lack of sufficient efficacy of vaccines in Africa. For rotaviruses, reverse genetics can be used for vaccine development, as well as for studying many basic research questions, including determinants of reassortment. An important question in rotavirus biology is what determines whether a genome segment or segments are compatible with each other, both on a genetic and functional level. Reverse genetics can be used to rationally modify genome segments to study how this affects virus replication and fitness. This can then give insight into whether genome segments reassort based purely on genetic compatibility, or whether the function of the proteins they encode has a mechanistic effect. This is especially important in elucidating the mechanisms of documented wild-type co-reassortment, such as that of GS6(VP6)/GS10(NSP4), which is of particular interest to this MSc. A better understanding of the underlying mechanisms of reassortment will allow the improvement of the safety profile of current live attenuated vaccines by rationally altering the determinants of reassortment to prevent reassortment between vaccine strains and wild-type strains.

1.2 Rotavirus burden of disease

Rotavirus A primarily affect children under five years of age. Before the introduction of vaccines, it was estimated that rotaviruses caused up to 1 million deaths per year (Tate et al., 2016). The introduction of two vaccines, Rotarix (GlaxoSmithKline Biologicals SA, Rixensart, Belgium) and RotaTeq (Merck & Co., Inc., West Point, PA, USA) in 2006 resulted in a decline to about 128 500 deaths per year and 260 000 episodes of diarrhoea in 2016 (Troeger et al., 2018). Half of these deaths occurred in four countries in Africa and South-East Asia. These countries were India, Pakistan, the Democratic Republic of the Congo, and Nigeria.

Rotavirus infections also cause an economic and agricultural burden due to treatment costs and subtarget weight animals suffering from calf-related diarrhoea, which causes significant losses during the first four weeks of life (Martella et al., 2010). Porcine rotavirus infections affect one to eight-week-old piglets and cause economic losses in commercial piggeries. Equine rotaviruses cause severe morbidity and mortality in foals aged up to three months of age (Martella et al., 2010).

There are no clear correlates of protection against rotavirus diarrhoea. Rotavirus vaccines have reduced efficacy in developing countries in sub-Saharan Africa and Asia, for reasons that are unclear (Henschke et al., 2022). Altough multiple factors have been suggested for reduced vaccine effectiveness, reasons for reduced efficacy are less clear (Desselberger, 2017a; Madhi et al., 2010). The circulating field strains in Africa are also different from those contained in the vaccine formulation, this is discussed in Section 1.9 (Page et al., 2018; Jere et al., 2018). This results in less optimal protection, especially if the dosing schedule is not completed. There are also some issues regarding vaccine safety. Vaccine strains are able to reassort with circulating field strains, which necessitates the investigation of reassortment mechanisms to allow the development of safe, rationally designed live-attenuated vaccine candidates that contain regional strains, as discussed in Section

1.10.3 (Donato et al., 2012; Rose et al., 2013).

The reassortment of the two genome segments encoding the outer capsid proteins of rotavirus, GS4(VP4) and GS9(VP7), has been extensively documented (Greenberg et al., 1982; Jere et al., 2018; Matsuno et al., 1980). These proteins are responsible for cell attachment and entry and are the primary immunological target (Estes & Greenberg, 2013). The reassortment of these two genome segments into other genetic backgrounds occurs quite readily and does not appear to reduce viral fitness (Martella et al., 2010). Reassortment of other genome segments has been less well documented, especially for the genome segments that co-reassort, such as GS6(VP6) and GS10(NSP4) (Iturriza-Gomara et al., 2003). Further investigation is required to ascertain whether these other, less frequent reassorments have an impact on vaccine safety, especially since rotavirus VP6 is highly immunogenic and is an attractive target for next-generation vaccines, as discussed in section 1.9 (Desselberger & Huppertz, 2011).

1.3 *Reovirales* overview

The *Reovirales* is an order of viruses that possess a segmented dsRNA genome encapsidated by one, two, or three concentric capsids. Viruses from this order are typically double-layered particles, apart from the triple-layered Rotavirus and the single-layered Cypovirus (Matthijnssens et al., 2022).The *Reoviriales* are divided into two families, the *Sedoreoviridae* and the *Spinareoviridae*. The two families are divided into 15 genera containing 97 species. The *Sedoreoviridae*, viruses whose core has a smooth non-turreted morphology, contain 6 genera, containing Orbivirus (containing the type species for this subfamily, Bluetongue virus), Cardoreovirus, Mimoreovirus, Phytoreovirus, Seadornavirus, and Rotavirus. The *Spinareoviridae*, viruses whose core particles have turrets or spikes, contain Aquareovirus, Coltivirus, Cypovirus, Dinovernavirus, Fijivirus, Idnoreovirus, Mycoreovirus, Orthoreovirus (containing the type species, Mammalian orthoreovirus), and Oryzavirus. Mature virions lack a lipid envelope (Estes & Greenberg, 2013).

1.4 Rotavirus discovery

Rotaviruses (RVs) were discovered in 1958 by Dr. Hubert Malherbe at the National Institute of Virology in Johannesburg, during routine monitoring of vervet monkeys used in the production of poliovirus vaccines. Dr. Malherbe took a rectal swab from an overtly healthy monkey and isolated a virus after passage in African green monkey kidney cells (Malherbe & Harwin, 1963; Malherbe & Strickland-Cholmley, 1967). This virus initially caused small inclusions in the cytoplasm of infected cells, which progressed to larger cytoplasmic inclusions and finally to cytoplasmic shrinkage and cell death. The virus was most likely an RNA virus, based on the fact that incubation with 5-bromodeoxyuridine did not inhibit replication. When the virus was inoculated intraperitoneally, subcutaneously, and intracerebrally into 24-hour-old mice, there were no observable symptoms. This virus was then designated Simian Agent 11 (SA11), with the specific strain in use named H-96. SA11 was not initially recognised as a rotavirus. SA11 is widely used in research labora-

tories today, due to the fact that it is nonpathogenic to humans and replicates well in cell culture, and is used as the prototype for studies in rotavirus biology (Estes et al., 1979).

In 1973 in Melbourne, Australia, Ruth Bishop, Ian Holmes and colleagues selected nine neonates, aged 9 to 31 months, who had acute gastroenteritis (Bishop et al., 1973). They performed duodenal biopsies, stained samples, and imaged them using electron microscopy. They saw virus particles in six of the nine patients. The particles had electron-dense cores and had a diameter of 67-87 nm. They concluded that this virus had a morphology similar to orbiviruses, including the bluetongue virus (BTV) and African horsesickness virus (AHSV), viruses that form part of the *Reoviridiae*.

A year later, in 1974 in Birmingham, United Kingdom, Flewett et al. used serology and electron microscopy to characterise viruses isolated from calves and young children, based on the work of Ruth Bishop and Ian Holmes (Flewett et al., 1974). Serum from affected patients was used to perform agglutination tests on both sets of viruses. This serum caused agglutination of both the calf and human viruses. Furthermore, electron microscopy showed that the viruses were indistinguishable based on both size and morphology. They did further work to show that these viruses were not related to reoviruses or bluetongue virus, as Ruth Bishop believed. Human and calf viruses exhibited a distinct appearance of spokes attached to a wide hub. Flewett et al. suggested the name rotavirus, where rota is Latin for wheel, based on this wheel-like appearance (Flewett et al., 1974).

1.5 Rotavirus classification

Rotaviruses are classified on both a serological and a genetic basis. Classical serological classification has been used to classify rotaviruses into 10 serogroups, designated A, B, C, E, F, G, H, I, and J (Matthijnssens et al., 2022). This was done using monoclonal antibodies (mAbs) against VP6, primarily using enzyme-linked immunosorbent assay (ELISA). This is still commonly used for RVA, as VP6 is highly immunogenic and represents the largest mass of the particle. However, there are problems with this approach, since some mAbs can cross-react with groups they were not raised against (Estes & Greenberg, 2013).

Rotavirus VP6 is used to divide rotavirus group A into four subgroups based on mAb binding (Greenberg et al., 1983, 1982). These are designated subgroup I, subgroup II, non-subgroup I, and non-subgroup II. Amino acids 172 or 305 affect subgroup I monoclonal antibody binding, double mutations in amino acids 305 and 306 affect subgroup II antibody binding (Lopez et al., 1994).

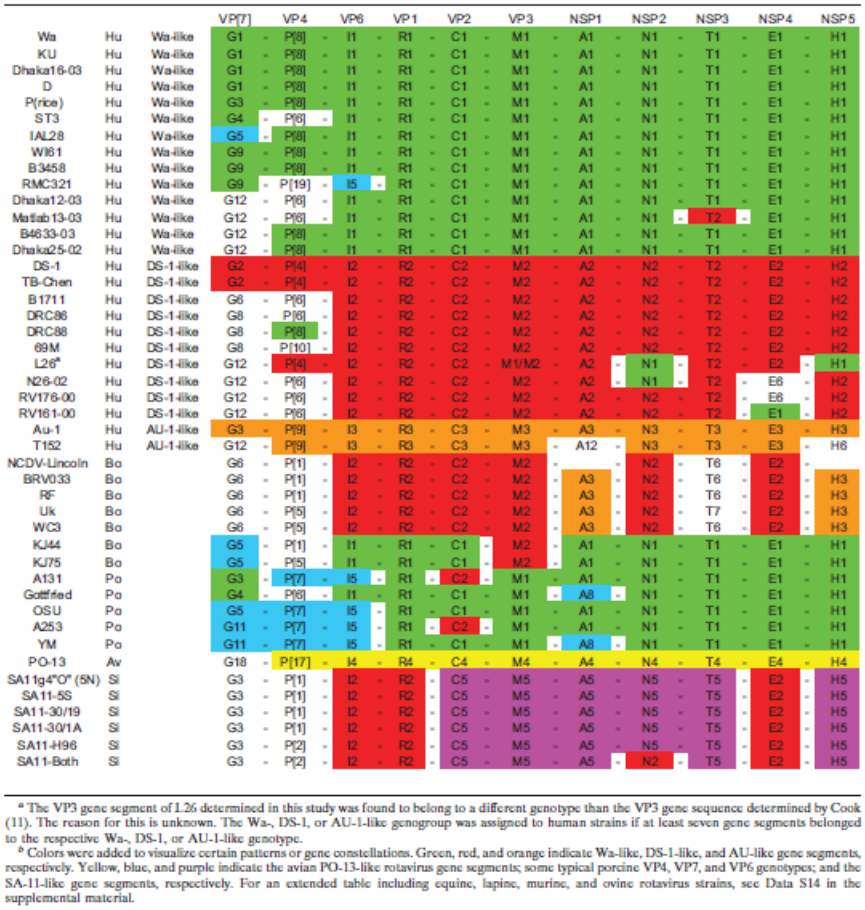
Group A rotaviruses (RVAs) are also classified into serotypes known as G- (based on the VP7 glycoprotein) and P-typing (based on the VP4 protease sensitive protein), using neutralization assays by using hyperimmune serum prepared in antibody-negative animals and more recently, genotyping (Estes & Greenberg, 2013). This has resulted in 42 G(VP7) types (Matthijnssens et al., 2022).

Sequence-based typing is also used for both GS6(VP6) and GS4(VP4)/GS9(VP7) using

PCR and then comparing nucleotide sequences. This has been used to classify novel RVs into serotypes. Many antibodies cross-neutralise different VP4 serotypes, resulting in mis-typing using serology, so P-typing has been done by sequence analysis of GS4. This has resulted in the classification of different 58 P types (Matthijnssens et al., 2022)f.

In 2008, a complete nucleic acid sequence-based genome classification system was suggested (Matthijnssens et al., 2008). This system utilises whole genome sequencing to classify each genome segment into a genotype based on the primary protein function using the designation of Gx-P[x]-Ix-Rx-Cx-Mx-Ax-Nx-Tx-Ex-Hx where x is an Arabic number. For a list of the genome segment to genotype designation, see Table 1.1. In 2011, a uniform system for sequence classification of strains was accepted, which designates the rotavirus strains in the following manner: RV group/species of origin/country of identification/common name/year of identification/G and P type (Matthijnssens et al., 2011). The strain used in this project is classified as RVA/Simian-tc/ZAF/SA11-H96/1958-N5/G3P5B[2].

Three main genetic backbones exist, representing the common genetic backbones present in circulating strains, Figure 1.1. These are classified according to the prototypic strains that were initially identified to contain these genetic backbones (Matthijnssens et al., 2008; Matthijnssens & Van Ranst, 2012). The first is known as the Wa-like backbone, classified as G1-P[8]-I1-R1-C1-M1-A1-N1-T1-E1-H1. The second are DS1-like backbones, classified as G2-P[4]-I2-R2-C2-M2-A2-N2-T2-E2-H2. These two backbones represent the most common genetic backbones in circulation. A third, rarer backbone is known as the AU-1-like backbone and is classified G3-P[9]-I3-R3-C3-M3-A3-N3-T3-E3-H3. These backbones are used to classify rotavirus genome segment reassortants, where one or more of a genome segment of a specific genotype can reassort into a backbone (Matthijnssens et al., 2008).



			VP[7]	VP4	VP6	VP1	VP2	VP3	NSP1	NSP2	NSP3	NSP4	NSP5
Wa	Hu	Wa-like	G1	P[8]	I1	R1	C1	M1	A1	N1	T1	E1	H1
KU	Hu	Wa-like	G1	P[8]	I1	R1	C1	M1	A1	N1	T1	E1	H1
Dhaka16-03	Hu	Wa-like	G1	P[8]	I1	R1	C1	M1	A1	N1	T1	E1	H1
D	Hu	Wa-like	G1	P[8]	I1	R1	C1	M1	A1	N1	T1	E1	H1
P(rice)	Hu	Wa-like	G3	P[8]	I1	R1	C1	M1	A1	N1	T1	E1	H1
ST3	Hu	Wa-like	G4	P[6]	I1	R1	C1	M1	A1	N1	T1	E1	H1
IAL28	Hu	Wa-like	G5	P[8]	I1	R1	C1	M1	A1	N1	T1	E1	H1
WI61	Hu	Wa-like	G9	P[8]	I1	R1	C1	M1	A1	N1	T1	E1	H1
B3458	Hu	Wa-like	G9	P[8]	I1	R1	C1	M1	A1	N1	T1	E1	H1
RMC321	Hu	Wa-like	G9	P[19]	I5	R1	C1	M1	A1	N1	T1	E1	H1
Dhaka12-03	Hu	Wa-like	G12	P[6]	I1	R1	C1	M1	A1	N1	T1	E1	H1
Matlab13-03	Hu	Wa-like	G12	P[6]	I1	R1	C1	M1	A1	N1	T2	E1	H1
B4633-03	Hu	Wa-like	G12	P[8]	I1	R1	C1	M1	A1	N1	T1	E1	H1
Dhaka25-02	Hu	Wa-like	G12	P[8]	I1	R1	C1	M1	A1	N1	T1	E1	H1
DS-1	Hu	DS-1-like	G2	P[4]	I2	R2	C2	M2	A2	N2	T2	E2	H2
TB-Chen	Hu	DS-1-like	G2	P[4]	I2	R2	C2	M2	A2	N2	T2	E2	H2
B1711	Hu	DS-1-like	G8	P[6]	I2	R2	C2	M2	A2	N2	T2	E2	H2
DRC86	Hu	DS-1-like	G8	P[6]	I2	R2	C2	M2	A2	N2	T2	E2	H2
DRC88	Hu	DS-1-like	G8	P[8]	I2	R2	C2	M2	A2	N2	T2	E2	H2
69M	Hu	DS-1-like	G8	P[10]	I2	R2	C2	M2	A2	N2	T2	E2	H2
L26[a]	Hu	DS-1-like	G12	P[4]	I2	R2	C2	M1/M2	A2	N1	T2	E2	H1
N26-02	Hu	DS-1-like	G12	P[6]	I2	R2	C2	M2	A2	N1	T2	E6	H2
RV176-00	Hu	DS-1-like	G12	P[6]	I2	R2	C2	M2	A2	N2	T2	E6	H2
RV161-00	Hu	DS-1-like	G12	P[6]	I2	R2	C2	M2	A2	N2	T2	E1	H2
Au-1	Hu	AU-1-like	G3	P[9]	I3	R3	C3	M3	A3	N3	T3	E3	H3
T152	Hu	AU-1-like	G12	P[9]	I3	R3	C3	M3	A12	N3	T3	E3	H6
NCDV-Lincoln	Bo		G6	P[1]	I2	R2	C2	M2		N2	T6	E2	
BRV033	Bo		G6	P[1]	I2	R2	C2	M2	A3	N2	T6	E2	H3
RF	Bo		G6	P[1]	I2	R2	C2	M2	A3	N2	T6	E2	H3
Uk	Bo		G6	P[5]	I2	R2	C2	M2	A3	N2	T7	E2	H3
WC3	Bo		G6	P[5]	I2	R2	C2	M2	A3	N2	T6	E2	H3
KJ44	Bo		G5	P[1]	I1	R1	C1	M2	A1	N1	T1	E1	H1
KJ75	Bo		G5	P[5]	I1	R1	C1	M2	A1	N1	T1	E1	H1
A131	Po		G3	P[7]	I5	R1	C2	M1	A1	N1	T1	E1	H1
Gottfried	Po		G4	P[6]	I1	R1	C1	M1	A8	N1	T1	E1	H1
OSU	Po		G5	P[7]	I5	R1	C1	M1	A1	N1	T1	E1	H1
A253	Po		G11	P[7]	I5	R1	C2	M1	A1	N1	T1	E1	H1
YM	Po		G11	P[7]	I5	R1	C1	M1	A8	N1	T1	E1	H1
PO-13	Av		G18	P[17]	I4	R4	C4	M4	A4	N4	T4	E4	H4
SA11g4"O" (5N)	Sl		G3	P[1]	I2	R2	C5	M5	A5	N5	T5	E2	H5
SA11-5S	Sl		G3	P[1]	I2	R2	C5	M5	A5	N5	T5	E2	H5
SA11-30/19	Sl		G3	P[1]	I2	R2	C5	M5	A5	N5	T5	E2	H5
SA11-30/1A	Sl		G3	P[1]	I2	R2	C5	M5	A5	N5	T5	E2	H5
SA11-H96	Sl		G3	P[2]	I2	R2	C5	M5	A5	N5	T5	E2	H5
SA11-Both	Sl		G3	P[2]	I2	R2	C5	M5	A5	N2	T5	E2	H5

[a] The VP3 gene segment of L26 determined in this study was found to belong to a different genotype than the VP3 gene sequence determined by Cook (11). The reason for this is unknown. The Wa-, DS-1, or AU-1-like genogroup was assigned to human strains if at least seven gene segments belonged to the respective Wa-, DS-1, or AU-1-like genotype.

[b] Colors were added to visualize certain patterns or gene constellations. Green, red, and orange indicate Wa-like, DS-1-like, and AU-like gene segments, respectively. Yellow, blue, and purple indicate the avian PO-13-like rotavirus gene segments; some typical porcine VP4, VP7, and VP6 genotypes; and the SA-11-like gene segments, respectively. For an extended table including equine, lapine, murine, and ovine rotavirus strains, see Data S14 in the supplemental material.

Figure 1.1: Rotavirus genome constellations. The three main genetic backbones are illustrated. Wa-like genotypes are coloured in green, DS-1 in red and AU-1 in orange. Genotypes that do not classify according to these three strains are each coloured separately. Note the multiple reassortments that have occured between genetic backbones. Used with permission Matthijnssens et al. 2008.

1.6 Rotavirus genome structure, coding assignment, and capsid structure

1.6.1 Genome structure and coding assignment

The rotavirus genome consists of 11 double-stranded (dsRNA) genome segments (GSs), Figure 1.2. The 11 genome segments encode 12 proteins. Ten genome segments are monocistronic, and one, genome segment 11, contains two overlapping open reading frames (ORFs) encoding NSP5 and NSP6. Genome segments are numbered from largest to smallest. For SA11-H96 the genome segments range from GS1 at 3300bp to GS11 at 660 bp (Mlera et al., 2013). The 11 GSs encode 6 structural proteins, namely VP1-4 and VP6 (VP5* and VP8* are products of trypsin cleavage of VP4) and 6 non-structural proteins, numbered NSP1-6, Figure 1.2. The structural proteins form the architecture of the mature virion, whereas the non-structural proteins perform essential functions of the virus replication cycle, but do not form part of the capsid.

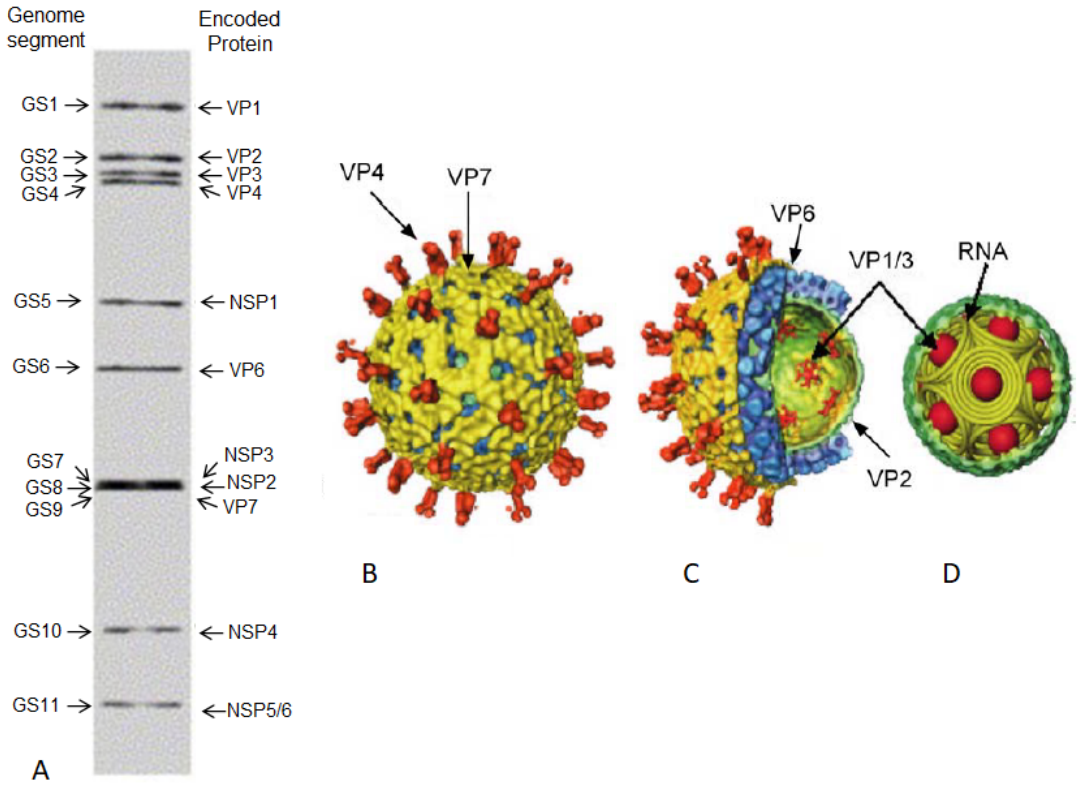


Figure 1.2: Rotavirus genome segments, coding assignment and capsid structure. (A) SDS-PAGE gel of the rotavirus dsRNA genome and corresponding genome segment coding assignment. Genome segments are numbered from largest to smallest. The protein products of each genome segment are listed next to its respective genome segment. (B) Rotavirus TLP structure showing the VP4 spike and VP7 trimer. (C) Cut-away of TLP showing VP6, which forms the middle protein layer known as the DLP and the core consisting of the replication complex, VP1 and VP3, and VP2 which forms the core structure. (D) Rotavirus core showing a theoretical genome organisation as well as the VP1/VP3 replication complex. Used with permission Jayaram et al. 2004

Table 1.1: Rotavirus A genome segment size, protein coding assignment, protein size, location, genotype, and main protein function. Used with permission Desselberger 2014

GS	Size (bp)	Protein	Size (kDa)	Location	Genotype	Protein function
1	3302	VP1	125	Core	R	RNA-dependent RNA polymerase; 3'-mRNA binding; forms transcription complex with VP3
2	2690	VP2	102	Core	C	Inner capsid structural protein; non-specific ssRNA and dsRNA binding; myristoylated; required for replicase activity of VP1.
3	2591	3VP3	98	Core	M	Guanylyltransferase and methyltransferase; non-specific ssRNA binding; part of transcription complex with VP1
4	2362	VP4	VP4:88 VP5*:60 VP8* 28	Outer Capsid	P	Outer capsid spike protein; P-type neutralization antigen; virulence determinant; cell-attachment protein; trypsin cleavage into VP5* and VP8* enhances infectivity; VP5* permeabilises membranes; VP8* contains the heamagglutinin domain (in some strains)
5	1611	NSP1	59	Cytoplasm	A	Associates with cytoskeleton; high degree of sequence variation; role in suppression of host interferon response
6	1356	VP6	48	Inner capsid	I	Major virion protein; middle capsid structural protein; homotrimeric structure; group- and subgroup-specific antigen
7	1105	NSP3	35	Cytoplasm	T	Homodimer; virus-specific 3'-mRNA binding; binds elongation factor eIF4G1 and circularises mRNA on translation initiation complex; involved in translational regulation and host shut-off
8	1059	NSP2	37	Cytoplasm	N	NTPase and helicase activity; non-specific ssRNA binding; major component of the viroplasm; binds NSP5 and VP1; essential for dsRNA synthesis and formation of infectious viral progeny
9	1062	VP7	37	Outer capsid	G	Outer capsid structural glycoprotein; G-type neutralization antigen; N-linked high mannose glycosylation and trimming; RER transmembrane calcium-binding
10	751	NSP4	20	Cytoplasm	E	Viral enterotoxin; receptor for double-layer particle budding through ER membrane; N-linked high mannose glycosylation; modulates intracellular calcium levels essential for viral RNA replication and formation of infectious viral progeny
11	667	NSP5/6	NSP5:22 NSP6:11	Cytoplasm	H	NSP5: viroplasm formation; multimerizes; O-linked glycosylation; hyper-phosphorylated; autokinase activity; enhanced by NSP2 interaction; binds ssRNA; component of viroplasm NSP6: interacts with NSP5 and localises to viroplasms

Each rotavirus genome segment contains an ORF flanked by non-coding untranslated regions (UTRs), designated the 5' and 3' UTRs, which vary in length from 9-48bp for the 5'-UTR and 17-182bp for the 3'-UTRs, Figure 1.3. During (+)ssRNA synthesis, transcripts are 5' – capped (5'-m7GpppG(m)), but not 3'-polyadenylated (Estes & Greenberg, 2013). It is thought that the UTRs contain cis-regulatory elements, which are essential for genome segment packaging. This is more fully discussed in Section 1.7.4.2.

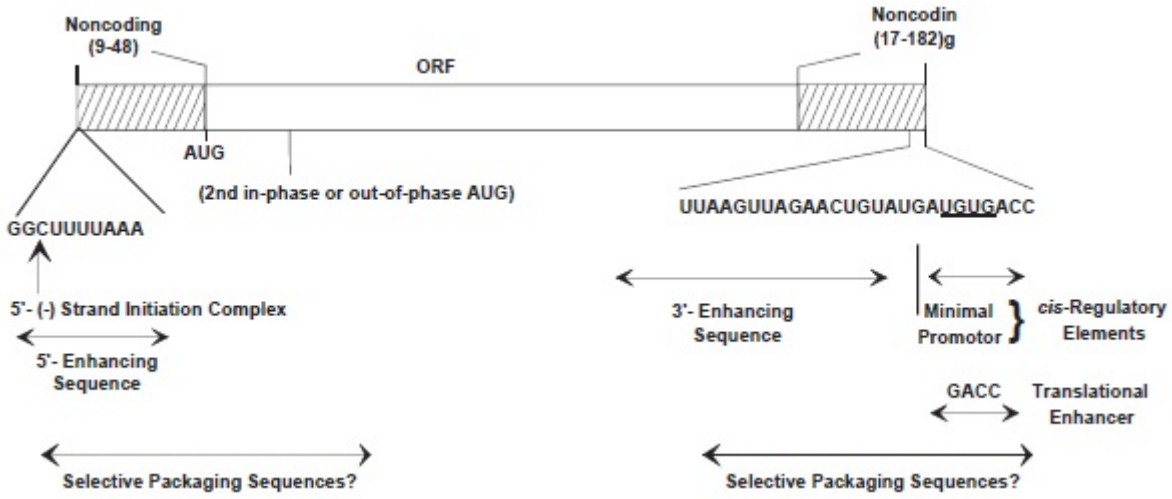


Figure 1.3: Rotavirus genome segment structure Note the 5'and 3'-UTRs that are required for genome segment selection, dsRNA genome replication from (+)ssRNA, and (+)ssRNA synthesis from (-)ssRNA during transcription. Each genome segment also contains an ORF encoding one, or in the case of GS11 2 proteins. Used with permission Estes & Greenberg 2013.

1.6.2 Capsid structure

The rotavirus dsRNA genome is encapsidated by three protein layers, Figure 1.2. Three particles are differentiated. Infectious particles are known as virions or triple-layered particles (TLPs), which are approximately 100 nm in diameter. Double-layered particles (DLPs) lack the outer capsid and are found only in the cytoplasm following virus internalisation and uncoating. Single-layered particles (SLPs), also known as cores, are only found immediately after genome packaging.

1.6.2.1 SLP structure

SLPs are composed of VP1, 2, and 3. 120 monomers of VP2 arranged into 60 dimers, giving the SLP a T=1 symmetry (McClain et al., 2010). Two isoforms of VP2 exist. VP2A forms a star-like structure around the five-fold hubs where VP1 and the (+)ssRNA exit channels are found (Ding et al., 2019; McClain et al., 2010). VP2B fills the space between the VP2A subunits, forming a decameric structure around the five-fold hub. Twelve of the VP2A/VP2B complexes exist in the SLP, in complex with VP1 and possibly VP3 (Ding et al., 2019). Both rotaviruses and orbiviruses perform all of their polymerisation and capping inside the inner shell.

1.6.2.2 DLP structure

The DLP is composed of the SLP proteins VP1, 2, 3, and 260 VP6 trimers attached to the core particle, Figure 1.4 (Mathieu, 2001). Rotavirus VP6 contains two domains, a head domain and a base domain, and contacts both the inner and outer capsids. VP6 is essential for cell entry and (+)ssRNA transcription (Chen et al., 2009; Lawton et al., 1997).

Rotavirus VP6 is a 48 kDa, 398 amino acid monomer encoded by GS6. VP6 serves a vital purpose both in the capsid structure and in the replication cycle. VP6 forms the inner capsid of rotaviruses and contacts both the core, consisting of VP2 and the outer capsid consisting of VP4 and VP7, performing an important architectural function in the virion (Mathieu, 2001). VP6 monomers consist of two domains, designated the head and base domains. Both of these domains participate in trimer formation with hydrophobic residues contacting the H domain and hydrophilic residues contacting the base domain, forming a large water-filled cavity in the trimer base (Mathieu, 2001). The head domain is essential for trimer formation and contains a Zn^{2+} ion coordinated to His153 of each subunit.

The base (B) domain consists of 8 consecutive α-helices designated αa-αh, formed by two polypeptide chains (Mathieu, 2001). α-αe (the first 150 N-terminal amino acids) form the first bundle, with the second bundle, αf-αh, being formed by amino acids 335-397. The head (H) domain (aa 151-334) is formed by a β-sandwich (2 β-sheets) folding into a jelly roll. The first β-sheet (CHEF) is found on the exposed side of VP6, while the second BIDG is found on the interior. The loop formed at positions 172, and 305/306 is responsible for determining the subgroup in RVAs (Lopez et al., 1994). Figure 1.4 illustrates the monomer and trimer structure.

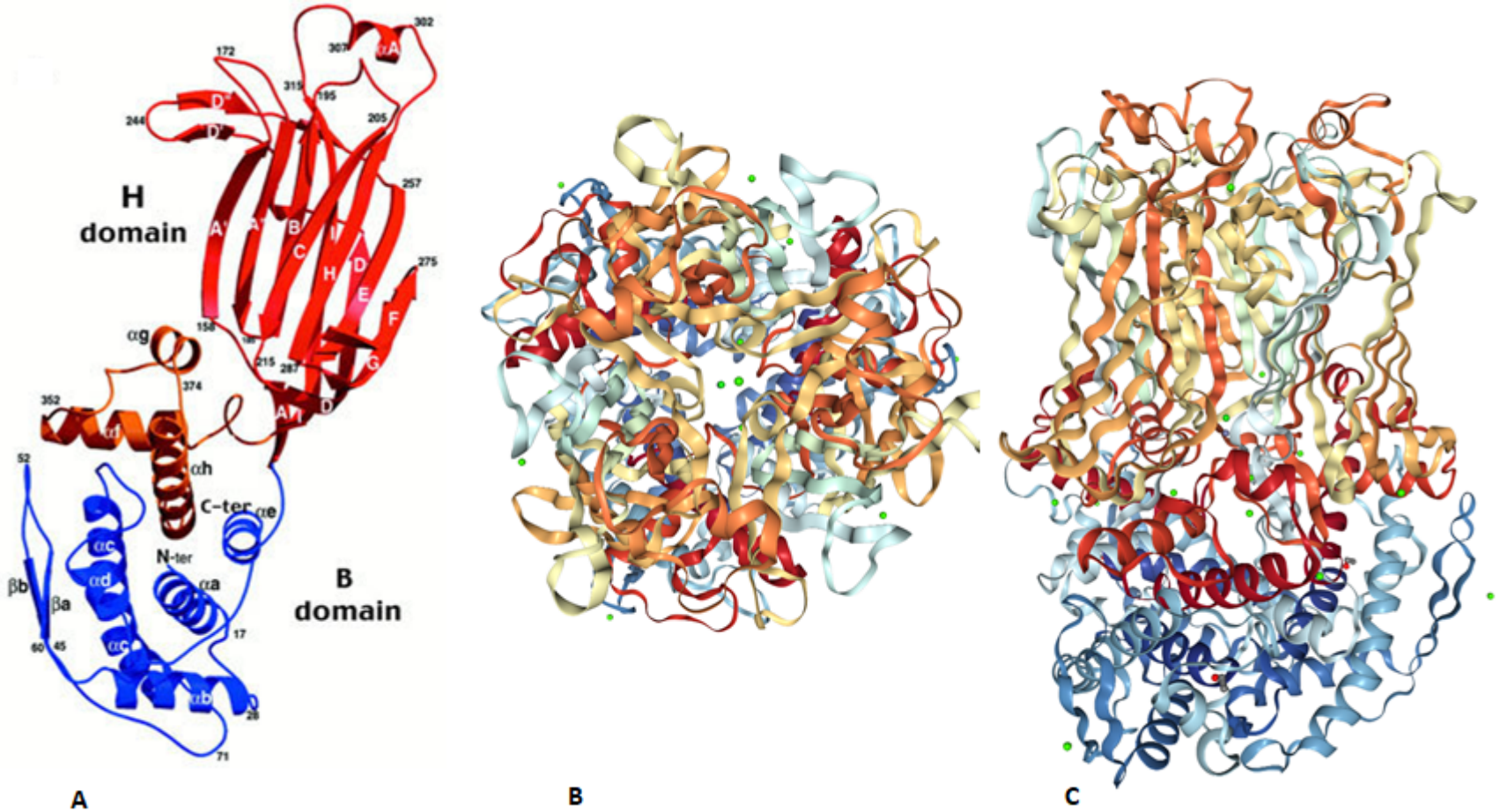


Figure 1.4: Rotavirus VP6 monomer and trimer structure. (A) Rotavirus VP6 monomer showing the head (H) and Base (B) domains. Note the loop at the top of the trimer whch contains amino acids 305 and 306 and the β-sheet CHEF on the exterior. (B) Top view and (C) Side view showing rotavirus VP6 trimer structure. Note the Zn^{2+} ion at the centre of the trimer, represented by the green sphere. Used with permission Mathieu 2001

1.6.2.3 TLP structure

Sixty trimers of VP4 extend from the VP6 layer (Crawford et al., 2001). VP4 is a spike protein that projects about 120Å from the outer layer (Settembre et al., 2011). VP4 contains a globular head domain, a symmetrical stalk domain, and a globular foot domain. Proteolysis cleaves VP4 into VP8* and VP5*, which are non-covalently associated. The spike is held in place by interactions with both VP7 and VP6. VP4 must first be attached to DLPs before VP7 is added during assembly, Figure 1.5 (Trask & Dormitzer, 2006). The outer capsid is then formed by 260 trimers of glycoprotein VP7, which consists of two domains: domain I with a disulphide bridge exhibits a Rossmann fold and domain II with three disulphide bridges which exhibits a jelly-roll β-sandwich fold. Three Ca^{2+} ions are bound on the surface of each subunit interface (Aoki et al., 2009). Three VP7 subunits interact to form a plate-like trimer that interacts with VP6, with the N-terminal arms contacting the VP6 trimers (Chen et al., 2009).

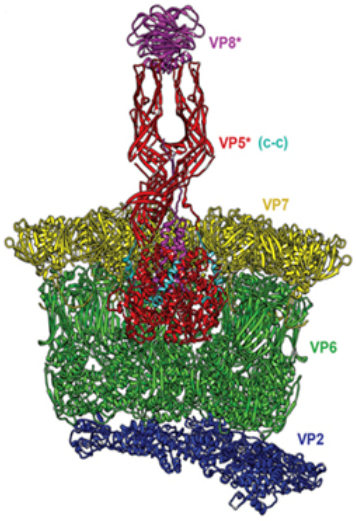


Figure 1.5: Rotavirus VP7, VP6, and VP2 position in the TLP. Cut-away view showing uncleaved VP4 (VP8* and VP5*) with the foot domain. VP7 is attached around the foot domain anchoring it in VP6. VP6 trimers attach to VP2 dimers via each monomer's base domain. Used with permission Settembre et al. 2011

1.7 Rotavirus replication cycle

The rotavirus replication cycle consists of five steps. These are attachment, penetration, and uncoating, (+)ssRNA synthesis and translation, viroplasm formation (including RNA packaging, (-)ssRNA synthesis and DLP formation), and virus particle maturation and release. Figure 1.6 and the following subsections describe each step in detail.

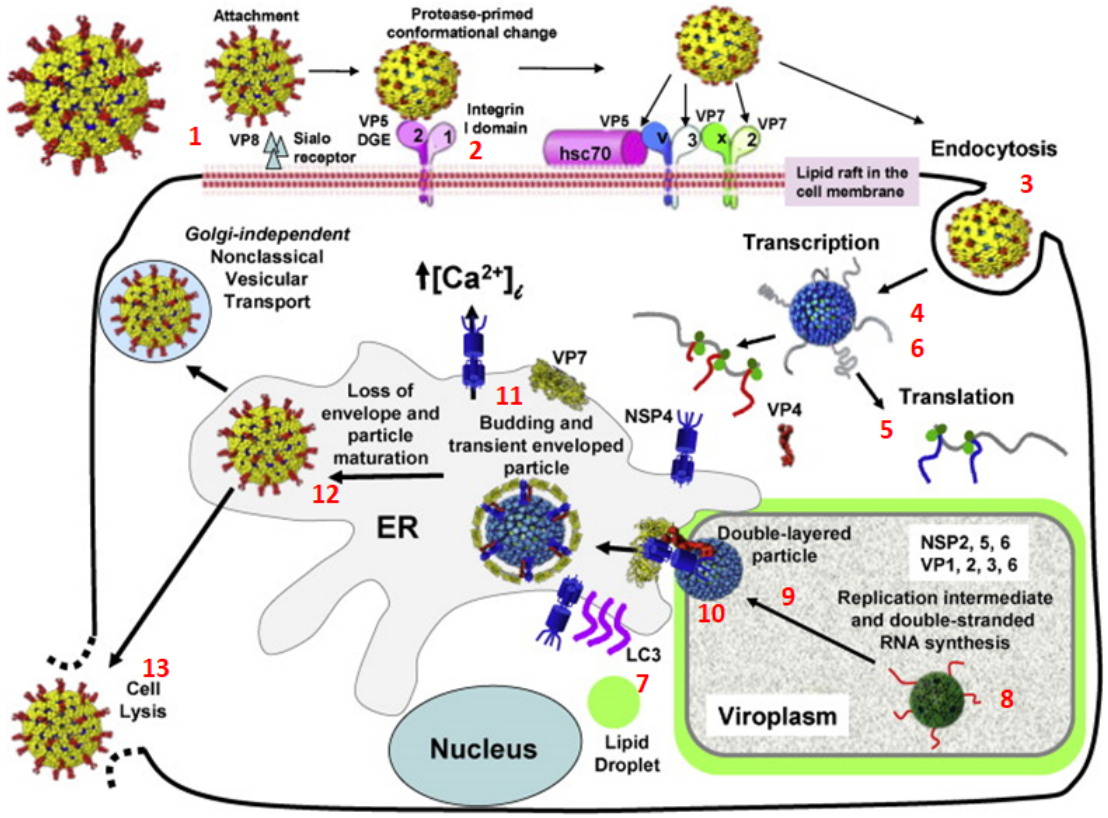


Figure 1.6: Rotavirus replication cycle. 1. Attachment of rotavirus to cell surface via interactions between VP8 and sialic acids. **2.** Interaction of various integrin motifs in VP5 and VP7 with integrins α2β1, αvβ3 and αxβ2 enabling viral attachment and initiation of viral entry via endocytosis. Interaction with hsp70 is also illustrated. **3.** Viral entry via endocytosis and formation of endosome. Uncoating of the outer VP4 and VP7 layer exposing the transcriptionally active DLP to the cytoplasm.**4.** Transcription of the viral genome.**5.** Translation of the viral (+)ssRNA resulting in viral protein synthesis. Formation of the viroplasm. NSP2 and NSP5 are essential to its formation.**6.** Transcription of viral mRNA for incorporation into cores.**7.** Recruitment of lipid droplets for the formation of the viroplasm. VP1, 2, 3 and 6 are also associated with the viroplasm.**8.** Formation of cores during which one of each of the 11 genome segments are encased in the core particle in association with VP1, VP3 and VP2.**9.** Attachment of VP6 to the core, forming the DLP and dsRNA synthesis within the core from VP1.**10.** Transport of DLP to ER for attachment of VP7 and VP4, particle is transiently enveloped.**11.** During initial uncoating and later maturation of the TLP, Ca^{2+} ion concentrations play a critical role in the stabilization of VP7 trimers. Low concentrations of Ca^{2+} (such as those found in the endosome) destabilize VP7 trimers and initiate uncoating. Increased concentrations of Ca^{2+} (facilitated through NSP4 activity) are required for proper coating of the DLP and maturation of the TLP.**12.** Maturation of TLP following the disassociation of the envelope and non-vesicle transport of virions to cell surface for viral egress. This process is independent of the Golgi apparatus and is not fully understood.**13.** Final release of matured viral particles through cell lysis or viral budding. Matured TLPs are now deemed infectious and spread to adjacent cells. Used with permission Desselberger 2014.

1.7.1 Attachment and entry

Attachment of rotavirus to cells is mediated by the protease-sensitive spike protein, VP4 (Ludert et al., 1996). It is believed that initial attachment occurs via common receptors, since rotavirus can infect multiple cell types, but with varying levels of efficiency (Estes et al., 1979). Post-attachment receptors may be essential for entry. The attachment is

probably mediated by the VP8* subunit of VP4, but cleavage of VP4 is required for entry.

Sialic acid receptors play a role in virus attachment since some rotaviruses, such as Rhesus rotavirus (RRV), hemagglutinate red blood cells, and neuraminidase treatment of cultured cells reduce the infectivity of hemagglutinin positive cells (Guerrero et al., 2000). This led to a classification scheme in which viruses are classified as neuraminidase sensitive and neuraminidase insensitive and the suggestion that the entry pathway is either sialic acid moiety dependent or independent (Ciarlet & Estes, 1999). Subsequent studies challenged this idea, showing that insensitivity to neuraminidase does not necessarily mean that binding is sialic acid independent (Haselhorst et al., 2009). However, neuraminidase sensitive strains bind to terminal sialic acid moieties and neuraminidase insensitive strains bind to sialic acid moieties in gangliosides, which are neuraminidase resistant (Haselhorst et al., 2009). It is clear that the VP8 * domain of both classes binds to sialic acid moieties in gangliosides (Dormitzer, 2002). Work by Ciarlet and collegues in 2002 showed that the mechanism of infection between the two classes was markedly different. Neuraminidase-sensitive strains enter on the apical side of the cell, whereas insensitive strains enter via both the apical and basolateral surfaces (Ciarlet et al., 2002).

After attachment, entry occurs via co-receptors. For this to occur, proteolytic cleavage of VP4 is required, which produces the N-terminal VP8* and C-terminal VP5* fragments. VP5* then binds to integrin co-receptors. Several integrins have been implicated in entry, namely $\alpha 2\beta 1$, $\alpha 4\beta 1$, $\alpha x\beta 1$, $\alpha v\beta 1$ (Coulson et al., 1997; Guerrero et al., 2000). The expression of these integrins in non-permissive cell lines increases binding and infectivity, but not to the same extent as fully permissible cell lines, showing that integrins may function as internalisation receptors (Ciarlet & Estes, 1999; Hewish et al., 2000).

1.7.2 Uncoating

Internalisation occurs via one of two mechanisms, through direct membrane penetration or clathrin-mediated endocytosis, both of which are under debate. Regardless of the mechanism, entry requires membrane permeabilisation (Cuadras et al., 1997; Falconer et al., 1995). A sequence motif in VP5* that bears homology to the fusion peptide sequence observed in enveloped viruses such as alphaviruses and influenza viruses has been implicated in the membrane permeabilisation activity of rotavirus cell entry (Denisova et al., 1999). The exact mechanism of uncoating is unclear, but it seems that the outer capsid (VP4 and VP7) is lost soon after entry, most probably in an endocytic vesicle at low Ca^{2+} concentrations (Ludert et al., 1987). DLPs are then transferred to the cytoplasm.

1.7.3 (+)ssRNA synthesis and translation

It is believed that conformational changes that occur upon loss of the outer capsid proteins, VP4 and VP7, activate transcription via VP6 interacting with VP2 (Sandino et al., 1986). DLPs are transcriptionally active in the cytoplasm. DLPs synthesise (+)ssRNAs from the dsRNA genome. Transcripts are detectable from one hour post infection (Ayala-

Breton et al., 2009). The (+)ssRNAs serve as templates for translation and are packaged for dsRNA synthesis. Rotavirus RNA-dependent RNA polymerase (VP1) performs both transcription (+)ssRNA synthesis and replication (-)ssRNA synthesis (Patton J T et al., 1997). (+)ssRNA from each genome segment is synthesised by a specific polymerase at the five-fold axes and transported from DLPs via type I channels that traverse the core and intermediate capsid. VP6 is essential for this function, as it is believed to cause a transcriptional change in VP2 in the core that results in transcription and (+)ssRNA extrusion from the DLP (Charpilienne et al., 2002). The transcripts exit at the five-fold axes of the DLP, Figure 1.7 (Chen et al., 2009; Lawton et al., 1997; Jayaram et al., 2004).

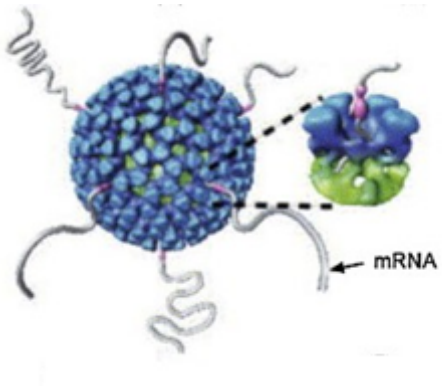


Figure 1.7: Rotavirus (+)ssRNA synthesis. (+)ssRNA exit from channels transversing the SLP and DLP. Note (+)ssRNA only exits at the five-fold axes. Used with permission Jayaram et al. 2004

The (+)ssRNA transcripts are not synthesised in equimolar amounts. The (+)ssRNAs of the larger genome segments are synthesised at a lower rate than the smaller ones, as shown in experiments carried out using RNA interference (RNAi) (Ayala-Breton et al., 2009). Rotavirus NSP3 binds to the 3' ends of (+)ssRNAs of the genome segments and interacts with the eukaryotic translation initiation factor eIF4GI and functions as an analogue for Poly(A) binding protein that would normally bind poly(A) tails, causing circularisation of viral (+)ssRNA genome segments, up regulating their translation (Piron, 1998; Piron et al., 1999). This then produces the required proteins for genome packaging and capsid assembly.

1.7.4 Viroplasm formation, genome packaging, and DLP assembly

1.7.4.1 Viroplasm formation

Rotavirus genome packaging and assembly of progeny DLPs occur in electron-dense cytoplasmic inclusion bodies, known as viroplasms. The formation of viroplasms requires three non-structural proteins, NSP2, NSP5, and NSP4. NSP4 co-localises with viroplasms. NSP4 is believed to direct NSP5 to viroplasms for viroplasm formation (Berkova et al., 2006). Proteins required for DLP assembly (VP1,2,3, and 6), as well as TLP assembly, VP4, and VP7 have also been found in proximity to viroplasms. (Garcés Suárez et al., 2019). Viroplasms appear 2 hours post infection (Eichwald et al., 2004). The number

of viroplasms peak and then decrease with time, but the surface area of viroplasms increases with time post-infection, suggesting fusion of viroplasms. Viroplasms associate with lipid droplets (Cheung et al., 2010). The components of lipid droplets are lipids, perilipin, adipocyte differentiation related protein (ADRP). Blocking of these components, thus interfering with lipid droplet formation, results in fewer functional viroplasms and a reduction in infectivity (Cheung et al., 2010).

NSP2 and NSP5 are essential for genome replication and packaging. NSP2 is a multifunctional octamer that possesses NTPase, NDP kinase, RNA triphosphatase(RTPase), and nucleic acid helix destabilizing activities (Bravo et al., 2018; Jiang et al., 2006; Kumar et al., 2007). Each monomer has two domains separated by a catalytic cleft. Monomers associate to form a doughnut-shaped octamer with a central hole along the fourfold axes. Each monomer has two domains separated by a catalytic cleft. The catalytic grooves are lined with basic residues and run across the two-fold axes (Jayaram et al., 2002). RNA binding activity of NSP2 requires formation of the octamer. RNA and NSP5 compete for the same binding site (Jiang et al., 2006). NSP2 octamers are essential for genome assortment prior to packaging (Borodavka et al., 2017; Bravo et al., 2018). NSP5 is a Ser/Thr rich phosphoprotein dimer. The biologically relevant form of NSP5 is a decamer (Martin et al., 2011). Although NSP2 binds to NSP5, it is hypothesised that some NSP2 remains free to bind RNA (Martin et al., 2011).

1.7.4.2 Genome packaging

A fundamental problem in rotavirus biology is how a set of eleven (+)ssRNAs of the genome segments are selected and packaged into the viral core. Genome packaging is poorly characterised for rotaviruses but better elucidated for two other dsRNA viruses, namely bluetongue virus (BTV), a 10 segmented dsRNA virus from the *Reoviridae* responsible for disease in livestock and φ6, the tri-segmented dsRNA bacteriophage from the *Cystoviridae* which infects *Pseudomonas* species.

Bacteriophage φ6 shares many similarities with members of the *Reoviridae*, such as a segmented genome that serves as template for (+)ssRNA synthesis. A major difference is that the three viral φ6 (+)ssRNAs are translocated into pre-assembled procapsids that lack the RNA-dependent RNA polymerase (RdRp) P2, showing that the role of the RdRp is limited in genome packaging (Borodavka et al., 2018; Juuti & Bamford, 1995). The φ6 (+)ssRNAs (referred to as s+, m , and l+) are sequentially packaged from the smallest to the largest segments (Borodavka et al., 2018). Fundamental to this process is the presence of packaging signals (pac) in the 5' ends of the (+)ssRNAs. The pac signal consists of 2 regions, an 18 nucleotide stretch in the 5' end, and a 200 nucleotide downstream stretch that forms a unique secondary structure, that binds to a recognition site on the capsid (Gottlieb et al., 1994; Pirttimaa & Bamford, 2000). Packaging of the s+ and m+ segments causes a conformational change in the pro-capsid, which exposes the l+ recognition site, allowing the packaging of the l+ segment (Poranen et al., 2001).

For the *Reoviridae*, (+)ssRNA selection and packaging occurs in viral inclusion bodies, known as viral factories or viroplasms. The viral (+)ssRNAs are divided into complexes that are then packaged into cores (Borodavka et al., 2018). For bluetongue virus (BTV), experiments indicate that (+)ssRNAs assemble into complexes prior to packaging into cores (Lourenco & Roy, 2011; Sung & Roy, 2014). In the case of genome segment 9 of BTV the 276 nucleotides in the 5' terminus and 393 nucleotides of the 3' terminus are important for packaging, suggesting that the 5' and 3'-UTRs along with adjacent segment-specific regions are required for packaging a specific segment (Matsuo & Roy, 2009) Figure 1.8.

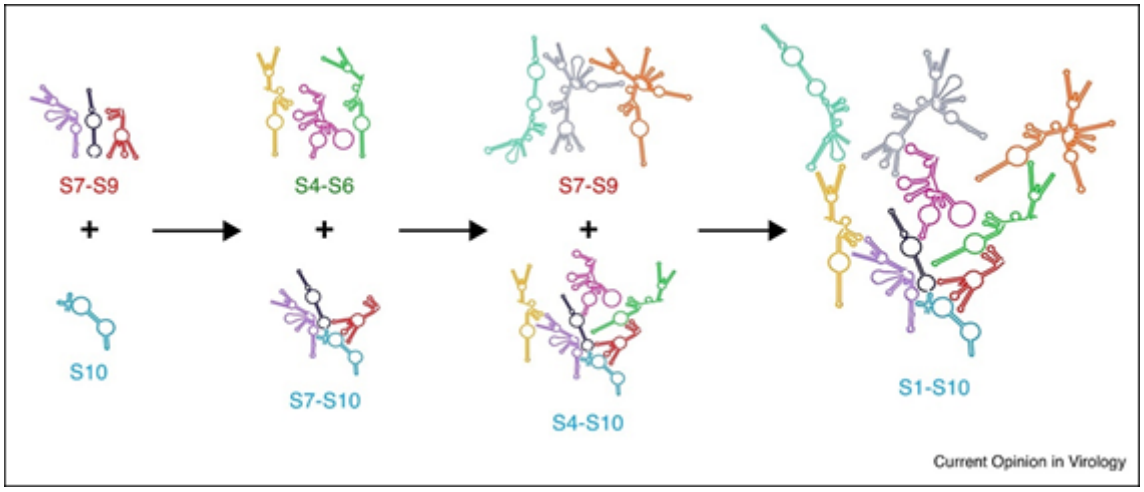


Figure 1.8: Current model of BTV genome packaging. Recruitment cascade of BTV virus (+)ssRNAs of genome segments, showing initial interaction of the small(+)ssRNA of the genome segments with the eventual recruitment of the larger (+)ssRNAs to form the complete set of (+)ssRNAs for packaging. Used with permission Roy 2017

Much less is known about (+)ssRNA packaging in rotaviruses. Specific intersegment interactions between (+ssRNA) of the genome segments are orchestrated by NSP2, which forms the viroplasm together with NSP5 (Borodavka et al., 2017; Bravo et al., 2018). Octameric NSP2 promotes the formation of sequence-specific intersegment interactions by remodelling the secondary structure of the (+)ssRNA, in the presence of a large molar excess of NSP2, a state that NSP2 may occur in, in viroplasms (Borodavka et al., 2018). This seems to suggest that intersegment interactions within coding regions of the individual (+)ssRNAs of genome segments are involved in the selection of genome segments, while packaging selectivity is determined by the UTRs, but this must still be experimentally proven, Figure 1.9. RNA-RNA interactions may also be a driver of reassortment between rotaviruses. What remains unclear for rotaviruses is how the (+)ssRNAs are selected for packaging into cores (McDonald & Patton, 2011). A prevailing idea is by binding the (+)ssRNAs to their respective RdRPs, which have a high affinity for the 3'-terminus of (+)ssRNAs. However, packaging signals have not been identified in rotavirus (+)ssRNAs, and it is difficult to explain why genome segments with sequence duplications outcompete wild-type segments during packaging (Troupin et al., 2011; Desselberger, 2020).

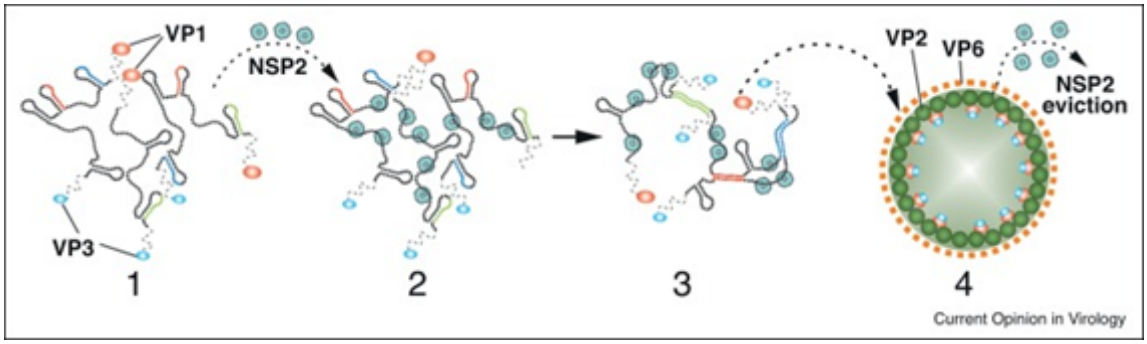


Figure 1.9: Model of the possible mechanism of rotavirus (+)ssRNA recruitment. VP1 binds to the 3'-UTR consensus sequence. NSP2 then binds and remodels the secondary structure. This exposes complementary sequences between the (+)ssRNA, which allows the formation of stable intersegment interactions. The resulting ribonucleoprotein complex may cause the formation of VP2 cores around the complex, after which NSP2 may be evicted prior to (-)ssRNA synthesis. Used with permission Borodavka et al. 2018.

1.7.4.3 Assembly of rotavirus DLPs

After (+)ssRNA packaging, VP6 is assembled onto SLPs to form progeny DLPs, which involves the attachment of VP6 onto packaged cores consisting of VP2 and VP1/3 complexes (Desselberger et al., 2013).

Assembly of VP6 onto rotavirus SLPs is highly regulated. Baculovirus-expressed rotavirus VP2 and VP6 are able to spontaneously form into DLP-like strucures (Zeng et al., 1994). Since rotavirus particle assembly is orchestrated in viroplasms containing NSP2/NSP5, it was assumed that NSP2 or NSP5 regulates both genome packing (as discussed in Section 1.7.4.2) and capsid assembly. Work by Berois and collegues showed that NSP5 co-immunprecipitates with VP2 (Berois et al., 2003). NSP5 was also shown to affect the cellular localisation of VP2. Fewer, but larger inclusions form when only VP2 is expressed in cells. Further pull-down experiments showed that NSP5 is capable of interacting with native SLPs, VP2/6 and VP1/2/3/6 VLPs, but not native DLPs (Berois et al., 2003). NSP5 is able to displace VP6 from VP2/6 VLPs, but not native DLPs. VP2 and VP6 interactions are stronger in native DLPs, than in VLPs, explaining why the effect of NSP5 eviction of VP6 is not seen in native DLPs. This shows that NSP5 competes for VP6 binding onto VP2 and modulates VP6 transcapsidation onto VP2, thereby regulating DLP assembly, and is thus necessary for DLP formation (Contin et al., 2010).

1.7.5 DLP Transport

Up to 2019, it was believed that DLPs transport from viroplasms to the ER by budding through the ER membrane (Dubois-Dalcq et al., 1984). The first identified function of NSP4 was that it acts as an intracellular receptor for DLPs. Using *in vitro* binding assays, it was shown that it most likely binds VP6 trimers (Au et al., 1989). The final C-terminal methionine 175Met of NSP4 was identified as essential for binding to DLPs, since its deletion completely abolishes DLP binding (Taylor et al., 1992). The binding

domain was mapped to the C-terminal, specifically to amino acids 161-175 by two separate groups using antibody binding experiments and protein truncations, Figure 1.10 (Au et al., 1993; Taylor et al., 1993). The cytoplasmic domain was then identified as consisting of a coiled-coil domain and a virus binding C-terminal, and it was hypothesised as essential for the structure of the DLP binding domain (O'Brien et al., 2000). During this, the budding DLPs gain an envelope that is lost as the DLPs reach the interior of the ER. It is important to note that all of this work was done without a fully tractable reverse genetics system, leaving important questions open regarding co-reassortment of GS6(VP6) and GS10(NSP4) that can now be investigated with the advent of rotavirus plasmid-based reverse genetics (Iturriza-Gomara et al., 2003).

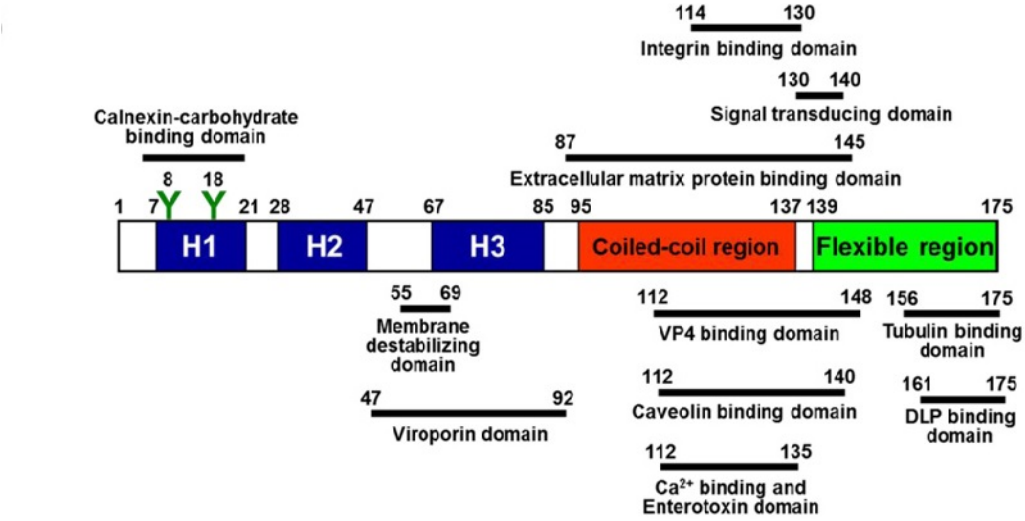


Figure 1.10: Rotavirus A NSP4 N and C-terminals, with various functional domains illustrated. H1-H3 comprises the hydrophobic domains that contain the membrane destabilising and viroporin domains. The C-terminal is hydrophilic and contains the coiled-coiled and flexible regions. The coiled-coil region contains the Integrin-binding domain, the signal transducing domain, the extracellular matrix protein binding domain, the VP4 binding domain, the caveolin binding domain, the Ca^{2+} binding and enterotoxin domains. The flexible region contains the tubulin binding and DLP domains. Used with permission Hu et al. 2012

However, there is new work that suggests that DLPs bud through autophagosome vesicles and not the ER as previously believed (Crawford et al., 2019). The authors showed that NSP4 is transported from the ER to viroplasms in COPII vesicles, a cellular transport mechanism that normally transports proteins from the ER to the Golgi apparatus, Figure 1.11. Using immunoprecipitation and confocal microscopy, it was shown that NSP4 exits the ER in COPII vesicles. Assembly of these vesicles depends on Sar1-GDP. Phosphorylation leads to the insertion of Sar1-GTP into the ER membrane and recruitment of Sec23 and Sec24 around the NSP4 cargo. Sar1 interacts with Sec23, allowing Sec24 to bind to the cargo protein. Following this, Sec13 and Sec31 form around the vesicle, Sec31 is phosphorylated by casein kinase II (CK2), and the vesicle leaves the ER. Following exit, the vesicle interacts with the autophagy protein LC3. These vesicles are then hijacked by the cellular autophagy machinery to transport NSP4 to viroplasms. The authors postulate that the membranes surrounding viroplasms are not endoplasmic reticulum as previously

believed, but are autophagy isolation membranes derived from COPII transport, since the ER marker proteins SERCA and calnexin were not found in membranes surrounding viroplasms. In addition, VP7 was shown to transport with NSP4 to viroplasms. This may present an alternative mechanism for DLP transport and particle maturation.

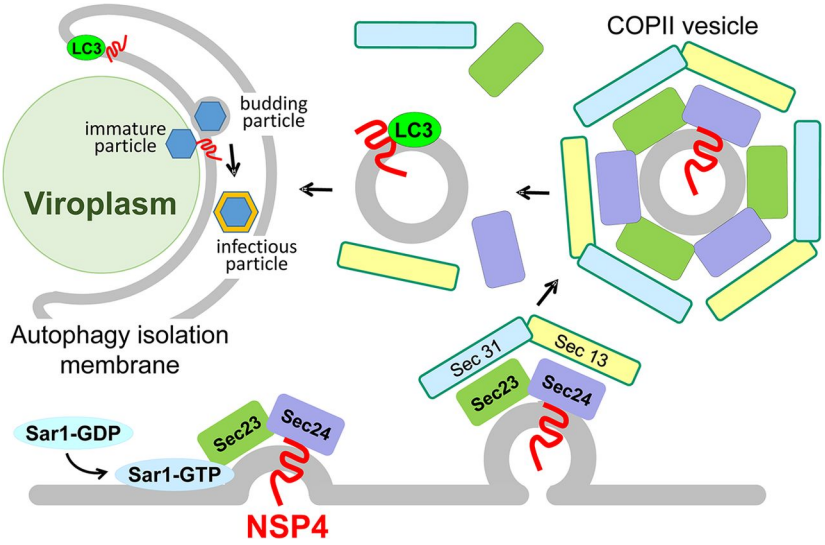


Figure 1.11: Proposed model of NSP4 transport in COPII vesicles. Sar1-GDP is phosphorylated to Sar1-GTP. Sar1-GTP interacts with Sec23, with Sec23 inturn interacting with Sec24, allowing binding of NSP4. This forms the inner coat of the vesicle. The Sec31/Sec13 heterotetramer then forms the outer coat around the vesicle. Phosphorylation of Sec31 by CK2 results in transport from the ER. These vesicles are then hijacked by the cellular autophagy machinery, where at some point LC3 interacts with NSP4. It is believed that autophagy isolation membranes then form around viroplasms, which allows transport of DLPs from viroplasms. Used with permission Crawford et al. 2019

1.7.6 Virus particle maturation and release

After DLP transport, nascent DLPs are coated with VP4 and VP7. It is believed that VP4 attaches to DLPs followed by VP7 which anchors VP4 in place (Trask & Dormitzer, 2006). TLP assembly is a calcium-dependent process, since VP7 forms calcium-dependent trimers (Chen et al., 2009). The N-termini of VP7 interact with VP6 trimers, Figure 1.5. Particle maturation is mediated by NSP4, which releases calcium from the calcium stores from the ER (Hyser et al., 2010). NSP4 is localised in the membranes surrounding the viroplasm and binds both VP6 and VP4. The function of NSP4 is more fully discussed in Section 1.8. The current model for outer capsid assembly has been suggested by Trask et al. (Trask et al., 2012). In this model, NSP4 recruits DLPs and VP4 to the cytosolic side of the ER. Interaction of DLPs with NSP4 tetramers results in deformation of the ER membrane and budding of NSP4, VP4 and DLPs into the ER. With VP4 assembled onto DLPs the transient envelope is lost and VP7 assembles into the capsid (Trask et al., 2012). Mature TLPs then exit the cell either by cell lysis of non-polarised cells, seen in work done in MA104 cells (McNulty et al., 1976). Rotaviruses exit polarised cells via a different budding mechanism that is not well understood (Gardet et al., 2006).

1.8 Rotavirus pathogenesis

The main symptom of rotavirus gastroenteritis is diarrhoea with little intestinal inflammation, a hallmark that distinguishes it from bacterial gastroenteritis (Greenberg & Estes, 2009). Rotavirus infects intestinal enterocytes, resulting in destruction of these cells, down-regulation of absorptive enzymes, and changes in tight junctions between cells that lead to paracellular leakage. Rotavirus pathogenesis is orchestrated by non-structural protein NSP4.

Rotavirus NSP4 is a 28 kDa, 175 amino acid glycoprotein encoded by genome segment 10. It is synthesised as an ER transmembrane protein, that functionally exists as a tetramer. Figure 1.10 shows the various NSP4 domains and their respective functions. The N-terminal contains three hydrophobic domains (Bergmann et al., 1989; Chan et al., 1988). The H1 domain contains two N-linked glycosylation sites that are orientated towards the luminal side of the ER (Bergmann et al., 1989). H2 is an uncleaved signal peptide that inserts into the ER membrane, with H3 serving as a viroporin that causes calcium efflux from the ER (Hyser et al., 2010). The N-terminal is followed by an extended cytoplasmic domain, that includes multiple functional domains, having diverse functions such as transcription modulation, VP4 binding, integrin binding, plasma membrane binding, viroplasm formation, (Berkova et al., 2006; Boshuizen et al., 2004; Lopez et al., 2005; Silvestri et al., 2005) and caveolin binding (Hyser et al., 2008; Parr et al., 2006; Seo et al., 2008). Importantly, as discussed in Section 1.7.5, rotavirus NSP4 serves as a receptor for DLPs transporting from the viroplasm for virus maturation (Taylor et al., 1996). Rotavirus NSP4 is central in many functional aspects of the replication cycle. The following is a discussion of some of the functional aspects.

In 1996, NSP4 was first identified as an enterotoxin (a toxin that affects the intestinal tract), when Judith Ball and colleagues expressed NSP4, and purified it for use in the production of anti-NSP4 serum (Ball et al., 1996). They discovered that intraperitoneal delivery of purified NSP4 induced diarrhoea in neonatal mice. This occurred in both an age-dependent and dose-dependent manner, since 0.1 nmol of NSP4 only affected 6-7-day-old mouse pups, and not 8-9-day-old mouse pups. Higher doses affected 8-9 day old mice, but not 17-18 day old mice. This was the first identification of a non-bacterial enterotoxin.

Enterotoxin activity is mediated by amino acids 114-135 by activating Ca^{2+}-activated Cl^- channel TMEM16A, and inhibiting Na^+ absorption via SGLT2, a Na^+/glucose transporter (Ousingsawat et al., 2011). Furthermore, this domain induces Ca^{2+} secretion by binding to phospholipase C and inducing transient inositol 1,4,5-trisphosphate (IP3) secretion.

Viroporin activity was identified in NSP4 in 2010 (Hyser et al., 2010). The authors identified a domain (aa 47-90) that inserts into the ER membrane. This domain consists of two subdomains, a pentalysine domain and an amphipathic helix domain. The pentalysine domain is believed to interact with negatively charged phospholipids in the ER membrane. Viroporin activity is mediated by the amphipathic helix subdomain, which is believed to

form a pore in the ER membrane upon tetramerization. This domain has also been found to activate calcium release from the ER store through activation of STIM1, a ER calcium sensor (Hyser et al., 2013). The authors showed that this interaction is required for rotavirus replication, since deletion of STIM1 significantly reduces virus yield. Figure 1.12 shows the proposed viroporin mechanism. Much of the pathogenesis of rotavirus is due to viroporin activity, which causes calcium efflux from the cell.

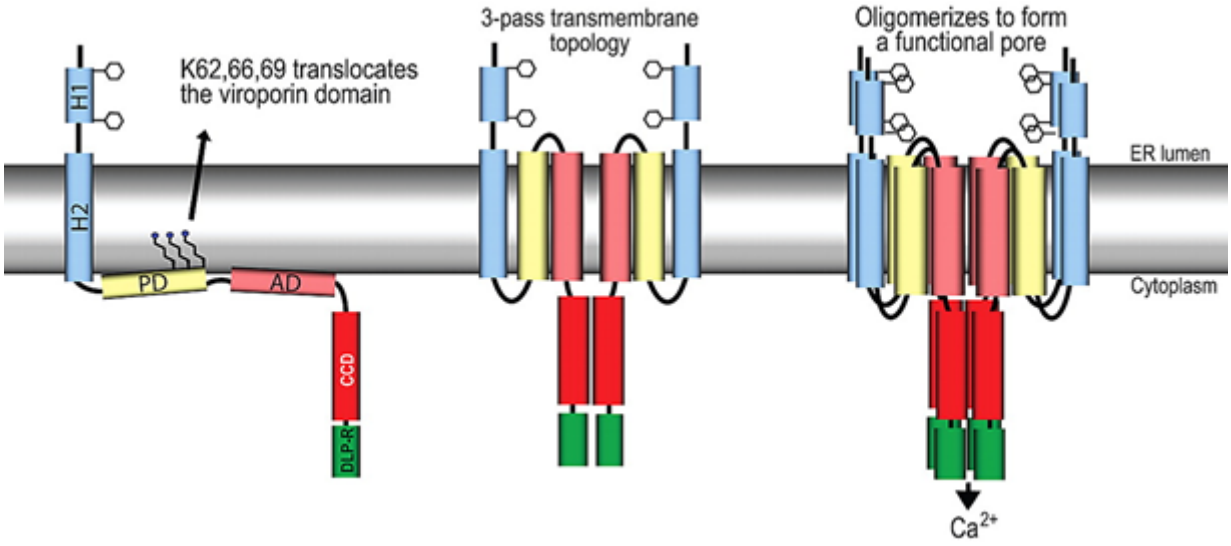


Figure 1.12: NSP4 viroporin activity proposed mechanism. The H2 signal domain inserts into the ER membrane, which in turn allows the insertion of the pentalysine domain into the ER membrane followed by the amphipathic helix domain, creating a 3- pass membrane topology. NSP4 tetramerises to forms a functional viroporin. Used with permission Hyser et al. 2010

The mechanism of rotavirus pathogenesis has been extensively characterised. Rotavirus infection in the ileum results in the expression of NSP4, during which NSP4 induces Ca^{2+} release from the ER. Virions exit the cell together with NSP4, Figure 1.13. Tight junctions are disrupted, allowing paracellular leakage of water and electrolytes (Greenberg & Estes, 2009). Extracellular NSP4 can then bind to neighbouring enterocytes and bind an unknown receptor, likely integrin $\alpha 2\beta 1$ since this integrin has been shown to bind NSP4 and elicit diarrhoea in neonatal mice (Seo et al., 2008). This causes a signalling cascade through phospholipase C (PLC) and inositol phosphatase (IP3) that results in both Ca^{2+} release and an increase in intracellular Ca^{2+}. Intestinal crypt cells can be acted upon directly by NSP4 or NSP4 can stimulate the enteric nervous system which signals intracellular Ca^{2+} release and stimulation of Cl^- secretion, which causes water loss (Lundgren, 2000).

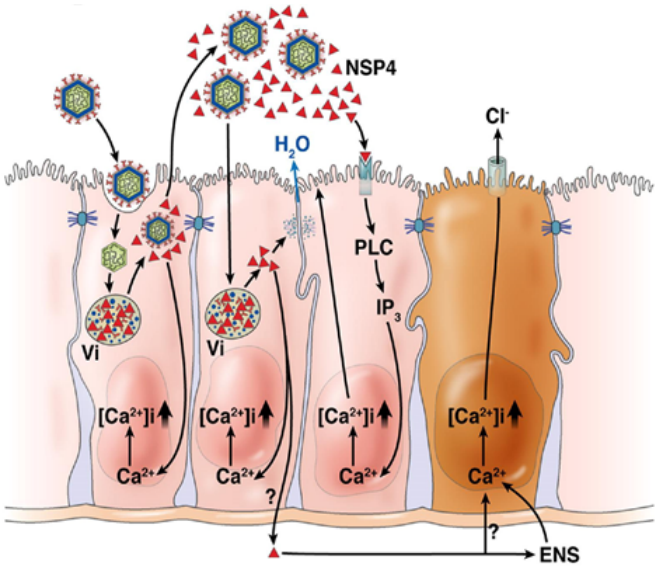


Figure 1.13: Mechanism of pathogenesis in rotaviruses. Cells are infected, resulting in expression of NSP4. NSP4 disrupts tight junctions of neighbouring cells. The extracellular form of NSP4 can interact with integrins which causes a signal cascade IP3 that causes calcium efflux from the cell. NSP4 also causes chloride ion loss from intestinal crypt cells, which causes water loss, the primary causes of dehydrating diarrhoea seen in rotavirus gastroenteritis. Used with permission Greenberg & Estes 2009

1.9 Rotavirus Vaccines

Currently, seven rotavirus vaccines are used in national immunisation programmes, Table 1.2. In 2006, two vaccines, Rotarix (GlaxoSmithKline Biologicals SA, Rixensart, Belgium) and RotaTeq (Merck & Co., Inc., West Point, PA, USA) were prequalified by the WHO and included in national immunisation programmes (Burke et al., 2019). This was followed in 2018 by Rotavac (Bharat Biotech, Hyderabad, India), and ROTASIIL (Serum Institute of India PVT. LTD., Pune, India). Two WHO-pre-qualified vaccines are currently in use in India and Palestine (Nair et al., 2019; Burke et al., 2019). The Rotavin-M1 and Lanzhou Lamb vaccines are not WHO-prequalified, but are currently in use in Vietnam and China, respectively. Vaccine strains can undergo ressortment with field strains, which impacts vaccine safety and efficacy (Rose et al., 2013). This will be discussed in detail in Section 1.10.3.

Table 1.2: Globally and locally licensed rotavirus vaccines (adapted from Burke et al. (2019))

Name	Manufacturer	Doses	Composition
Rotarix	GSK	3	G1P[8]
RotaTeq	Merck	2	G1,G2,G3,G4, P[8]
Rotavac	Bharat Biologicals	3	G9P[11]
ROTASIL	Serum Institute of India	3	G1,G2,G3,G9, P[5]
Rotavin-M1	POLYVAC	3	G1P[8]
Lanzhou Lamb rotavirus vaccine	Lanzhou Institute of Biological products	1	G10P[15]

Rotavirus vaccines are highly effective in developed countries, with up to 90% efficacy. RotaTeq (RV5), introduced in 2006, was shown to have an efficacy of 74% (Block et al., 2007; Vesikari et al., 2007). Rotarix (RV1) was tested in two separate phase III trials in Europe and the United States (Ruiz-Palacios et al., 2006; Vesikari et al., 2007). They are less effective in developing countries, such as those in Africa. Efficacy in South Africa after two doses of Rotarix was originally reported at 72% in the phase III clinical trial, but was later reported at 54% after follow-up surveillance (Groome et al., 2014; Madhi et al., 2010; Henschke et al., 2022). The reasons for low efficacy are unclear, but differences in circulating field strains compared to those in vaccine formulations could be a reason for poor vaccine efficacy, especially since it is not clear to what extent rotavirus vaccines exert heterotypic (cross-reactive) immunity (Desselberger & Huppertz, 2011; Page et al., 2018; Jere et al., 2018).

Correlates of protection for rotavirus are not well defined, altough antibodies against VP6 and VP5* may have a role (Angel et al., 2012; Nair et al., 2016, 2017). Animal models have shown that humoral immunity is most probably associated with protection and that it is mediated by both neutralising (mediated by the outer capsid proteins VP4 and VP7) and non-neutralising antibodies (mediated by the inner capsid protein VP6) (Desselberger & Huppertz, 2011). There are some indications that high titres of gut IgA (also known as copro-antibodies) directed against VP6 correlate with protection, but this has not been definitively proven.

1.9.1 Live-attenuated vaccines

Rotarix is a monovalent vaccine containing a G1P[8] strain. This vaccine is derived from the rotavirus strain 89-12, which was obtained from a symptomatic neonate in 1988 (Bernstein et al., 1990; Ward et al., 1997, 2009). It was attenuated by passaging 26 times in primary African Green Monkey cells, followed by 7 passages in Vero cells. The initial material showed some residual virulence, but was improved during subsequent plaque purification and passaging by GlaxoSmithKline. The molecular basis for attenuation is unknown, but was speculated to be due to GS10(NSP4) mutations, which was found not to be the case when comparing virulent and passage gene sequences (Ward et al., 1997). This strain was shown to provide protection G1, G3, G4, and G9 strains that contained a P[8] GS4(VP4) (Ward et al., 2009).

RotaTeq is a live-attenuated pentavalent human-bovine reassortant vaccine that contains five pairs of human VP4/VP7s on a bovine backbone with G1-G4 for GS9(VP7) and a P[8] for GS4(VP4). The genetic backbone for these strains is the bovine WC3 strain, a naturally attenuated cell culture-adapted bovine strain (Heaton et al., 2005). The G1-4 strains express the VP7s from the WI78, SC2, WI78 and Bricout B strains together with a P7[5] VP4 from the WC3 strain. The P[8] strain expresses the VP4 for the WI79 strain and a G6 VP7 form the WC3 strain (Heaton et al., 2005).

Rotavac contains a naturally attenuated G9P[11] strain isolated in India that was shown

to be asymptomatic in neonates and was not previously identified in humans (Bhan et al., 1993). This strain was isolated after a 1986 outbreak of rotavirus in a New Delhi neonatal ward. Infection did not result in diarrhoea and elicited a strong salivary antibody titre (Jayashree et al., 1988). Rotasiil is a human-bovine reassortant vaccine that contains G1-4 and a G9 strain on the Bovine UK strain backbone (Kulkarni et al., 2017). This vaccine has a 60.5% efficacy against severe disease.

Other nationally licenced vaccines are in use in Vietnam and China. The first is known as Rotavin-M1 (Centre for Research and Production of Vaccines and Biologicals (POLYVAC, Hanoi, Vietnam) and is a naturally attenuated G1P[8] strain isolated from an infant (Anh et al., 2012). The second is the Lanzhou Lamb rotavirus vaccine (Lanzhou Institute of Biological Products Co., Ltd., Lanzhou, China) that contains a G11P[15] strain isolated in 1985 and is exclusively licensed in China (Fu et al., 2007). The third is based on the asymptomatic Australian RV3 neonatal strain, known as RV3-BB (PT BioFarma, Bandung, Indonesia), and is undergoing clinical trials in Indonesia (Bines et al., 2018). This vaccine was originally developed in Australia and contains an asymptomatic G3P[6] strain. This vaccine is aimed at being used as a neonatal vaccine, since this strain has the ability to replicate in the neonatal gut, even in the presence of maternal antibodies (Chen et al., 2017). Maternal serum IgG and breast milk IgA are more prevalent in mothers from developing countries than developed countries, the hypothesis being that repeated reinfection occurs more often in developing countries due to poor sanitation and living conditions (Moon et al., 2010). Maternal antibodies function by crossing both the placenta during pregnancy and are transferred to breast milk and are believed to reduce the efficacy of commercial vaccines by neutralising them after administration (Chan et al., 2011).

1.9.2 Non-replicating and dead-subunit vaccines

Non-replicating vaccines will be able to bridge the gap in live-attenuated vaccine efficacy by acting as a booster vaccine because live-attenuated boosters will not be effective due to varying levels of partial immunity. One such vaccine, currently in clincial trial, is known as P2-VP8-P[8] a rotavirus VP8 subunit fused to a P2 epitope of tetanus toxin (Groome et al., 2017). Norovirus virus-like particle (VLPs) together with a rotavirus VP6 has been trialled as a vaccine candidate that acts as a norovirus-rotavirus combination vaccine (Blazevic et al., 2011).

Non-live rotavirus VLPs have been suggested as a booster vaccine, to improve poor live-attenuated vaccine efficacy (Jere et al., 2014). VLPs only contain the structural components of the virus without genetic material, eliminating the risk of reassortment and avoiding inhibition from partial immunity. Rotavirus VLPs did confer complete protection in a mouse model, but did not protect when used alone in gnotobiotic pigs (Azevedo et al., 2013; O'Neal et al., 1997). VLPs can then elicit a cellular and humoral immune response but are non-replicating, meaning that repeated doses will be required for long-term immunity.

1.10 Reassortment in segmented RNA viruses

Segmented RNA viruses are unique in their characteristic of maintaining their genomes as distinct RNA molecules referred to as genome segments (McDonald et al., 2016). Currently, 11 segmented RNA virus families have been identified that infect a wide variety of hosts (Marshall et al., 2013; Ramig, 1997). These viruses differ in their virion structure, genome architecture, and host tropism, but share the ability to exchange genome segments during co-infection of the same cell with two parent viruses. This is known as reassortment (McDonald et al., 2016). Recombinant progeny particles with single-genome segment reassortments are most common.

Reassortment in segmented RNA virus families that package their genomes into a single capsid, families such as the *Cystoviridae* (φ6 bacteriophage), *Orthomyxoviridae*, and the *Reoviridae* require packaging signals in the form of RNA-RNA and/or RNA-protein interactions as discussed in Section 1.7.4.2. Therefore, strain- and species-specific differences in RNAs and packaging proteins can severely restrict, completely prohibit the generation of reassortant progeny, or prevent observation in the population due to a reduction in fitness. Initially, it was postulated that reassortment is a means of purging deleterious mutations. McDonald *et al.* believed that reassortment is not a driver of evolutionary fitness, but an artefact of segmented genome replication, since it is not required to maintain fitness for non-segmented RNA viruses (McDonald et al., 2016).

1.10.1 *Orthomyxoviridae* genome reassortment

The 8 segmented (-)ssRNA influenza viruses appear to require specific RNA-RNA interactions for reassortment to occur. Using reverse genetics, influenza A and B (two distinct species) have been reassorted *in vivo* by exchanging the hemagglutinin (HA) encoding genome segment of influenza A with that of influenza B (Baker et al., 2014). This was done by swapping the packaging signals of the influenza B segment with those of the influenza A segment. This, however, does not represent a possible wild-type reassortment, since using a reverse genetics system does not take into account the competition between homologous segments. With reverse genetics, reassortants can be produced that cannot be produced by co-infection, such as the work done for influenza A/avian influenza reassortment (Essere et al., 2013). For influenza viruses, it has also been shown that there are few barriers to genome segment exchange when genome segments are genetically compatible (Marshall et al., 2013).

1.10.2 *Cystoviridae* genome reassortment

Viruses from the tri-segmented dsRNA genome *Cystoviridae* have less specific determinants for reassortment. Genome segments with highly divergent sequence similarity can reassort both *in vitro* and in nature (Diaz-Muñoz et al., 2013). However, bacteriophage φ13 has been shown to package the bacteriophage φ6 medium (+)ssRNA, but the reverse, where the φ13 medium (+)ssRNA is used to package into φ6 procapsids, is not possible,

showing that some level of RNA-RNA complementarity is required (Qiao et al., 2000).

1.10.3 *Reoviridae* genome reassortment

Viruses from the *Reoviridae*, which contain 10-12 dsRNA genome segments, cannot reassort between species. Even some closely related Rotavirus A (RVA) strains are not capable of reassorting (Ramig, 1997). This has also been observed for mammalian orthoreoviruses and bluetongue viruses (Nibert et al., 1996; Ramig et al., 1989). The *Reoviridae* have RNA-RNA complementarity when (+)ssRNAs are first packaged into capsids (Section 1.7.4.2) as well as protein-RNA compatibility during genome replication, where (+)ssRNAs are used as templates for dsRNA production (Lu et al., 2008).

1.10.3.1 Rotavirus genome reassortment

The 3'-terminal(+)ssRNA terminal of rotavirus genome segments contains a consensus recognition sequence. This sequence is inserted into the polymerase and serves as a recognition sequence for the polymerase to begin transcription, Figure 1.14. Phylogenetically, this sequence segregates into two clades. Clade A contains RVA, RVC, RVD, and RVF and Clade B, RVB, RVG, and RVH. The 3'-terminal sequence for clade A is 5'- UGUGACC - 3' or 5'- UGUGGCU- 3', and for clade B is 5'- AAAACCC -3', 5' - AAGACCC - 3' or 5'- UAUACCC - 3', Table 1.3 (Ogden et al., 2012). (+)ssRNAs are bound via their 5'-cap and the 3'-end of the (+)ssRNA insert into the RNA polymerase VP1. A three-amino acid insertion in the template entrance tunnel of VP1 of the RVB/RVG/RVH clade reduced entrance tunnel width, Figure 1.15. This insertion appears to be responsible for this difference in 3'-CS length. This means that a further restriction, based on narrowing of the template entrance tunnel may be a determinant of reassortment.

	U7	G6	U5G4		A3C2C1	
	(414)	(185)	(699)	(591)	(417)	(396)
RVA SA11	TIFST	HNAKYRYE	EK~~~RGQS	SGEKQTKA	STKKN	SMSSASN
RVG 03V0567	KIKTT	RNRKWSMT	ERPYGTDVS	SGEKTTKI	TTKKM	SLANTSN
	(458)	(225)	(751)	(647)	(461)	(440)
	A7	A6	G5A4		C3C2C1	

Figure 1.15: Insertion of 3 amino acids in RVG 03V0567 as compared to RVA SA11. This is believed to narrow the template entrance tunnel width, which is linked with the different 3' consensus sequence in clade B. Used with permission Ogden et al. 2012

1.10.3.2 The effect of rotavirus genetic complementarity on reassortment

Multiple field reassortments of rotavirus strains have been documented that seem to suggest that reassortment might be due to intergenome segment complementarity and whether the interactions occurring are compatible. These reassortments show that protein structure or function within RVAs is probably not a restriction of reassortment because viruses with incompatible proteins would be replication incompetent.

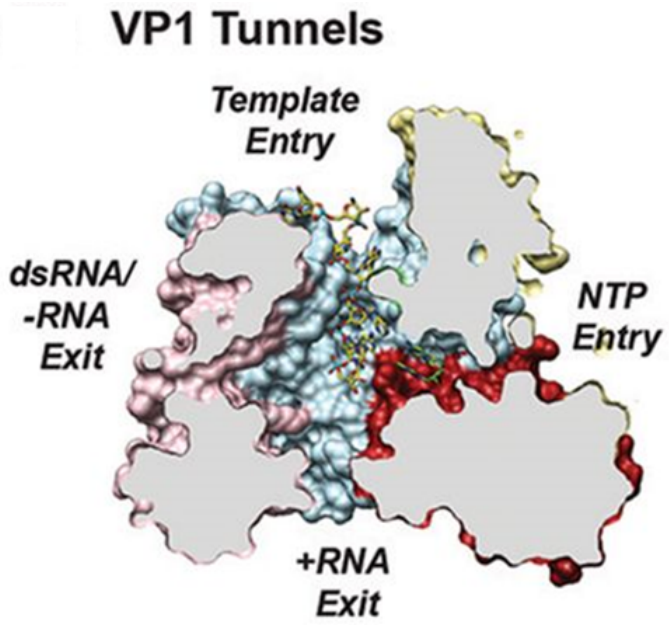


Figure 1.14: Rotavirus VP1 structure showing the template entrance tunnel, the dsRNA/(+)ssRNA exit tunnel, the (+)ssRNA exit tunnel, and the NTP entrance tunnel. The template entrance tunnel is pictured with an RNA encoding the 3'-consensus sequence bound to the tunnel. The 3'-CS inserts into the template entrance tunnel and is required for transcription to be initiated. Used with permission Steger et al. 2019

Table 1.3: Ogden *et al.* terminal sequences of of RV (+)RNA GS1(VP1)[a].

Clade	Species	Strain	5' end[b]	3' end[b]
A	RVA	SA11	GGCUAUUAAA	AGAUGUGACC
A	RVA	RRV	GGCUAUUAAA	AGAUGUGACC
A	RVA	UK	GGCUAUUAAA	AGAUGUGACC
A	RVA	ETD	GGCUAUUAAA	CGAUGUGACC
A	RVA	PO-13	GGCUAUUAAA	AGAUAUGACC
A	RVA	02V0002G3	GGCUAUUAAA	CGAUGUGACC
A	RVC	Bristol	GGCUAAAAAA	UAUUGUGGCU
A	RVD	05V0049	GGCAAUUAAA	ACUUGUGACC
A	RVF	03V0568	GGCAAUUAAU	UAAUGUGACC
B	RVB	Bang373	GGCACAAUAU	AUAAAAACCC
B	RVB	DB176	GGCAAUAAUG	GUAAAAACCC
B	RVG	03V0567	GGCAUAUAUU	AUAAAGACCC
B	RVH	B219	GGCACUAUGG	UAAUAUACCC
B	RVH	J19	GGCACUAUGG	UAAUAUACCC

[a] reproduced with permission Ogden et al. (2012) [b] Sequences are written 5' to 3'.

In Malawi, strains were monitored pre- and post- Rotarix vaccine introduction (Jere et al., 2018). The predominant strains before vaccine introduction possessed Wa-like genetic backbones (I1-R1-C1-M1-A1-N1-T1-E1-H1) with either G1P[8], G3P[8], G4P[8],G9P[8] or G12P[8] as G- and P-type combination. After vaccine introduction, this reverted to a DS-1 like backbone (I2-R2-C2-M2-A2-N2-T2-E2-H2) with a G1P[8] G- and P-type, classifying

these as double reasssortants. Triple reassortants were also detected with a Wa-like VP1 (R1) or a Wa-like NSP3 (T1) reassorted with the Wa-like VP4/7 into this DS-1 genetic backbone. This suggests an intrinsic compatibility between the Wa-like and DS-1-like backbones. The authors speculate that the generation of these novel double reassortments occurred due to the positive selection of these novel strains in response to herd immunity (Jere et al., 2018). In South-East Asia, where vaccination is less prevalent, novel Wa-like / DS-1-like reassortments have been observed (Komoto et al., 2016, 2015; Nakagomi et al., 2017). This presents a problem for rotavirus vaccination, and it is possible for vaccine strains to reassort with circulating field strains (Donato et al., 2012; Rose et al., 2013). VP4 reassortment between RotaTeq and a G6P[8] as well as G1P[8]has been identified (Donato et al., 2012). Work in Brazil also identified a reassortment between Rotarix and an AU-1 strain, generating a GS7(NSP3) reassortant (Rose et al., 2013).

Two different reassortments have been documented between the bovine rotavirus O-agent and SA11. These are a GS8(NSP2) reassortment between SA11-H96 and O-agent and GS4(VP4) reassortment in the SA11-4F with O-agent. The rotavirus O agent was isolated in 1965 from abattoir waste in the same laboratory where SA11-H96 was isolated (Malherbe & Strickland-Cholmley, 1967). The determination of a consensus sequence for SA11 revealed two viruses in an SA11 sample of unknown passage history (Mlera et al., 2013). It contained two strains, SA11-N5, which is a close derivative of SA11-H96, and a second strain, SA11-N2, which was found to be a GS8(NSP2) monoreassortant with the bovine virus O-agent. Reassortment between SA11-4F-like viruses and the O-agent has also been detected (Small et al., 2007). Sequencing of multiple SA11 strains found that the SA11-4F GS4(VP4) to be unrelated to the SA11-H96 GS4(VP4). It possessed a GS4(VP4) from O-agent, most probably due to contamination of the original cell culture aliquot. Furthermore, they found that SA11-Both has an N2 GS8 (NSP2), showing another SA11 able to reassort GS8(NSP2)s. Taken together, this shows that SA11 and the O-agent possesses substantial sequence complementarity, since these two strains were able to reassort two different genome segments.

Determinants of GS8(NSP2) reassortment were investigated in 2017 using a helper-virus based reverse genetics system (Mingo et al., 2017). The authors were able to reassort Wa-like and DS-1 like GS8(NSP2)s into SA11 but not the AU-1 like GS8(NSP2). They then exchanged regions of the SA11 GS8 until they were able to map the restriction of AU-1/SA11 reassortment to a 36-nucleotide region at nucleotides 784-820 near the 3'-end of the genome segment that was designated as the sub-region. The rescued reassortant only rescued with 15% efficiency. If this is a real reduction in fitness or poor rescue efficiency of the helper-based reverse genetics system could not be ascertained. The authors speculated between whether this region is important for RNA-RNA complementary during packaging or represents a functional change to NSP2, see Figure 1.16. This opens up exciting possibilities for testing the role of genome segments and their mutations in reassortment using the recent plasmid-only reverse genetics systems, see Section 1.11.4.

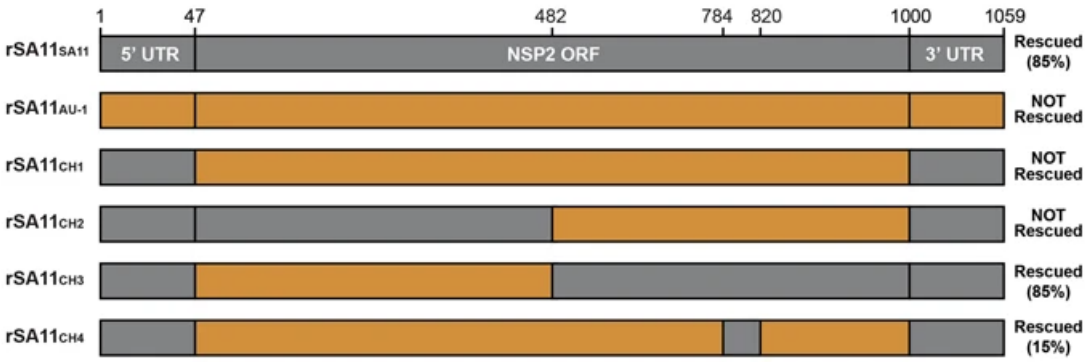


Figure 1.16: Mingo *et al.* mapping of GS(NSP2) sub-region. Full length AU-1 GS8(NSP2) could not be reassorted into the SA11 genetic background using reverse genetics. A construct was then used which only contained the ORF for NSP2, which also could not be rescued. Two constructs were then tested where the first 440 bp of the SA11 ORF was used to replace the AU-1 genome segment, which could not be rescued or the second where bp 482 to 1000 of the SA11 genome segment was placed in the AU-1 ORF, which could be rescued. The sub-region was then mapped to position 784-820. Used with permission under a Creative Commons Attribution 4.0 International License.

1.10.3.3 Protein function considerations affecting reassortment

As discussed in Section 1.10.3 RNA-RNA and RNA-protein interactions determine reassortment capacity, but unfavourable protein-protein interactions can also restrict reassortment. This has been documented in two cases. In 2003, 78 RVA GS6 (VP6) and GS10 (NSP4) sequences were sequenced (Iturriza-Gomara et al., 2003). As discussed in Section 1.7.5 NSP4 functions as an intracellular receptor to mediate DLP transport from viroplasms to what was thought up to 2019 to be the ER. The authors found that specific genotypes of GS10(NSP4) also cluster with specific subtypes of VP6, see Section 1.5 for a discussion on subtypes. This implied that specific sets of GS6(VP6)/GS10(NSP4) can co-reassort. It was hypothesised that this may be due to a required complementarity of NSP4 to VP6 to be able to bind DLPs, showing functional complementarity driving reassortment instead of RNA-RNA complementarity. This is a hypothesis that can only be investigated using reverse genetics.

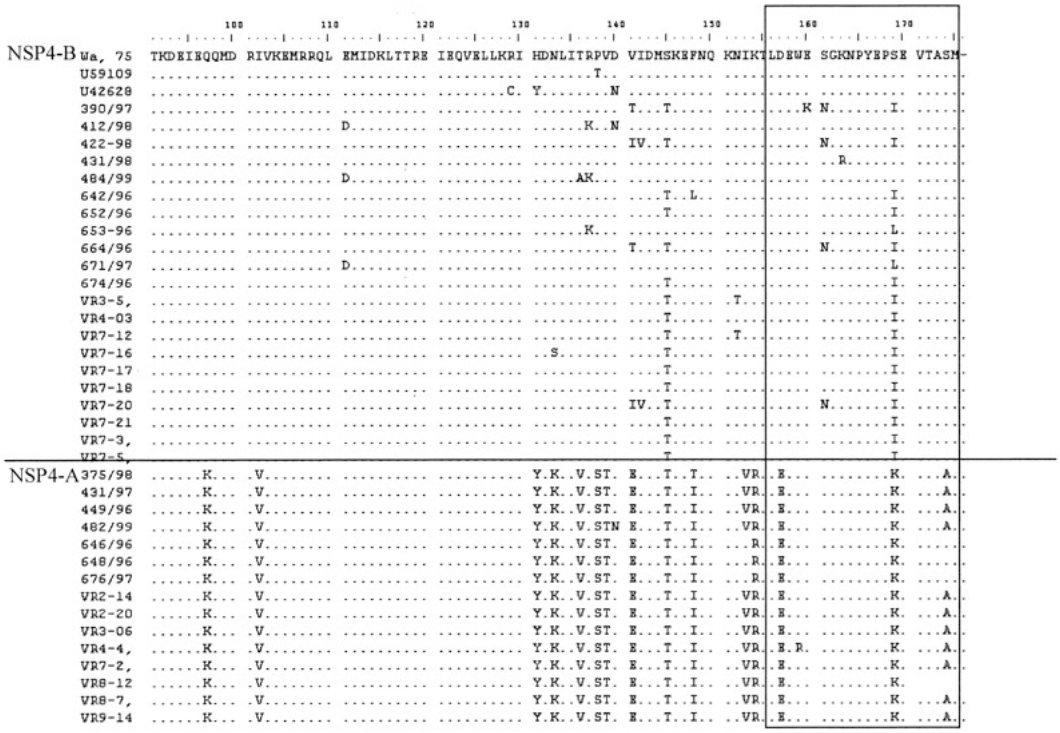


Figure 1.17: NSP4 amino acid sequences clustering into distinct Wa-like and DS-1-like groups designated as NSP4-B and NSP4-A respectively. The box indicates the DLP binding domain. These genotypes were found to be linked to a specific VP6 subgroup. Used with permission Iturriza-Gomara et al. 2003.

Using genome segment-specific RT-PCR, co-reassortment of GS6(VP6)/GS10(NSP4) was also observed in a 2019 study of 74 RVA strains from Pakistan. A marked incidence of these double reassortants with clustering of specific VP6 and NSP4 genotypes was detected, Figure 1.4 (Tamim et al., 2019). Whether this is due to functional complementarity remains to be determined and is of interest to the present study. Although a small sample size was used, the authors showed that an I2 GS6(VP6) can reassort into a Wa-like backbone containing an E1 GS10(NSP4), but not a E2 GS10(NSP4) into a Wa-like backbone (containing an I1 GS6(VP6)). A GS6(VP6)/GS10(NSP4) I2/E2 reassortant possessing a Wa-like backbone was also detected, suggesting that GS6(VP6)/GS10(NSP4) co-reassortment may be required in certain cases to maintain viral fitness. Other studies have shown mono-reassortment of either GS6(VP6) or GS10(NSP4) or dual reassortment GS6(VP6)/GS10(NSP4) (Benati et al., 2010; Chaimongkol et al., 2012; Khamrin et al., 2010; Phan et al., 2020; Tatte & Chitambar, 2012; Tatte et al., 2010). Only one field strain has been detected that possesses an I1/E2 reassortment, however this E2 NSP4 has a mutation at amino acid 174 that is usually found in E1 NSP4, suggesting that without compensatory mutations this genome segment combination is incompatible (Zeng et al., 2020). GS6(VP6)/GS10(NSP4) amino acid conservation is more fully discussed in Chapter 3.

Table 1.4: GS6 and GS10 genotypes showing reassortments documented in Pakistan. Adapted, used with permission Tamim et al. 2019

Strain	No. strains with the indicated combination	VP6 genotype	NSP4 genotype
G1P[8]	18	I1	E1
	1	I2	E1
G1P[8]	3	I1	E1
	6	I2	E2
G2P[4]	13	I2	E2
	1	I2	E1

1.11 Overview of *Reoviridae* reverse genetics

Classical genetics is defined by the observation of a specific phenotype, for example, an enzyme possessing an altered activity such as seen in inborn errors of metabolism, and trying to deduce which gene or genes are responsible for this phenotype. Reverse genetics is the exact opposite, where changes are made to a gene sequence to deduce its function by observing its phenotype (Bridgen, 2012). In viral reverse genetics, specifically RNA virus reverse genetics, this occurs by making changes to the cDNA copies of the viral gene. Fundamentally, reverse genetics of RNA viruses refers to the generation of an RNA virus directly from cDNA copies of its genome. RNA viruses have double-stranded, or single-stranded positive or negative sense genomes and are either segmented or non-segmented (Bridgen, 2012).

Most RNA virus reverse genetics systems started out as helper virus and/or transcript-based systems where cells are transfected with either a set of transcripts, a set of transcripts together with a helper virus, or cells are infected with a helper virus and transfected with the cDNA for a genome segment that is to be modified. This was followed by plasmid-based systems using a plasmid or plasmids that contain the viral genome in cDNA form, which can then be transfected into cells. The first mammalian RNA virus reverse genetics system was published in 1981 for poliovirus, a (+)ssRNA virus (Racaniello & Baltimore, 1981). This was followed by rabies virus, a negative-sense RNA virus, in 1993. Reverse genetics for segmented RNA viruses proved to be more difficult. Reverse genetics for Bunyamwera virus, a negative-sense tri-segmented virus, was reported in 1996 (Bridgen & Elliott, 1996). Influenza virus, with a (-)ssRNA segmented genome, was initially rescued using a helper virus and transfecting single modified RNA segments. This was followed by a 12 component cDNA plasmid set. Today, a single plasmid, containing the complete influenza virus cDNA genome, is used for transfection (Fodor et al., 1999; Zhang et al., 2009).

Viruses that were especially difficult to rescue are those with segmented dsRNA genomes. The first dsRNA virus to be rescued was bacteriophage φ6 (Olkkonen et al., 1990). This was followed by the first animal dsRNA virus to be rescued, infectious bursal disease virus (IBDV) in 1996 using a transcript-based system (Mundt & Vakharia, 1996). Members of the *Reoviridae* proved especially difficult to rescue, with the first plasmid-based systems

only being reported in 2007 (Kobayashi et al., 2007). The *Reoviridae* reverse genetics systems were either first designed as transcript-based systems or helper-virus-based systems, and all were finally moved to plasmid-only systems. Various optimisations were subsequently applied to the plasmid-only systems.

1.11.1 Reovirus reverse genetics

The first reverse genetics system for the *Reoviridae* was developed for reovirus (Roner et al., 1990). This system involved transfecting a complete set of (+)ssRNA or dsRNA from the reovirus strain ST3 and using strain ST2 as a helper virus. This system had extremely poor efficiency, with virus only being harvested from 4% of cells. This system could generate a chimeric virus, with a CAT gene inserted into one of the genome segments (Roner & Joklik, 2001).

In 2007 the first plasmid-only reverse genetics system for reovirus was developed (Kobayashi et al., 2007). This was the first reverse genetics system for mammalian dsRNA viruses. This system used cDNA transcription cassettes of each of the 10 dsRNA genome segments that generates (+)ssRNAs with exact 5'- and 3'-termini. The viral cDNA was flanked by a T7 promoter at the 5' end and a antigenomic hepatitis delta virus (HDV) ribozyme at the 3' end, Figure 1.18. All reovirus genome segments (+)ssRNAs have a guanosine at their 5'end. T7 RNA polymerase prefers to initiate transcription from a guanosine (Milligan et al., 1987). The ribozyme was used to generate a precise (+)ssRNA 3' end, which is essential for Reoviridae genome packaging. A T7 terminator was placed downstream of the ribozyme. This transcription cassette was then cloned into a pT7 plasmid backbone. The cell line to be transfected was infected with a vaccinia virus expressing T7 RNA polymerase and the 10-plasmid set, representing the 10 genome segments, was then transfected into L929 murine fibroblast cells. After 5 days, virus was harvested by freeze-thaw of the cells and rescued viruses were isolated by plaque assay. This system was later improved by cloning the 10 cDNAs into four plasmids, with 3 of the plasmids carrying two cDNAs and one carrying four (Kobayashi et al., 2010). The authors, however, reported in 2011 that rescue was not consistent with this system, attesting to the fact that *Reoviridae* reverse genetics systems are complex and require substantial optimisation (Boehme et al., 2011).

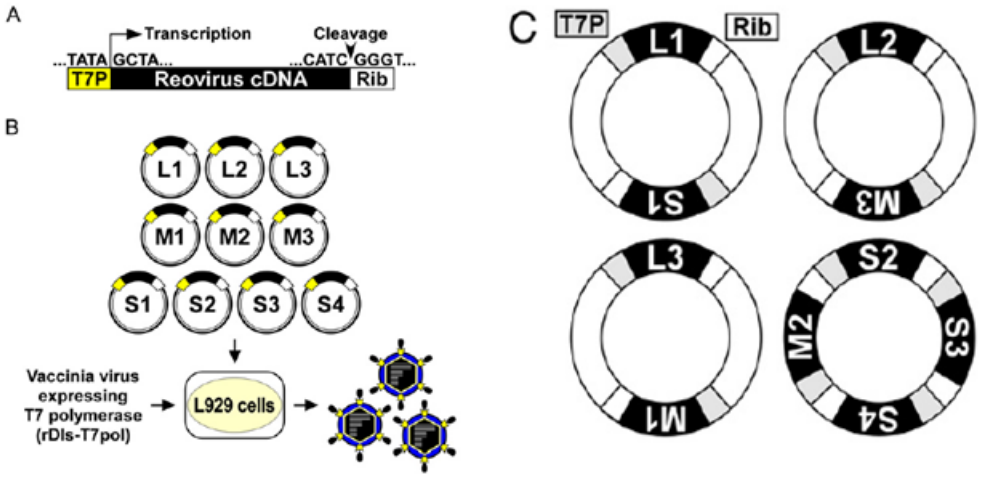


Figure 1.18: Reovirus plasmid-based reverse genetics. (A) cDNAs of each genome segment is flanked by a T7 promoter and a HDV ribozyme. (B) The 10 plasmid set is transfected into L929 cells, and the cells are infected with a vaccinia virus expressing T7 RNA polymerase. (C) Schematic of the reovirus 4 plasmid system showing each cDNA genome segment flanked by a T7 promoter and HDV ribozyme. Used with permission from Kobayashi et al. 2007 and Boehme et al. 2011

1.11.2 Bluetongue and African horsesickness reverse genetics

Two other members of the *Reoviridae* that have been rescued using both transcript and plasmid-based systems are from the genus Orbivirus. These are bluetongue virus (BTV), which causes substantial losses in the sheep industry, and African horsesickness virus (AHSV), which can lead to the death of more than 90% of unvaccinated horses (MacLachlan, 1994; Erasmus, 1972). The BTV and AHSV reverse genetics systems are very similar. Both started out as transcripts derived from active open cores, then followed by synthetic transcripts derived from cDNAs, followed by the transfection of expression plasmids together with run-off transcripts and finally plasmid-only systems (Boyce & Roy, 2007; Boyce et al., 2008; Matsuo et al., 2010; Van Gennip et al., 2012; Pretorius et al., 2015; Conradie et al., 2016). The evolution of the BTV and AHSV reverse genetics systems are important, since much of the rationale behind the rotavirus SA11-N5 system developed in our laboratory at the NWU was derived from the plasmid-only systems of these two viruses, as discussed in Section 1.11.3.3. Further, these systems have shown the application of a fully tractable reverse genetics system in the context of rational vaccine design and optimising vaccine safety. This will be more fully discussed in Section 1.11.4.

1.11.2.1 Bluetongue virus reverse genetics

BTV was initially rescued by transfecting transcripts derived from open cores (Boyce & Roy, 2007; van Dijk & Huismans, 1980; Verwoerd & Huismans, 1972). This was followed by cloning cDNAs of the 10 genome segments into plasmids and synthesising transcripts *in vitro* using T7 RNA polymerase. Using BTV serotype 1 (BTV-1) as a backbone, It was possible to exchange two genome segments (GS2(VP2) and GS5(VP5)) of BTV-10 by using synthetic transcripts (Boyce et al., 2008). Using a kit-based method to introduce a

cap analogue on the 5' end of the (+)ssRNAs of the genome segment, the authors were also able to rescue viable virus by transfecting 10 synthetic transcripts derived from the cDNA plasmids. This system was used in 2012 to rescue both virulent and avirulent BTV strains (Van Gennip et al., 2012).

The original synthetic transcript BTV system was improved in 2015 (van de Water et al., 2015). Rescue could not be achieved repeatably by only using synthetic transcripts. The ORFs for BTV VP1,VP3,VP4,VP6,VP7,NS1, and NS2 were cloned into pSMART-HC or pSMART-LC under control of a CMV promoter for mammalian expression. This contruct was designated phCMVDream (Prof. P.A. van Rijn, personal communication). The rationale behind this was to have formation of viral factories (NS2) (the rotavirus viroplasm analogue), the replication complex (VP1, VP4, VP6), the core (VP3), the intermediate capid (VP7), as well as the interferon antagonist NS1 prior to transfection of the synthetic capped RNAs. In subsequent work, it was shown that transfection of these expression plasmids prior to the transcripts encoding the viral genome segments are essential for rescue (van Rijn et al., 2016). When transcripts were capped prior to transfection, rescue was not possible if the VP1 or NS2 plasmids, or the complete set of expression plasmids were left out. When transcripts were not capped, rescue was not possible if VP3 was left out. Rescue was also not possible if only the plasmids encoding VP1 and NS2 or VP1, VP3, NS2 were transfected prior to transfection of uncapped transcripts.

In 2015 a complete plasmid-only reverse genetics system for BTV was developed (Pretorius et al., 2015). This system is similar to the reovirus system in that a cDNA copy of a genome segment is flanked by a T7 promoter and an anti-genomic HDV ribozyme. These ten plasmids were transfected into BSR-T7/5 cells (BSR cells are a clone of baby hamster kidney cells, known as BHK cells) and viruses were harvested 3-5 days later (Figure 1.19).

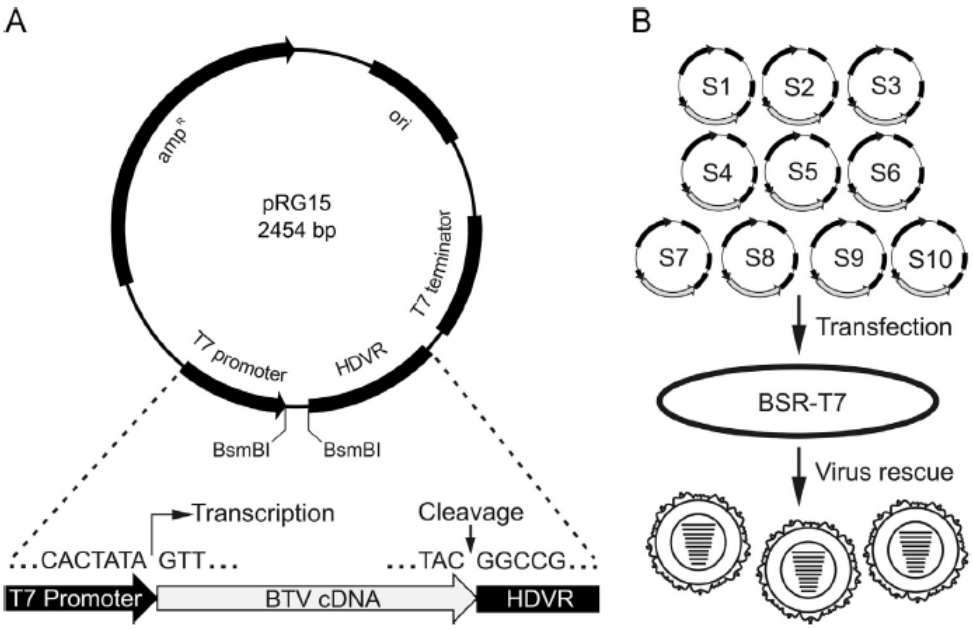


Figure 1.19: Bluetongue virus plasmid-based reverse genetics. (A) A transcription cassette, consisting of a BTV genome segment cDNA flanked by a T7 promoter and an HDV ribozyme, is cloned into a pRG15 backbone. (B) The 10 plasmid set is transfected into BSR5-T7 cells and virus is rescued. Used with permission Pretorius et al. 2015.

1.11.2.2 African horsesickness virus reverse genetics

Reverse genetics for AHSV followed in 2010, two years after BTV, by also using a combination of core-derived and *in vitro* capped synthetic transcripts (Matsuo et al., 2010). This was followed by transfecting expression plasmids (containing VP1, VP3, VP4, VP6, VP7, NS1, and NS2) 24 hours before transfecting 10 capped run-off transcripts (van de Water et al., 2015). The expression combination that facilitates rescue was determined in the same manner as discussed in Section 1.11.2.1 (van Rijn et al., 2016).

The transcript-based systems were later replaced by transcription plasmids using the same design as for the BTV system with an initially ten-plasmid set, with the cDNA flanked by a T7 promoter and an antigenomic HDV ribozyme and transfecting into BSR-T7/5 cells (Conradie et al., 2016). Figure 1.20 shows the AHSV reverse genetics system. The plasmid backbone for this system was derived from pSMART-HC.

1.11.3 Rotavirus reverse genetics

To develop a robust and effective rotavirus reverse genetics system proved to be especially challenging. Initially, helper-virus-based systems were developed and implemented. Transcript-based systems were attempted in our laboratory and elsewhere, but did not yield any results. Finally, multiple plasmid-based systems were developed between 2017 and 2019.

Rotavirus plasmid-based reverse genetics systems based on the original design developed in

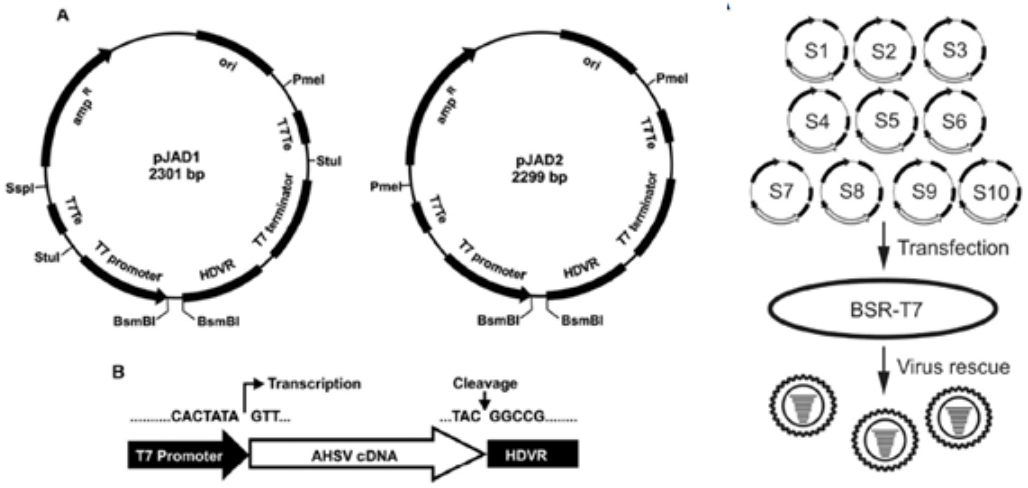


Figure 1.20: AHSV plasmid-based reverse genetics. (A) pJAD1 has a StuI restriction enzyme site flanking the T7Te terminators, whereas pJAD2 has PmeI sites. (B) A transcription cassette, consisting of an AHSV genome segment cDNA flanked by a T7 promoter and an HDV ribozyme, is cloned into a pRG15 backbone. (C) The 10 plasmid set is transfected into BSR-T7/5 cells and virus is rescued. Used with permission Conradie et al. 2016.

2017 by Kanai *et al.* have been implemented around the world, allowing the construction of chimeric viruses and novel studies in virus biology (Criglar et al., 2020; Falkenhagen et al., 2019; Kanai et al., 2020; Song et al., 2020; Sanchez-Tacuba et al., 2020).

The following sections describe the successive rotavirus helper virus and plasmid-based reverse genetics systems with their optimisations.

1.11.3.1 Helper-virus-based rotavirus reverse genetics

In 2006, a reverse genetics system for rotavirus was developed using the rotavirus strain KU as a helper virus and a strong selection system in the form of a neutralising monoclonal antibody raised against VP4 of strain KU (Komoto et al., 2006). This system employed plasmids with transcription cassettes where the genome segment to be reassorted was flanked by a T7 RNA polymerase promoter and a hepatitis delta virus ribozyme, followed by a T7 RNA polymerase terminator to allow production of (+)ssRNA transcripts possessing the correct rotavirus genome segment 5' and 3' termini, as in the reovirus, BTV, and AHSV RG systems, Figure 1.21. Cells were transfected with the plasmid and then infected with the helper virus a day later.

Another helper virus-based genetics system was developed using a dual selection strategy by employing a temperature-sensitive mutant which only grows at 31 °C and RNAi degradation of GS8(NSP2) (+)ssRNA, with an engineered RNAi target site that is resistant to degradation (Trask et al., 2010). This allowed the selection of recombinant virus at a higher (39 °C) temperature. In conjunction, an MA104 cell line was transduced to express an SA11 GS8 shRNA, thus engineering a cell line that silences RV strains that possess a GS8 targeted by RNAi. This allowed rescue of recombinant viruses after two rounds of selection, with a population that is nearly 100% recombinant.

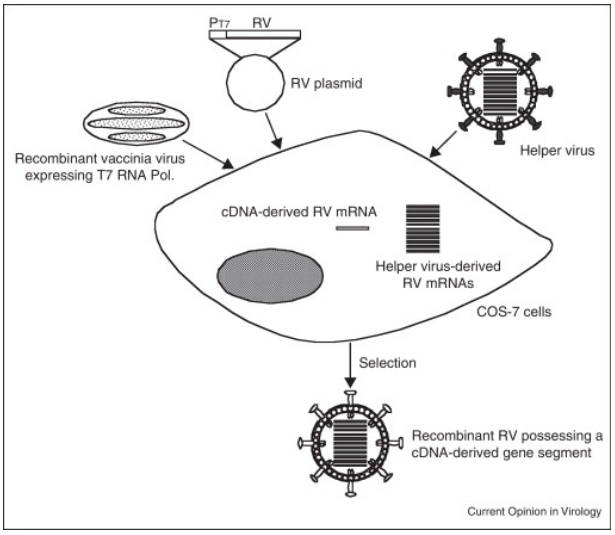


Figure 1.21: Komoto et al. helper virus system. Cos-7 cells are infected with a vaccinia virus expressing T7 RNA polymerase. transfection with a plasmid containing a recombinant genome segment flanked by a T7 promoter and HDV ribozyme. After transfection, the cells are infected with a rotavirus KU helper virus. Used with permission Taniguchi & Komoto 2012

1.11.3.2 Transcript-based rotavirus reverse genetics

Two successive rotavirus transcript-based systems were attempted by PhD students in our laboratory. The first was by Dr. L. Mlera in 2012 (Mlera, 2012). This entailed sequencing the SA11-N5 genome and using consensus sequence to generate a transcription plasmid set. This was then used to synthesise *in vitro* transcripts that were transfected into cells. Rescue was not achieved with this system, since the transcripts elicited a very strong innate immune response, the cDNAs generated in L. Mlera's project were the basis for all our subsequent RV RG work.

Dr. J.F. Wentzel attempted to reduce using DLP-derived transcripts. He designed expression plasmids containing the MA104 codon-optimised ORFs for VP1, VP2, VP3, VP6, NSP1, NSP2, NSP5, and NSP6 for transfection 24 hours before the DLP-derived transcripts (Wentzel et al., 2013). The expression plasmids were designed to result in the expression of the viroplasm proteins (NSP2, NSP5, NSP6), as well as the replication complex (VP1 and VP3), core (VP2), and DLP (VP6). J.F. Wentzel also took a multigenome segment plasmid approach in 2014 by designing and constructing four transcription plasmids (Wentzel, 2014). pAlpha contained GS1(VP1), GS8(NSP2) and GS11(NSP5/6). pBeta contained GS2(VP2) and GS3(VP3). pDelta contained GS7(NSP3), GS10(NSP4), and GS9(VP7). pGamma contained GS4(VP4), GS6(VP6) and GS5(NSP1). Each genome segment was flanked by a T7 promoter and HDV ribozyme. This system did not result in rescue due to a design error which resulted in an extra guanosine being incorporated in the extreme 5' end of each cDNA genome segment. Protein expression was, however observed. The transcription plasmids he constructed were used to construct the 11 pSMART SA11-N5 cDNA plasmids for the NWU SA11-N5 pSMART plasmid-only reverse genetics system (Geldenhuys, 2018; Huyzers, 2020).

1.11.3.3 Plasmid-based RV reverse genetics

The advent of a plasmid-only reverse genetics system for SA11-L2 was a major breakthrough in the field (Kanai et al., 2017). It opened a major bottleneck in technology that prevented progress in rotavirus research for two decades. It is now possible to start to investigate many aspects of the rotavirus replication cycle, including what determines reassortment of certain genome segments, and to rationally design live attenuated vaccine candidates.

This system was based on the plasmid-based system for reovirus, but had two additional features provided by three helper plasmids. A set of 11 transcription plasmids was used for the 11 rotavirus genome segments flanked by a T7 promoter and the genomic HDV ribozyme, using pT7 as plasmid backbone, Figure 1.22. The system requires three helper plasmids, that are not encoded by the rotavirus genome, but are required for efficient virus rescue from plasmids. One contained the ORF for a fusion-associated small transmembrane protein (FAST) to allow cell to cell fusion, which ensures that the complete plasmid set is present in a one large fused cell. The other two contained ORFs encoding the subunits (D12L and D1R) of a vaccinia virus capping enzyme to produce a 5' cap on transcripts. This 14-plasmid set was transfected in an equimicrogram ratio into BHK/T7-9 cells. After 48 hours, the transfection cell line was co-seeded with MA104 cells and incubated until cytopathic effect (CPE) was visible. The culture was freeze-thawed three times, passaged in MA104 cells again, and then visualised using an *in vitro* imaging system. In 2019 genes encoding fluorescent reporter proteins were incorporated into this system in GS5(NSP1) (Kanai et al., 2019). This system has been widely implemented in laboratories around the world and was patented in 2019 (Kobayashi & Kanai, 2019).

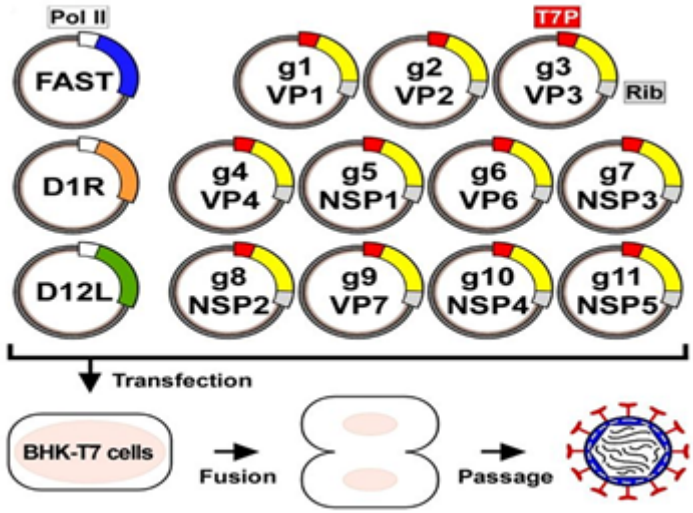


Figure 1.22: The Kanai *et al.* plasmid-only reverse genetics system. The first plasmid-only rotavirus reverse genetics system consisting of 14 plasmids. 11 cDNA plasmids encoding the 11 genome segments, 2 plasmids for the subunits of the vaccinia virus capping enzyme and 1 for the FAST protein. The 14 plasmid set is then transfected into BHK-T7 cells. Used with permission Kanai et al. 2017

In 2018 another Japanese group showed that the capping and FAST proteins are not essential for rescue, Figure 1.23. They achieved rescue by using only the 11 cDNA plasmids encoding the rotavirus genome, but increasing the amount of plasmids that encode NSP2 and 5 three-fold, Figure 1.23 (Komoto et al., 2018). They were also able to incorporate eGFP and mCherry fluorescent reporters into GS5(NSP1), with native GS5(NSP1) being supplied in the form of an expression plasmid added to the transfection mix. Komoto and colleagues also replaced the MA104 co-seeding cell line with CV-1 cells, which are also derived from African green monkeys.

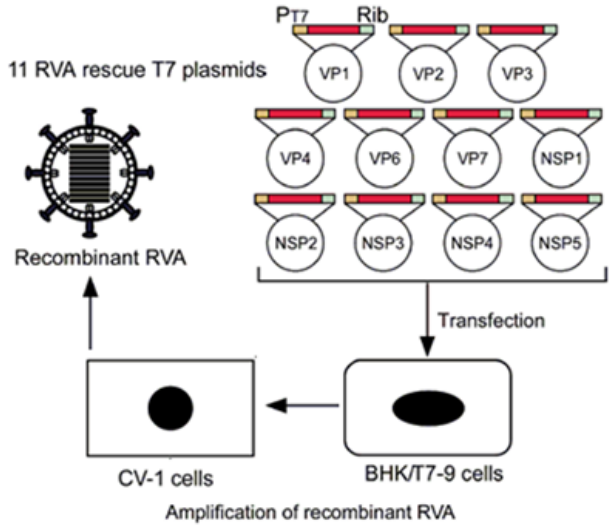


Figure 1.23: Komoto *et al.* adaptations. As in the original Kanai *et al.* system, cDNAs of each genome segment is flanked by a T7 polymerase and HDV ribozyme. only the 11 cDNA plasmid set is transfected into BHK-T7 cells, with 3x the amount of the GS8(NSP2) and GS11(NSP5/6). This is followed by co-seeding with CV-1 cells 48 hours after transfection. Viruses are rescued following passage on MA104 cells. Used with permission Komoto et al. 2018

In 2019, the same group succeeded in developing the first RV RG system for the human strain KU, Figure 1.24 (Komoto et al., 2019). This was significant, since human rotaviruses replicate at a much lower rate than the SA11 strains. They were also able to exchange the KU VP4 with an SA11 VP4, this will be discussed at length in Section 1.11.4.

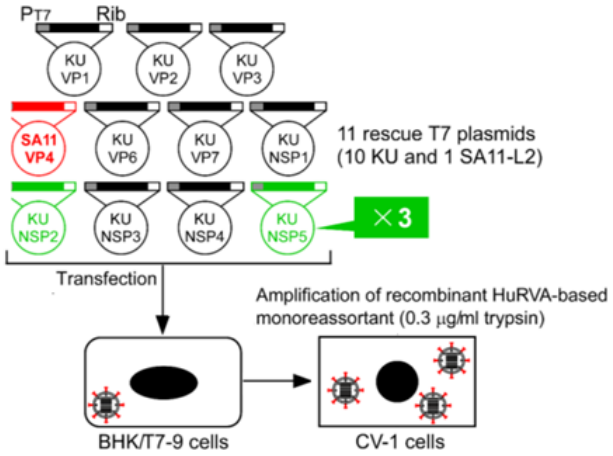


Figure 1.24: Rotavirus human strain KU reverse genetics system. Note exchange of plasmid containing the KU GS4 cDNA replaced with an SA11 GS4. The design is identical to the Komoto *et al.* adaptations published in 2018. Used with permission Komoto et al. 2019.

As part of his MSc M.GJ. Huyzers developed a plasmid-only reverse genetics for SA11-N5 in our laboratory (Huyzers, 2020). He used pSMART-T7 as plasmid backbone for the 11 cDNAs. As discussed in Section 1.19 this backbone was originally used as an expression plasmid backbone in the BTV reverse genetics system. This plasmid backbone is 1000 bp smaller than the pT7 backbone used for the SA11-L2 reverse genetics system. This reduced plasmid load by almost 10 000 bp and should theoretically increase rescue efficiency. This system used a antigenomic HDV ribozyme. He exchanged the VV capping enzyme with an African swine fever virus (ASFV) capping enzyme and constructed a fusion protein with the ASFV capping enzyme and a T7 RNA polymerase, separated by a glycine-serine-glycine linker in a phCMVDream backbone (Eaton et al., 2017). He also replaced the transfection cell line with BSR-T7/5 cells (as in the BTV and AHSV systems) and the co-seeding cell line with swine testicular (ST) cells (Welter et al., 1991). The 13-plasmid set was transfected in an equimolar ratio into the BSR-T7/5 cells, co-seeded with ST cells, incubated until 100% CPE and was then passaged in MA104 cells. Figure 1.25 shows the rationale behind this system.

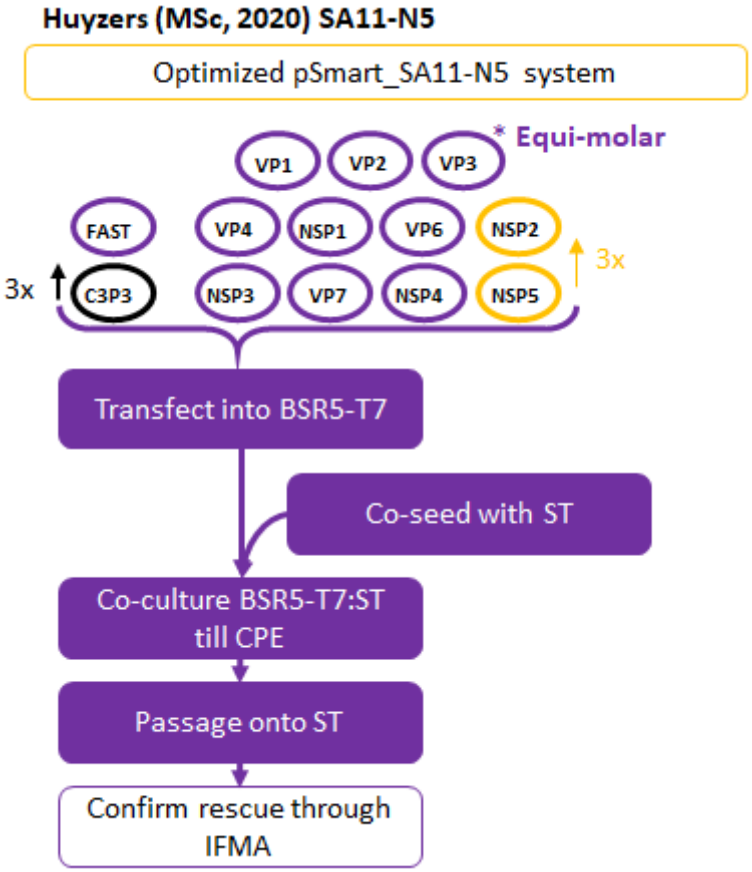


Figure 1.25: SA11-N5 plasmid-based reverse genetics system developed by M.GJ Huyzers. The 11 SA11-N5 cDNAs are cloned into pSmart. C3P3 and FAST are cloned on phDream. The 13 plasmid set is transfected in an equimolar ration into BSR5-T7 cells, co-seeded with ST cells 48 hours later and incubated until CPE. The whole lysate is passage on ST cells and rescue is confirmed via IFMA. Used with permission Huyzers 2020

Unfortunately, the NWU SA11-N5 pSMART reverse genetics system has not been repeatable. Soon after starting to use this system, M.J. Visser discovered that most of the plasmids had deletions or mutations (M.J. Visser, personal communication). M.J. Visser and I tested multiple bacterial cell lines in an attempt at improved plasmid stability. These attempts were not successful. This led to the rationale to reorientate the transcription cassettes of the SA11-N5 plasmid set.

Plasmids contain origins of replication, which are required to replicate the plasmid. There are multiple types of origins of replication, that result in different mechanisms of replication (Lilly & Camps, 2015). The one of interest to this project is known as a pMB1 origin of replication, which is derived from the pBR322 origin of replication, and results in about 500-700 plasmid copies per cell (Lilly & Camps, 2015; Wu & Liu, 2010). This origin of replication results in the plasmid being replicated unidirectionally, instead of bi-directionally as in the *Escherichia coli* genome, known as class B theta replication, Figure 1.26 (Lilly & Camps, 2015; Nakasu & Tomizawa, 1992) . Since antibiotic resistance and other genes are transcribed in the plasmid, run-on transcription of the insert can occur, resulting in a toxic protein product. This causes deletions in the insert by the bacterium

in order to alleviate the toxicity (Kimelman et al., 2012). Furthermore, constitutive transcription of inserts in plasmids can occur, even when placed under a strongly selective promoter, due to the presence of bacterial promotor-like sequences. Inserts can be orientated in the same direction or in the opposing direction that replication of the plasmid would occur, Figure 1.26 (Brewer, 1988). It has been documented that *E. coli* prefers to have genes in the same direction as replication would occur, whether in its genome or plasmids (Brewer, 1988; Hamperl & Cimprich, 2016).

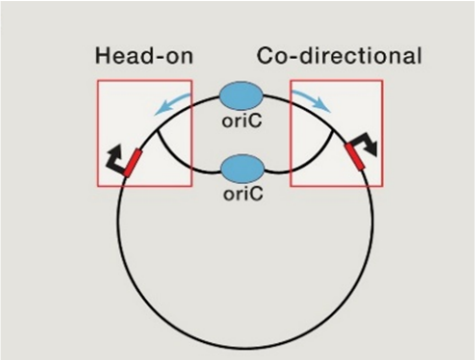


Figure 1.26: Schematic showing plasmid replication and transcription. This shows the possible scenarios arising from the different orientations of the transcription cassette. Replication and transcription can occur either in the same direction, or different directions. Used with permission Hamperl & Cimprich 2016

In 2020, Sanchez-Tacuba and colleagues generated both a new murine D6/2 rotavirus reverse genetics system and a Rhesus rotavirus reverse genetics system (Sanchez-Tacuba et al., 2020). This allows modification of determinants of pathogenesis and reassortment to study the effects *in vivo* in a relevant animal model, This reverse genetics system has already been used to identify that NSP1 contributes to host range and pathogenesis, a previously unknown role (Hou et al., 2021). The authors also generated a MA104 cell line that expresses the V protein of parainfluenza 5 (PIV5) and the N^{pro} protein of bovine viral diarrhoea virus (BVDV). This prevents expression of IRF3 and STAT1. Finally, the authors showed that by including C3P3 rescue of rhesus rotavirus (RRV) could be achieved, a strain that was not previously able to rescue.

1.11.4 Applications of the rotavirus and orbivirus RG systems

The BTV and AHSV RG systems have demonstrated the utility of having a fully tractable plasmid-based RG system. Both systems have been used in developing rationally-designed, safer vaccine candidates. Following is a discussion of what has been achieved with the BTV and AHSV systems and what so far has been applied in the rotavirus system.

Non-structural protein 3 (NS3) of both BTV and AHSV was long believed to be associated with virulence. Its knockout in BTV led to strongly reduced viremia and avirulence in sheep (Feenstra et al., 2014). NS3 is required for egress from cells, which is required for

replication in the *Cullicoides* midges that serves as a vector for both BTV and AHSV, and causes CPE in infected mammalian cells. Disabled Infectious Single Animal (DISA) candidate vaccines have been developed for both BTV and AHSV by deleting GS10 (NS3/NS3a) and exchanging outer capsid proteins consisting of VP2 (Feenstra et al., 2014; van de Water et al., 2015). DISA vaccines improved the safety of vaccine candidates since viruses cannot spread between hosts via the insect vector since virus cannot egress from insect cells. These vaccine candidates have shown good efficacy in sheep studies (Feenstra et al., 2015; van Rijn et al., 2018; Van Rijn et al., 2017).

BTV VP6 serves as a helicase and is essential for the replication cycle (Matsuo & Roy, 2011). This fact has led to the design of Disabled Single Cell vaccine (DISC) candidates (van Rijn, 2019). These viruses are replication incompetent, meaning that they cannot replicate in cells, and can thus not leave cells that are infected. They were produced in a trans-complementing cell line expressing BTV VP6. The BTV DISC vaccine candidates evoke a full immune response in sheep (Matsuo et al., 2011).

Using reverse genetics, it has been shown that deletion of AHSV GS9(VP6/NS4) results in virus attenuation in horses. AHSV NS4 antagonises the host immune response. Its ORF encodes two forms, designated NS4-I and NS4-II (Zwart et al., 2015). NS4-II localises proportionally higher to the cytoplasm (Boughan et al., 2020). Work on BTV NS4 has shown that nuclear localisation is related to its virulence and that it antagonises the host interferon response by down-regulating the type I IFN transcripts as well as interferon stimulated genes (Ratinier et al., 2016) A modified NS4 provided an attenuated vaccine strain which could be used to construct a DISC AHSV vaccine candidate. Boughan and colleagues showed that NS4 co-localises with promyelocytic leukaemia nuclear bodies (PML-NBs), which have a role in the host interferon response. AHSV-5 with a mutation that abolishes NS4 expression was rescued (Boughan et al., 2020). Absence of AHSV NS4 expression resulted in elongated PML-NBs. Subsequent work using rAHSV-5 NS4 deletion mutants showed that knockdown of NS4 had no effect on replication in cell culture. In horses, however, it results in viral attenuation(Wall et al., 2021).

Reverse genetics has also been used to exchange the BTV and AHSV outer capsid proteins, VP2 and VP5, by using a universal BTV-1 core particle (Nunes et al., 2014; van de Water et al., 2015). The authors constructed a panel of all VP2/VP5 reassortant viruses 16 serotypes of BTV that either contained a universal BTV-1 backbone. They also rescued chimeric viruses containing the VP2 of BTV-14 and the VP5 of BTV-6 or the VP2 of BTV-24 and the VP5 of BTV-4. Finally, they rescued the outer capsid proteins of BTV-5, BTV-7, BTV-10, BTV-12,BTV-15, BTV-16, BTV-18, and BTV-19 including the use of Seg-2 with the UTRs of BTV-1 and the use of VP2, VP5, and VP7 from the strain being rescued. They showed that sheep inoculated with the BTV-8 VP2/VP5 reassortant were protected against BTV-8. They were able to construct a chimeric VP2 that contains regions from both BTV-1 and BTV-8, and rescued a chimeric virus containing this chimeric VP2. This virus is neutralised by both BTV-1 and BTV-8 antisera. This might allow the construction of multi-serotype vaccines.

Some applications have already been reported for rotaviruses. Another human strain reverse genetics system was generated for the rotavirus strain Odelia, similar to that discussed in Section 1.11.3.3. This was used to design a panel of mono-reassortant viruses (Kawagishi et al., 2020). Using SA11-L2 as a universal backbone, each of the 11 genome segments were exchanged one at a time with that of rotavirus Odelia, to develop an 11-member panel of monoreassortant viruses. This shows that reassortants between human and simian strains can be generated and has extensive application in rational vaccine design.

Outer capsid VP4/VP7 reassortants have also been generated for SA11. Using SA11-L2 DLPs as a backbone, viruses containing VP4s or VP7s from porcine, bovine, bat, pheasant, and chicken rotavirus As have been rescued (Falkenhagen et al., 2019). Further work in rescuing SA11 with VP4s and VP7s from African human strains showed that human GS7(VP7) has a high reassortment capability but that human VP4s may be limiting as human VP4 reassortment results in markedly lower virus titre (Falkenhagen et al., 2020). Chimeric human VP4s have been rescued in two separate studies. The first has shown the utility of using reverse genetics to generate candidate vaccine seed strains. The authors showed that the VP8* fragment directly affects replication efficiency in MA104s when rescuing an SA11 expressing a human VP4. By replacing the human VP8* with SA11 VP8* they were able to improve viral titre in MA104s (Kanai et al., 2020). This shows that the immunogenic proteins (VP4,VP7, and VP6) can be reassorted into SA11 and used as a live-attenuated vaccine candidates, since there are no documented cases of SA11 pathogenicity in humans.

The above-mentioned applications show some of the first examples of the wide range of applications in rational vaccine design that a plasmid-based reverse genetics system offers. It will allow us to not only investigate the mechanisms of reassortment, but also construct tailor-made reassortant viruses as vaccine candidates for specific regions. Reverse genetics can further be applied in this project to investigate the observed co-reassortment of VP6/NSP4, as it allows rapid testing of constructs.

1.12 Problem statement

Rescue of rotaviruses with the SA11-N5 rotavirus reverse genetics system could not yet be repeated in our laboratory, since the plasmid set is unstable in bacterial cell lines. To be able to use reverse genetics to investigate reassortment, this problem must be alleviated. Reassortment between vaccine strains and field strains have been documented. Rotavirus A readily reassorts the outer capsid protein-encoding genome segments GS4(VP4) and GS9(VP7) in the field and has been investigated using reverse genetics. Field reassortment of other genome segments have been documented, but the capacity of other genome segments to reassort has not been investigated using reverse genetics. Co-reassortment of GS6(VP6)/GS10(NSP4) in field strains has been documented in two separate studies. For this project, the particular focus was to investigate co-reassortment of GS6(VP6) and GS10(NSP4) using plasmid-based rotavirus reverse genetics. The knowledge gained

from this study should be useful to improve vaccine safety by introducing restrictions of reassortment to prevent vaccine strain/field strain reassortment.

1.13 Aims and Objectives

This project had two main aims:

1. To reorientate the transcription cassettes in the NWU SA11-N5 RV RG system so that the transcription cassettes are transcribed in the same direction that plasmid replication occurs, for improved plasmid stability.
2. To reassort GS6(VP6) from a RV strain that does not readily reassort GS6(VP6) into SA11 by using the SA11-N5 based reverse genetics system and exchanging the SA11 GS10(NSP4) DLP binding domain with that from an E1 strain.

   The objectives for Aim 2 were as follows:

   2.1 To design and order plasmids containing full-length GS6(VP6) open-reading frames (ORFs) for use in the reverse genetics system.

   2.2 To attempt to rescue a Wa-like (I1) VP6 in an SA11 E2 background to show whether this combination is unable to rescue or has reduced fitness.

   2.3 To use a separate DS-1 like (I2) VP6 to show whether a VP6 of the same genotype as SA11 can be rescued in an SA11 background.

   2.4 To use a SA11 NSP4 with an exchanged DLP-binding domain to determine if rescue is possible with the VP6 constructs that did not rescue with the SA11 NSP4 and whether rescue of the exchanged DLP-binding domain NSP4 with a SA11 VP6 is possible.

   2.5 To perform mutagenesis to mutate the amino acids 169 and 174 in the DLP binding domain of SA11 NSP4 to determine if this has an effect on the NSP4/VP6 interaction.

Chapter 2

Troubleshooting the NWU pSMART SA11-N5 reverse genetics system

2.1 Introduction

As discussed in Chapter 1, Kanai and colleagues achieved plasmid-only reverse genetics in 2017, this system is known as the pT7 SA11-L2 reverse genetics system. This was followed by multiple optimisations, both by other groups and our laboratory, which resulted in a marked improvement in rescue efficiency. M. GJ. Huyzers designed and constructed a plasmid-only reverse genetics system using another SA11 strain, known as the pSMART SA11-N5 system; in parallel to the SA11-L2 system. The pSMART SA11-N5 system gave a theoretical 6 log $TCID_{50}$ improvement over the original SA11-L2 system, at initial rescue (Huyzers, 2020). This was achieved with the inclusion of the C3P3 plasmid, exchange of the transfection and co-seeding cell lines and increasing the amounts of the plasmids that encode NSP2 and NSP5. This uniquely positions this system to rescue reassortant and chimeric viruses, which normally rescue less efficiently than SA11.

However, both our laboratory and our collaborators at the University of the Free-State have detected mutations in the pSMART SA11-N5 plasmid set following growing up of overnight cultures (Prof. H.G. O'Neill, UFS, personal communication). Prior to this project, a single base insertion was detected in pSMART-T7_RV-SA11_GS2_VP2 that results in a frame-shift causing a 30 amino acid truncation of the VP2 C-terminal (M.J. Visser, personal communication). Mutations in GS8(NSP2) and GS10(NSP4) were also detected by our collaborators (S.S. van der Schyff and Prof. H.G O'Neill, personal communication). pSmart-T7_RV-SA11_GS2(VP2) was subsequently recloned with the correct SA11 GS2(VP2) (S.S. van der Schyff, University of the Free State, personal communication). New transcription cassettes containing SA11 GS8(NSP2) and SA11 GS10(NSP4) were synthesised by Genscript and cloned into pUC57 (M.J. Visser, personal communication).

Currently, we hypothesise that the instability observed in the plasmid set may be due to the orientation of the insert in the plasmids of the pSMART SA11-N5 system. The pT7 SA11-L2 system has the inserts in the same direction as the origin of replication, and thus

far no instability has been reported.

The aims of the experiments described in this chapter were: To reanalyse previously generated Sanger and NGS sequencing data to determine which genome segments were commonly problematic. Secondly, to design primers that would allow the use of In-Fusion and NEBuilder seamless cloning to sub-clone the 11 transcription cassettes in the reverse orientation, to determine whether this would result in improved plasmid stability, and to test multiple different transfection and infection cell lines to evaluate whether exchange of the commonly used cell lines could contribute to rescue or improve rescue efficiency.

2.2 Materials and Methods

2.2.1 Design and construction of the pSMART-T7_SA11-N5_inline plasmid set

To construct the plasmids described in this project, seamless cloning was used to remove the transcription cassettes from the pSMART backbone and re-clone them in the new orientation. Two different methods were used, namely In-Fusion and NEBuilder seamless cloning.

In-Fusion cloning (Takara Bio, Shiga, Japan) is a commercialisation of a method that was published as FastCloning (Li et al., 2011). In-Fusion cloning is completely ligation and sequence independent. It involves generating 15bp ends that are complementary to the ends of the linearised vector when amplifying the insert. It uses vaccinia virus DNA polymerase 3'→5' exonuclease activity to create single-strand ends that can then base pair with the ends of the vector. The mixture is transformed into competent cells, and ligated by the bacteria.

NEBuilder (New England Biolabs, Ipswich, USA) utilises a different approach. 15 bp complementary overhangs are also added to the insert or vector during amplification, but NEBuilder utilises a three-enzyme system. A 3'-exonuclease to generate single-strand ends to allow spontaneous base pairing of the vector and insert, a DNA polymerase to fill any gaps, and a ligase to repair the sugar-phosphate backbone. NEBuilder can assemble lower concentrations of vectors and insert than In-Fusion.

To determine, the amount, in picomoles (pmol) of vector and insert, gel extracted vector and insert were quantified using Nanodrop spectrophotometry. Both In-Fusion and NEBuilder require a vector:insert ratio of 1:2. Amounts of DNA was determined using the following equation:

$$\text{pmol DNA} = \frac{\text{weight in ng} \times 1000}{\text{size in bp} \times 650\,\text{Da}}$$

The In-Fusion reaction set-up is shown in Table 2.1 and NEBuilder reaction set-up in Table 2.2. Each system has a range of DNA amount that results in successful cloning.

For In-Fusion, the EcoDry kit (which contains the reaction components in a lyophilised pellet(Takara Bio, Shiga, Japan) was used due to better reagent stability of this kit (Prof. A.C. Potgieter, personal communication).

Table 2.1: In-Fusion HD reaction composition

Component	10µl reaction
Purified PCR fragment (insert)	100-200 ng
Linearised vector	50-200 ng
Nuclease-free water	to 10 µl

Table 2.2: NEBuilder reaction composition

Component	20µl reaction
Total amount of fragments (vector and insert) in reaction	0.03-0.2 pmol
Master mix (2x)	10µ l
Nuclease-free water	to 20 µl

For In-Fusion cloning, vector and insert were mixed in a 1:2 molar ratio, made up to 10µl using nuclease-free water and added to the lyophilised pellet. The mixture was pipetted up and down to mix. The reaction was then placed in a T100 thermocycler (Biorad, California, USA) and incubated at 37°C for 15 minutes followed by 50°C for 15 minutes. The reaction was then kept at 4°C until transformed.

For NEBuilder cloning, vector and insert were also mixed in a 1:2 molar ratio, 10µl NEBuilder HiFi DNA Assembly Master Mix (2x) was added, and the reaction made up to 20µl (New England Biolabs, Ipswich, USA). Incubation was then carried out in a T100 thermocycler at 50°C for 15 minutes.

As mentioned in Chapter 1 the SA11-N5 genome segments are flanked by a T7 promoter at the 5'-end and a ribozyme at the 3'-end. Downstream of the ribozyme is a T7 terminator. This means that the transcription cassette is configured as 5'- T7 promoter - RV genome segment – ribozyme-T7 terminator-3'. The transcription cassette was re-orientated using In-Fusion and NEBuilder seamless cloning, See Figure 2.1 and Figures S1-S3.

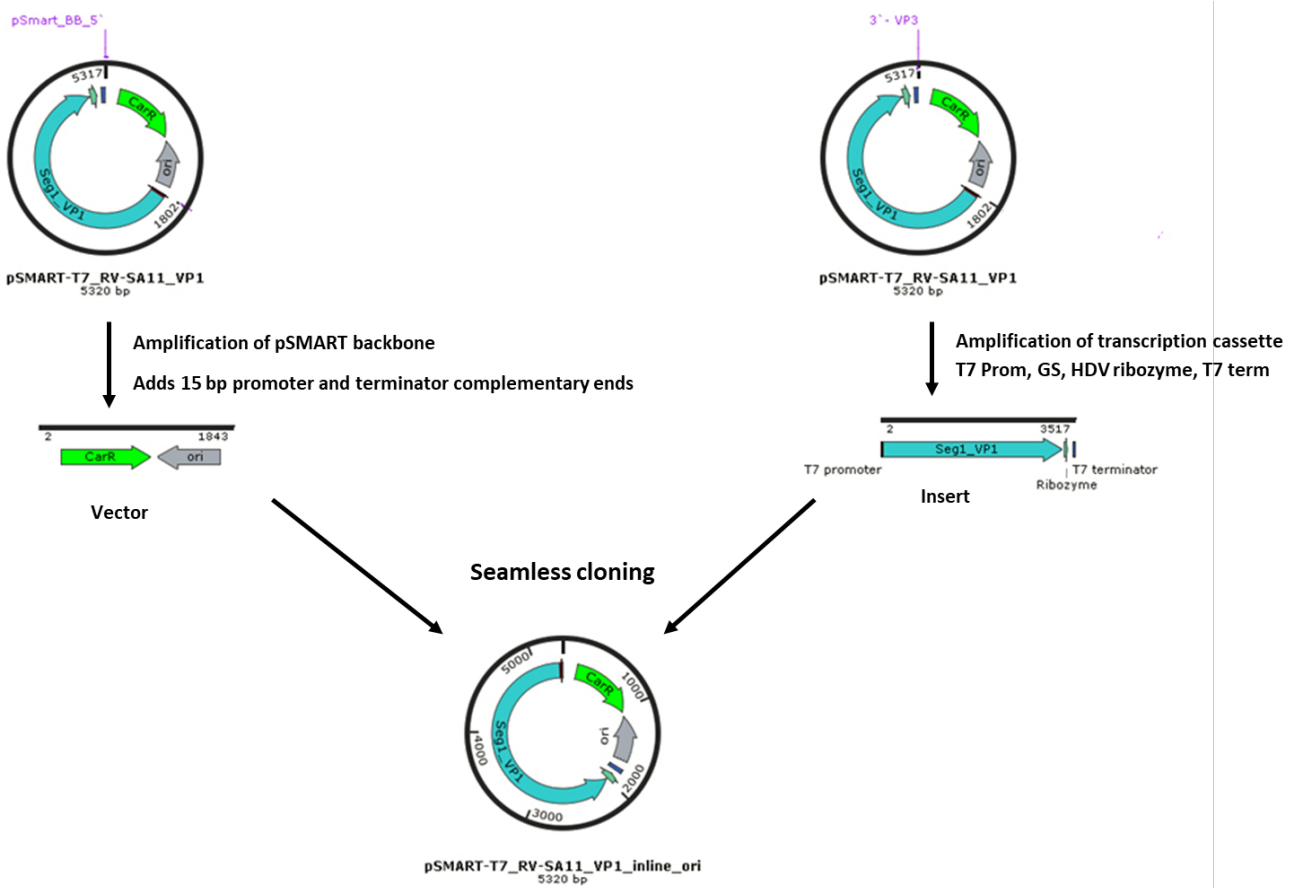


Figure 2.1: Schematic of rationale used to re-orientate transcription cassette, the pSMART_T7 reverse genetics plasmid set. The pSMART backbone was amplified using primers pSMART-BB-T7p and pSMART-BB-T7t (discussed in Section 2.2.1.1). Primers T7-ins-p and T7-ins-t were used to amplify the complete transcription cassette. The new plasmid set was then constructed using InFusion or NEBuilder seamless cloning.

2.2.1.1 Primer design for seamless cloning

Two primer sets were designed that would allow re-orientation of the transcription cassette using InFusion (Takara Bio, Shiga, Japan) and NEBuilder seamless cloning. Both methods require 15 bp overhangs between the vector and insert for ligation to occur. It was decided that 15 bp overhangs would be created on the pSMART backbone that are complementary to the T7 promoter and T7 terminator. Primers pSMART-BB-T7p and pSMART-BB-T7t were used to amplify the plasmid backbone and generate the complementary ends that would allow the transcription cassettes to be ligated in the opposing orientation. Primers T7-ins-p and T7-ins-t were used to amplify the transcription cassettes (from promoter to terminator) from the 11 plasmids. Table 2.1 gives the primer names, annealing temperatures, sequence, and length.

Table 2.3: Primers used for seamless cloning of transcription cassettes.

Primer name	Sequence	T_m	Length
pSMART-BB-T7p	5'-cctatagtgagtcgtattaggatatcgctcaatactgacc-3'	47°C	40-mer
pSMART-BB-T7t	5'-gtcttgaggggttttttgatatcattcaggacgagc-3'	49°C	36-mer
T7-ins-p	5'-ctaatacgactcactatagg-3'	54°C	20-mer
T7-ins-t	5'-caaaaaaacccctcaagac-3'	52°C	18-mer
SA11corGS7F	5'-taatacgactcactataggcatttaatgc-3'	56°C	29-mer
SA11GS7iNR	5'-gggaccatgccggccggccacataacgccc-3'	54°C	30-mer
SA11corGS9F	5'- taatacgactcactataggctttaaaaagag-3'	52°C	31-mer
SA11GS9iNR	5'- gggaccatgccggccggtcacatcatacaattc-3'	54°C	33-mer

2.2.1.2 Thermal gradient polymerase chain reaction

PCR was used to amplify and create overhangs on the vector backbone from pSMART-T7_RV-SA11_VP1 plasmid to remove the insert and to amplify the transcription cassette from each RG plasmid. Templates were selected that were previously endotoxin-free purified and verified with next-generation sequencing. The templates for GS8 and GS10 were purchased from Genscript, and these plasmids were verified using Sanger sequencing. Templates that were used for PCR are shown in Table 2.4. Q5 HF DNA polymerase (New England Biolabs, Ipswich, USA) together with its 5X Q5 reaction buffer was used. The master mix was set up as shown in Table 2.5. Generally, templates were diluted to 100 ng/µl, with primer concentrations being 10µM as working stock concentration. PCRs were set up as follows: a cycle of initial denaturation was run for 1 minute at 98°C, followed by 19 cycles of a 10 second 98°C denaturation step, an annealing step for 30 seconds set up as thermal gradients (44.9°C, 49°C, 52.6°C, and 55.1°C) and an elongation step at 72°C for 2 minutes. This was followed by a final extension at 72°C for 10 minutes and was then held at 4°C. Four reactions were run for each plasmid.

Table 2.4: PCR template designations for seamless cloning

Template name	Use
pSMART-T7_RV-SA11_VP1	Vector and insert
pSMART-T7_RV-SA11_VP2	Insert
pSMART-T7_RV-SA11_VP3	Insert
pSMART-T7_RV-SA11_VP4	Insert
pSMART-T7_RV-SA11_NSP1	Insert
pSMART-T7_RV-SA11_VP6)	Insert
pDelta or pSMART-T7_RV-SA11_NSP3	Insert
pUC57-T7_RV-SA11_NSP2	Insert
pDelta or pSMART-T7_RV-SA11_VP7	Insert
pUC57-T7_RV-SA11_NSP4	Insert
pSMART-T7_RV-SA11_NSP5/6	Insert

Table 2.5: Q5 DNA polymerase PCR master mix components:

Component	Volume for 50 µl reaction	Final concentration
5X Q5 reaction buffer1	10 µl	1X
10 mM dNTPs	1 µl	200 µM
10 µM Forward primer	2.5 µl	0.5 µM
10 µM Reverse primer	2.5 µl	0.5 µM
Template DNA	1 µl	≤1000 ng
Q5 HF DNA polymerase (2000 U/µl)	0.5 µl	0.02 U/µl
Nuclease-free water	32.5 µl	-

2.2.1.3 Agarose gel electrophoresis

The principle underlying gel electrophoresis is using agarose dissolved in a buffer to construct a gel matrix with holes of uniform size to resolve DNA or RNA fragments of different sizes (Feinstein, 1968; Aaij & Borst, 1972). This is done by placing a gel in a buffer and applying an electrical current across it. Since DNA and RNA is negatively charged, fragments will travel from the cathode to the anode. Resistance provided by the gel matrix will result in fragments interacting with the matrix to varying degrees, with large fragments experiencing greater interaction, and small fragments experiencing less interaction. This separates fragments based on size, with smaller fragments moving faster, and large fragments slower. The resolving capacity can be varied by varying the concentration of agarose, with lower concentrations ($\leq 1\%$) able to resolve fragments of between 1000 and 10 000 bp, whereas higher concentrations ($\geq 2\%$) resolve fragments of less than 1000 bp.

All gels were 1% w/v agarose gels, using either tris-borate EDTA (TBE) or tris acetic acid EDTA (TAE) as a buffer. TBE has both greater buffering capacity and provides higher resolution than TAE, and was used for RNA work (Rio et al., 2010a; Sambrook & Russell, 2001). 0.5 g-2.0 g Agarose were dissolved in 50-200 mL TAE or TBE depending on mould size and heated in a microwave until the solution was clear. The solution was allowed to cool to about 45 °C and ethidium bromide (0.25 µg/µl final concentration) was

added, the solution mixed, and the gel was cast in a 10x7x0.5 cm or 22x15x0.5 cm mould and allowed to set. Ethidium bromide intercalates with DNA and fluoresces when excited with UV light. For all moulds, the appropriate comb was used to form wells (normally 10-12 wells or 52 wells for a large gel two comb configuration). Gels were allowed to set for at least 1 hour at 23 °C and a further 30 minutes at 4 °C. 1 µl GeneRuler 1Kb ladder (ThermoFisher scientific. Waltham, USA) was loaded in the first and last wells. Samples were loaded as follows: For PCR amplicons, 4 µl amplicons and 1 µl Qiagen GelPilot 5X loading dye; for restriction enzyme digestion: 8 µl restriction enzyme digestion mixture mixed 1µl NEB purple 5X loading dye. Gels were run at 70 V for 60 minutes (7V per cm) and 130V for 90 minutes for large gels, and imaged on a ChemiDoc XRS+ system, using the manufacturer's software.

2.2.1.4 Restriction enzyme digestion to eliminate plasmid templates from PCR amplicons

To eliminate plasmid templates that may still be present after amplification and result in colonies growing under antibiotic resistance but not containing the intended engineered plasmid, a double endonuclease digestion strategy was devised using BsaI and DpnI. DpnI cleaves dsDNA only when its recognition site is methylated, allowing the selective removal of the PCR template since PCR amplicons are not methylated, whereas plasmid templates are methylated as part of bacterial mismatch repair following DNA replication (Fukui, 2010). BsaI is used additionally, since previous work in our laboratory has shown that DpnI is unable to completely eliminate PCR template. BsaI cleaves 10 of the 11 plasmids once, in the plasmid β-galactosidase gene, linearising the plasmid and virtually reducing parent plasmid background and preventing its transformation following cloning. Reactions components are shown in Table 2.6.

Table 2.6: Overnight restriction endonuclease digestion composition

Component	Volume for 50 µl reaction	Final concentration
5X CutSmart buffer (NEB, Ipswich, USA)	5 µl	1X
DpnI (NEB, Ipswich, USA)	1 µl	0.4 U/µl
BsaI (NEB, Ipswich, USA)	2 µl	0.4 U/µl
PCR amplicon	43 µl	Unknown

2.2.1.5 Gel extraction of vector and insert for seamless cloning

44 µl of the overnight restriction enzyme digested PCR amplicon was mixed with 10 µL loading dye and run on 8 well gels. To prevent DNA damage such as thymine dimers, which is caused by exposure to UV light, a dark reader (Clare Chemical Research, Dolores, USA) was used to visualise DNA. To perform gel extraction, a Qiagen QIAquick Gel Extraction kit was used (Qiagen, Hilden, Germany). Bands with the correct size in base pairs were excised from the gel by cutting out the band with a scalpel and leaving as little residual gel as possible. 2.0 ml microcentrifuge tubes were pre-weighed, to determine the mass of

gel for each band, which determines the volume of buffer QC needed. In addition of buffer QC, the samples were placed in a heat block at 60°C for 1 hour, with vortexing at 15-minute intervals to allow complete mixing. One gel volume of isopropanol was then added and mixed by up-and-down pipetting. Separate 800 µl volumes were applied one at a time to a spin column and centrifuged at 17 900 x *g* for 1 minute until the complete volume was applied to the column, with flow-through being discarded after each centrifugation. The columns were then washed with 750 µl of buffer PE and centrifuged. Products were eluted using 60 µL nuclease-free water (pre-warmed to 70°C) into new 1.5 ml microcentrifuge tubes.

2.2.1.6 Transformation of commercial chemically competent cells with InFusion and NEBuilder cloning reactions

Transformation refers to the introduction of exogenous DNA, into bacterial cells. For this project EPI400 CopyCutter™ (Lucigen, Wisconsin, USA) *E. coli* cells were used to more readily clone unstable DNA sequences. JM109 cells (Zymo Research, Irvine, USA) cells were also selected as the chemically competent cell lines for the expression plasmids used in this project. EPI400 CopyCutter™ cells were selected because they contain a modified pcnB gene under an inducible promoter. This allows plasmids that are normally high copy number, up to 500-700 copies per cell, to be kept at low copy number (approximately 9 copies). In EPI400 cells induction of *pcnB*, results in the formation of poly(A) polymerase polyadenylates RNAI, which is an antisense primer that binds RNAII, the primer required for plasmid replication (Masters et al., 1993). This prevents RNAI binding and increases plasmid copy number. This allows plasmids that contain toxic cDNA sequences (AT and GC rich sequences, and sequences that have strong secondary structure) to be kept at low copy number following transformation, when bacterial cells are under substantial stress. In EPI400s, plasmids can be induced to high copy number for plasmid extraction or endotoxin-free plasmid purification, where high plasmids yields are required. *E. coli* JM109 cells have a mutation in their *RecA* gene, termed *RecA1.* This results in a lower rate of recombination.

Incubation on ice followed by a 45-second heat shock at 42°C has two purposes. Firstly, it produces a temperature imbalance between the cell interior and exterior, allowing Brownian motion to push plasmids into the cell. Secondly, incubation on ice is believed to result in protein loss from the exterior of the cell, with the heat shock causing lipid loss, enlarging the pores formed during induction of competency (Panja et al., 2008).

Competent EPI400 or JM109 cells were retrieved from -80°C storage and allowed to thaw on ice. This protocol does not require transformation tubes and is performed in the supplied tubes. When the ice crystals have just disappeared, 2.5 µl of each cloning reaction was added to the tubes and incubated on ice for 30 minutes. Following this, cells were heat shocked at 42 °C for 30 seconds and immediately replaced on ice for 2 minutes. 250 µl SOC medium, warmed to 37 °C, was then added to bring up the final volume to 500 µl, after which the cells were incubated for 1 hour at 37 °C while shaking horizontally at 350

rpm. Serial dilutions (10^0 to 10^{-2}) of cells were prepared using SOC medium and spread on LB agar plates containing carbenicillin (50 µg/ml) and incubated for 16 hours at 37 °C.

Individual colonies were picked to verify their plasmids using a 10 µl tip and streaked onto a master plate. This master plate was then also used for archiving glycerol stocks of the individual plasmids after confirming the plasmid sequences.

2.2.1.7 Plasmid extraction

The Qiaprep spin miniprep kit (Qiagen, Hilden, Germany) was used to perform small scale plasmid purification for sequence verification, restriction endonuclease digestion and to have a stock of plasmids for further use. The Qiaprep miniprep plasmid extraction protocol is based on the method of Birnboim and Doly (Birnboim & Doly, 1979). This method uses selective denaturation of the genomic DNA by utilising an alkaline buffer. It exploits the fact that DNA denatures at between pH 10 - 12, resulting in the genomic DNA and plasmid DNA denaturing but remaining in the supernatant. Due to topological constraints, plasmid dsDNA can be held together at neutralisation and be renatured. At neutralisation, the genomic DNA cannot renature due to its size, causing large insoluble aggregates to form. These are then pelleted by centrifugation. This allows the plasmid DNA to remain in the supernatant, which is applied to a silica column at high salt concentration, allowing DNA binding to the column, washed and eluted at low salt concentration.

If using EPI400 cells, the OD_{600} of 5 mL overnight cultures (prepared in LB containing 50 µg/ml carbenicillin) was measured and used to determine the amount of overnight culture and induction solution to be added to fresh LB-carbenicillin to a final volume of 5 ml. Induction was performed at 37 °C with 350 rpm shaking for four hours. Cultures were then centrifuged at, 6800 x *g* for 5 minutes to pellet the cells. The supernatant was discarded, and the pellets allowed to dry upside down for 5-10 minutes. Cells were resuspended in 250 µl buffer P1, which contains LyseBlue a pH indicator, and RNaseH to digest RNA released by cell lysis, which would also bind to the silica column and contaminate the plasmid extracts. Buffer P1 also contains EDTA and Tris-Cl. The EDTA functions by chelating divalent ions required for DNase function, and Tris-Cl acts as a buffer.

The homogenised cells were then transferred to new 2 ml microcentrifuge tubes and 250 µl of the lysis buffer P2, was added turning the solution blue, giving an indication of when the buffer has been mixed completely. Buffer P2 contains sodium dodecyl sulphate (SDS) and NaOH. SDS is a detergent that solubilises the bacterial cell wall, NaOH denatures genomic DNA, and cellular proteins. These reactions should not proceed for more than 5 minutes

Adding 350 µl of buffer N3 then neutralised the alkaline lysis buffer, precipitating the genomic DNA and SDS. Buffer N3 contains potassium acetate, which lowers the pH of the solution and provides a high-salt environment for binding of the plasmid DNA to the

silica column. The samples were then centrifuged for 10 minutes at 17900 x *g*. A volume of 800 µl of the supernatant was applied to the column, centrifuged for 1 minutes at 17900 x *g*, and the flow-through discarded. The column was then washed with 750 µl buffer PE, centrifuged for 1 minute at 17900 x *g*and the flow-through discarded and then centrifuged again to remove residual buffer. Elution was done into a new 1.5 ml microcentrifuge tube by applying 60 µl of nuclease-free water (pre-warmed to 70 °C) to the centre of the column and centrifuging at 17900 x *g* for 1 minute.

2.2.1.8 Endotoxin-free plasmid purification

Bacterial lipopolysaccharides(LPS) form the outer leaflet of the outer membrane of Gram-negative bacteria (Wang & Quinn, 2010). LPS have of a hydrophilic polysaccharide domain and a hydrophobic lipid A domain. Lipid A is known as the bacterial endotoxin and is responsible for bacterial virulence. Transfection of plasmids contaminated with endotoxins results in changes to cell morphology, cell death, and severely reduces transfection efficiency of mammalian cells; which directly impacts the efficiency of rescue when performing reverse genetics (Butash et al., 2000; Reitmeyer & Peterson, 1988). This necessitates removal of endotoxins before transfection. The Qiagen EndoFree plasmid maxi kit is based on the same principles as the Birnboim & Doly method for the Qiagen miniprep kit, but binds DNA at a low salt concentration and elutes DNA at high salt concentration, the inverse to the miniprep technique. Plasmids are bound using an anion exchange resin consisting of diethylaminoetheyl (DEAE) on a silica support, instead of a silica based column. The positive DEAE groups interact with the negatively charged backbone of DNA at low salt concentration to allow washing and removal of RNA and proteins at medium salt concentration, while plasmid DNA remains bound at a broad range of salt concentrations. Plasmid DNA is eluted at high salt concentration and de-salted using isopropanol precipitation.

Colonies were picked from a master plate and inoculated into 5 ml LB broth containing carbenicillin (50 µg/ml) and incubated for 16 hours at 37°C and 250 rpm. Cells were then induced as indicated in the protocol of the manufacturer. The amount of overnight culture required is determined by the OD_{600}. The determined volume of overnight culture was added to fresh LB-carbenicillin broth and CopyCutter induction solution in a 1:1000 dilution was added to a final volume of 100 ml. Cultures were incubated at 350 rpm for 4 hours. The cells were then pelleted at 6800 x *g* for 10 minutes and resuspended in 10 ml buffer P1. 10 ml buffer P2 was then added and mixed by inverting, followed by incubation at room temperature for 5 minutes. 10 ml of chilled buffer P3 was added and mixed by inverting 4-6 times. The lysate was then poured into the prepared filter cartridge and incubated for 10 minutes. The plunger was then inserted into the cartridge and the nozzle cap removed. The lysate was then filtered by pressing the plunger down slowly. 2.5 ml of buffer ER was added to the lysate, mixed by inverting, and incubated on ice for 30 minutes. A Qiagen-tip 500 was then prepared by equilibrating with 10 ml of buffer QBT. After equilibration, the lysate was applied to the tip and allowed to enter the resin. The resin was then washed twice with buffer QC and DNA was then eluted with 15 ml buffer

QN. DNA was precipitated using 0.7 volumes of isopropanol and then centrifuged at 15 000 x *g* for 30 minutes, after which the supernatant was decanted. The DNA pellet was then washed with 5 ml 70% ethanol. Centrifugation was then performed at 15 000 x *g* for 10 minutes, and the supernatant decanted. The pellet was then air dried for 5-10 minutes and resuspended using 100 µl nuclease-free water, pre-warmed to 70 °C.

2.2.1.9 Spectrophotometric determination of DNA purity and quantity

DNA from gel extractions, plasmid purifications, and endotoxin-free plasmid purifications was evaluated with a Nanodrop spectrophotometer (ThermoFisher Scientific, Waltham, USA). The stage was cleaned using nuclease-free water and then blanked using either nuclease-free water or buffer, depending on which the DNA was stored in. DNA absorbs maximally at 260 nm, whereas RNA absorbs maximally at 280 nm. A_{260}/A_{280} ratios of between 1.7 to 1.9 were indicative of high-quality DNA. Values lower than this was indicative of protein contamination, whereas values high than this was indicative of RNA contamination. DNA yield for plasmid extractions were commonly between 50 ng/µl and 400 ng/µl. Endotoxin-free plasmid purification yielded DNA of between 700 ng/µl and 8000 ng/µl.

2.2.1.10 Sequencing

Sanger Sequencing: To verify plasmids following cloning and plasmid extraction, Sanger sequencing was used. Plasmids for sequencing were prepared by diluting to 100 ng/µl. Upstream_pSMART and Downstream_pSMART primers were used for sequencing to verify that the transcription cassette has been orientated in the correct direction, Table 2.7. All Sanger sequencing was done by the Central Analytical Facilities DNA sequencing core at Stellenbosch University. After sequencing, correct sequences were verified by aligning to the designed reference sequences using MEGA7 (Kumar et al., 2020).

Table 2.7: Primers used to verify succesful cloning using Sanger sequencing

Primer name	Sequence	T_m	Length
Upstream_pSMART	5'-ggcaaacaaaccaccgctggc-3'	61°C	20-mer
Downstream_pSMART	5'-ggcatcttttactttcaccagcgtttctgc-3'	60°C	28-mer

NGS: After endotoxin purification, plasmids that were to be used for reverse genetics transfection were verified by next generation sequencing. This was done at the Next generation sequencing core facility at the National Institute of Communicable Diseases (Sandringham, Johannesburg) using an Illumina NextSeq. Samples were sent as transcription plasmid mixes. Files were received as FASTQ files.

2.2.1.11 *De novo* assembly and read alignment of NGS data

All FASTQ read files were trimmed at the NICD sequencing core by the in-house bioinformatitian. These files were then used to construct a *de novo* assemmbly of the 11 plasmids and align the contigs to *in silico* references of the plasmids.

De novo assembly was performed using ABySS (Jackman et al., 2017). ABySS employs a probalistic Bloom filter to encode a de Bruijn graph. Bloom filters are probabilistic data structures use to represent a set of elements, allowing insertion of a new element into the set and querying the presence of that element within a set. de Bruijn graphs use k-mers, where k-mers are defined as k length subsequences of a specific length, to determine overlap between reads and so construct a contiguous sequence (contig). ABySS then stores reads in a de Bruijn graph by dividing them into a defined k-mer length, and then determining which k-mers overlap. Assemblies are performed from paired end FASTQ read files and the contigs are written to a FASTA file. For this project, k-mer size was set to 96, which is standard practice for 150 bp Illumina paired-end sequencing reads, giving substantial overlap between reads.

Alignment was performed using the graph-based sequence aligner HiSAT2 (Kim et al., 2019). Genome graphs are created by taking a linear reference sequence and storing each base as a string. These are then indexed, assigning a hierarchy to each base. Since each base has a hierarchy if single nucleotide polymorhisms (SNPs) or insertion/deletions (indels) are present reads that differ substantially from the reference sequence can still be mapped since the areas of the read that still map to the reference are aligned non-linearly using the hierarchy assignment made to each base in the reference. HiSAT outputs the alignment as a SAM file. SAMtools was used to convert the SAM file to a BAM file (Li, 2011). The BAM file was then sorted and indexed. Integrated Genomics Viewer (IGV) was used to visualise alignments (Robinson et al., 2011)

2.2.2 Reverse genetics

2.2.2.1 Cell-culture

For rotavirus reverse genetics, transfection and viral propagation cell lines had to be prepared. For transfection, different clones of baby hamster kidney epithelial cells, BSR-T7/5, BHK-C3P3 clone 8, BSR-C3P3 clone 4, and African Green Monkey kidney eppithelial Vero-E6-C3P3 clone 5 cells were selected (all transfection cell lines were kindly provided by Prof. A.C. Potgieter). A transfection cell line is required, since rotavirus does not replicate well in either BSR-T7/5 or BHK-T7 cells. However, these cell lines are highly transfectable. For infection, African Green Monkey kidney epithelial MA104, Swine testis ST, and African Green Monkey CV-1 cells were selected. MA104 cells were provided by Prof. H.G. O' Neill, University of the Free State, and ST and CV-1 cells were provided by Prof. A.C. Potgieter. Most Rotavirus A viruses (including SA11) reaches the highest titre in MA104 cells and MA104 cells are as such the cell line of choice for rotavirus A

infection (Desselberger, 2017b; Estes et al., 1979; Whitaker & Hayward, 1985).

BSR-T7/5, BSR-C3P3 clone 4, BHK-C3P3 clone 8, Vero-E6-C3P3 clone 5, CV-1 and MA104 cells were propagated in Dulbecco's Modified Eagle Medium (DMEM) (Gibco, Waltham, USA) supplemented with 5% foetal bovine serum for Vero-E6-C3P3 clone 5 and 10% foetal bovine serum (FBS) for CV-1 (Gibco, Waltham, USA). ST cells were cultured in Minimal Essential Medium (MEM) (Gibco, Waltham, USA) with 10% FBS. All cell lines were supplemented with 1% non-essential amino acids (NEAA) (Gibco, Waltham, USA) and 100 units/ml penicillin, 100 µg/ml streptomycin and 0.25 µg/ml amphotericin B (Anti-Anti) (Gibco, Waltham, USA).

All cell lines were retrieved from liquid nitrogen or - 80°C storage and thawed in a 37°C water bath. Once thawed, the cells were mixed by pipetting up and down and transferred to a 25 cm^3 Nunc flask containing 5 ml growth medium supplemented with 20% FBS, 1% Anti-Anti, and 1% NEAAs. For BSR-T7/5, BSR-C3P3 clone 4, BHK-C3P3 clone 8, Vero-E6-C3P3 clone 5 cells, geneticin was added to a final concentration of 1 mg/ml, to select for the T7 polymerase or C3P3 expression plasmid. The flasks were then incubated for 1 hour at 37°C and 5% CO_2 to allow cell attachment.

All cell-lines were cultured in either 25 cm^3 or 75 cm^3 cell culture flasks. Cells were sub-cultured after reaching 90% confluence. Cells were sub-cultured by removing the medium and washing the monolayer twice with 2 ml phosphate-buffered saline (PBS, Gibco/her). After discarding the PBS, 2 ml 0.05% trypsin-EDTA for 25 cm^3 flask was added to the monolayer and placed in a 37°C humidified incubator. Trypsinisation was generally 2-3 minutes. The trypsin was then discarded and 1 ml FBS was used to initially detach the monolayer. Depending on the sub-cultivation ratio, the FBS was divided among the required number of flasks and FBS added, giving 5% or 10% v/v and 4.75 ml of sub-culturing medium. Before transfection, monolayers from 25 cm^3 flasks were detached as discussed above and seeded into 6 well plates using 5% FBS and 1.8 ml sub-culturing medium per well. For 75 cm^3 flasks, cells were sub-cultured in the same manner with a final medium volume of 15 ml.

2.2.2.2 Mycoplasma testing

Mycoplasma is a genus of pleomorphic bacteria that do not possess a cell wall (Young et al., 2010). *Mycoplasma* is relevant in cell culture, since contamination with *Mycoplasma* can cause a reduction of protein expression and an activated interferon state (Rottem & Naot, 1998). In this project, a PCR-based method was used to test for contamination of cell-lines with different *Mycoplasma* species. The LookOut PCR Mycoplasma testing kit tests for 20 different species of *Mycoplasma* by using primers that are specific for *Mycoplasma* 16S rRNA genes (Sigma-Aldrich, St-Louis, USA). 2 µl of medium from actively growing cells are boiled at 95 °C for 5 minutes. During this time, a master mix of 25 µl per reaction rehydration buffer and 0.5 µl per reaction JumpStart Taq DNA Polymerase is prepared. PCR tubes are provided with a lyophilised pellet that contains the primers and

the reaction internal control. 23 µl of master mix is added to a PCR tube together with 2 µl of the boiled medium. Mixing is done by pipetting up and down to dissolve the pellet. Cycling conditions for PCR were as follows 94 °C for 2 minutes, followed by 40 cycles of 94 °C for 30 seconds, 55 °C for 30 seconds, and 72 °C for 40 seconds. The reactions are then cooled down to 4 °C and 8 µl of amplicon is run on a 2% agarose gel.

2.2.2.3 Preparation of plasmid transfection mixture

Prior to transfection, the concentrations of all endotoxin-free purified plasmids were verified using Nanodrop spectrophotometry, Section 2.2.1.9. Plasmid mixtures for transfection were prepared in one of two ways, either an equimicrogram or an equimolar mixture. The total amount of DNA in the mixture for both methods was 4µg per well in a 6 well plate.

Equimicrogram mixtures were prepared by mixing equal µg amounts of plasmids. Due to the large variation of rotavirus genome segment size (3300 bp-660 bp) the plasmids vary in size. This results in the number of copies of plasmids in the mixture of the smaller plasmids being greater than that of the larger plasmids.

Equimolar mixtures were prepared by determining the molecular mass (MW) of each plasmid and then mixing molar amounts of plasmids, to result in an equal number of copies of the plasmids in the plasmid set. This mirrors what is present in rotavirus virions and leads to the large genome segment (GS1-4) plasmids contributing more to the total DNA amount for transfection. MWs of each plasmid was calculated *in silico* using DNAMAN (Lynnon Biosoft, USA). Equations 2.1 and 2.2 illustrate the rationale of preparing a plasmid mixture, (Huyzers, 2020).

For an equimicrogram plasmid mixture:
For a final mixture mass of 4µg and selecting 250 ng per plasmid
Where *[DNA]* is the concentration of DNA in ng/µl and V is the volume of DNA required to obtain the required ng of DNA in relation to the plasmid mixture.

$$\textit{Plasmid volume required} = \frac{\textit{250 ng plasmid}}{[\mathrm{DNA}]} \tag{2.1}$$

For an equimolar mixture: For a mixture of mass 4µg the molar mass *(P*$\mathrm{M_r}$*)* of each plasmid in kDa is determined
This is then used to calculate the mass required to keep each plasmid in an equimolar mixture.
The molar mass of the mixture is defined as: *M*$\mathrm{M_r}$

$$\textit{Mass of plasmid required} = 4(\frac{\mathrm{PM_r}}{\mathrm{MM_r}}) \tag{2.2}$$

Mixtures are then measured using NanoDrop spectrophotometry to determine their concentration. This is then used to calculate the volume of mixture required to transfect 4µg per well. The required volume was then pipetted into opti-MEM, an FBS-free medium,

buffered with HEPES and sodium bicarbonate, and supplemented with hypoxanthine, thymidine, sodium pyruvate, L-glutamine, and growth factors (Gibco). This medium was used since it is specifically designed for lipid-mediated transfections.

2.2.2.4 Rescue protocol for rotavirus reverse genetics

All transfections were performed in 6 well plates. Transfection was performed on 80-90% confluent monolayers, since more confluent monolayers have reduced transfection efficiency, metabolic activity, and viral yield. Prior to transfection, the media was discarded, and the monolayer was washed twice with 2 ml 1x PBS to remove FBS and accumulated cellular waste products prior to transfection. 2 ml fresh complete medium was then placed on the cells, containing 5% FBS, 1% Anti-anti, and 1% NEAA.

The monolayers were then transfected with the desired plasmid mixture, using TransIT-LT1 (Mirius Bio, Madison, USA) as the main transfection reagent of choice. TransIT-LT1 functions by forming a cationic lipid complex with DNA, which is able to bind to the phospholipid membrane and be internalised into cells (Montier et al., 2008; Hoekstra, 2001).

Transfection mixtures were prepared in an equimicrogram or equimolar ratio, as indicated. Final mixtures did not exceed a total 4 µg DNA. This mixture was then added to 250 µl opti-MEM in a 2 ml Eppendorf lo-bind tube and mixed by pipetting. Following this, the TransIT-LT1 was mixed by gentle flicking and added to the diluted DNA in a ratio of 2.5 µl to 1 µg DNA. For this project, 10 µl transfection reagent was added to the diluted DNA by breaking the meniscus of the medium and gentle pipetting the transfection reagent into the mixture, while being careful to not touch the side of the tube. This was then mixed by vortexing for 2 seconds. The mixture was then incubated for 30 minutes. The monolayers were transfected by holding the plate to expose the monolayer and adding the transfection mixture dropwise to the monolayer, to ensure that the complete monolayer was transfected and incubated at 37 °C and 5% CO_2. After 16-18 hours the medium was removed, the monolayers washed twice with PBS and growth medium without FBS placed on the monolayers, since it has been observed that the transfection reagent damages cells and negatively impacts rescue (Prof. A.C. Potgieter, personal communication). Cells were incubated for a total 48 hours in a humidified incubator at 37 °C and 5% CO_2.

Two days after transfection, the co-seeding cell line was detached using trypsin and FBS as described. Cells were the pelleted at 100 x *g* and the pellet resuspended in 1 ml growth medium warmed to 37 °C twice to remove residual FBS. Cells were then counted using a stage haemocytometer. The amount of cells per ml were calculated and between 2 x 10^5 and 5 x 10^5 cells were seeded into each well by pipetting the cells under the meniscus. Porcine trypsin type IX (Sigma-Aldrich, St.Louis, Missouri) was added to a final concentration of 0.5 µg/ml to each well and incubated for a further 3 days. Cells were then freeze-thawed by placing flasks in a -20°C freezer and allowing the monolayer to freeze. Flasks were removed, allowed to thaw and homogenised by pipetting. This was

done three times. The whole lysate was then transferred to a 2 ml tube, labelled and stored at 4°C until passage.

When other transfection reagents were used conditions were as follows: For jetOPTIMUS (Polyplus, Illkirch-Graffenstaden, France) a 1:1 µl transfection reagent to µg DNA ratio was used, XtremeGene-360 (Sigma-Aldrich, St.Louis, USA) 2:1, and for Lipofectamine 2000 (ThermoFisher Scientific, Waltham, USA) (, jetPRIME (Polyplus, Illkirch-Graffenstaden, France) and jetPEI (Polyplus, Illkirch-Graffenstaden, France) 2.5:1. For Lipofectamine 2000 the 250 µl opti-MEM was divided into two 125 µl volumes, and transfection reagent was added to one and DNA to the other. Following a 2 second vortexing of each, the DNA was added to the diluted lipofectamine and vortexed for 10 seconds. Prior to transfection with Lipofectamine opti-MEM was warmed to 37 °C and 1 ml placed on the cells 30 minutes prior to transfection after washing twice with PBS. This was exchanged with 37 °C pre-warmed opti-MEM immediately prior to transfection. The following morning, the monolayer was washed with 37 °C FBS-free medium and replaced with 37 °C pre-warmed FBS-free DMEM. jetPEI was prepared as for Lipofectamine 2000, but in a 10 mM NaCl buffer, diluted transfection reagent was added to the DNA. jetOPTIMUS and jetPRIME transfection reagents were prepared as with TransIT-LT1, but in their own respective buffers. XtremeGene-360 was prepared in opti-MEM, in the same manner as TransIT-LT1.

2.2.2.5 Viral propagation

Prior to infection using lysates from transfected cells or viral stocks, rotaviruses need to be activated using porcine trypsin. This is done to cleave the VP8* subunit from VP4 to allow VP5* interaction with cellular integrins. To activate the inoclulum, the whole lysate from the co-seeded cells is removed, and 1 mg/ml Porcine trypsin type IX (Sigma, St Louis, USA) was then added in a final concentration of 10 ug/ml. After addition of trypsin, the stock was incubated for 30 minutes at 37°C. For viral stocks, the required volume of stock is removed and place in a separate tube. The viral stock is then activated in the

To propagate rescued virus on 80-100% confluent monolayers of the infection cell lines, MA104, ST, or CV-1 cells, were prepared in 25 cm^3 or 75 cm^3 flasks. At infection, the growth medium was removed, and the monolayer washed twice with PBS. The activated lysate was then added to the monolayer and allowed to incubate for 1 hour at 37°C with agitation. After 1 hour, the activated lysate was removed, stored, and replaced with propagation medium. Propagation medium is FBS-free and contains 0.3-0.5 µg/ml porcine trypsin. Incubation was then for 3-5 days until 80%-100% CPE is visible. The medium was then removed as a first passage (P0) supernatant and the monolayer was used for immunofluorescent monolayer assay (IFMA) if 80% CPE had occured. If CPE was 100% the cell debris was pelleted at 2500 x g and used for dsRNA extraction.

2.2.3 Rescue verification

2.2.3.1 Immunofluorescence monolayer assay

One of the methods used to verify rescue, is known as immunofluorescence monolayer assay (IFMA). Primary rabbit polyclonal serum against SA11 DLPs, NSP2 and NSP4 was provided by Prof. A.C Potgieter and Prof. H.G. O' Neill. A fluorophore-conjugated secondary antibody was then used against the primary antibodies to visualise rescue.

This principle of this method is to fix infected cells grown as monolayers to the flask using methanol:acetone. This also precipitates cellular proteins and virus particles and permeabilises cell membranes to allow interaction of antibodies with the virus particles. For this method, the permeabilisation step is not necessary, since organic solvent is sufficient to solubilise cellular lipids and dehydrate cells (Jamur & Oliver, 2010a,b). The cells are then incubated with primary polyclonal antibody serum, washed, and incubated with a secondary antibody raised against the constant region of the primary antibody.

After passaging, cell lysates from infected MA104 or ST cells were removed and 5 ml ice cold 50:50 methanol:acetone was added, and the cells incubated at -20°C in order to fix the monolayer. The methanol:acetone was then removed and 5 ml blocking buffer (containing 1x PBS, 0.05% Tween-20 and 1% (w/v) tryptone) was added and incubated for 30 minutes at 37°C. The anti-SA11 DLP rabbit, rabbit anti-SA11 NSP2, or rabbit anti-SA11 NSP4 serum provided by Prof. A.C. Potgieter, Deltamune, RSA and Prof. H.G. O'Neill, University of the Free State, RSA) were diluted 1:2000 in 5 ml blocking buffer, added to the cells and incubated for 1 hour at 37 °C. The primary antibodies were then removed, and the fixed cells washed three times with washing buffer (containing 1x PBS, 0.05% Tween-20). Alexa Fluor 488 goat anti-rabbit IgG (Invitrogen, Waltham, USA) was then diluted 1:2000 as for the primary antibodies, added to the cells and incubated for 1 hour at 37°C. Alex Fluor 488 has an excitation range of Ex: 495 nm and emission range of Em: 519 nm. The secondary antibody was then removed, and the fixed cells washed twice with 5 ml PBS, and then visualised on a Nikon Eclipse TE-2000-S microscope with the appropriate filter to verify rescue.

2.2.3.2 dsRNA extraction

The dsRNA extraction protocol used for this project was developed by Potgieter and colleagues (Potgieter et al., 2009). After 100% CPE was visualised in a 25 cm^3 flask, normally 3-5 days after infection, any remaining cells were manually detached by scraping or pipetting. The complete content of the flask was emptied into a 15 ml Falcon tube and cells were pelleted at 2500 x g for 10 minutes. The supernatant was then decanted and used as a virus stock for subsequent passage if required. The pelleted cells were used for dsRNA extraction using TRIzol using the manufacturer's instructions.

TRIzol is a monophasic solution of guanidinium chloride and phenol that both solubilises

biological material (cell membranes and lipids) and denatures proteins (virus particles). It is particularly useful for preserving RNAs when endogenous RNases are present (Rio et al., 2010b). This is combined with phenol to provide an organic phase for organic phase:aqueous phase extraction where proteins enter the organic phase, DNA is found at the organic phase: aqueous phase interface and all RNA remains in the aqueous phase.

Extraction was done by adding 750 µl of TRIzol to the pellet and resuspending by pipetting up and down and incubated on the bench for 10 minutes (Invitrogen, Waltham,USA).The complete contents of the tube were then transferred to a 2 ml microcentrifuge tube. Then 250 µl chloroform was added, the sample vortexed, and incubated on the bench for 2 minutes. The sample was centrifuged at 16 000 x *g* for 30 minutes. The aqueous phase (containing RNA) was then removed and a 1:1 volume of isopropanol added, mixed and incubated at room temperature for 10 minutes to facilitate RNA precipitation.

Following this, RNA was pelleted at 16 000 x *g* for 30 minutes and the supernatant discarded. The pellet was then resuspended in 30µl LiChrosolv HPLC water (Merck, Darmstadt, Germany) at room temperature.

To remove ssRNA lithium chloride (LiCl) was added to a final concentration of 2M and incubated overnight at 4°C. The following morning ssRNA was pelleted using centrifugation at 16 000 *g* for 30 minutes and the supernatant was transferred to a new microcentrifuge tube. LiCl was removed using a MEGAclear kit (Invitrogen, Waltham, USA) since it distorts agarose gels.

The LiCl containing dsRNA sample was brought up to 100µl using the elution buffer. 350 µl binding solution was added to the sample and mixed by pipetting. This was followed by 250 µl of ethanol. The solution was then transferred to a binding column and the column placed into the provided collection tube. The column was then centrifuged at 13 000 x *g* for 1 minute to allow RNA to bind to the membrane. Flow-through was discarded and the membrane washed twice with washing solution by centrifuging for 1 minute at 13 000 x *g*. The column was centrifuged to dry and remove residual wash buffer. The column was then placed into a new 1.5 ml microcentrifuge tube and dsRNA eluted using 50 µl of 95°C nuclease-free water twice, by adding 50 µl and centrifuging to elute the RNA. This yielded a final volume of 100 µl. dsRNA was visualised through agarose gel electrophoresis.

2.3 Results and Discussion

2.3.1 Sequence analysis of the original pSMART SA11-N5 reverse genetics plasmids

Due to the failure to repeat the rescue of the NWU SA11-N5 pSMART reverse genetics system and reports of instability of various plasmids, both in our laboratory and by our collaborators at the University of the Free-State it was decided that original and more recently generated Sanger sequencing data as well as previously generated NGS data be

reanalysed to determine which genome segments were most prone to deletions and mutations.

Sanger sequencing of the transcription cassette of pSMART-T7_RV-SA11_GS7_NSP3 that was extracted from glycerol stocks generated by L. Geldenhuys was compared to Sanger sequencing of the transcription cassette of pSMART-T7_RV-SA11_GS7_NSP3 performed by in this project in 2020 (Geldenhuys, 2018). Previous Sanger sequencing data generated by M.J. Visser for pSMART-T7_RV-SA11_GS9_VP7 was also analysed.

Multiple glycerol stocks of pSMART-T7_RV-SA11_NSP3 generated during L. Geldenhuys's MSc were grown up overnight and plasmid extracted. The extracted plasmids were sent for Sanger sequencing at Central Analytical Facilities, Stellenbosch University. M.J. Visser provided pSMART-T7_RV-SA11_VP7 sequencing data generated previously. Alignment of the sequences obtained with GS7(NSP3) and GS9(VP7) reference sequences showed that both the HDV ribozyme and T7 terminator sequences of both constructs were deleted, Figures 2.2 and 2.3. These same glycerol stocks were used by M.GJ. Huyzers in his MSc to generate the complete plasmid set for reverse genetics. This implies that any subsequent plasmids extracted for pSMART-T7_RV-SA11_GS7_NSP3 and pSMART-T7_RV-SA11_GS9_VP7 most probably did not contain a ribozyme, since the master glycerol stocks used by both M.GJ. Huyzers and L. Geldenhuys did not contain the ribozyme.

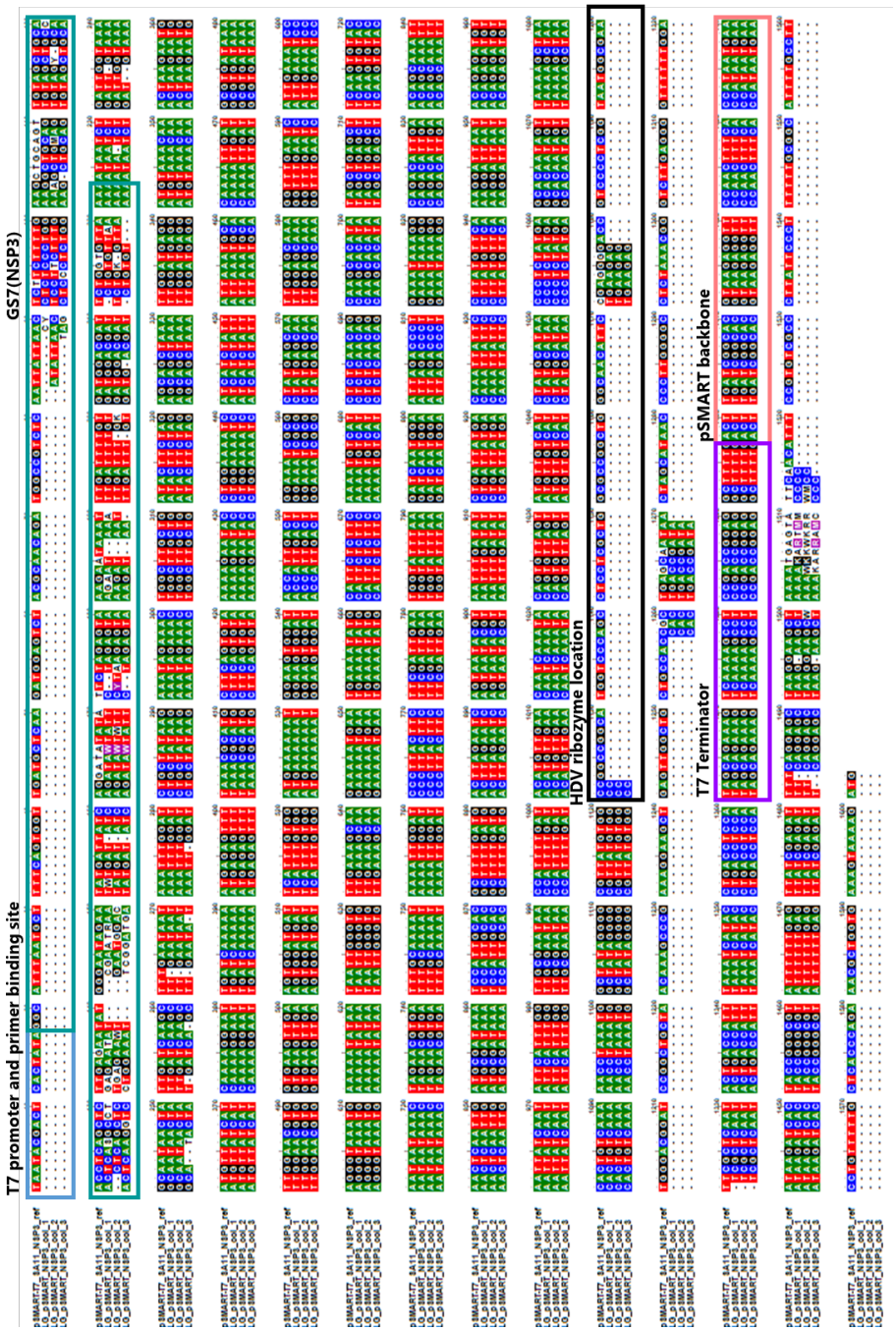


Figure 2.2: Alignment of Sanger Sequencing of pSMART-T7_RV-SA11_NSP3 obtained from plasmid generated by L. Geldenhuys. The plasmid shows a complete deletion of the HDV ribozyme. The T7 promoter, genome segment, ribozyme location, terminator, and part of the pSMART backbone sequence is indicated.

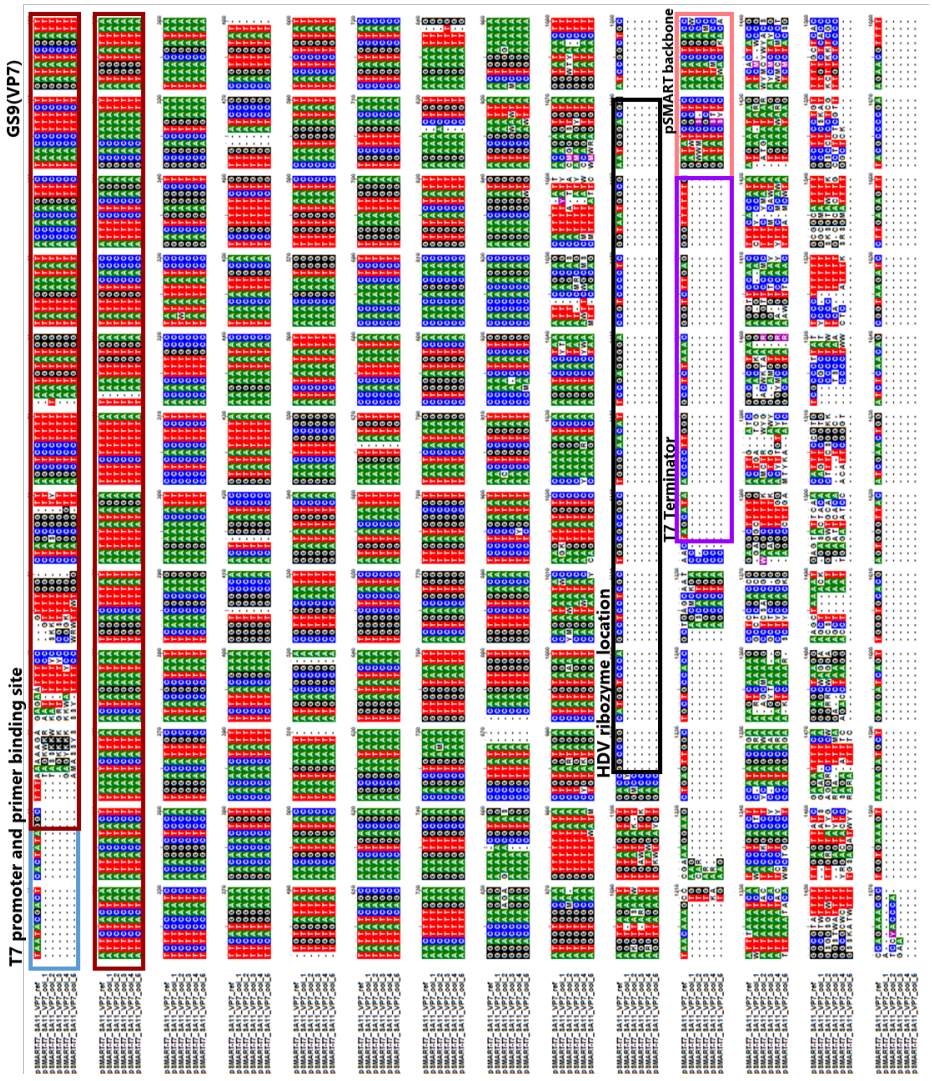


Figure 2.3: Alignment of Sanger Sequencing performed by M.J. Visser of pSMART-T7_RV-SA11_VP7 from plasmid generated by L. Geldenhuys and used by M.GJ Huyzers. The plasmid show a complete deletion of the HDV ribozyme. The T7 promoter, genome segment, ribozyme location, terminator, and part of the pSMART backbone sequence is indicated.

During both M. GJ. Huyzers's and L.Geldenhuys's MSc projects plasmids were not verified using Sanger sequencing after cloning (Huyzers, 2020; Geldenhuys, 2018). Plasmids were most often sent as mixtures for NGS as a single library. This has both positive and negative implications. NGS allows sequencing depth, which allows the identification of sub-populations of mutations that may be present in the sequence that will only show as a double peak on a Sanger sequencing chromatogram. The negative result is that often large deletions are not immediately verifiable, especially if endotoxin-free plasmid preparations mixtures are directly sent for NGS. Further, the way in which the alignments of reads were performed, by mapping directly to a reference using CLC Genomics Workbench that aligns reads linearly, resulted in reads being forcibly aligned to the ribozyme and terminator locations in these plasmids from plasmids in the mixture that did contain a ribozyme and T7 terminator. Reads were also not aligned as paired-end libraries. Paired-end technology allows the use of two reads that are paired to each other, with a known specific distance between the reads. If one of the reads cannot align to the reference, both reads will not be aligned to the reference. This would have made it impossible to visualise the ribozyme deletion. This makes NGS sequencing of plasmids as a mixture and then aligning with CLC Genomics Workbench, a poor choice to verify sequence. Plasmids were also not verified with Sanger sequencing to confirm elements that are common between all plasmids.

During his MSc, M. GJ. Huyzers also sequenced each individual plasmids of the pSMART SA11-N5 reverse genetics plasmid set as separate libraries. This allows the analysis of the complete plasmid, including the plasmid backbone. The single plasmid NGS data was reanalysed as this would allow a complete and accurate picture of the complete transcription cassette, since there are no contaminating reads that could align with the ribozyme sequence if it is not present in a specific plasmid. NGS was reanalysed by performing a *de novo* assembly to show whether any reads contained the ribozyme sequence.

In this project, *de novo* assemblies of M. Huyzers' single plasmid sequence data were performed using AbySS (Jackman et al., 2017). This is a Linux-based *de novo* assembler that has been shown to produce high N50 values, a measure of the shortest contig for which equal or longer contigs cover at least 50% of the assembly (Castro & Ng, 2017). The N50 value can be seen as the midpoint of read length distribution across the sequence being analysed. This results in very robust assemblies. The *de novo* assemblies were then mapped to the plasmid references using HiSAT2, a graph-based sequence aligner which uses a genome graph to align reads more accurately. To verify that the assemblies were performed correctly, assembly was performed of the pSMART-T7_RV-SA11_GS1_VP1 library. This plasmid was previously verified using Sanger sequencing and has been shown to contain the correct T7 promoter, ribozyme, and T7 terminator sequences, and has had no reported stability problems, Figure 2.4a. Of the eleven reverse genetics plasmids only two, pSMART-T7_RV-SA11_NSP3 and pSMART-T7_RV-SA11_VP7 did not contain ribozyme sequences, Figures 2.4b and 2.5a.

(a) pSMART-T7_RV-SA11_GS1(VP1)*de novo* assembly read mapping



(b) pSMART-T7_RV-SA11_GS7(NSP3) *de novo* assembly read mapping

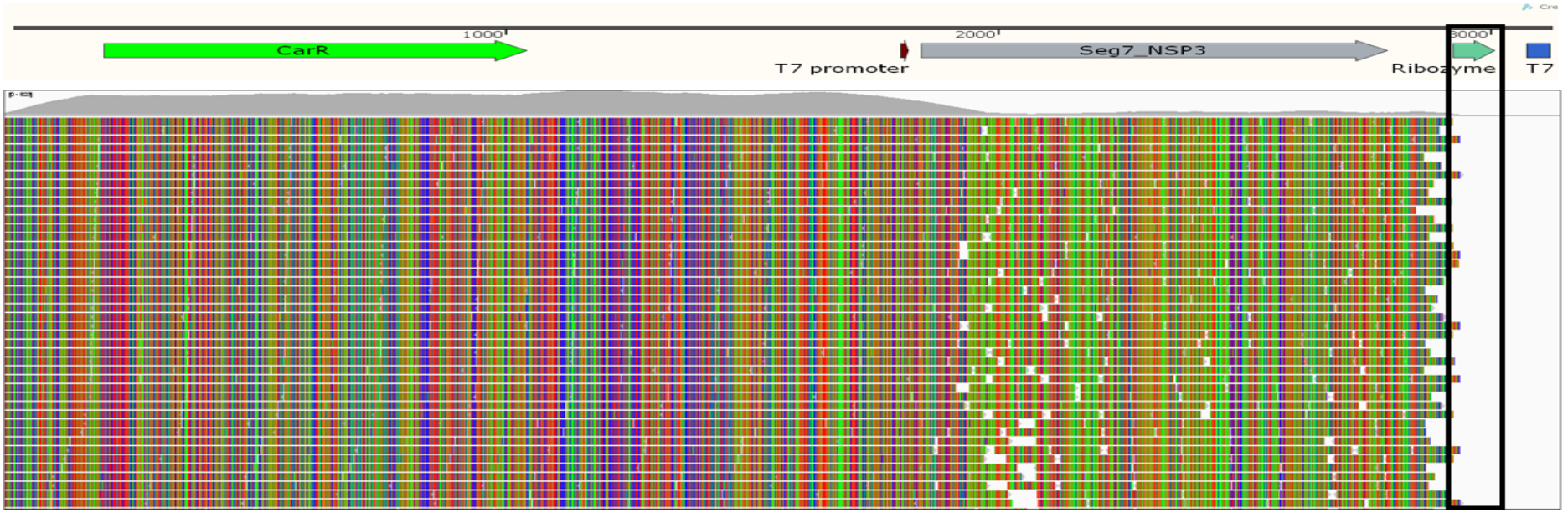
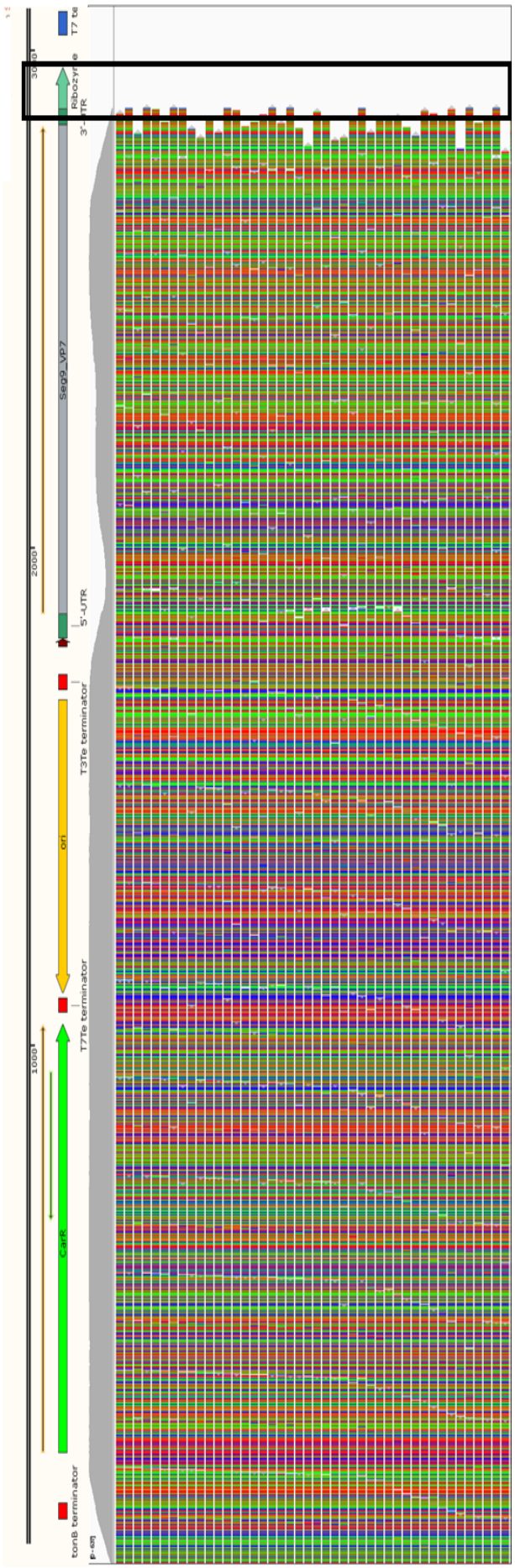


Figure 2.4: Alignments of pSMART-T7_RV-SA11_VP1 and pSMART-T7_RV-SA11_NSP3. (a) Alignment of *de novo* assembly of sequencing of pSMART-T7_RV-SA11_VP1 using ABySS and HiSAT2. The black box indicates the position where the ribozyme is expected in this plasmid. The assembly confirms that this plasmid does contain a ribozyme. This assembly was performed in order to show that the assembly is occurring correctly, since it has been shown via Sanger sequencing that this plasmid contains a ribozyme and T7 terminator.(b) Alignment of the *de novo* assembly of sequencing of pSMART-T7_RV-SA11_NSP3. The black box indicates the position where the ribozyme is expected in this plasmid. The assembly confirms that this plasmid does not contain a ribozyme or T7 terminator.



(a) pSMART-T7_RV-SA11_GS9(VP7)*de novo* assembly read mapping

Figure 2.5: Alignment of the *de novo* assembly of sequencing of pSMART-T7_RV-SA11_VP7. The black box indicates the ribozyme in this plasmid. The assembly confirms that this plasmid does not contain a ribozyme or T7 terminator.

There was substantially higher coverage of the pSMART backbone (600x) than the transcription cassettes (40x). This may be due to multiple reasons. Firstly, it is possible that a sub-population of plasmids exists that only consist of the plasmid backbone. Secondly, the way in which the libraries were prepared has a substantial influence on how reads are generated for specific genes (Sun et al., 2013). This can influence the alignment rate, how many genes are detected, and how many reads are mapped to specific locations in genomes. In the case of this study, the ribozyme deletions were verified by Sanger sequencing. Further, although there was substantially reduced coverage for the transcription cassette, the transcription cassette still has an average 40x coverage. Therefore, since Sanger sequencing confirmed the absence of a ribozyme, lower coverage does not account for the lack of a ribozyme in the NGS data.

These results imply that L. Geldenhuys's rescue attempts were unsuccessful due to both pSMART-T7_RV-SA11_NSP3 and pSMART-T7_RV-SA11_VP7 not possessing a ribozyme. In *Reoviridae* reverse genetics, the HDV ribozyme ensures a native and precise 3'-end on each (+)ssRNA genome segment. This ensures that the required terminal 5'-UGUGACC-3' consensus sequence that is required for genome packing is present (Kobayashi et al., 2007). Since the rescue results from M. GJ. Huyzers's MSc were not reproducible, it is also probable that virus was never rescued during that project. With the deletions of the ribozymes in pSMART-T7_RV-SA11_GS7_NSP3 and pSMART-T7_RV-SA11_GS9_VP7 rescue would not have been possible, since correct 3' (+)ssRNA genome segment ends for those genome segments would not have been generated during transcription. Wild-type SA11-N2 was used in M. GJ. Huyzers' project as a positive control for IFMA and dsRNA extraction. As discussed in Chapter 1, SA11-N2 is a GS8(NSP2) reassortant that possesses the GS8(NSP2) from the bovine O-Agent. It is plausible that what was seen as rescue was most probably never rescue, but contamination from the wild-type SA11-N2. The sequence of the GS8(NSP2) from the rescued virus was never compared to SA11-N2 GS8(NSP2) in the MSc of M.GJ Huyzers.

Instability of an RNA virus genome in cDNA form has been experienced in (+)ssRNA viruses (Almazán et al., 2000; Jo et al., 2021; Rice et al., 1989). In the reverse genetics system for transmissible gastroenteritis coronavirus the cDNA viral genome was unstable when cloned into a bacterial artificial chromosome (BAC), unless a fragment of the genome that was identified as toxic to bacteria was only introduced in the final cloning step (Almazán et al., 2000). In the next-generation respiratory syncitial virus (RSV) reverse genetics system, a low-copy number pSMART-BAC was used as a backbone, together with incubation at room temperature for several days to select positive clones (Jo et al., 2021). In the original yellow-fever virus (YFV) reverse genetics system, cDNA fragments had to be ligated *in vitro* (Rice et al., 1989). The ligated fragments were then used to generate *in vitro* transcripts. The main drawback of (+)ssRNA reverse genetics systems is that the genomes are often in excess of 30Kb, which makes them inherently difficult to clone. Size is not a problem in the rotavirus reverse genetics system, which has a 18Kb genome, that is divided into genome segments that are not larger than 3.5Kb.

It is important to note that the 2017 Kanai *et al.* pT7 SA11-L2 plasmid set is stable, whereas the NWU SA11-N5 pSMART plasmid set is not. There have been no published reports of the plasmids from the Kanai *et al.* system being unstable, and our laboratory has no problems in growing up the glycerol stocks for plasmid extraction. As discussed in Chapter 1, a survey of the literature on bacterial plasmid replication showed that *E. coli* prefers to have the replication and transcription of its genes in such an order to allow these processes occur in the same direction. Since both myself and M.J. Visser previously attempted different bacterial cell lines and incubation conditions for growing up overnight cultures for plasmid extraction, it was decided that reorientating the complete NWU SA11-N5 pSMART reverse genetics plasmid set had to be investigated as a means to improve plasmid stability.

2.3.2 PCR amplification of pSmart backbone and SA11-N5 transcription cassettes for reorientation

To improve the stability of the pSMART SA11-N5 reverse genetics plasmid set, the direction of the transcription cassette needed to be changed in the plasmid backbone using seamless cloning. For seamless cloning, PCR is required to generate vector and transcription cassette amplicons to be used for cloning. Initially, all eleven plasmids used by M. GJ. Huyzers were used to amplify each respective plasmid's transcription cassette. This was done for completeness' sake to confirm the results obtained for pSMART-T7_RV-SA11_NSP3 and pSMART-T7_RV-SA11_VP7 using the previously generated NGS data. Following this PCR, the GS7(NSP3) and GS9(VP7) transcription cassettes were amplified from the previously generated multi-genome segment transcription plasmid, pDelta (Wentzel, 2014).

Both In-Fusion and NEBuilder require an insert with 15 bp overhangs flanking the insert that are complementary to the vector to allow insert-vector annealing and subsequent ligation. The newly designed pSmart-BB-T7p and pSmart-BB-T7t primers were used to amplify the pSmart backbone. T7-ins-p, and T7-ins-t were used to amplify the transcription cassette from each plasmid containing the cDNAs of the 11 genome segments, Figure 2.1. The 15 bp overhangs were generated on the vector using the pSmart-BB-T7p and pSmart-BB-T7t primers, that are complementary to the T7 promoter and T7 terminator on the transcription cassette.

First, the primers were used to generate amplicons for a pSmart backbone and a GS1(VP1) transcription cassette to assess the specificity of the primers. This was done to test the newly purchased primers and to show that cloning could be successfully performed using the procedure developed. The primer annealing step was run as a thermal gradient to determine the optimal primer set annealing temperature for both the primer sets. The theoretical primer T_m are shown in Table 2.3. To find the optimal primer annealing temperature, temperatures above and below the theoretical annealing temperatures (44.9°C, 49°C, 52.6°C, and 55.1°C) were selected. After amplification, amplicons were run on a 1% agarose gel. Figure 2.6 illustrates the four reactions each for the backbone and GS1

amplification. Amplicons of the correct size were generated, 1806 bp for the pSMART backbone amplicon and 3516 bp for the GS1(VP1) transcription cassette amplicon. No non-specific amplicons were visible on the gel, although some ladder spillover was visible in the 44.9°C pSMART backbone lane.

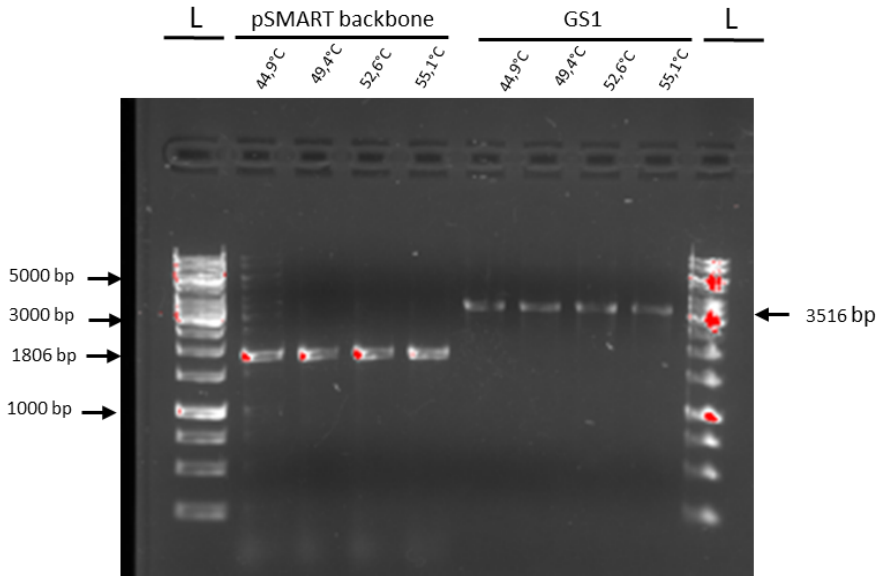


Figure 2.6: 1% agarose gel of amplicons from a thermal-gradient PCR of the pSMART backbone and GS1 transcription cassette. The pSmart backbone amplicon has a size of 1800 bp, the correct size for the backbone without the T7 promoter and T7 terminator. The GS1 amplicon has a size of 3500 bp, equating to a size of 3300 bp for the genome segment and 200 bp for the T7 promoter and T7 terminator.

Following the initial thermal gradient for pSMART and GS1(VP1) amplicon generation the same thermal gradients were run for the plasmids carrying the cDNA of the other genome segments and amplicons were run on a 1% gel, Figure 2.7. Amplicons of the following size were obtained for each transcription cassette: GS2 = 3000 bp, GS3 = 2900 bp, GS4 = 2500 bp, GS5 = 1700 bp. GS11 amplicon size = 800 bp GS10 = 1000 bp, GS6 = 1500 bp, GS7 = 1500 bp, GS8 = 1200 bp, GS9 = 1200 bp. Non-specific amplicons were detected for each reaction, except for the GS8 and GS10 reactions.

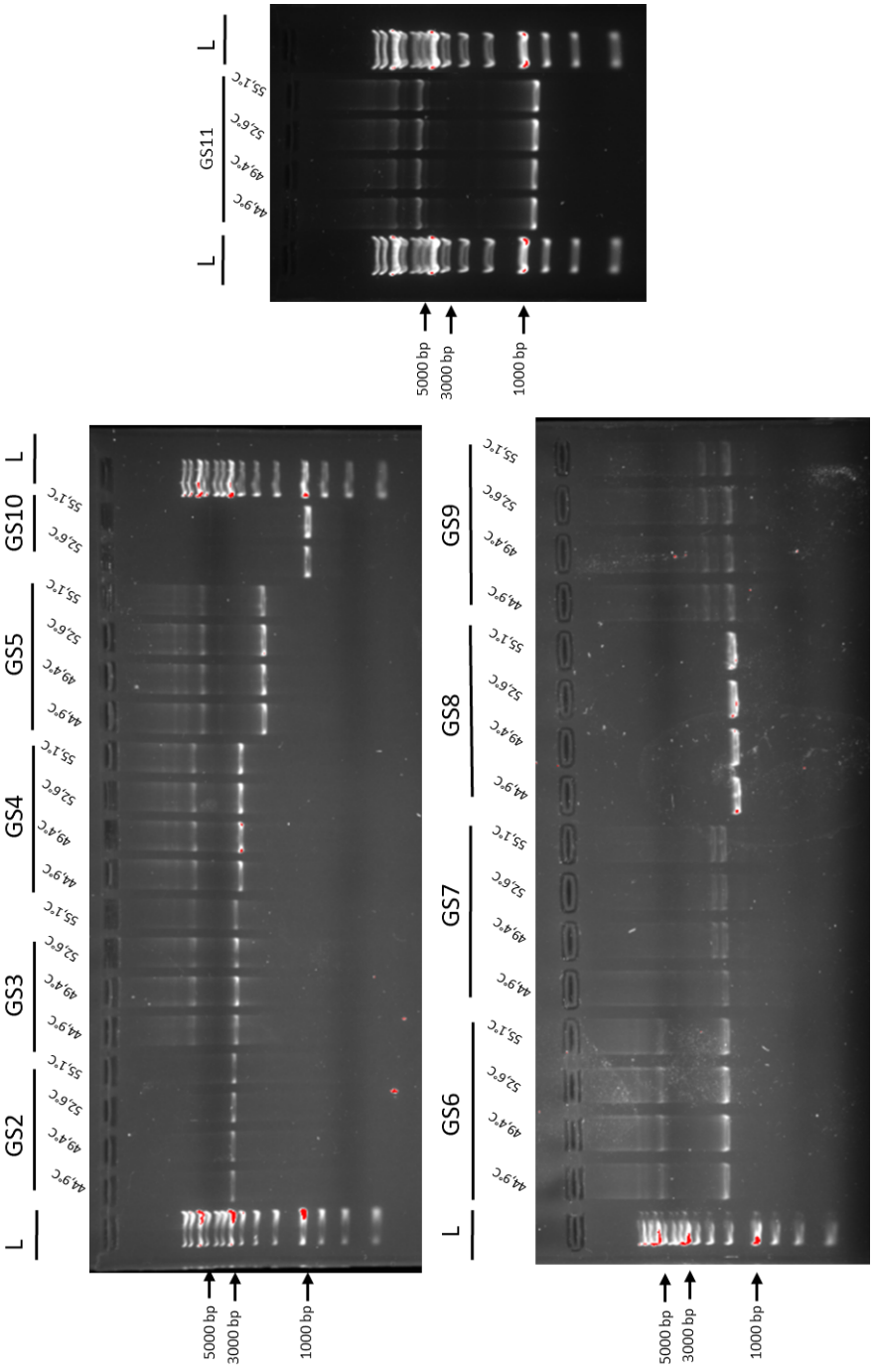


Figure 2.7: 1% agarose gel of the thermal-gradient PCR amplicons for the GS2-GS11 transcription cassettes. Amplicon size: GS2 = 3000 bp, GS3 = 2900 bp, GS4 = 2500 bp, GS5 = 1700 bp. GS11 amplicon size = 800 bp GS10 = 1000 bp, GS6 = 1500 bp, GS7 = 1500 bp, GS8 = 1200 bp, GS9 = 1200 bp.

Amplicons of the expected size were obtained for the transcription cassettes of nine of the eleven genome segments, Figures 2.6-2.7. This was not obtained for GS7(NSP3) and GS9(VP7). The wide range of temperatures used in the thermal gradient gave similar yields during amplification, which was unexpected, since the expectation would be for amplification yield to decrease as the annealing temperature increases. Further, substantial non-specific amplification was seen in all reactions except for the GS8 and GS10, which have substantially less non-specific amplification. InFusion primers often result in non-specific amplification during PCR, since the primers are localised to a specific location, and this location is fixed because of the amplicon that needs to be generated for cloning. The relative sizes of the non-specific amplicons are the same. This might be attributed to random primer binding, resulting in random backbone amplification, generating the large amount of non-specific amplicons seen. Addition of $MgCl_2$ and further optimisation of the PCR might have reduced the amount of non-specific bands.

This result also showed that none of the available pSMART GS7 and GS9 plasmids from L. Geldenhuys and M. GJ. Huyzers could be used as templates for recloning. GS7(NSP3) gave amplicons that were 200 bp (1400 bp) and 400 bp larger (1600 bp) than the excpected size (1400 bp) and GS9(VP7) gave three amplicons (1200 bp, 1400 bp, and 1600 bp), with the 1200 bp amplicon being of the correct size. The yield of the GS7(NSP3) and GS9(VP7) amplicons were also poor. During his PhD J.F. Wentzel constructed four plasmids that were designed to be multicistronic transcription plasmids to rescue SA11-N5. These plasmids were not suitable to rescue SA11-N5, due to an extra guanosine incorporated in the 5'- GGC consensus sequence. This results in a 5'-GGGC. These plasmids were designated pAlpha, pBeta, pGamma, and pDelta. pDelta contains GS7, GS9, and GS10 and was subsequently used as a template for GS7 and GS9, Figure 2.8. Full length transcription cassettes could not be amplified due to two reasons. Firstly, the plasmid pDelta contains three transcription cassettes and primers for the T7 promoter and T7 terminator would amplify all three. Secondly, the GGGC consensus needed to be corrected prior to cloning. It was decided to use the primers L. Geldenhuys used to prepare amplicons to clone the transcription cassettes from the pDelta into the pSMART backbone, Figure 2.8. The forward primer in this set removes the extra guanosine via site directed mutagenesis.

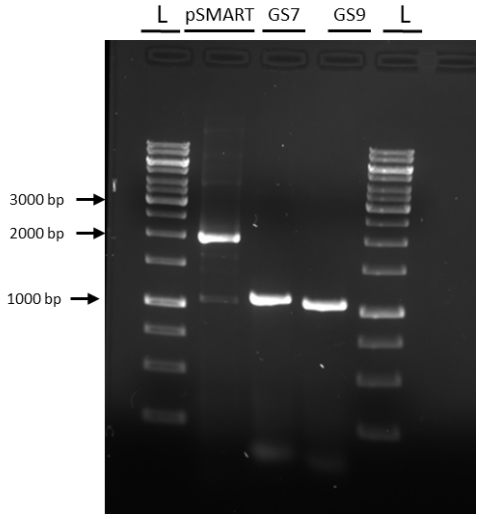


Figure 2.8: 1% agarose gel of pSMART backbone, GS7, and GS9 PCR amplicons. pSMART backbone amplicon size= 2018 bp GS7= and GS9 = GS11 amplicon size = 800 bp. All amplicons have equal amplification efficiency.

The correct size amplicons were obtained for both GS7(NSP3) and GS9(VP7) at 1100 bp and no non-specific amplicons visualised. The generation of backbone generated multiple non-specific amplicons. These primers were designed during L. Geldenhuys' MSc, these primers were not designed optimally and have substantially different annealing temperatures.

2.3.3 Seamless cloning of the SA11-N5 RG transcription cassettes in the same orientation as the origin of replication

To clone the eleven transcription cassettes into the pSMART backbone, the PCR amplicons generated in Section 2.3.2 needed to be purified prior to the cloning reactions. The aim was to use the purified amplicons in InFusion and NEBuilder cloning to re-orientate the transcription cassettes into the pSMART backbone. Following transformation, colonies were selected, plasmid extracted, and Sanger sequenced to assess the clones generated.

Plasmid templates are still present after PCR. To eliminate these templates, the amplicons were digested with restriction enzymes overnight. Following digestion, all amplicons of the correct size amplicons were purified by gel extraction as described in Section 2.2.1.5. This provided pure vector and insert amplicons. Seamless cloning of the transcription cassettes of eleven genome segments was performed over multiple weeks using both Infusion and NEBuilder kits and transformed into competent EPI400 cells. Reactions were set up as described in Section 2.2.1. Cloning reactions were immediately cooled to 4°C during thawing of the competent EPI400 cells. 2.5 µl of each cloning reaction was transformed into cells and plated onto LB-carbenicillin agar plates and incubated for 16 hours at 37 °C as described in Section 2.2.1.6.

To assess the success of seamless cloning, plasmids were purified from distinct bacterial

colonies generated following transformation of the cloning reaction. Plasmids from the selected colonies were purified as described in Section 2.2.1.7 by inoculating a colony in 5 ml overnight LB-carbenicillin cultures and inducing for higher plasmid copy number the following day. After plasmid extraction, DNA quality as well as concentration were assessed using Nanodrop spectrophotometry. DNA concentrations varied between 100 and 400 ng/µl.

Sanger sequencing was performed on the purified plasmids using the pSmart_Upstream and pSmart_Downstream primers, Figure 2.9. For GS1(VP1)-4(GS4), sequencing was initially performed at the Central Analytical Facilities at Stellenbosch University on an ABI 3500 sequencer. Sequencing for the GS5(NSP1)-GS11(VP7) of the plasmid set was performed on an ABI 3730XL. The limitation of Sanger sequencing is length. This meant that for GS1-GS4, the sequence of the complete transcription cassette could not be verified. These primers bind upstream and downstream of the transcription cassette and allows the assessment of both sequence and orientation of the transcription cassette. All transcription cassettes sequenced were found to be in the correct inline orientation and showed the correct sequence. Figures 2.10-2.20 plasmid sequence from one colony per genome segment as an example. Sequencing results were of high quality for all plasmids except those of pSMART-T7_RV_SA11_GS11, where a sequence from the Upstream primer could not be obtained. The figure shows a reverse complement from the Downstream primer, which shows that the sequence across the 5'-UTR and T7 promoter is correct. For each genome segment, the colony with the plasmid that was confirmed to be correct by sequencing was used for endotoxin-free plasmid purification for transfection into mammalian cell culture.

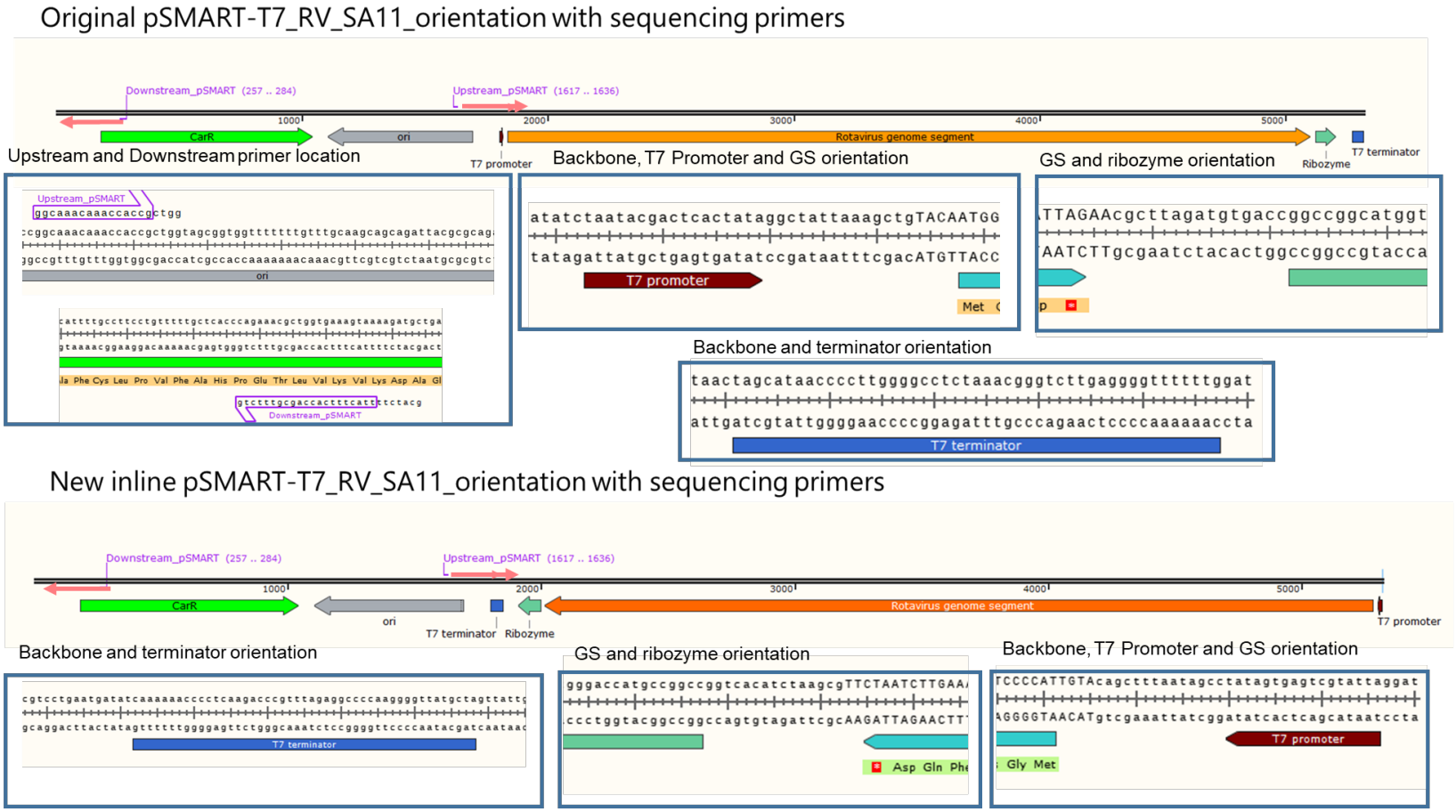


Figure 2.9: Schematic showing the orientation of sequencing primers with respect to the transcription cassette. Note that in the previous orientation, Sanger sequencing from the pSMART_Downstream would have sequenced the T7 terminator and HDV ribozyme. In the new orientation, it sequences across the T7 promoter and 5'-end of the genome segment. The Upstream primer previously sequenced across the T7 promoter, it now sequences across the T7 terminator, HDV ribozyme, and 3'- end of the cDNA genome segment. Selected sequences of each element in the plasmid are shown to illustrate how the sequenced changed with respect to the sequencing primers.

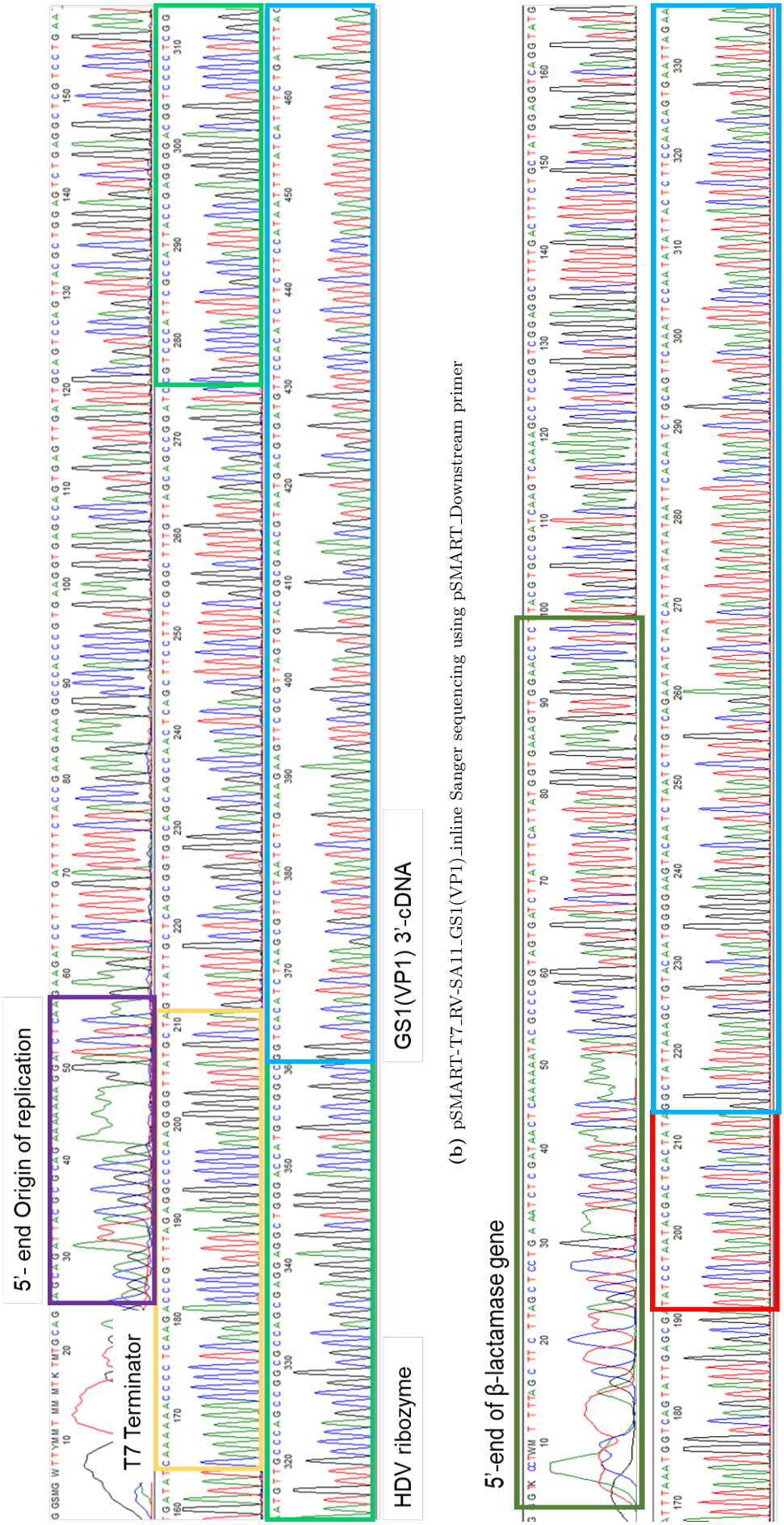
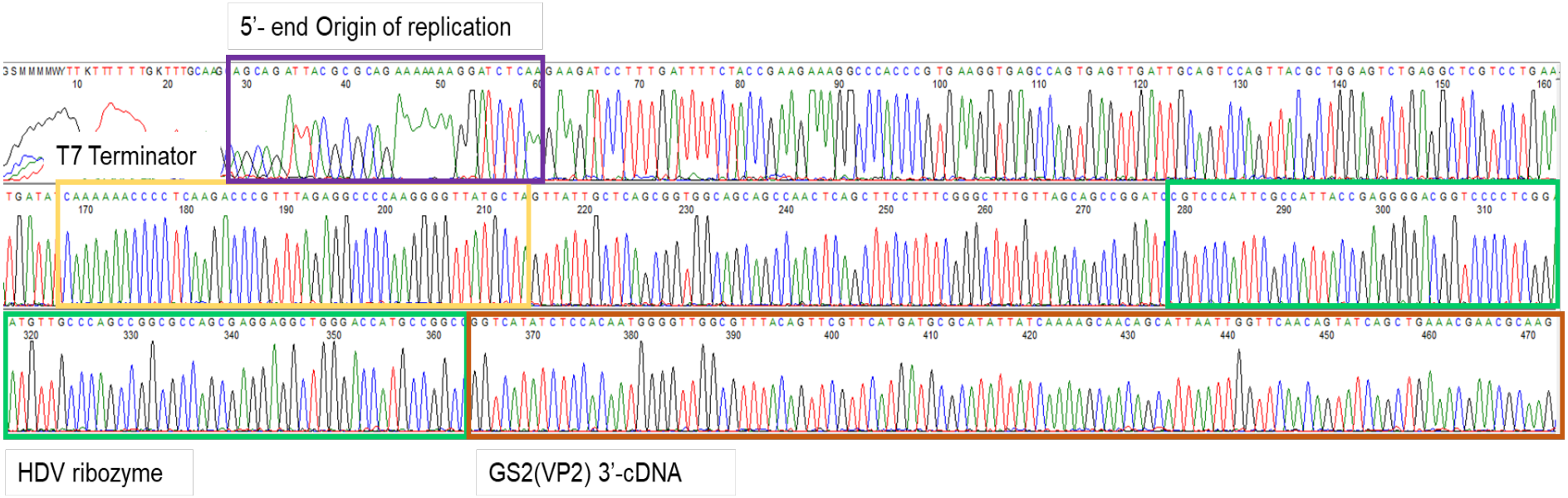


Figure 2.10: Sanger sequencing of the pSMART-T7_RV-SA11_GS1(VP1)_inline transcription cassette using the pSMART_Upstream and Downstream primers. This shows that the orientation of the cassette was successfully changed and that the T7 promoter, cDNA genome segment, HDV ribozyme, and T7 terminator are present.

(a) pSMART-T7_RV-SA11_GS2(VP2)_inline Sanger sequencing using pSMART_Upstream primer



(b) pSMART-T7_RV-SA11_GS2(VP2)_inline Sanger sequencing using pSMART_Downstream primer

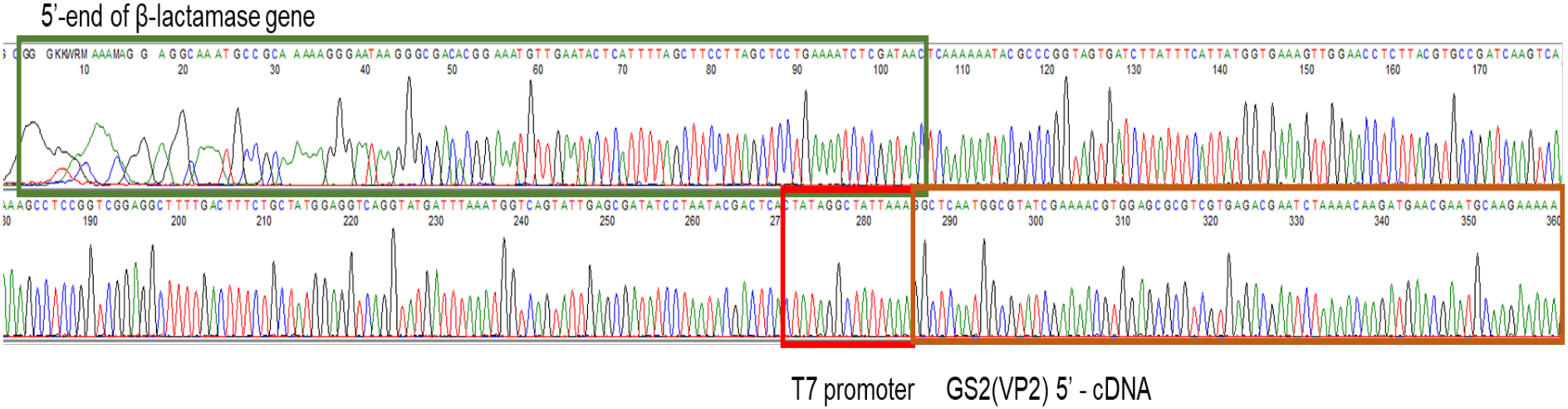
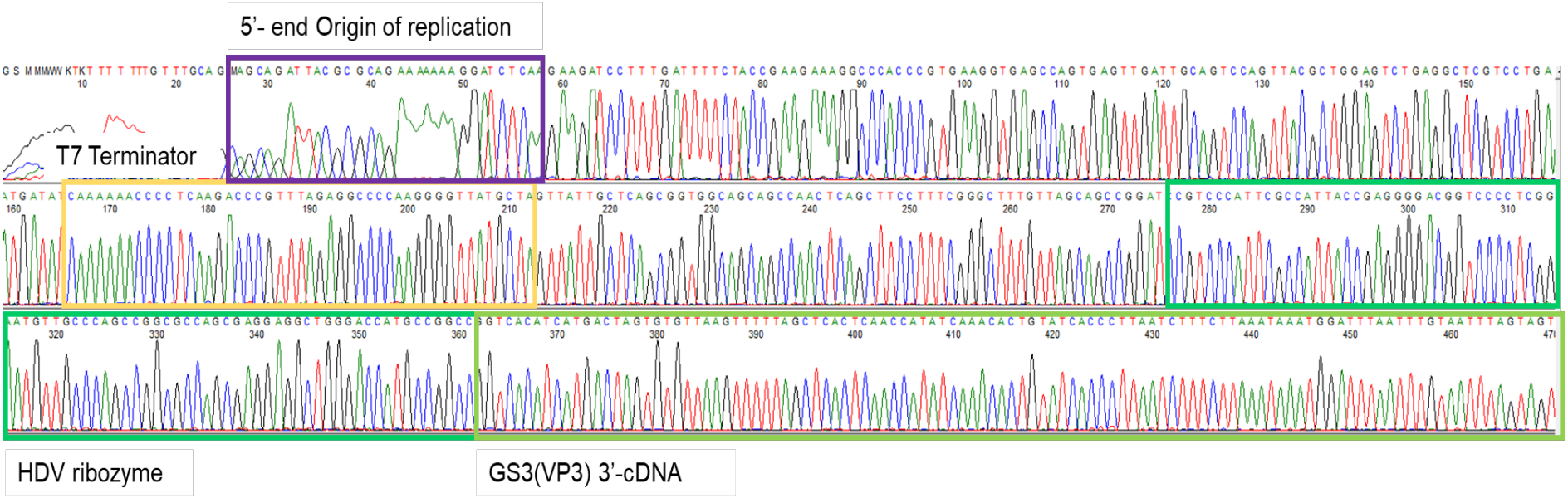


Figure 2.11: Sanger sequencing of the pSMART-T7_RV-SA11_GS2(VP2)_inline transcription cassette using the pSMART_Upstream and Downstream primers. This shows that the orientation of the cassette was successfully changed and that the T7 promoter, cDNA genome segment, HDV ribozyme, and T7 terminator are present.

(a) pSMART-T7_RV-SA11_GS3(VP3)_inline Sanger sequencing using pSMART_Upstream primer



(b) pSMART-T7_RV-SA11_GS2(VP2)_inline Sanger sequencing using pSMART_Downstream primer

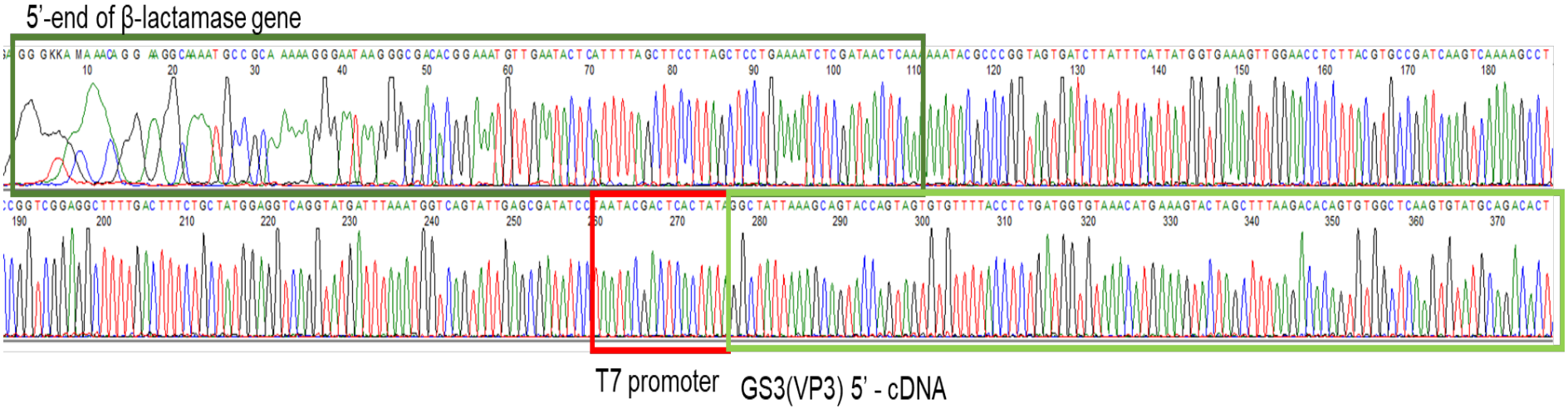


Figure 2.12: Sanger sequencing of the pSMART-T7_RV-SA11_GS3(VP3)_inline transcription cassette using the pSMART_Upstream and Downstream primers. This shows that the orientation of the cassette was successfully changed and that the T7 promoter, cDNA genome segment, HDV ribozyme, and T7 terminator are present.

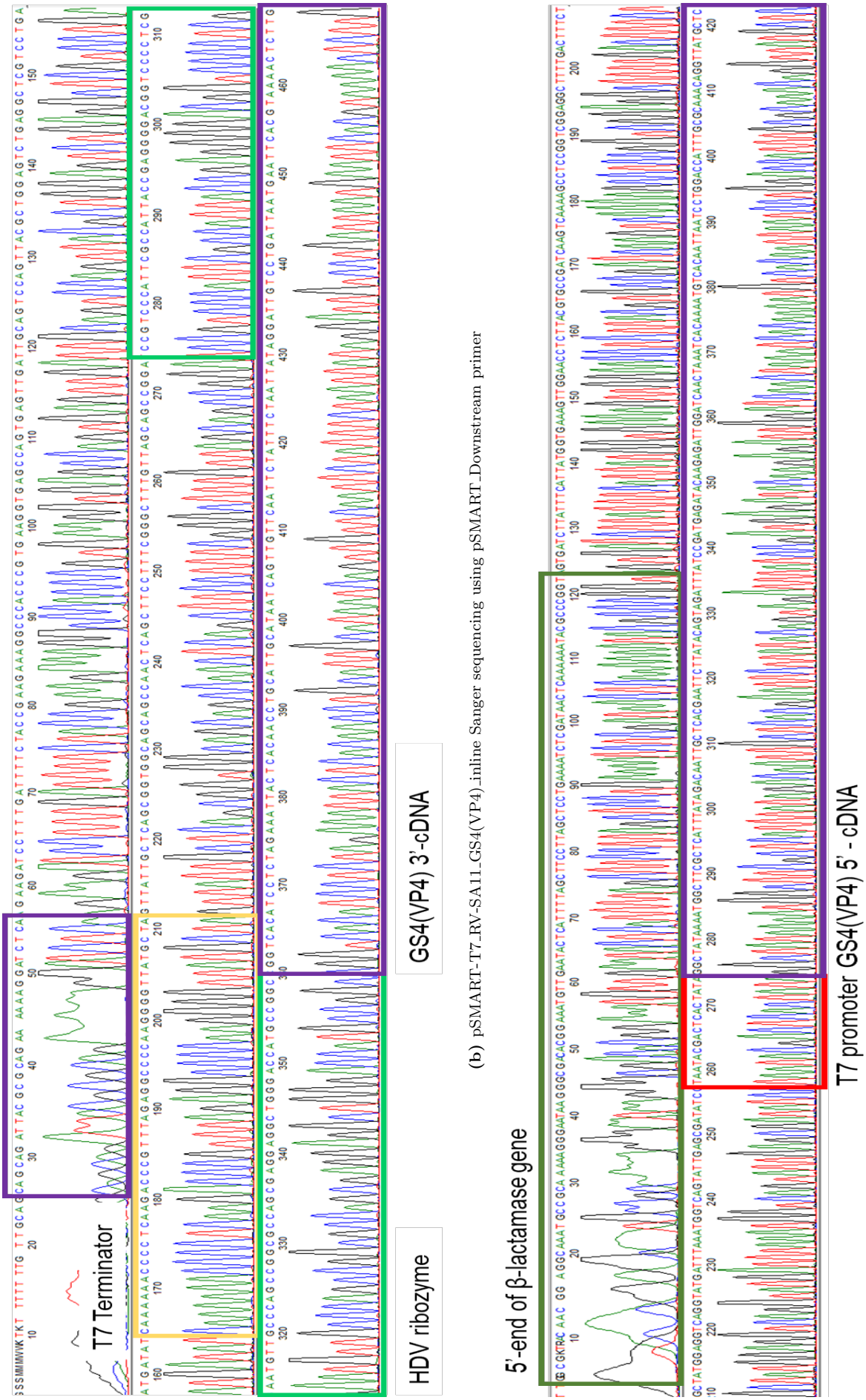
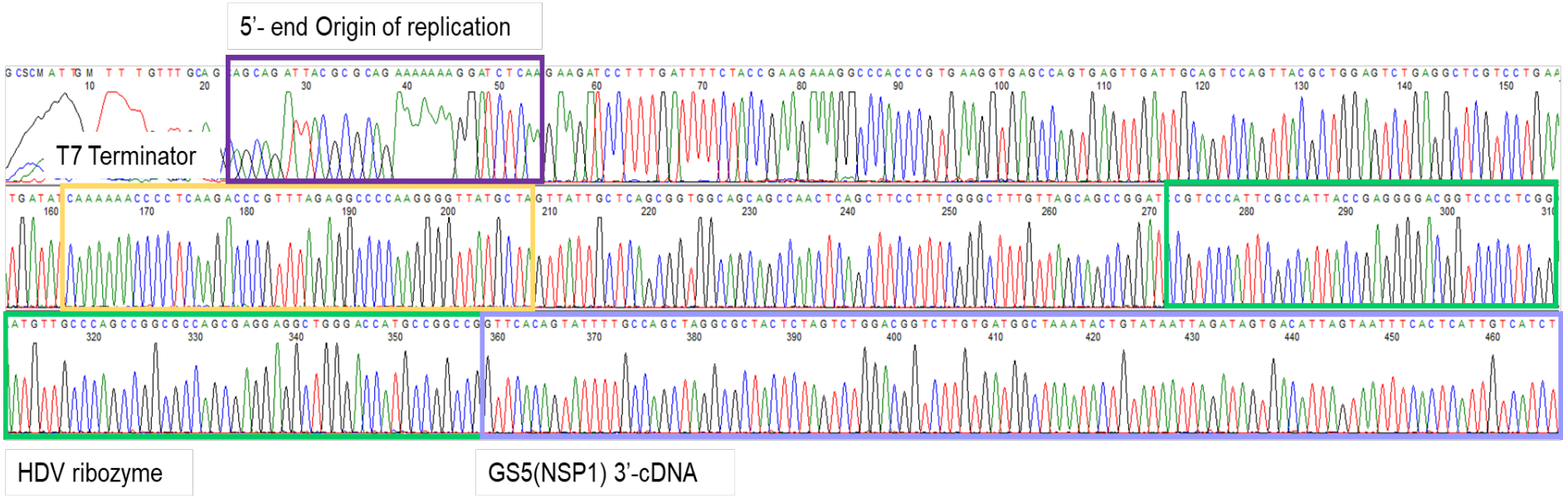


Figure 2.13: Sanger sequencing of the pSMART-T7_RV-SA11_GS4(VP4)_inline transcription cassette using the pSMART_Upstream and Downstream primers. This shows that the orientation of the cassette was successfully changed and that the T7 promoter, cDNA genome segment, HDV ribozyme, and T7 terminator are present.

(a) pSMART-T7_RV-SA11_GS5(NSP1)_inline Sanger sequencing using pSMART_Upstream primer



(b) pSMART-T7_RV-SA11_GS5(NSP1)_inline Sanger sequencing using pSMART_Downstream primer

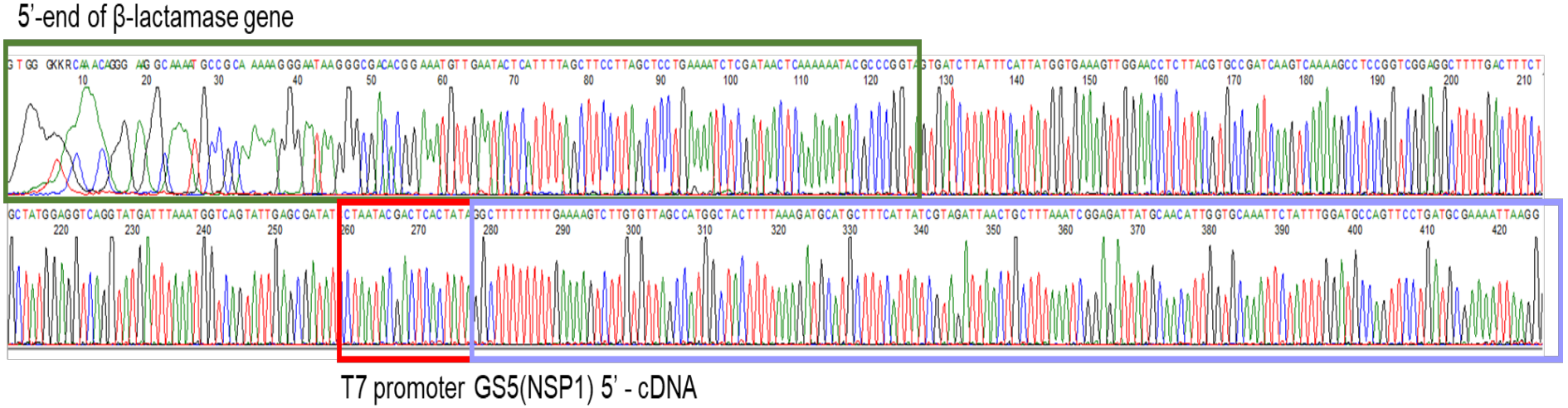


Figure 2.14: Sanger sequencing of the pSMART-T7_RV-SA11_GS5(NSP1)_inline transcription cassette using the pSMART_Upstream and Downstream primers. This shows that the orientation of the cassette was successfully changed and that the T7 promoter, cDNA genome segment, HDV ribozyme, and T7 terminator are present.

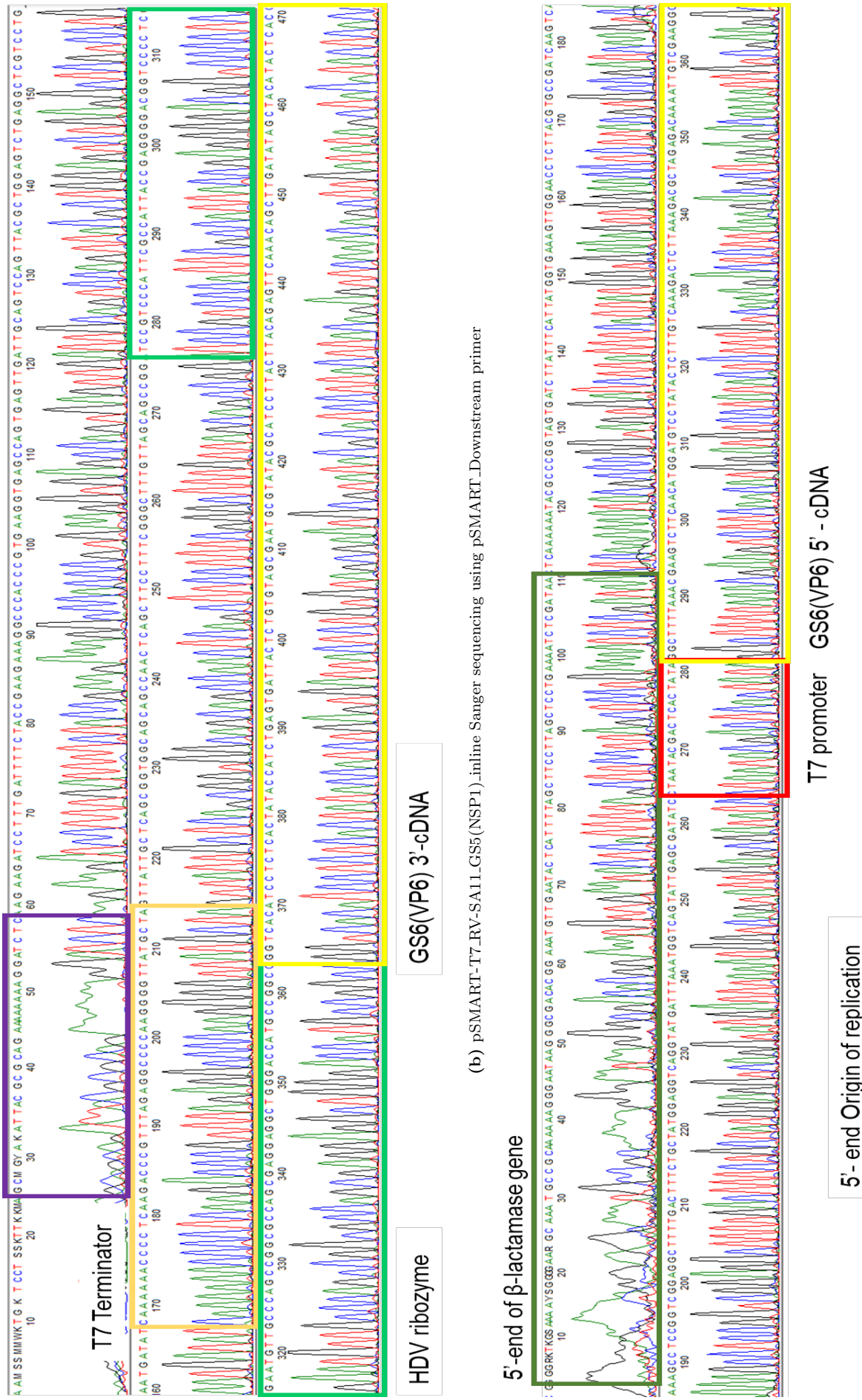
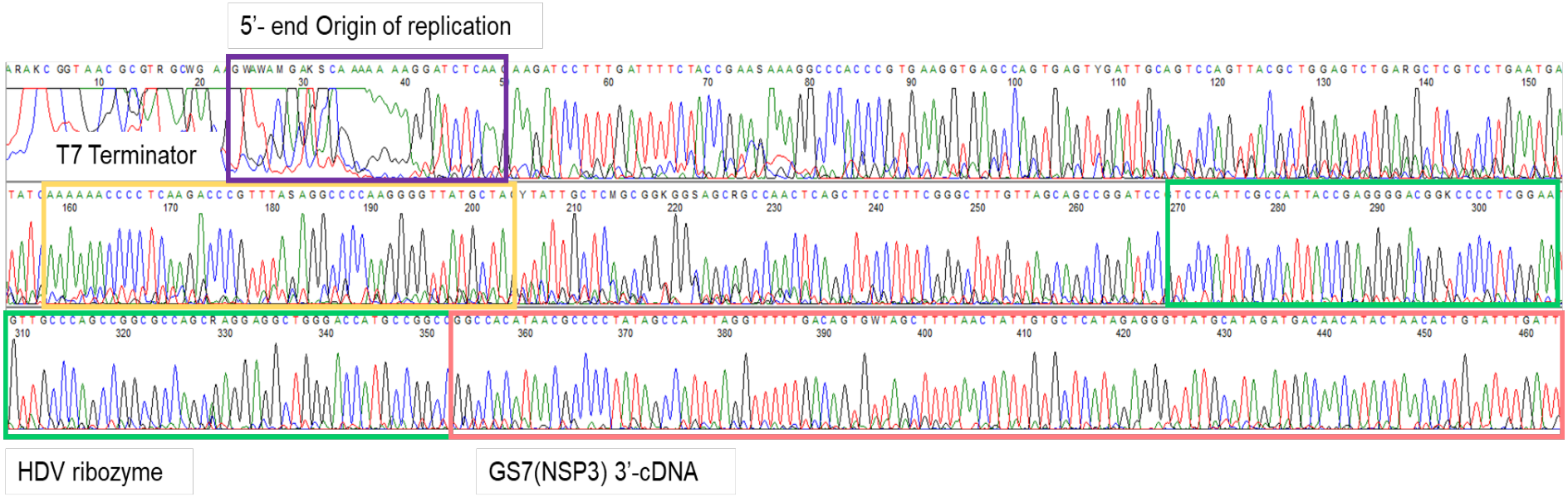


Figure 2.15: Sanger sequencing of the pSMART-T7_RV-SA11_GS6(VP6)_inline transcription cassette using the pSMART_Upstream and Downstream primers. This shows that the orientation of the cassette was successfully changed and that the T7 promoter, cDNA genome segment, HDV ribozyme, and T7 terminator are present.

(a) pSMART-T7_RV-SA11_GS7(NSP3)_inline Sanger sequencing using pSMART_Upstream primer



(b) pSMART-T7_RV-SA11_GS7(NSP3)_inline Sanger sequencing using pSMART_Downstream primer

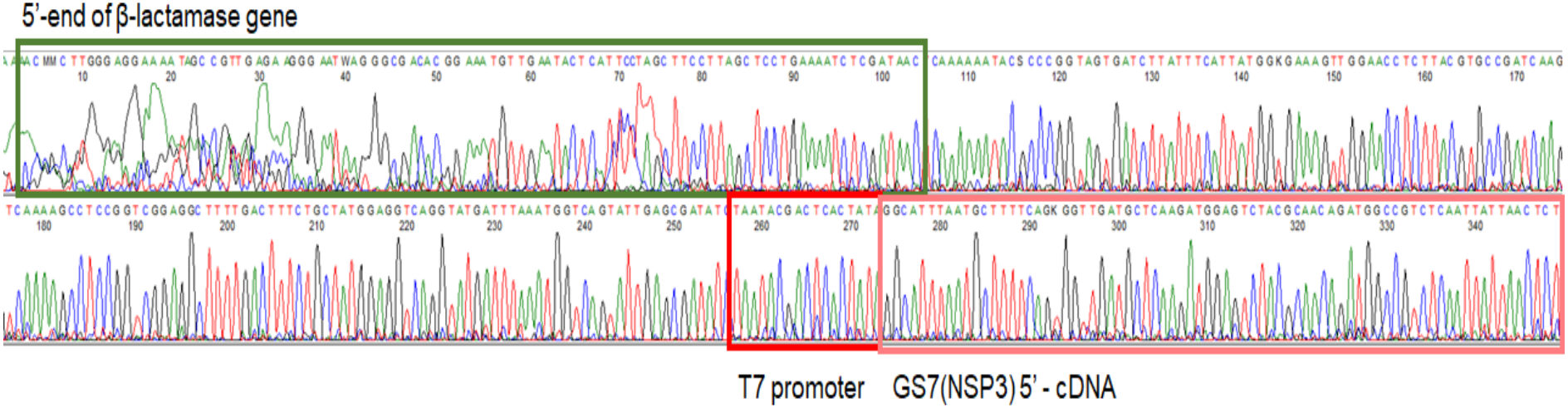
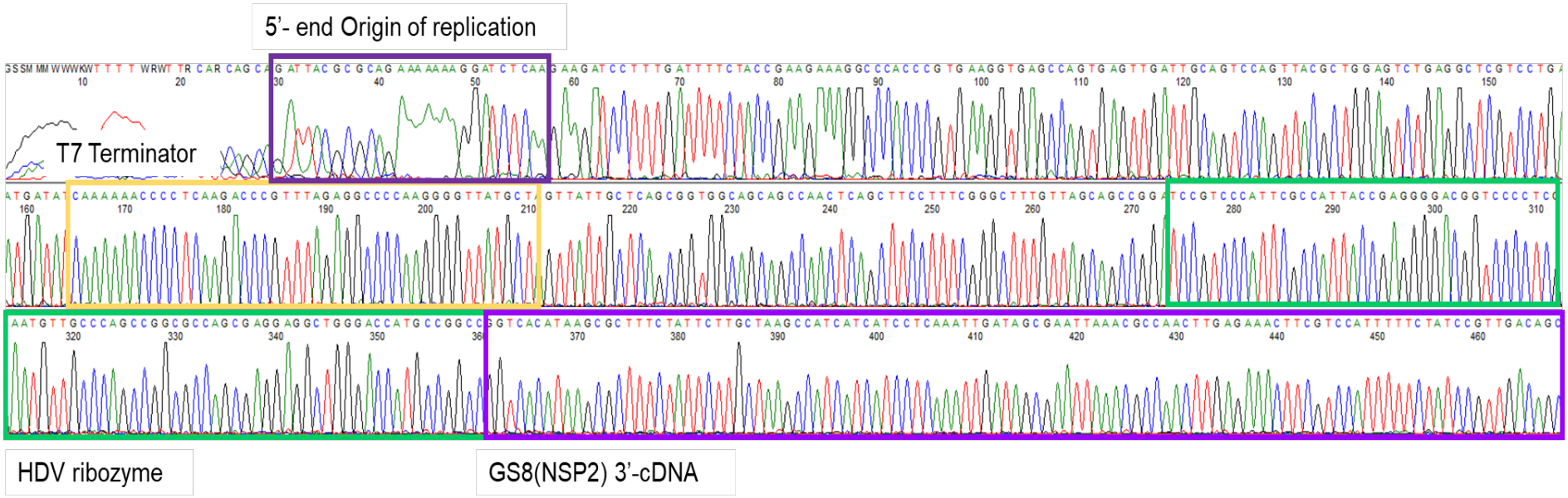


Figure 2.16: Sanger sequencing of the pSMART-T7_RV-SA11_GS7(NSP3)_inline transcription cassette using the pSMART_Upstream and Downstream primers. This shows that the orientation of the cassette was successfully changed and that the T7 promoter, cDNA genome segment, HDV ribozyme, and T7 terminator are present.

(a) pSMART-T7_RV-SA11_GS8(NSP2)_inline Sanger sequencing using pSMART_Upstream primer



(b) pSMART-T7_RV-SA11_GS7(NSP3)_inline Sanger sequencing using pSMART_Downstream primer

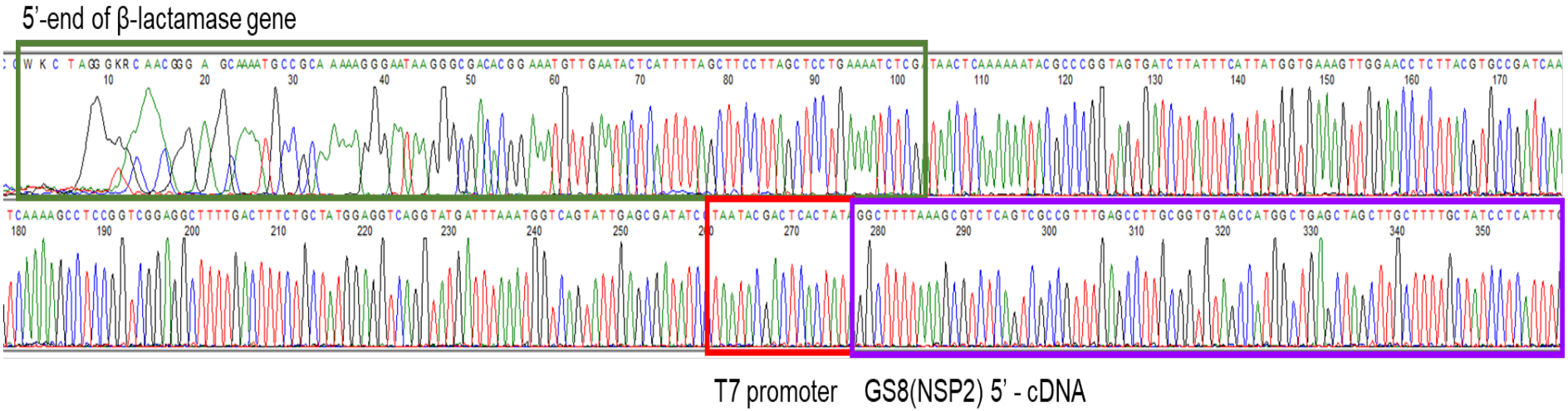


Figure 2.17: Sanger sequencing of the pSMART-T7_RV-SA11_GS8(NSP2)_inline transcription cassette using the pSMART_Upstream and Downstream primers. This shows that the orientation of the cassette was successfully changed and that the T7 promoter, cDNA genome segment, HDV ribozyme, and T7 terminator are present.

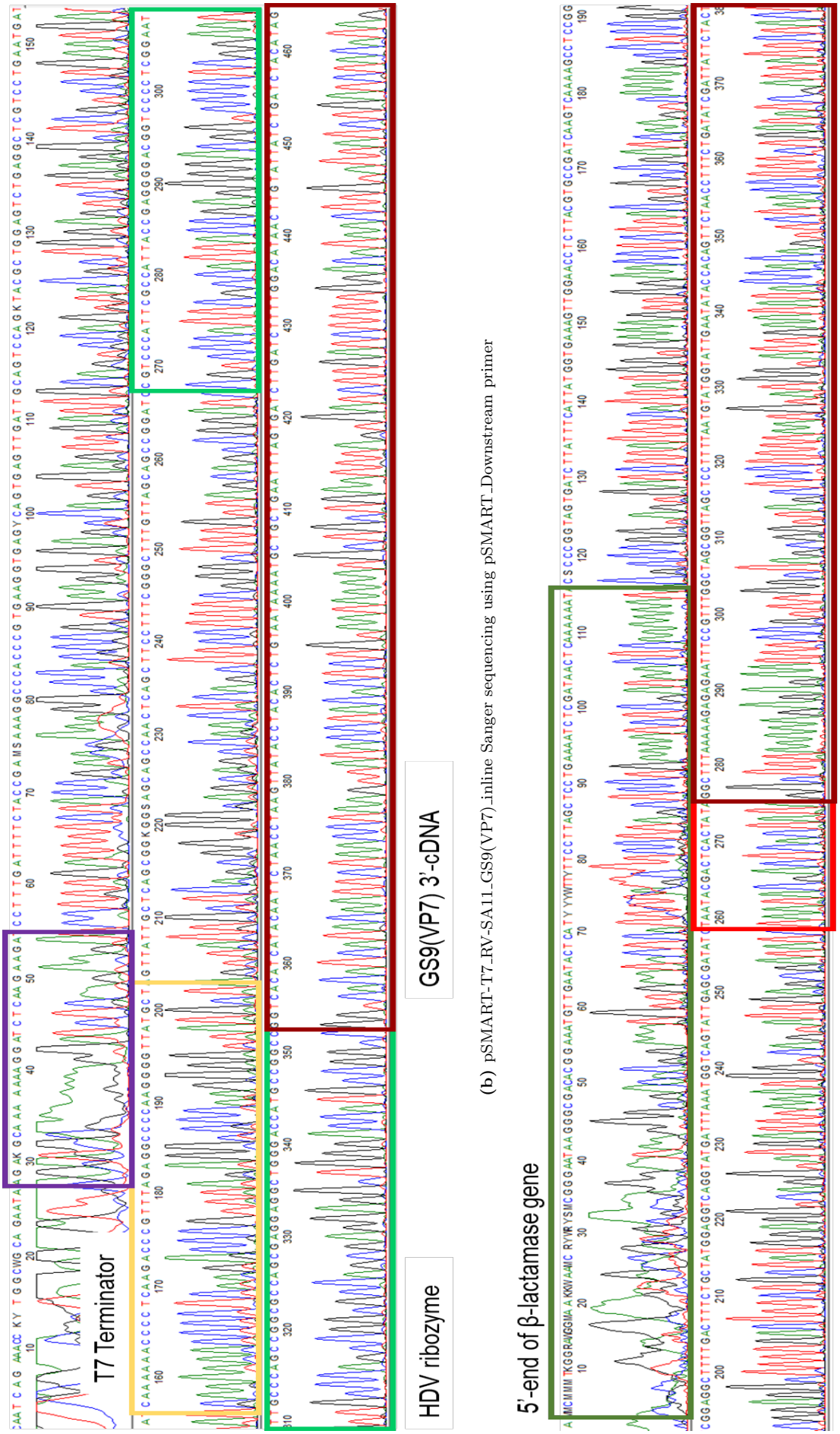
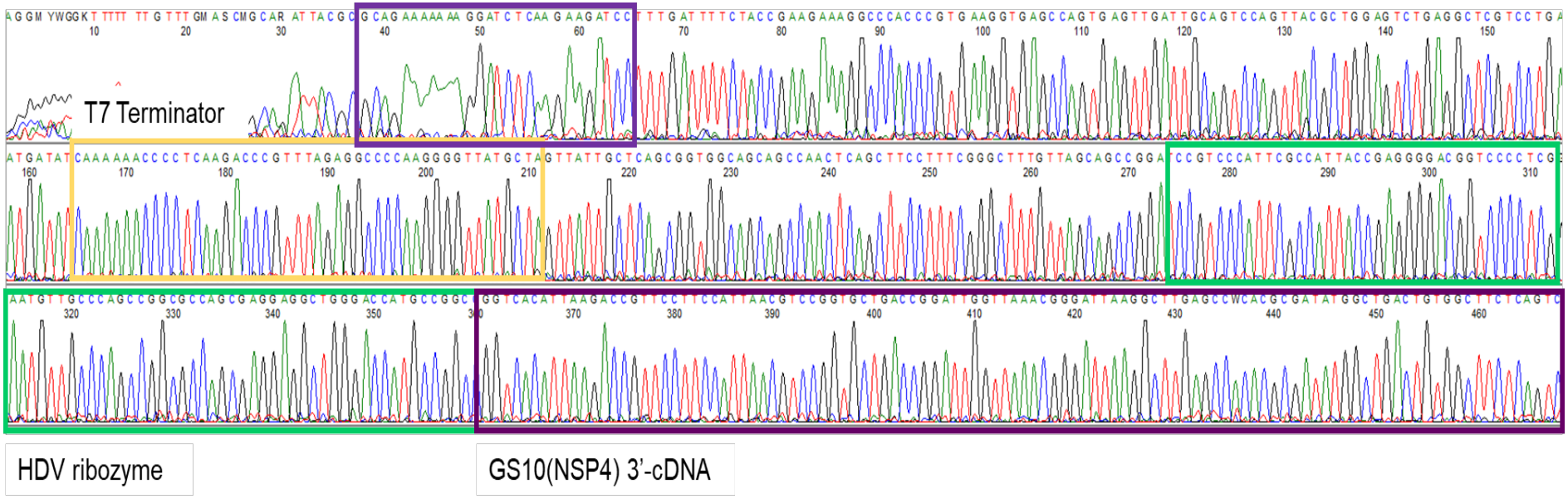


Figure 2.18: Sanger sequencing of the pSMART-T7_RV-SA11_GS9(VP7)_inline transcription cassette using the pSMART_Upstream and Downstream primers. This shows that the orientation of the cassette was successfully changed and that the T7 promoter, cDNA genome segment, HDV ribozyme, and T7 terminator are present.

(a) pSMART-T7_RV-SA11_GS10(NSP4)_inline Sanger sequencing using pSMART_Upstream primer



(b) pSMART-T7_RV-SA11_GS10(NSP4)_inline Sanger sequencing using pSMART_Downstream primer

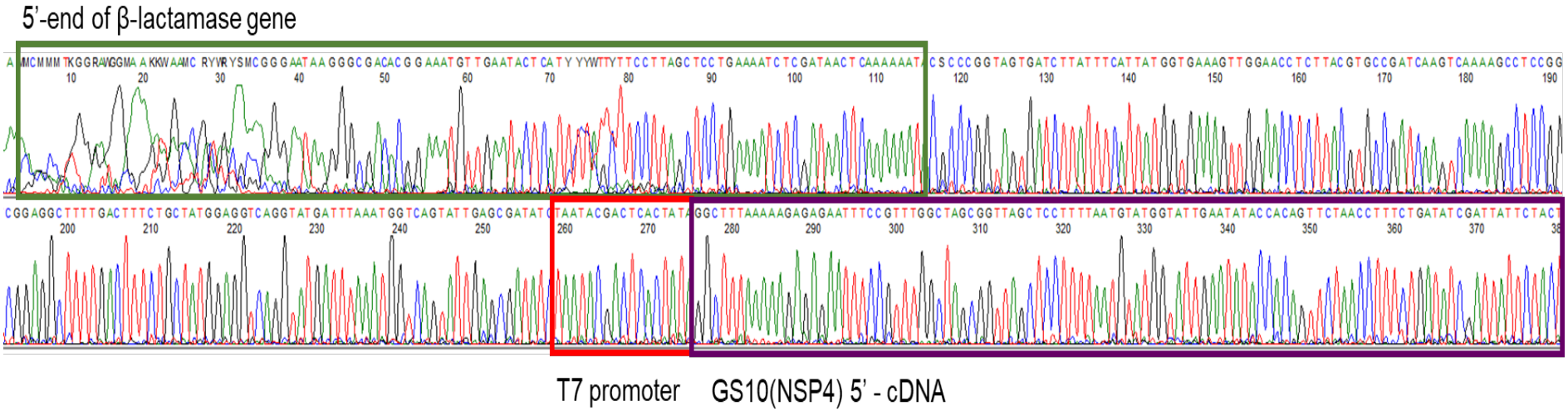
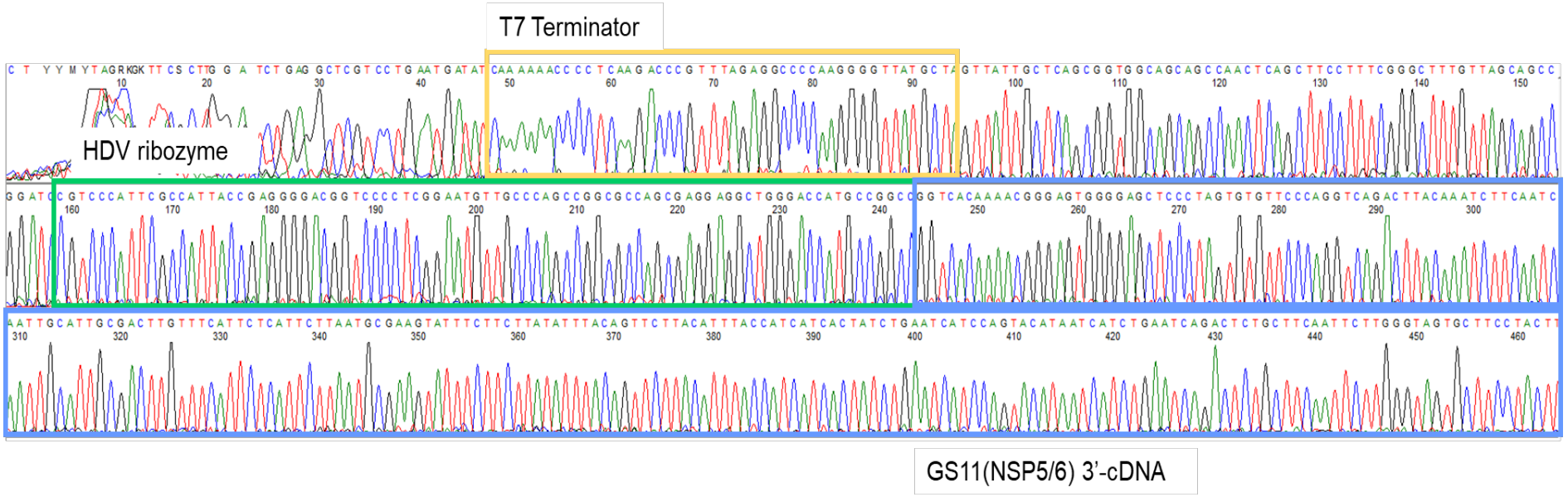


Figure 2.19: Sanger sequencing of the pSMART-T7_RV-SA11_GS10(NSP4)_inline transcription cassette using the pSMART_Upstream and Downstream primers. This shows that the orientation of the cassette was successfully changed and that the T7 promoter, cDNA genome segment, HDV ribozyme, and T7 terminator are present.

(a) pSMART-T7_RV-SA11_GS11(NSP5/6)_inline Sanger sequencing using pSMART_Upstream primer



(b) pSMART-T7_RV-SA11_GS11(NSP5/6)_inline Sanger sequencing using pSMART_Downstream primer

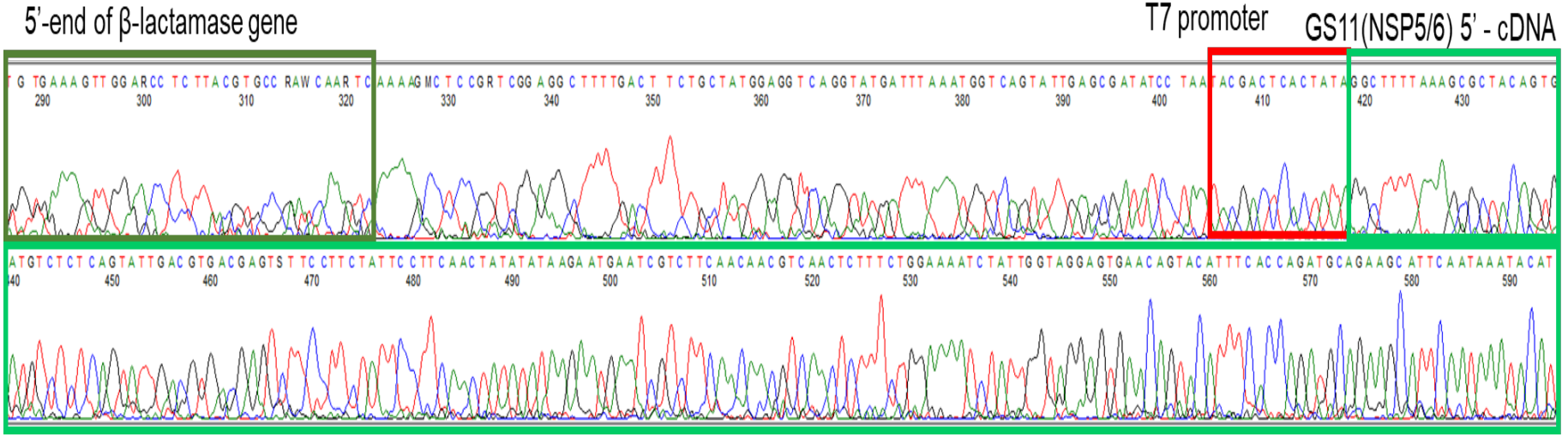


Figure 2.20: Sanger sequencing of the pSMART-T7_RV-SA11_GS11(NSP5/6)_inline transcription cassette using the pSMART_Upstream and Downstream primers. This shows that the orientation of the cassette was successfully changed and that the T7 promoter, cDNA genome segment, HDV ribozyme, and T7 terminator is present. Note that the Downstream sequence was generated from the reverse complement of the Upstream sequence, due to a technical error with the Upstream sequencing.

2.3.4 Endotoxin-free plasmid purification for transfection and sequence verification using Next-Generation sequencing

As discussed in Section 2.2.1.8 endotoxins severely inhibit transfection and impact viral rescue efficiency. This required that a Sanger sequence verified plasmid for each genome segment be endotoxin-free purified for transfection into mammalian cell culture. Further, prior to use in reverse genetics, all complete reverse genetics plasmids needed to be verified using NGS to provide higher sequencing depth and allow identification of sub-populations.

From each set of colonies, one was selected for each genome segment for endotoxin-free purification and transfection into mammalian cell culture. 15 ml overnight cultures were prepared. Induction for plasmid replication was performed the following morning on overnight cultures. Plasmids were then extracted and endotoxin-free purified according to the manufacturer's instructions. Nanodrop spectrophotometry showed that concentrations generally ranged between 500 and 3500 ng/µl.

To verify that the plasmids did not contain large deletions prior to next-generation sequencing, BsaI was selected for the digestion, since this enzyme cuts the pSmart backbone in the β-lactamase gene, except for the GS6(VP6) plasmid, where the enzyme cuts in the GS6(VP6) ORF as well. This allows linearisation of the plasmid containing the transcription cassette, Figure 2.21. Table 2.8 shows the expected fragment sizes for each digestion, All plasmids digested and were of the correct size. No large deletions were detectable by restriction digestion. Between 100-500 ng was loaded for digestion of plasmids carrying the transcription cassettes of GS1-GS10. For the GS11 plasmid, less than 50 ng was loaded for pSMART-T7_RV-SA11_GS11_NSP5-6_inline_ori. This was due to low yield of the plasmid after endotoxin-free plasmid purification. DNA amounts less than 50 ng result in low signal intensity on the gel. Although signal intensity was low, successful digestion of pSMART-T7_RV-SA11_GS11_NSP5-6_inline_ori could be verified.

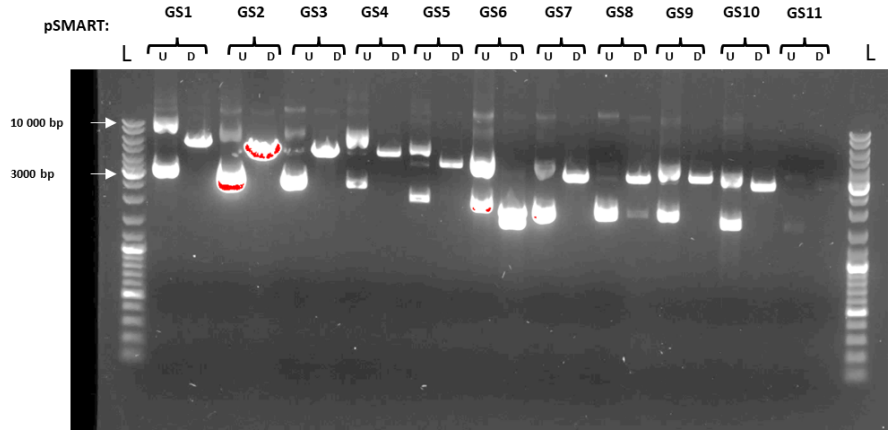


Figure 2.21: 1% Agarose gel of BsaI restriction enzyme digestion of the pSmart_SA11-N5_inline_ori reverse genetics plasmid set. This shows correct plasmid size following recloning of the transcription cassettes in the new orientation. U = Undigested. D = Digested.

Aliquots of the complete plasmid set were then pooled as one library for NGS at the National Institute of Communicable diseases. Sequencing was done in this way to reduce costs, as this allows the preparation of a single library for the complete plasmid set, instead of individual libraries for each plasmid. The concentration was 100 ng/µl and was delivered to the NICD sequencing core for 2 x 150 bp whole genome sequencing on the Illumina NextSeq with a required minimum 1000x read depth. This approach only allowed the verification of individual transcription cassettes and not the plasmid backbones, since reads for the plasmid backbones are not specific to a single plasmid. Because the backbone sequence is found in every plasmid, it does not allow construction of contigs in the *de novo* assembly that are a complete contig for each plasmid since the backbone is not unique, meaning backbone reads will not form a contig that includes each separate transcription cassette. Even though the promoter and ribozyme occur in each plasmid, paired-end sequencing technology allows *de novo* assembly of the promoter and ribozyme. A read that is generated in the cDNA genome segment will be part of a pair. The second member of the pair can then be successfully assembled that arose from the ribozyme or promoter, since the distance between the pair is known and there is read overlap between the ribozyme and genome segment. *De novo* assembly as well as alignment with HiSAT2 was performed in order to ensure that an accurate alignment was obtained of the transcription cassettes, with no reads for the T7 promoter, T7 terminator, or ribozyme being mapped to a plasmid that has a deletion of once of these components because of reads being generated from another plasmid in the mixture. The trimmed reads from the sequenced library were *de novo* assembled using AbySS and the contigs were then aligned to their *in silico* designs, Figure 2.22 - Figure 2.27.

Figures 2.22 - 2.27 show that all the 11 transcription cassettes were successfully re-orientated. Reads were mapped to each *in silico* construct, showing that the 11 transcription cassettes were present in the plasmid mixture sent for sequencing, Figures S6-S16. No reads aligned with the backbone, as was expected. Reorientation resulted in the sequence that was previously 5'-3' on the positive strand, now being 5'-3' on the negative strand.

Table 2.8: Expected fragments and size of the SA11-N5 pSMART_inline_ori plasmid set after BsaI digestion

Plasmid name	Expected fragment size
pSMART-T7_RV-SA11_GS1_VP1_inline_ori	5320 bp
pSMART-T7_RV-SA11_GS2_VP2_inline_ori	4711 bp
pSMART-T7_RV-SA11_GS3_VP3_inline_ori	4609 bp
pSMART-T7_RV-SA11_GS4_VP4_inline_ori	4380 bp
pSMART-T7_RV-SA11_GS5_NSP1_inline_ori	3632 bp
pSMART-T7_RV-SA11_GS6_VP6_inline_ori	1832 and 1542 bp
pSMART-T7_RV-SA11_GS7_NSP3_inline_ori	3123 bp
pSMART-T7_RV-SA11_GS8_NSP2_inline_ori	3077 bp
pSMART-T7_RV-SA11_GS9_VP7_inline_ori	3081 bp
pSMART-T7_RV-SA11_GS10_NSP4_inline_ori	2769 bp
pSMART-T7_RV-SA11_GS11_NSP5/6_inline_ori	2685 bp

Reads were created from the positive strand in a 5'-3' direction. The sequence was thus the complement of the coding sequence on the negative strand. A mixture of the 11 plasmids were sequenced as a single library. This resulted in the amount of reads in the library being much higher for the backbone, than for the transcription cassettes, since there is more backbone present. Since Illumina paired-end sequencing technology was used and aligning to a single reference for each plasmid, only read pairs that have a mapped to be the backbone and the transcription cassette will show in the alignment. This is because we are defined that we only want to see reads that were mapped to a single plasmid as pairs.

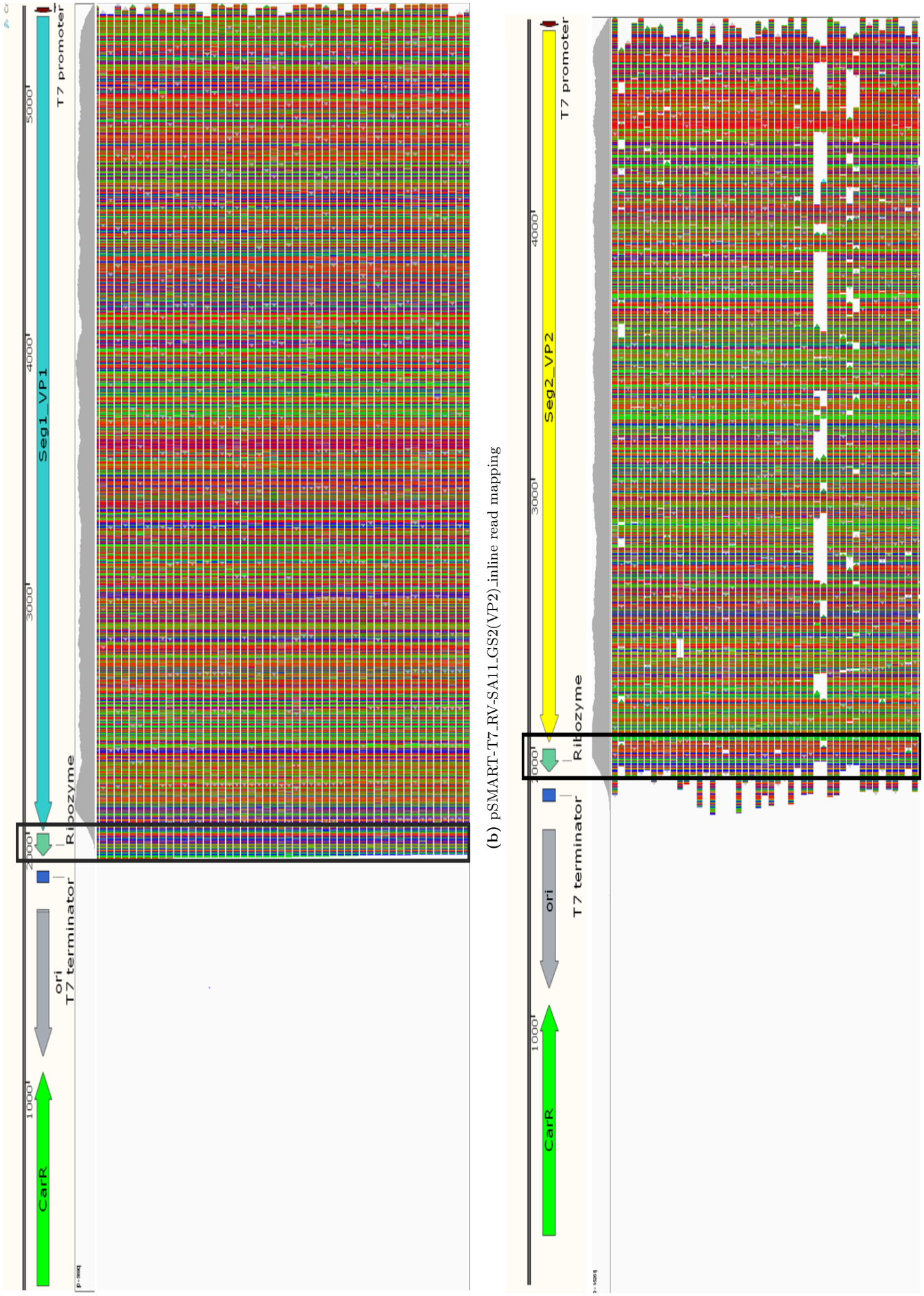


Figure 2.22: (a) *De novo* **assembly and alignment of trimmed reads of pSMART-T7_RV-SA11_GS1(VP1)_inline and (b)** *de novo* **assembly and alignment of pSMART-T7_RV-SA11_GS2(VP2)_inline.** The black box indicates the ribozymes in each plasmid. The alignment confirms that these plasmids do contain a ribozyme.

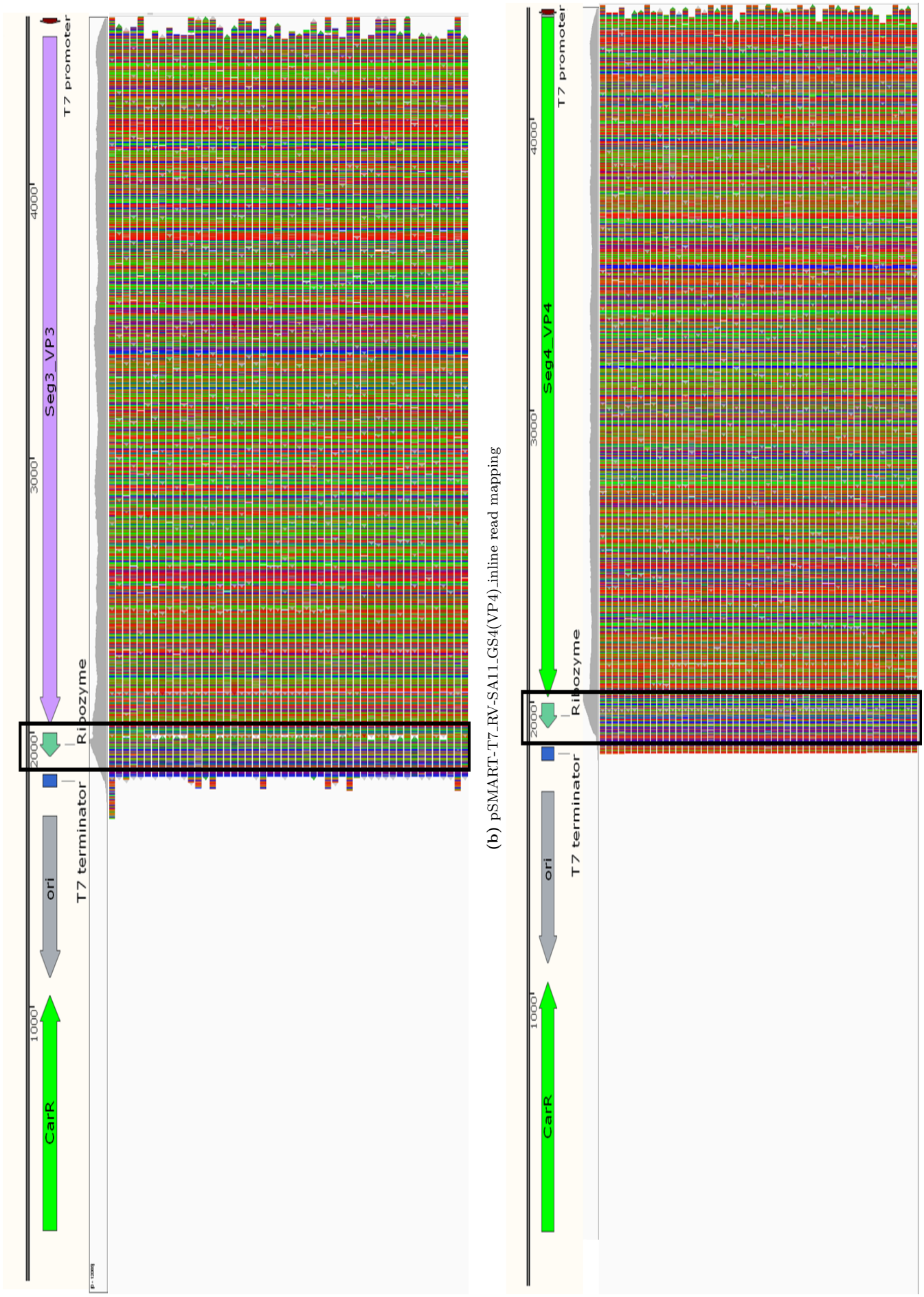


Figure 2.23: (a) *De novo* **assembly and alignment of trimmed reads of pSMART-T7_RV-SA11_VP3(GS3)_inline and (b)** *de novo* **assembly and alignment of pSMART-T7_RV-SA11_GS4(VP4_inline.** The black box indicates the ribozymes in each plasmid. The alignment confirms that these plasmids do contain a ribozyme.

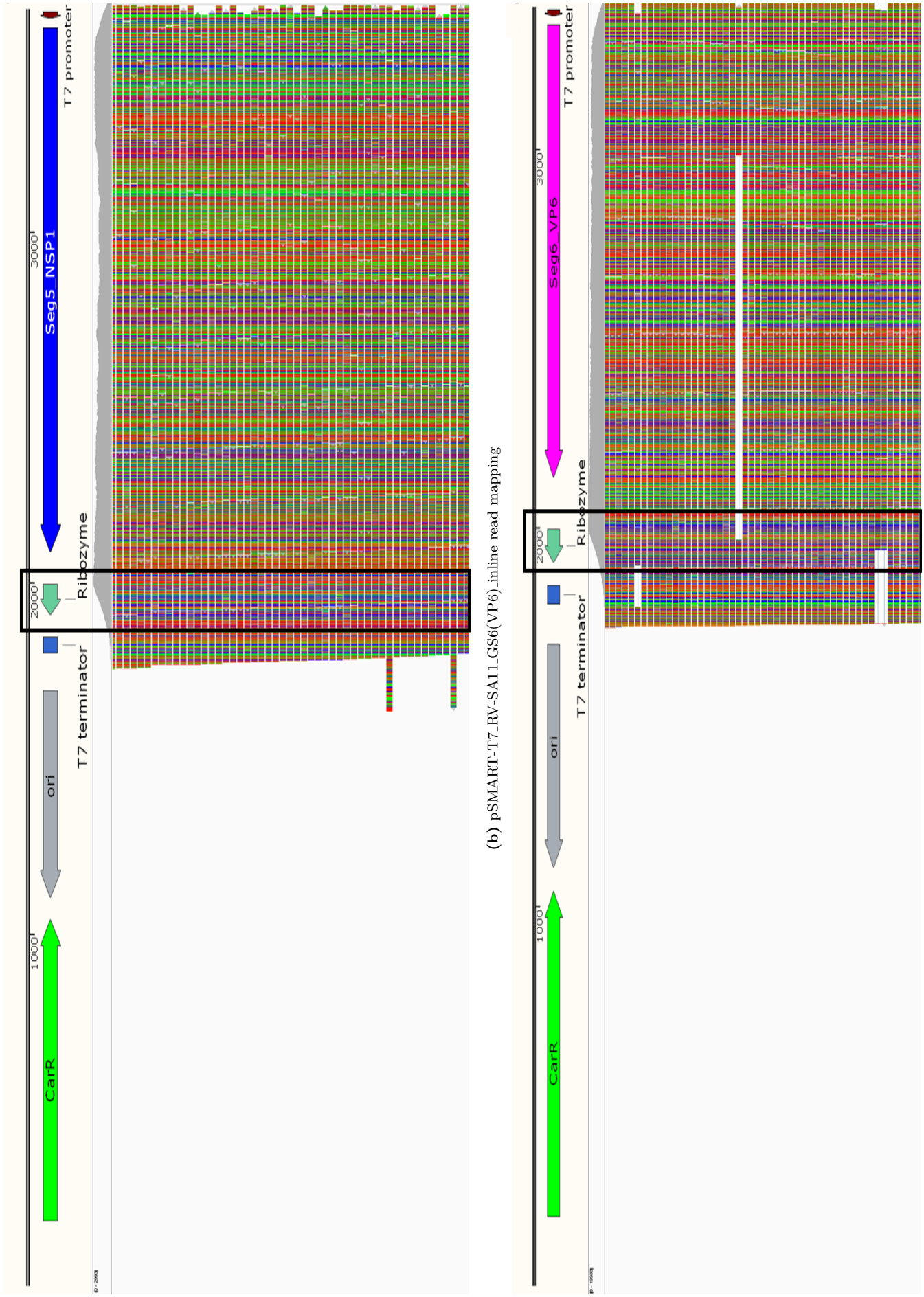
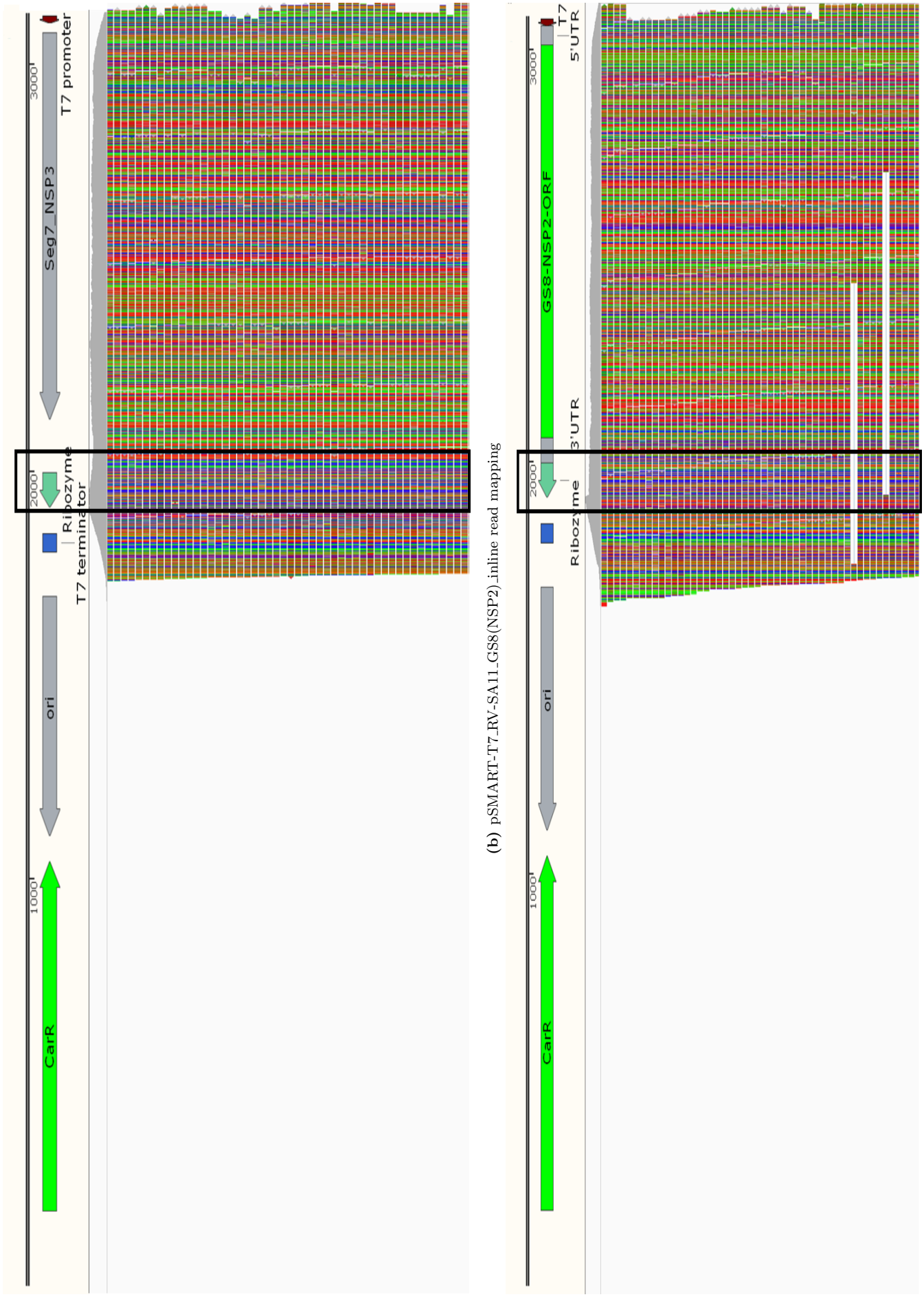


Figure 2.24: (a) *De novo* assembly and alignment of trimmed reads of pSMART-T7_RV-SA11_GS5(NSP1)_inline and (b) *de novo* assembly and alignment of pSMART-T7_RV-SA11_GS6(VP6)_inline. The black box indicates the ribozymes in each plasmid. The alignment confirms that these plasmids do contain a ribozyme.



(a) pSMART-T7_RV-SA11_GS7(NSP3)_inline read mapping

(b) pSMART-T7_RV-SA11_GS8(NSP2)_inline read mapping

Figure 2.25: (a) *De novo* **assembly and alignment of trimmed reads of pSMART-T7_RV-SA11_GS7(NSP3)_inline and (b)** *de novo* **assembly and alignment of pSMART-T7_RV-SA11_GS8(NSP2)_inline.** The black box indicates the ribozymes in each plasmid. The alignment confirms that these plasmids do contain a ribozyme.

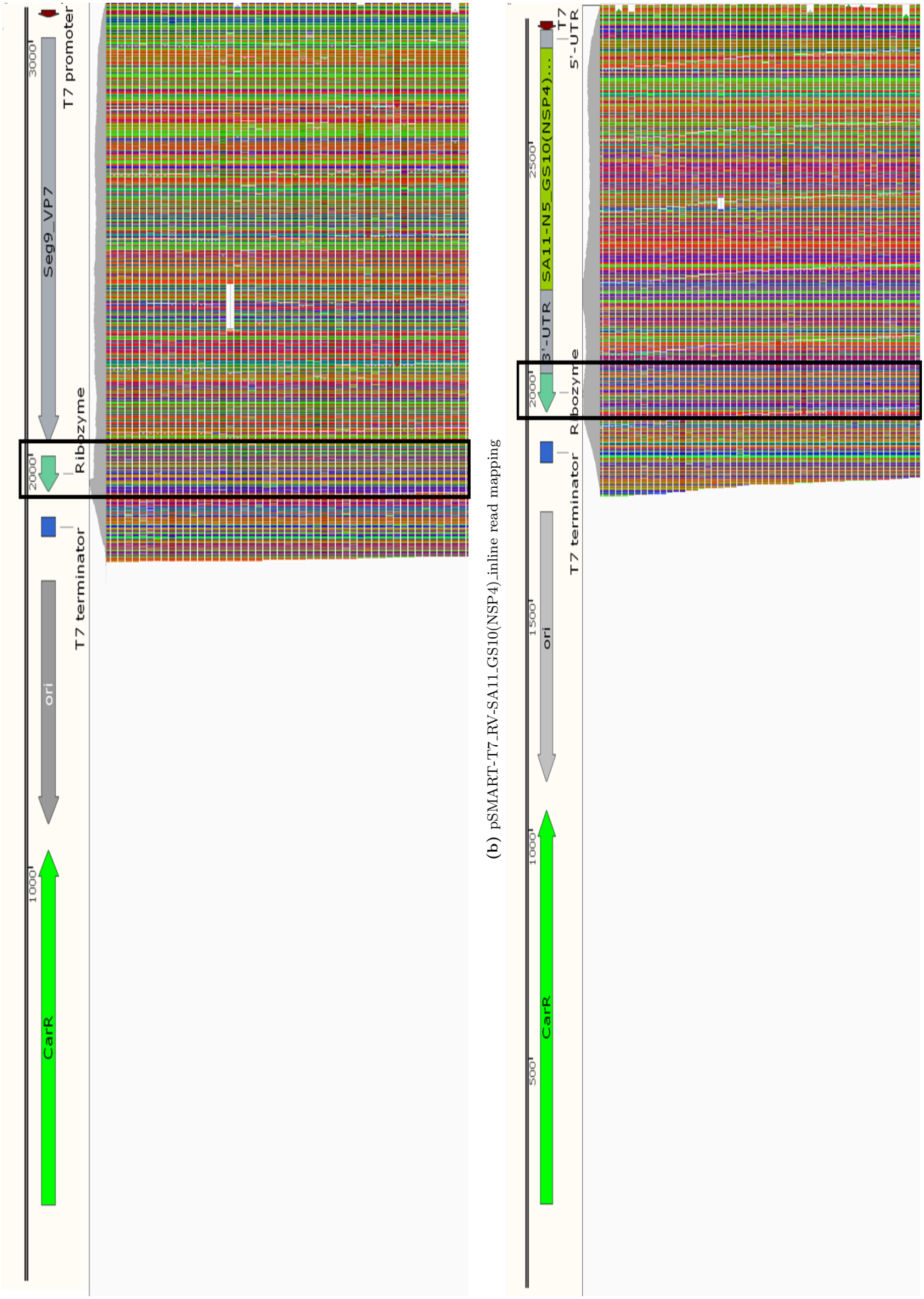
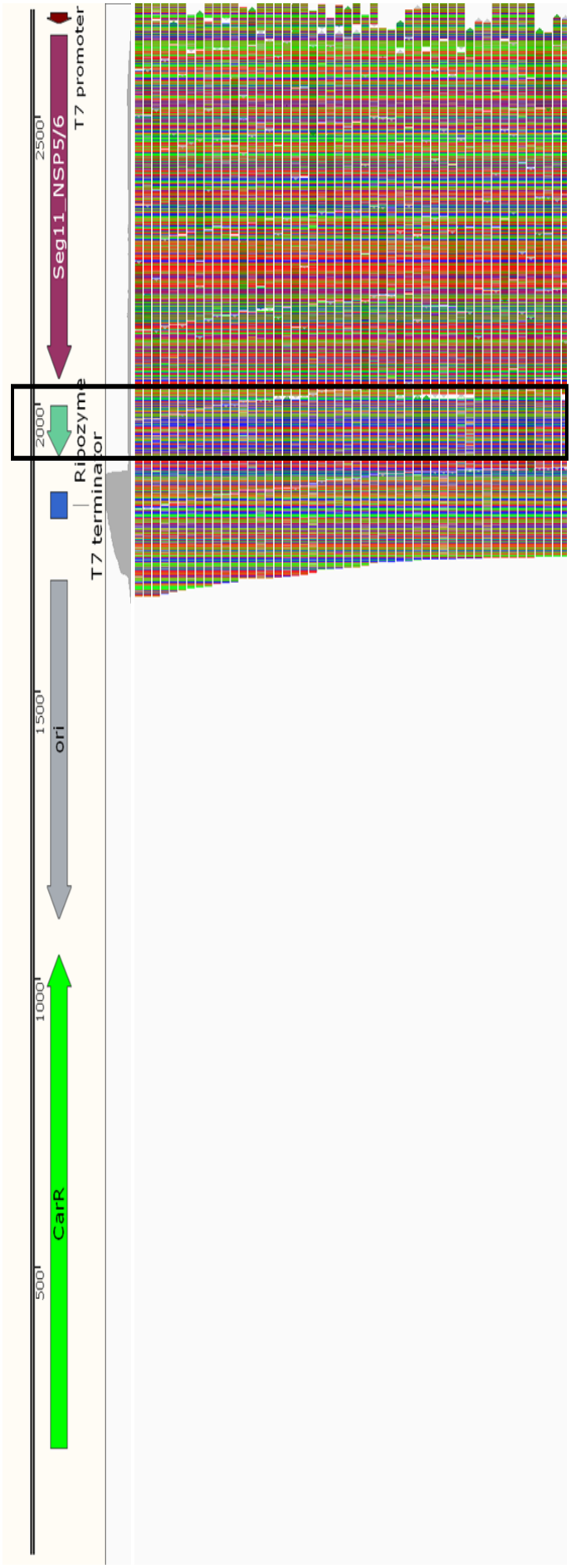


Figure 2.26: (a) ***De novo*** **assembly and alignment of trimmed reads of pSMART-T7_RV-SA11_GS9(VP7)_inline and (b)** ***de novo*** **assembly and alignment of pSMART-T7_RV-SA11_GS10(NSP4)_inline.** The black box indicates the ribozymes in each plasmid. The alignment confirms that these plasmids do contain a ribozyme.



(a) pSMART-T7_RV-SA11_GS11(NSP5/6)_inline read mapping

Figure 2.27: Alignment of trimmed reads of pSMART-T7_RV-SA11_GS11(NSP5/6.) The black box indicates the ribozyme in this plasmid. The alignment confirms that this plasmid does contain a ribozyme.

The stability substantially improved for the pSMART_inline_ori plasmid set. What was especially apparent during the recloning of the plasmid set was that the cloning efficiency improved, with almost 100% of colonies screened containing the correct construct. This was especially evidenced for what were previously seen as difficult or problem genome segments, such as GS7(NSP3), GS9(VP7), and GS10(NSP4), and for the ribozyme region, which had previously been undergoing deletions in many of the plasmids, Section 2.3.1.All the plasmids were stable after cloning with no large deletions or mutations seen during the course of this project, even when working from glycerol stocks. Glycerol stocks were shown to be stable for more than a year, where previously glycerol stocks were unusable after 3 months, with large deletions occurring when retrieved from -80°C storage (data not shown).

2.3.5 Attempted viral rescue with the SA11-N5 pSMART_inline plasmid set

To assess whether the new plasmid set could be used for rescue and whether rescue was repeatable, transfection mixes needed to be prepared for transfection. Rescue of SA11-N5 was attempted using both an equimolar and equimicrogram approach.

BSR-T7/5 stat(-) clone 16, ST, MA104 cells were in use in our laboratory at this stage. BSR-T7/5 stat(-) clone 16 cells were chosen to replace the BSR-T7/5 cells used by M.GJ Huyzers, since rescue could be achieved with these cells for AHSV and BTV, and they have STAT1 knocked out (Prof. A.C. Potgieter, personal communication). The approach was that these cells may generate a higher titre at initial rescue, since they cannot mount an interferon response.

One day prior to transfection, BSR-T7/5 stat(-) clone 16 cells were seeded into 6 well plates. Plasmids were measured using Nanodrop spectrophotometry and equimolar or equimicrogram mixes prepared. Mixes were measured prior to transfection in order to transfect the correct mass of DNA. BSR-T7/5 stat(-) clone 16 cells were transfected using 4 μg of DNA as described in Section 2.2.2.4. The medium was changed the following day and transfections incubated for 5 days. The BSR-T7/5 stat(-) clone 16 cells were then freeze-thawed three times, porcine trypsin activated and passaged on ST cells, this was designated as the P0 passage. After complete cell death, freeze-thaw and activation was again performed, and the clarified supernatant passaged on ST cells again. The P1 lysate was then used to infect MA104 cells.

What appeared as cytopathic effect (CPE) was visualised in ST cells, Figure 2.28. A negative control was included, where untransfected BSR-T7/5 cellls from the same plate was passaged in the same manner as the rescue attempts. There was a clear progression from a monolayer that appears uninfected to a monolayer that presented 90% CPE. CPE was also observed in the subsequent passaging in MA104 cells. At 80% CPE cells were fixed for immunofluorescence and the supernatant kept for further passaging. IFMA was then performed as described in Section 2.2.3.1 and the monolayers visualised using a Nikon TE-2000S epifluorescence microscope (data not shown). No fluorescence was

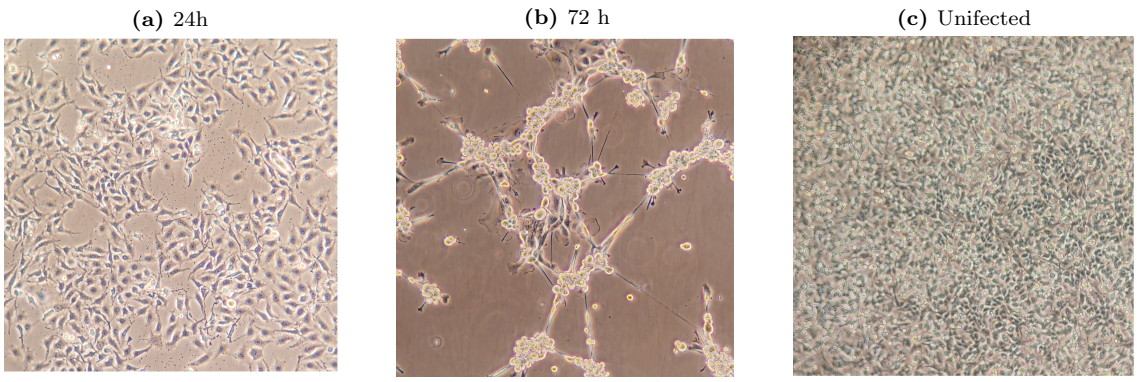


Figure 2.28: Cytopathic effect in ST cells (a) Cell morphology 24 hours post infections (b) Cell morphology 72 hours post infection. Note that the monolayer progressed from 80 % confluent 24 hours post-infection to 10% confluent 48 hours later, with amorphic patches of cells forming. (c) Infection of transfection negative control (No serum, 0.3 µg/ml trypsin) in ST cells, 72 hours post infection

observed on the IFMA. Despite signs of CPE being observed, it was often difficult to differentiate actual viral infection from a monolayer that is reacting poorly to the medium conditions required for infection. Since the negative control showed no signs of CPE, it is probable that there additional toxcicity from the transfected BSR-T7/5 cells, that resulted in cell death in the ST cells. In the future a mock-transfected negative control may be a more valid comparison. Rescue of SA11-N5 was not successful, despite multiple attempts.

The utility of a fluorescent reporter virus is that fluorescence is usually visible 24-48 hours after infection. This would allow us to rapidly transfect, passage, and visualise rescue, allowing more attempts at rescue in the same space of time. This also eliminates the need to passage blind and the use of CPE as an indicator of infection. pSMART-T7_SA11-N5_NSP1-ZsGreen was generated previously during my honours project. The construct design was based on that of Kanai *et al.* (Kanai et al., 2019). This plasmid was still available for use, and it was decided to attempt the rescue of SA11-N5_NSP1-ZsGreen using the re-orientated plasmid set in parallel to the rescue of SA11-N5.

Rescue was attempted for SA11-N5_NSP1-ZsGreen by exchanging the NSP1 plasmid with pSMART-T7_RV_SA11_NSP1-ZsGreen and transfecting the rescue plasmid mixture in BSR-T7/5 stat(-) cells as for SA11-N5. Transfections were incubated for 5 days, whole lysates passaged on ST cells, and then passaged on MA104 cells. Fluorescence was visualised in single cells 48 hours post infection in the P1 passage, a result that was taken to be indicative of infection. "r"SA11-N5_NSP1-ZsGreen1 initially propagated very poorly, with no visible cytopathic effect after five passages, in infection or plaque assay.

Due to how the infection progressed, with what appeared as single cells being infected, but with no viral spread to neighbouring cells, it was postulated that the porcine trypsin was not effective and viral activation may not have been occurring prior to infection. Fresh porcine trypsin was purchased. The substitution with fresh porcine trypsin had no effect

on "r"SA11-N5_NSP1-ZsGreen propagation.

As a separate experiment to assess whether reduced trypsin cleavage efficacy or lack of expression of NSP1, which inhibits the cellular interferon response, prevented efficient viral spread, the "r"SA11-N5_NSP1-ZsGreen viral stock was only infected in ST cells, since they are more susceptible to infection (Prof. A.C. Potgieter, personal communication).

"r"SA11-N5_NSP1-ZsGreen passage 4 was infected in ST cells and fixed after 72 hours for IFMA. Fig 2.29 shows immunofluorescence using Alexa Fluor 555, co-localising with the ZsGreen signal. No CPE was visible, but immunofluoresence overlays with the ZsGreen signal, seemed to show that infection, but not viral spread occurred. Signal intensity was extremely low. This was initially taken to be rescue, but is now believed to be background. Firstly, it is common for secondary antibodies to bind to clusters of cell debris. Secondly, cell debris also fluoresces when blue light is used for excitation, resulting in green fluorescence. After multiple blind passages, a dsRNA genome could not be isolated. This result showed that the NWU SA11-N5 pSMART system did not support rescue, even after plasmid stability was improved by reorientating the transcription cassettes.

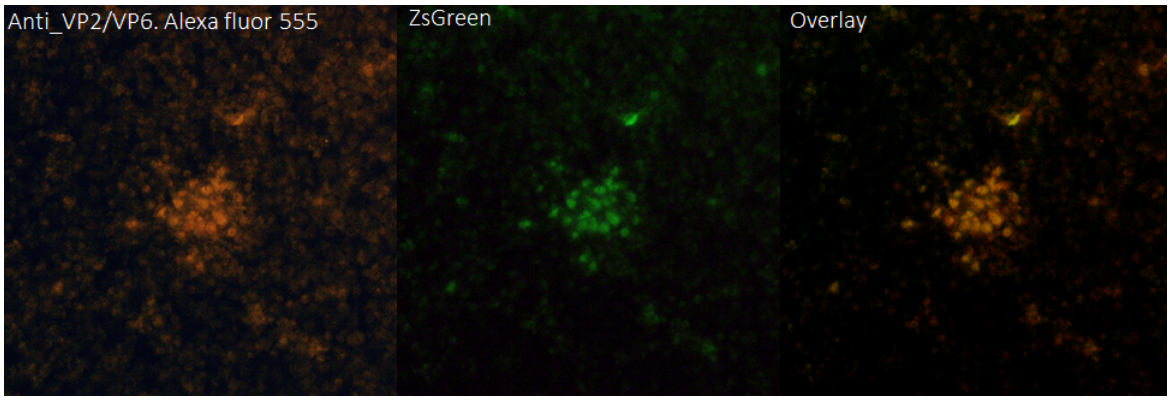


Figure 2.29: Immunofluorecence showing ZsGreen1 and Alexa555 fluorescence in the green and red channels during epifluorescence. Both green and red fluorescence can be visualised on their respective channels. Overlaying of the channels shows exact overlap between the two signals

2.3.6 Various modifications applied to facilitate rescue with the SA11-N5_inline pSMART system

The lack of success of the NWU SA11-N5 pSMART reverse genetics system in the present study led to three hypotheses. The first was that there was a fundamental problem in the mammalian cell lines we were using. The second was that there was a problem with both the cell lines and/or transfection reagents, and the the third that there was a fundamental problem with the pSMART_inline plasmid set.

The main transfection cell line in use at this time was BSR-T7/5 stat(-) clone 16. This cell line is a STAT1 knockout selected for its high transfection efficiency (prepared by Prof. A.C. Potgieter, personal communication). Since we could not rescue with this cell line, other cell lines were selected to test whether the transfection cell line or infection cell line

we were using was not allowing rescue. Many of the transfection cell lines we were using were clones of transfection cell lines used for AHSV and BTV reverse genetics. Since the plasmid design of the AHSV, BTV and RV pSMART reverse genetics systems are similar, transfection reagent efficiency for each cell line was tested by Prof. A.C Potgieter (data not shown, personal communication). This showed that TransIT-LT1, jetPEI, and jetPRIME worked most effectively for BSR-T7/5 stat(-) clone 16 and BSR-C3P3 clone 4. XtremeGene 360 and jetOPTIMUS worked most effectively for BHK-C3P3 clone 8 and Vero-E6-C3P3 clone 5. ST cell transfection efficiency was tested in this project, which showed that Lipofectamine 2000 was most effective.

Replacing of MA104 with CV-1 cells and ST cells were also attempted as a method to facilitate rescue and were each used as the co-seeding and infection cell line. ST cells were chosen because they are more susceptible to infection and are believed to express a larger amount of the receptors required for viral attachment and internalisation (Prof. A.C. Potgieter, personal communication). CV-1 cells were chosen since they have been previously shown to be susceptible to rotavirus infection (Komoto et al., 2018; Estes et al., 1979).

Table 2.9 shows the rescue attempts made with each transfection reagent/transfection reagent/infection cell line combination. A total of 7 transfection reagents (TransIT-LT1, XtremeGene 360, jetPEI, jetPrime, jetOptimus, Lipofectamine 2000, and FuGene HD, 5 transfection cell lines (BSR-T7/5 stat(-) clone 16, BSR-C3P3 clone 4, BHK-C3P3 clone 8, Vero-E6-C3P3 clone 5, and ST cells, and 3 infection cell lines (MA104, ST, and CV-1) were tested. Different transfection reagent/cell line combinations were also tested to determine whether rescue was possible if a specfic transfection reagent was used. The rationale of using cell lines expressing C3P3 was to further reduce the plasmid load during transfection by omitting this plasmid in the transfection mixture, since the phCMVDream_C3P3 plasmid is large (9Kb). The rationale of using both the vaccinia virus (VV) and African Swine Fever Virus (ASFV) capping enzyme was to test whether capping was possibly happening sub-optimally with one of the two capping enzymes. ST cells do not contain a T7 polymerase and phCMWDream_C3P3 was co-transfected in a 1:1 ratio to provide T7 polymerase.

Rescue was not achieved in any attempt.

Table 2.9: Variations applied to the basic rescue protocol to facilitate rescue with the SA11-N5_inline pSMART reverse genetics system

Transfection reagent	Transfection cell line	Capping enzyme	Infection cell line	Rescue
TransIT-LT1	BSR-T7/5 stat(-) clone 16	C3P3	MA104	No
			ST	No
			CV-1	No
		ASFV	MA104	No
			ST	No
			CV-1	No
	BSR-C3P3 clone 4	C3P3	MA104	No
			ST	No
			CV-1	No
		ASFV	MA104	No
			ST	No
			CV-1	No
		VV	MA104	No
			ST	No
			CV-1	No
Lipofectamine 2000	BSR-T7/5 clone 16 stat (-)	C3P3	MA104	No
		ASFV	MA104	No
	BSR-C3P3 clone 4	C3P3	MA104	No
			ST	No
			CV-1	No
		ASFV	MA104	No
			ST	No
			CV-1	No
	ST	C3P3	ST	No
XtremeGene-360	BHK-C3P3 clone 8	C3P3	MA104	No
		ASFV	MA104	No
	Vero-E6-C3P3 clone 5	C3P3	MA104	No
jetPEI	BSR-T7/5 clone 16 stat(-)	C3P3	MA104	No
			ST	No
			CV-1	No
		ASFV	MA104	No
			ST	No
			CV-1	No
	BSR-C3P3 clone 4	C3P3	MA104	No
			ST	No
			CV-1	No
		ASFV	MA104	No

Table 2.9 – continued from previous page

Transfection reagent	Transfection cell line	Capping enzyme	Infection cell line	Rescue
			ST	No
			CV-1	No
jetPrime	BSR-T7/5 clone 16 stat(-)	C3P3	MA104	No
			ST	No
			CV-1	No
		ASFV	MA104	No
			ST	No
			CV-1	No
	BSR-C3P3 clone 4	C3P3	MA104	No
			ST	No
			CV-1	No
		ASFV	MA104	No
			ST	No
			CV-1	No
jetOptimus	Vero-E6-C3P3 clone 5	C3P3	MA104	No
FuGene HD	Vero-E6-C3P3 clone 5	C3P3	MA104	No

Since no virus could be rescued using these optimisations, it was hypothesised that a previously undetected mutation in one of the plasmids may be abrogating rescue.

During the experiments summarised in Table 2.9 NGS for the SA11-N5_inline pSMART plasmid set was repeated to confirm that the plasmid set was correct. A plasmid mixture was sent as a single library to Inqaba biotec and sequenced on an Illumina NextSeq. Analysis was done as in Section 2.3.4. No mutations were detected (data not shown).

After the cell-line/transfection reagent variations gave no rescue, it was tested whether a transcription plasmid/expression plasmid combination could facilitate rescue. A 2-step transfection procedure was developed for AHSV where six expression plasmids expressing the AHSV replication complex (VP1, VP3, VP4, VP6) as well as NS1, the interferon antagonist, and NS2 which participates in the formation of viral factories were transfected first (Kaname et al., 2013). Transfection resulted in the expression of the replication complex, the viral factories, and interferon antagonist prior to the transfection of capped (+)ssRNA synthetic transcripts in step 2, 18 hours later. The 2-step transfection approach was also used in 2016 to optimise BTV and AHSV transcript-based reverse genetics (van Rijn et al., 2016). J.F. Wentzel also used this approach to attempt rescue of SA11-N5 using DLP-derived transcripts (Wentzel, 2014).

For this MSc project, the addition of an MA104 codon optimised expression plasmid set was used in conjunction with the transcription plasmid set. The idea was to test whether co-transfection with the 11 transcription plasmids or a two-transfecion rationale where the expression plasmids were transfected 18 hours before the transcription plasmids could

facilitate rescue of SA11-N5. Either the plasmids encoding the viroplasm (NSP2, NSP5, and NSP6), or the complete set encoding the replication complex, the core, DLP, the innate immune antagonist, and viroplasm (VP1, VP2, VP3, VP6, NSP1, NSP2, NSP5, and NSP6) were transfected. Table 2.10 shows the rescue attempts using the expression plasmid set. No rescue could be achieved using any of the described variations.

Table 2.10: Use of transcription and expression plasmid co-transfection to facilitate rescue

Expression mix composition	Expression mix transfection reagent	Expression mix transfection time point	Ratio[a] Tr:Ex	Rescue
phCMVDream VP1,2,3, 6 and NSP1,2,5,6	TransIT-LT1	18h before	1:3	No
			2:2	No
			3:1	No
	Lipofectamine 2000	18h before	1:3	No
			2:2	No
			3:1	No
	TransIT-LT1	co-transfection	2:2	No
phCMVDream NSP1,2,5,6	TransIT-LT1	18h before	1:3	No
			2:2	No
			3:1	No
	Lipofectamine 2000	18h before	1:3	No
			2:2	No
			3:1	No
	TransIT-LT1	co-transfection	2:2	No

[a] Tr = Transcription plasmid mixture mass in µg, Ex = Expression plasmid mixture mass in µg

2.3.7 Mycoplasma contamination in cell lines

In 2020 a paper was published detailing the authors' rotavirus reverse genetics protocol (Philip et al., 2020). They discussed factors that impact rescue. The first factor was the transfection cell line being allowed to grow to over confluence. This was believed to cause cells to enter senescence and the cell line could not recover, even after multiple passages. The second was the presence of mycoplasma in the BHK-T7 cells being used. The authors stated that mycoplasma was most often associated with their transfection cell line, and they were unable to rescue in the presence of mycoplasma.

Mycoplasma *Spp.* are round or filamentous bacteria that are characteristic due to their lack of a cell wall and small size (Young et al., 2010). Mycoplasma is commonly found in the human respiratory and urogenital tracts (Rottem & Naot, 1998). Mycoplasmas contaminate up to 35% of cell cultures, and contamination completely alters cell physiology. Mycoplasma *Spp.* do not possess the genes necessary for amino acid biosynthesis, and compete with the host for amino acids (Himmelreich et al., 1997). Most importantly, Mycoplasma use the arginine dihydrolase pathway for generating ATP (Pollack et al., 1997). This depletes cellular arginine and impacts protein synthesis, and thereby cell growth and

division. Further, this results in chromosomal aberrations in the host cell, since histones are rich in arginine. These aberrations include chromosomal breakage, translocations, a reduction in chromosome number and new or additional chromosome varieties (Rottem & Barile, 1993).

Contamination can occur readily, since the standard 0.22 μM filter pore size allows mycoplasma to pass through. Mycoplasma are 100 nm in size and are pleomorphic, allowing them to pass through or be forced through the filter membrane. Cell cultures are most commonly contaminated with *M. orale*, *M. arginini*, or *Acholeplasma laidlawii*.

The cell lines used in our laboratory were then tested using the LookOut PCR mycoplasma detection kit. None of our transfection cell lines were positive. The internal control band is 260 bp in size, and the positive band is at 480 bp. Our MA104 and ST cell lines were found to be positive, Figure 2.30. No positive but an internal control band were detected for BSR5-T7/5, which only showed amplification of the 260 bp internal control band. MA104 and ST cells both only had amplification of the positive 480 bp band, indicating very heavy contamination. CV-1 cells were then used as the primary infection cell line. However, rescue could still not be attained when using this cell line. A plaque assay with SA11-N2 showed that CV-1 cells only support SA11 to titres of approximately 10^5 or 10^6 (data not shown). This resulted in the CV-1 cells being abandoned for all our subsequent work. The BSR-T7/5, BHK-C3P3 clone 8, BSR-C3P3 clone 4, Vero-E6-C3P3 clone 5 cells, and CV-1 cells were also tested, and tested negative (data not shown).

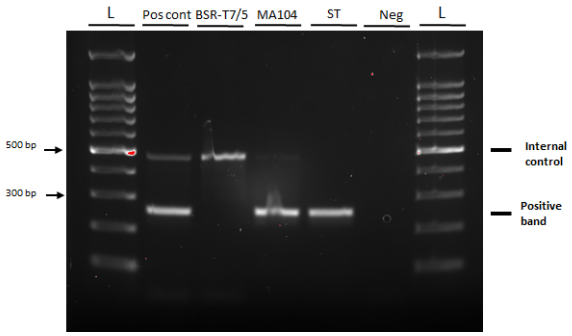


Figure 2.30: 2% Agarose gel of Sigma LookOut Mycoplasma amplicons from BSR-T7/5, MA104 and ST cells. When compared to the positive control, MA104 and ST cells were heavily contaminated, since the ratio of the amplification efficiency of the internal control band at 480 bp to the positive band at 280 bp determines the amount of contamination.

Mycoplasma free BSR-T7/5 and MA104 cells were obtained from Prof. H.G. 'O Neill (University of the Free State, Bloemfontein). The BSR-T7/5 cells were confirmed to be transfectable and capable of transcription from a T7 promoter of a GFP construct. The MA104s were also confirmed to be permissive of infection by plaque assay.

However, two attempts at rescuing with the SA11-N5 pSMART system in mycoplasma-free cells were also not successful.

2.3.8 Summary

The initial success of the SA11-N5 pSMART system claimed a significant (6-log) improvement over the SA11-L2 pT7 system, however rescue of the NWU SA11-N5 reverse genetics system could not be repeated. This led to the following approach, results, and conclusions in this chapter to troubleshoot the NWU SA11-N5 pSMART reverse genetics system:

Reorientation of the transcription cassette

1. The NWU SA11-N5 pSMART plasmid set was extremely unstable. There were mutations and deletions in multiple plasmids.
2. Sanger and NGS sequencing data was reanalysed and showed that both pSMART-T7_RV-SA11_GS7_NSP3 and pSMART-T7_RV-SA11_GS9_VP7 used by previous students in our laboratory did not possess a ribozyme or T7 terminator. This may have made rescue impossible.
3. The literature showed that changing the orientation of the transcription cassette so that replication of the plasmid and transcription of the transcription cassette occurs in the same direction, may improve stability.
4. Transcription cassettes were reorientated using InFusion and NEBuilder seamless cloning.
5. Sanger sequencing and NGS showed that cloning was successful, and the orientation being successfully changed. Furthermore, no mutations or deletions were detected following cloning and repeated extraction of the plasmids. This showed that the stability was markedly improved.

Rescue with the pSMART SA11-N5 plasmid set

6. The plasmids were endotoxin-free purified, and transfected into BSR-T7/5 cells, but no rescue could be achieved. Seven different cell lines and five transfection reagents were used to determine if they could facilitate rescue, also without any success.
7. An expression plasmid approach was used where plasmids expressing the replication complex, SLP, and DLP were either co-transfected with the transcription plasmids or transfected 18h before the transcription plasmids. Rescue was not achieved.

Mycoplasma contamination in cell lines

8. Mycoplasma was detected in our MA104 and ST cells. This may have made rescue impossible, due to the damage sustained to the cell lines' genomes and protein expression capacity.
9. After replacing these cell lines with new, uncontaminated cells, rescue was still not possible with the NWU SA11-N5 plasmid set.

   Since we could not rescue with our reorientated SA11-N5 pSMART system, we switched to the 2017 Kanai *et al.* pT7 reverse genetics plasmid set which we extracted

from glycerol stocks. This system did support rescue and was used for all experiments in Chapter 3.

The results described in this chapter indicate that rescue was actually never achieved with the SA11-N5 pSMART system due to multiple problems with the plasmid set developed by L. Geldenhuys (2017) and M. GJ. Huyzers (2020). My results show that the plasmids contained deletions, mutations, and insertions that could be traced back to the original archived glycerol stocks frozen away by L. Geldenhuys. This indicated that the plasmid set was inherently unstable, especially since M.J. Visser observed multiple different deletions or mutations when growing up bacteria for plasmid extraction. In this chapter, I was able to show that by reorientating the transcription cassette in the plasmid backbone, the stability of all eleven reverse genetics transcription plasmids was improved. Unfortunately, I was unable to demonstrate whether this plasmid set supported rescue, since it was discovered that our infection cell lines were heavily contaminated with mycoplasma. Due to time constraints, we were unable to extensively test new transfection and infection cell lines that replaced our mycoplasma contaminated ones.

Chapter 3

Investigation of GS6(VP6)/GS10(NSP4) co-reassortment using SA11-based reverse genetics

3.1 Introduction

An important understudied aspect of live-attenuated rotavirus vaccines is the reassortment safety profile of live-attenuated rotavirus vaccines. Live-attenuated rotavirus vaccine strains have been shown to be able to reassort with rotavirus field strains (Donato et al., 2012; Rose et al., 2013). This may have two implications. It could result in reduced vaccine effectiveness or in reassortant vaccine strains that are no longer attenuated. This is especially relevant in an environment where there are high rates of rotavirus infection, which increases the likelihood of reassortment events. To eventually apply rotavirus reverse genetics to the production of rationally designed live attenuated vaccines, the identification of determinants of reassortment is important to facilitate the introduction of novel safety features into next-generation vaccines to prevent or reduce reassortment.

GS6(VP6)/GS10(NSP4) co-reassortment is a relevant field reassortant that may represent a protein function reassortment restriction. This protein-protein interaction is essential for the production of rotavirus TLPs from DLPs. In work done by Itturiza-Gòmara and colleagues in 2003 it was shown that GS10(NSP4) genotypes segregate according to RVA subgroup (SG). Wa-like (E1) GS10(NSP4) segregates with Wa-like VP6 SGII, while DS-1 like NSP4s (E2) segregates with VP6 SGI, which is found in DS-1 like strains (Iturriza-Gomara et al., 2003). The only documented interaction between VP6 and NSP4 is the DLP binding domain in NSP4 that transports DLPs from the viroplasm by interacting with VP6 (Au et al., 1989; Taylor et al., 1993; Au et al., 1993; Taylor et al., 1996). This led to the hypothesis that this protein interaction may have an effect on the reassortment of the genome segments that encode for VP6 and NSP4. As discussed in Chapter 1, the sequencing performed by Tamim and colleagues identified multiple GS6(VP6)/GS10(NSP4) field reassortants (Tamim et al., 2019). Their work identified that an I2/E1 combination, but no I1/E2 reassorants were sequenced. They also documented an I2/E2 co-reassortment into a Wa-like backbone. This raises an important question whether this possible restriction of reassortment can be applied to improve vaccine safety.

Reverse genetics now allows the interrogation of specific amino acids by rescuing mutant or chimeric viruses. All GS6 (VP6) / GS10 (NSP4) receptor interaction work was performed *in vitro*, and the results generated needed to be analysed using replicating virus in cell culture (Au et al., 1989, 1993; Taylor et al., 1992, 1993, 1996). The aim of this study was to place a Wa-like (I1) VP6 into the SA11 E2 background to show whether this combination is unable to rescue or has reduced fitness. A separate DS-1 like (I2) VP6 was included in the study to show whether a VP6 of the same genotype can be rescued in an SA11 background. Mutagenesis was also performed to mutate amino acids 169 and 174 in the C-terminal of NSP4 to determine if this has an effect on the NSP4/VP6 interaction. This showed whether this protein interaction places selective pressure on GS6(VP6)/GS10(NSP4) reassortment and if it influences whether these genome segments co-reassort or not.

3.2 Materials and methods

All methods used in this Chapter are described in Chapter 2, except for the methods described below.

3.2.1 Plasmid construction

To design VP6(GS6) encoding plasmids for this study, two Mozambican strains: RVA/Human-wt/MOZ/0308/G2P[4] GS6(VP6) (MG926729.1) and RVA/Human-wt/MOZ/0060a GS6(VP6) (MG926762.1) were selected since they are Wa-like SGII and DS-1 like SGI strains respectively (Strydom et al., 2019a,b).Three transcription plasmids were designed and ordered from Genscript. For GS6(VP6), pSMART-T7_RV-Moz_308_GS6_VP6 and pSMART-T7_RV-Moz-0060a_GS6_VP6 were designed to contain the ORF for the respective proteins but to contain the SA11 5' and 3' UTRs to ensure genetic compatibility, Figure S4.

For the NSP4(GS10) encoding plasmid RVA/Human-wt/MOZ/0060a /2012/G12P[8]P[14]_GS10(NSP4) (MG926762.1) was selected and pSMART-T7_RV-SA11 _NSP4_Moz_0060a_NSP4_DLP-BD, was designed so that nucleotides 521-566 (encoding aa 161-175) in the SA11-N5 GS10(NSP4) were replaced with those of RVA/Human-wt/MOZ/0060a/2012/G12P[8]P[14]_GS10(NSP4), Figure S5.

The above-mentioned plasmids were synthesised by Genscript (Piscataway, USA) and received as lyophilised plasmids. The plasmids were transformed into EPI400 cells. Plasmids were extracted from colonies of each construct and sent for Sanger sequencing. One colony of each construct was selected for endotoxin-free plasmid purification, Sections 2.2.1.6 - 2.2.1.10.

Two additional plasmids with mutations in SA11-N5 GS10(NSP4) were generated by site-directed mutagenesis. These mutations were NSP4 R169I and NSP4 A174S. Primers were designed to amplify the complete pSMART_RV_SA11-

N5_GS10(NSP4) plasmid and simultaneously mutate single nucleotides to induce amino acid changes. For the NSP4 R169I mutation, the plasmid was amplified using NSP4_mut_R169I_For (5'- GAAGTGACTGCAGCAATGTAAGAGG-3') and NSP4_mut_R169I_Rev (5'- CTGCAGTCACTTCTATTGGTTCATAAGG-3'). The reverse primer was used to mutate 547.C>A. For the NSP4 A174S mutation, A174S_mut_For (5'-GAGAAGTGACTGCATCAATGTAAGAGG-3') and A174S_mut_rev (5'-GCAGTCACTTCTCTTGGTTCATAAGG-3') was used to amplify the plasmid and induce a 561.G>T mutation using the forward primer. Infusion seamless cloning was then used to anneal the overhangs generated. All Infusion reactions were then transformed into EPI400 cells. Plasmids were purified using an Endofree Maxi plasmid kit from Qiagen (Hagen, Germany), Section 2.2.1.8. Figure 3.1 shows the design of each construct.

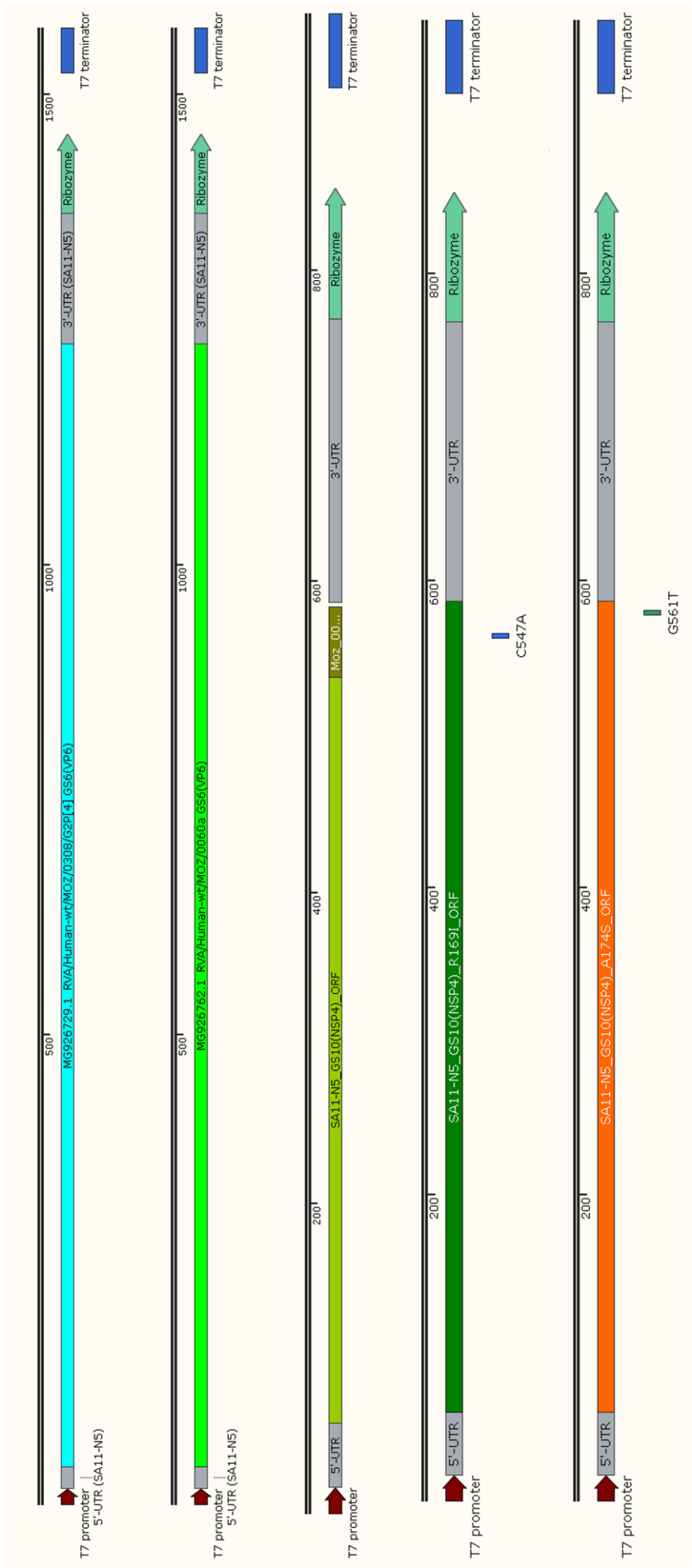


Figure 3.1: Schematic showing the design of the transcription cassettes of GS6(VP6) and GS10(NSP4) constructs used in this project. pSMART-T7_RV-Moz_308_GS6_VP6, pSMART-T7_RV-Moz-0060a_GS6_VP6, and pSMART-T7_RV-SA11_NSP4_Moz_0060a_NSP4_DLP-BD were ordered from Genscript. pSMART_RV_SA11-N5_NSP4_A174S, and pSMART_RV_SA11-N5_NSP4_R169I were constructed from pSMART_RV_SA11-N5_GS10(NSP4) using site-directed mutagenesis.

3.2.2 SA11-L2 pT7 reverse genetics protocol

All transfections were performed in mycoplasma-free BSR-T7/5 cells seeded in 6 well plates, Section 2.2.2. The original Kanai *et al.* 2017 plasmid set was used with the following modifications. Both *Cricetinae* (Hamster) codon-optimised D1R and D12L were previously ordered from Genscript in phCMVDream, and replaced the D1R and D12L plasmids from the plasmid set purchased from Addgene. The plasmid encoding FAST was also not included in transfection mixtures, since multiple groups have shown that it is not required for rescue. All plasmids were measured using Nanodrop spectrophotometry and equimicrogram mixtures were prepared by adding 250 ng each of pT7_SA11_GS1, pT7_SA11_GS2,pT7_SA11_GS3,pT7_SA11_GS4, pT7_SA11_GS5, pT7_SA11_GS6, pT7_SA11_GS7, pT7_SA11_GS9, pT7_SA11_GS10, phCMVDream_D1R, phCMVDream_D12L and 750 ng of pT7_SA11_GS8 and pT7_SA11_GS11. The required plasmids were exchanged if a reassortant was being rescued.

The plasmid mixture was vortexed and measured using nanodrop spectrophotometry to ensure that the correct mass of DNA was being transfected. 250 µl of Opti-MEM was added to a 2 ml lo-bind Eppendorf tube and Transit-LT removed from 4 °C storage. The reagents were allowed to reach room temperature. 4 µg of the plasmid mixture was pipetted into the Opti-MEM and 10 µl (2.5 µl per µg DNA) added, and vortexed for 2 seconds. Transfection mixtures were incubated for 30 minutes. Before transfection, the growth medium was removed and the monolayer washed once with 2 ml of PBS. Transfection was then performed by adding the transfection complexes dropwise directly onto the monolayer, and the plate was incubated on the bench for 3 minutes. Complete medium (DMEM, 5% FBS, 1% NEAA, 1%AA) was placed on the monolayer and the cells were incubated for 16-18 hours at 37 °C and 5% CO_2 in a humidified incubator.

The following morning, the medium was removed, and washed twice with 2 ml PBS. 2 ml fresh FBS-free DMEM (1% NEAA, 1%AA) The transfected cells were then incubated for another 24 hours. 48 hours after transfection, coseeding was performed by detaching MA104 cells in FBS, pelleting at 100 x *g*, and resuspending in 1 ml 37°C DMEM to remove the FBS, Section 2.2.2.3. This was repeated, and the cells counted using a stage haemocytometer by adding 10 µl of cells suspesion to 10 µl 0.4% trypan blue. The 1 ml suspension was then divided amongst the number of wells to be co-seeded. The seeding density was between 2 x 10^5 and 5 x 10^5 cells per well. 1 hour after seeding, 1 mg / ml of porcine trypsin type IX was added to a final concentration of 0.5 µg/ml.

Passaging of viruses were performed as described in Section 2.2.2.4.

3.2.3 Genome segment-specific single-step cDNA synthesis

In order to sequence the rotavirus genome, dsRNA must be converted to cDNA. When Sanger sequencing is performed, the rotavirus genome segments are amplified in separate reactions using primers that are specific to a single genome segment. For this project,

a SuperScript III one-step RT-PCR kit (Invitrogen, Waltham, USA) was used. This kit works on two principles. First, RNA is converted to cDNA by using a M-MLV reverse transcriptase (RT) engineered to have both reduced RNaseH activity and to be more thermally stable. After cDNA synthesis, the RT is denatured and normal PCR is performed to amplify the cDNA.

In this project, an additional step was added prior to performing cDNA synthesis. dsRNA is extremely stable and usually requires denaturation using heat and DMSO or methylmercury hydroxide (MMOH) in order to properly denature ssRNA when performing two-step cDNA synthesis. For single-step synthesis, 1µl of extracted dsRNA was added to the required primer concentration for the RT-PCR reaction, and then diluted in the required volume of nuclease-free water. Primers are listed in Table 3.1. This was then heated to 95°C for 30 seconds and immediately placed on ice. The rationale behind this is that heat will momentarily denature the dsRNA to linear ssRNA (Prof. A.C. Potgieter, personal communication). As the reaction is cooled, the primers will anneal to the ssRNA, preventing reannealing to dsRNA. This may allow dsRNA to be preferentially amplified above any plasmid that may still be present from the transfection step. To this the required volumes of reaction buffer and RT / DNA polymerase were added, Table 3.2. The reaction conditions were as follows, For the cDNA synthesis: 1 cycle of 50°C for 30 minutes and 94 °C for 2 minutes, for PCR: 40 cycles of 94 °C for 15 seconds, 55 °C for 30 seconds, 68 °C for 1 minute 30 seconds, and a final extension at 68 °C for 5 minutes.

Table 3.1: Primers used for the synthesis of cDNA from GS6 (VP6) and GS10 (NSP4)

Primer name	Sequence	T_m	Length
SA11corGS6F	5'-taatacgactcactataggcttttaaacgaag-3'	45°C	32-mer
SA11 GS6iNR	5'-gggaccatgccggcctcacatcctctcac-3'	49°C	29-mer
SA11corGS10F	5'-taatacgactcactataggcttttaaaagttc-3'	42°C	32-mer
SA11GS10iNR	5'-gggaccatgccggccggtcacattaagacc-3'	43°C	30-mer

Table 3.2: SuperScript III RT-PCR reaction compostion

Component	final volume or concentration
2x Reaction Mix	25 µl
Template RNA	1µl
Forward primer	0.5 µM
Reverse primer	0.5 µM
SuperScript RT/Plaqtimum Taq mix	2 µl
Nuclease-free water	to 50 µl

3.2.4 Plaque assay and growth kinetics

Viral replication is analysed by growth curves, in which viral multiplication is measured with respect to time. Growth curves allow the comparison of viral growth under different conditions or the comparison of replication of different viral mutants. This allows the assessment of growth dynamics with respect to a wild-type virus.

Prior to the plaque assay, MA104 cells were seeded in 12 well plates and grown to 100% confluence and 2.4% Avicel RC-581 (FMC biopolymer, Philadelphia, USA) was prepared in distilled water and autoclaved. Serial dilutions (10^0 to 10^{-10}) of trypsin-activated viral stocks were prepared in DMEM and placed on the 12 well plates for 1 hour. During incubation, growth medium was prepared containing 2x DMEM, 2% NEAA, 2% Anti-Anti and 2 µg/ml porcine trypsin type IX. The overlay was then prepared by adding growth medium to Avicel in a 1:1 ratio, giving a final Avicel concentration of 1.2%, 1x DMEM, 1% NEAA, 1% Anti-Anti, and 1 µg/ml porcine trypsin. After one hour, the incoculum was removed and 1 ml of the overlay was placed in each well. Plates were incubated at 37 °C, 5% CO_2 for 3 days without disturbing the plates. After 3 days, the overlay was removed by pipetting, washed once with PBS, and fixed with 4% formaldehyde for 30 minutes at room temperature. Plaque assays were stained with crystal violet (0.25% crystal violet in 20% methanol,(Sigma-Aldrich, St-Louis, USA). Plaques were then counted to determine the titre. This gave a maximum titre in PFU/ml for each virus.

To perform growth curves, seven 25 cm^3 flasks, representing 7 time points, 12 hours apart, were infected with whole lysates at an MOI of 0.001. At 0, 12, 24, 36, 48, 60, and 72 hours, each flask designated for that time point was frozen at -20 °C. After completion of the time points, each flask was freeze/thawed three times. The whole lysates were then serially diluted in separate experiments in triplicate by activating the whole lysate on separate days and performing a plaque assay as described above to assess the titre at that specific time point. The plaque assays were then incubated and stained as described. The average of each time point's maximum titre was then plotted against the number of hours. To perform statistical analyses, each time point was normalised to the 0 hour time point by dividing each time point by the 0 hour time point. This was then log transformed by calculating the $\log_{10}$ of each value after normalisation in order to achieve a normally distributed data set. IBM SPSS (IBM, Armonk, USA) was then used to perform a two-way Analysis of Variance (ANOVA) using a least significant difference (LSD) post hoc test. This compares each virus with all viruses in the experiment. Since for this project only each virus compared to SA11 was of interest, the p-values of this comparison were selected. $p < 0.05$ was considered statistically significant.

3.3 Results and Discussion

3.3.1 Analysis of selected VP6 and NSP4 amino acid sequences to inform rational construct design

To confirm the results reported in the literature, additional sequences of GS6 (VP6) and GS10 (NSP4) were obtained to determine whether GS10(NSP4) genotype segregates with GS6(VP6) subgroup. These data were then used to inform the rational design of the constructs to test the effect of the NSP4 DLP binding domain on the co-reassortment of GS6(VP6) and GS10(NSP4).

Random sequences of rotavirus A strains (RVA) were selected that were part of recent

whole genome sequences of circulating field strains. Sequences were only included if they were generated using NGS. Full-length nucleic acid sequences of GS6 (VP6) and GS10 (NSP4) were downloaded from Genbank. This project required an analysis of the amino acid sequences of the DLP binding domain in NSP4 and the amino acids that determine the VP6 subgroup. The ORFs were extracted from full-length genome segment sequences and converted to amino acid sequences using MEGA7. The amino acid alignment was then performed in MEGA7.

The NSP4 amino acid sequences were aligned in order to compare the DLP-binding domains between Wa-like (E1) NSP4s and DS-1 like (E2) NSP4s, Figure 3.2. This figure shows the C-terminal end of NSP4. 38 sequences were aligned as representatives of Wa-like and DS-1-like NSP4s.

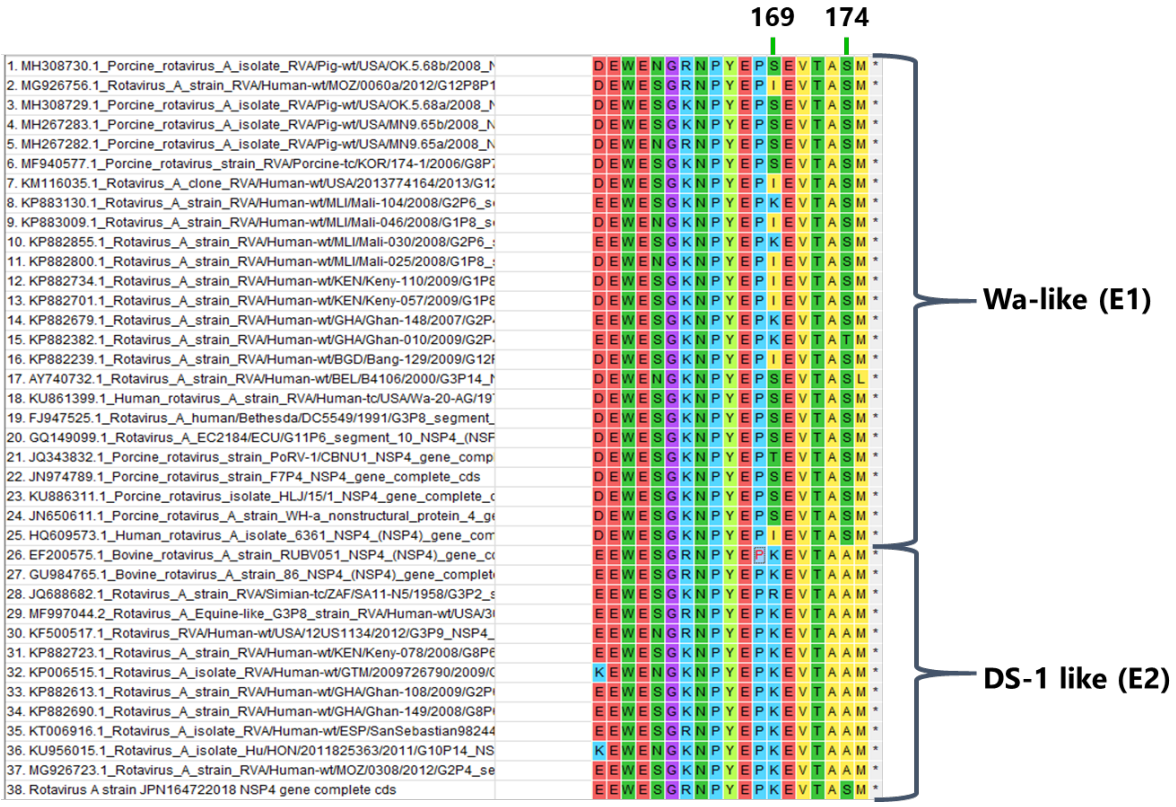


Figure 3.2: RVA NSP4 DLP binding domain amino acid sequence alignment. This figure shows E1 and E2 NSP4s. Note the clear segregation of amino acid sequence between E1 and E2 NSP4 genotypes at amino acid 174.

The amino acid alignment analysis showed that the DLP-binding domain amino acid sequence only varies at two positions, namely positions 169 and 174. At position 169 there were three different amino acids. Amino acids varied between polar serine, nonpolar isoleucine, and positively charged lysine. DS-1-like (E2) strains seem to prefer lysine at position 169, while there is more variation between serine, isoleucine, and lysine for Wa-like (E1) NSP4s.

At NSP4 amino acid 174 there was clear segregation between Wa-like (E1) and DS-1-like

(E2). Wa-like (E1) NSP4s have a polar serine at this position, whereas DS-1 like E2 NSP4s have a nonpolar alanine. This showed possible strong selection of this amino acid, and since position 174 segregates between the genotypes, it may function as a restriction of reassortment.

The VP6 ORFs of the strains analysed in Figure 3.2 were also aligned and analysed. Work from Lopez *et al.* showed that positions 305 and 306 in VP6 determines SGII, whereas positions 172 and 305 determine SGI (Lopez et al., 1994). This work was carried out using monoclonal antibodies, so in this study it was decided to interrogate the amino acid sequence more widely to see if there is still variation at position 172 in SGII stains and at 306 in SGI strains, even though these amino acids do not determine the subgroup. Alignment showed that 3 separate groups of strains could be visualised. The first group had the following mutations: 172A, 305A, and 306N and could not be assigned to a subgroup. The second group had 172M or 172I, 305N, and 305A, classifying them as SGII strains. The third group had mutations 172A, 305A, and 306A, and could be classified as SGI strains.

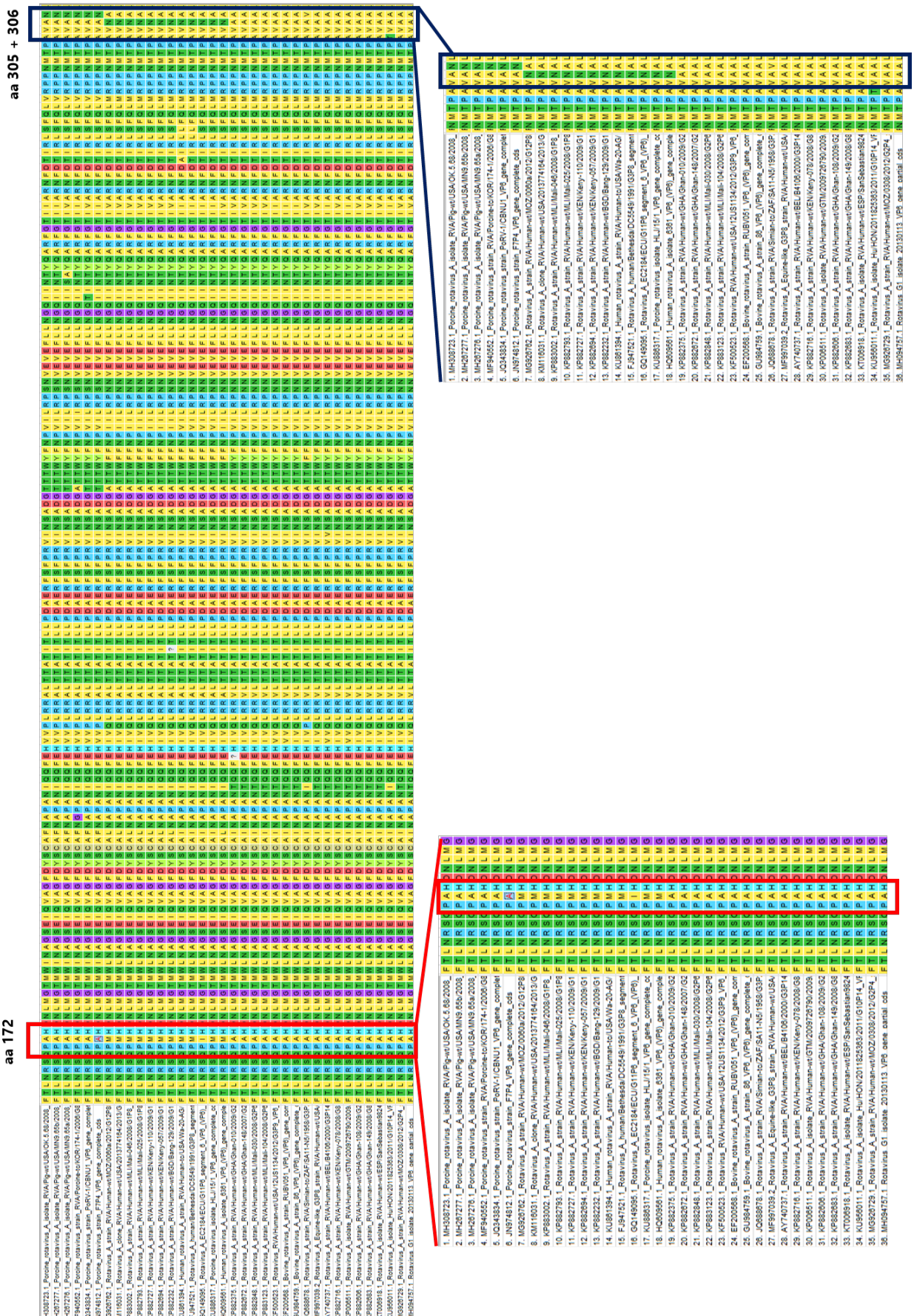


Figure 3.3: Alignment of RVA VP6 amino acid sequences obtained from Genbank. These sequences correspond to the viruses for which the NSP4s were aligned in figure 3.2. The red box indicates amino acid position 172. The blue box indicates amino acids 305 and 306.

The results from the NSP4 and VP6 amino acid alignments were then collated in Table 3.3. These results provide three insights into GS6(VP6)/GS10(NSP4) co-reassortment. First, of note are the five I5 VP6 strains that possess E1 NSP4s wherein there were the following three variations in VP6 (172A, 305A, 306N) and three variations in NSP4 (169S, 169T, and 174S). All five strains could be classified as non-SGI / SGII. Second, with one exception (Rotavirus_A_EC2184/ECU/G11P6), all the I1 VP6 strains had the same amino acids 172M, 305N, 306A and clustered with NSP4 169I or 169S and 174S. Third, I2 VP6 strains with 172A, 305A, 306A clustered with NSP4 169K or, in one case, 169S. It is important to note that SA11-N5 (which has an identical amino acid sequence to SA11-L2) possesses a K169I mutation in NSP4.

These results show that there is segregation between the three groups of strains analysed and may point to a selection that occurs among wild-type strains to maintain these constellations of amino acids. Mutation of these amino acids may result in weaker interaction of VP6 and NSP4, although mutation of the amino acids may not be lethal. This may result in a reduction in fitness, which is lethal to a virus cocirculating with viruses that are more fit. This may explain why other combinations of GS6 (VP6) / GS10 (NSP4) are not observed in field strain sampling.

Table 3.3: Summary of GS6(VP6) and GS10(NSP4) of strains analysed in this study

Strain name	VP6 relevant mutations	NSP4 DLP-BD	VP6/NSP4 Genotype	Accession numbers
Porcine_rotavirus_A_isolate_RVA/Pig-wt/USA/OK.5.68/2008	172A, 305A, 306N	169S, 174S	I5-E1	MH308723.1, MH308730.1
Porcine_rotavirus_A_isolate_RVA/Pig-wt/USA/MN9.65b/2008	172A, 305A, 306N	169S, 174S	I5-I1	MH267277.1, MH267283.1
Porcine_rotavirus_A_isolate_RVA/Pig-wt/USA/MN9.65a/2008	172A, 305A, 306N	169S, 174S	I5-E1	MH267276.1, MH267282.1
Porcine_rotavirus_strain_PoRV-1/CBNU1	172A, 305A, 305N	169T, 174S	I5-E1	JQ343834.1, JQ343832.1
Porcine_rotavirus_strain_RVA/Porcine-tc/KOR/174-1/2006/G8P7	172A, 305A, 306N	169S, 174S	I5-E1	MF940552.1, MF940577.1
Porcine_rotavirus_strain_F7P4	172A, 305A, 306N	169S, 175S	I5-E1	JN974812.1, JN974794.1
Porcine_rotavirus_isolate_HLJ/15/1	172M, 305N, 306A	169S, 174S	I1-E1	KU886317.1, KU886311.1
Rotavirus_A_strain_RVA/Human-wt/MOZ/0060a/2012/G12P8P14	172M, 305N, 306A	169I. 174S	I1-E1	MG926762.1, MG926756.1
KM116031.1_Rotavirus_A_clone_RVA/Human-wt/USA/2013774164/2013/G12P8	172M, 305N, 306A	169I, 174S	I1-E1	KM116031.1, KM116035.1
Rotavirus_A_strain_RVA/Human-wt/MLI/Mali-046/2008/G1P8	172M, 305N, 306A	169I, 174S	I1-E1	KP883002.1, KP883009.1
Rotavirus_A_strain_RVA/Human-wt/MLI/Mali-025/2008/G1P8	172M, 305N, 306A	169I, 174S	I1-N/A	KP882793.1, KP882700.1
Rotavirus_A_strain_RVA/Human-wt/KEN/Keny-110/2009/G1P8	172M , 305N, 306A	169I, 174S	I1-E1	KP882727.1, KP882734.1
Rotavirus_A_strain_RVA/Human-wt/KEN/Keny-057/2009/G1P8	172M, 305N, 306A	169I, 174S	I1-E1	KP882694.1, KP882701.1
Rotavirus_A_strain_RVA/Human-wt/BGD/Bang-129/2009/G12P6	172M, 305N, 306A	169I, 174S	I1-E1	KP882232.1, KP882239.1
Human_rotavirus_A_strain_RVA/Human-tc/USA/Wa-20-AG/1974	172M, 305N, 306A	169S, 174S	I1-E1	KU861394.1, KU861399.1
Rotavirus_A_human/Bethesda/DC5549/1991/G3P8	172M, 305N, 306A	169S, 174S	I1-E1	FJ947521.1, FJ947525.1
Rotavirus_A_EC2184/ECU/G11P6	172I, 305N, 306A	169S, 174S	I1-E1	GQ149095.1, GQ149099.1
Human_rotavirus_A_isolate_6361	172M, 305N, 306A	169I, 174S	I1-E1	HQ609561.1, HQ609573.1
Rotavirus_A_strain_RVA/Human-wt/MLI/Mali-030/2008/G2P6	172A, 305A, 306A	169K, 174S	I2-E2	KP882848.1, KP882855.1
Rotavirus_A_strain_RVA/Human-wt/GHA/Ghan-148/2007/G2P4	172A, 305A, 306A	169K, 174S	I2-E2	KP882672.1, KP882679.1
Rotavirus_A_strain_RVA/Human-wt/GHA/Ghan-010/2009/G2P4	172A, 305A, 306A	169K, 174T	I2-E2	KP882375.1, KP882382
Rotavirus_A_strain_RVA/Human-wt/MLI/Mali-104/2008/G2P6	172A, 305A, 306A	169K, 174S	I2-E2	KP883123.1, KP883130.1
Rotavirus_RVA/Human-wt/USA/12US1134/2012/G3P9	172A, 305A, 306A	169K, 174A	I2-N/A	KF500523.1, KF500517
Bovine_rotavirus_A_strain_RUBV051	172A, 305A, 306A	169K, 174A	I2-E2	EF200568.1, EF200575
Bovine_rotavirus_A_strain_86	172A, 305A, 306A	169K, 174A	I2-E2	GU984759.1, GU98476
Rotavirus_A_strain_RVA/Simian-tc/ZAF/SA11-N5/1958/G3P2	172A, 305A, 306A	169R, 174A	I2-E2	JQ688678.1, JQ688682.1
Rotavirus_A_Equine-like_G3P8_strain_RVA/Human-wt/USA/3000390639/2015/G3P8	172A, 305A, 306A	169K 174A	I2-E2	MF997039.2, MF997044.2
Rotavirus_A_strain_RVA/Human-wt/BEL/B4106/2000/G3P14	172A, 305A, 306A	169S, 174S	I2-E5	AY740737.1, AY740732.1
Rotavirus_A_strain_RVA/Human-wt/KEN/Keny-078/2008/G8P6	172A, 305A, 306A	169K, 174A	I2-E2	KP882716.1, KP882723.1
Rotavirus_A_isolate_RVA/Human-wt/GTM/2009726790/2009/G8P14	172A, 305A, 306A	169K, 174A	I2-E2	KP006511.1, KP006515.1
Rotavirus_A_strain_RVA/Human-wt/GHA/Ghan-108/2009/G2P6	172A, 305A, 306A	169K, 174A	I2-E2	KP882606.1, KP882613.1
Rotavirus_A_strain_RVA/Human-wt/GHA/Ghan-149/2008/G8P6	172A, 305A, 306A	169K, 174A	I2-E2	KP882683.1, KP882690.1
Rotavirus_A_isolate_RVA/Human-wt/ESP/SanSebastian98244047_DS-1/2015/G3P8	172A, 305A, 306A	169K, 174A	I2-E2	KT006918.1, KT006916.1
Rotavirus_A_isolate_Hu/HON/2011825363/2011/G10P14	172A, 305A, 306A	169K, 174A	I2-N/A	KU956011.1, KU956015.1
Rotavirus_A_strain_RVA/Human-wt/MOZ/0308/2012/G2P4	172A, 305A, 306A	169K, 174A	I2-E2	MG926729.1, MG926723.1

3.3.2 Generation of plasmids to evaluate the effect of variations in VP6 and NSP4 on NSP4/DLP binding

In this project, we wanted to investigate the effect of the amino acid mutations identified in Section 3.3.1 on NSP4/DLP binding. To do this, the following rationale was developed. Firstly, we wanted to select a strain with the same VP6 subgroup (SGI) as SA11 to show whether a VP6 of the same subgroup affects growth and thereby possibly NSP4 binding. Secondly, we wanted to select a SGI strain to determine whether a VP6 of a different subgroup could be rescued. Thirdly, we wanted to design an SA11 NSP4 that contains the DLP binding domain from the SGI strain. Fourthly, we wanted to analyse NSP4 amino acids 169 and 174, by mutating the SA11 NSP4 amino acids to those observed in Wa-like E1 strains. We selected two strains. Rotavirus_A_strain_RVA/Human-wt/MOZ/0308/2012/G2P4 and Rotavirus_A_strain_RVA/Human-wt/MOZ/0060a/2012/G12P8P14 sequenced by our collaborators at the University of the Free State (Strydom et al., 2019a,b). Rotavirus_A_strain_RVA/Human-wt/MOZ/0308/2012/G2P4 is a SGI strain. Rotavirus_A_strain_RVA/Human-wt/MOZ/0060a/2012/G12P8P14 is a SGII strain.

As indicated in Section 3.2.1, five constructs were designed to evaluate the effect of the VP6 and the DLP binding domain on NSP4 on the GS6 (VP6) / GS10 (NSP4) co-reassortment, Table 3.4. Two VP6 constructs, Moz308 (SGII) and Moz0060a (SGI) VP6, and one SA11 NSP4 containing the Moz0060a NSP4 DLP binding domain, were purchased from Genscript. Two SA11 NSP4s, containing the R169I and A174S mutations, were generated using site-directed mutagenesis. Both plasmids received from Genscript, pSMART-T7_RV-SA11_NSP4_R169I, and the pSMART-T7_RV-SA11_NSP4_A174S were transformed into EPI400 cells as described in Section 2.2.1.6. Plasmids were purified from overnight cultures using a Qiagen miniprep kit. To evaluate the transcription cassette of the plasmids prior to use in reverse genetics, purified plasmids were sent for Sanger Sequencing at Inqaba biotec. Sequences were analysed using MEGA 7. Figures 3.4 and 3.5 show the sequence alignment of the forward and reverse Sanger sequences of the plasmid extracted from a selected colony with each respective reference. The reverse complement of the Upstream_pSMART sequences were aligned with the Downstream_pSMART sequences.

Table 3.4: Summary of GS6(VP6) and GS10(NSP4) constructs designed in this study

Plasmid name	Relevant mutations	Strain	Genotype
pSMART-T7_RV-Moz308_GS6(VP6)	172A, 305A, 306A	Rotavirus_A_strain_RVA/Human-wt/MOZ/0308/2012/G2P4	I2
pSMART-T7_RV-Moz0060a_GS6(VP6)	172M, 305N, 306A	Rotavirus_A_strain_RVA/Human-wt/MOZ/0060a/2012/G12P8P14	I1
pSMART-T7_RV-SA11_NSP4_0060a_DLP-BD	169I, 174S	Rotavirus_A_strain_RVA/Human-wt/MOZ/0060a/2012/G12P8P14	E1/E2
pSMART-T7_RV-SA11_GS10(NSP4)_A174S	169R, 174S	Rotavirus_A_strain_RVA/Simian-tc/ZAF/SA11-N5/1958/G3P2	I2
pSMART-T7_RV-SA11_GS10(NSP4)_R169I	169I,174A	Rotavirus_A_strain_RVA/Simian-tc/ZAF/SA11-N5/1958/G3P2	I2

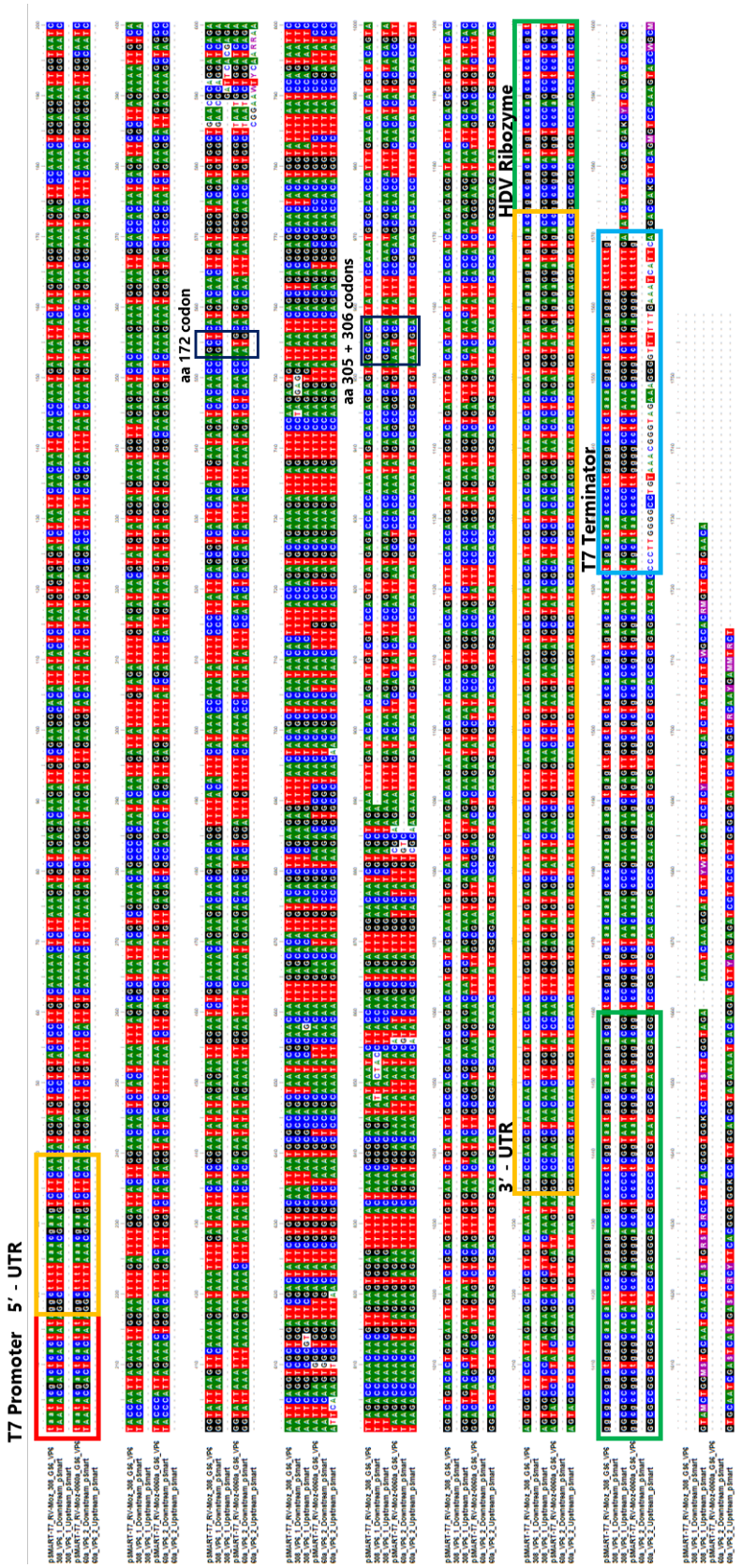


Figure 3.4: Multiple sequence alignment of the forward and reverse Sanger sequences of the Moz308 and Moz0060a GS6(VP6) transcription cassettes. This shows that plasmids from each selected colony aligned correctly with their reference sequence. The T7 promoter, 5'-UTR, 3'-UTR, HDV ribozyme, and T7 terminator sequences are indicated. The red box indicates the T7 promoter, the gold boxes the 5' and 3'UTRs, the blue boxes indicate the codons that code for amino acids 172, 305, and 306, the green box the HDV ribozyme, and the light blue box the T7 terminator.

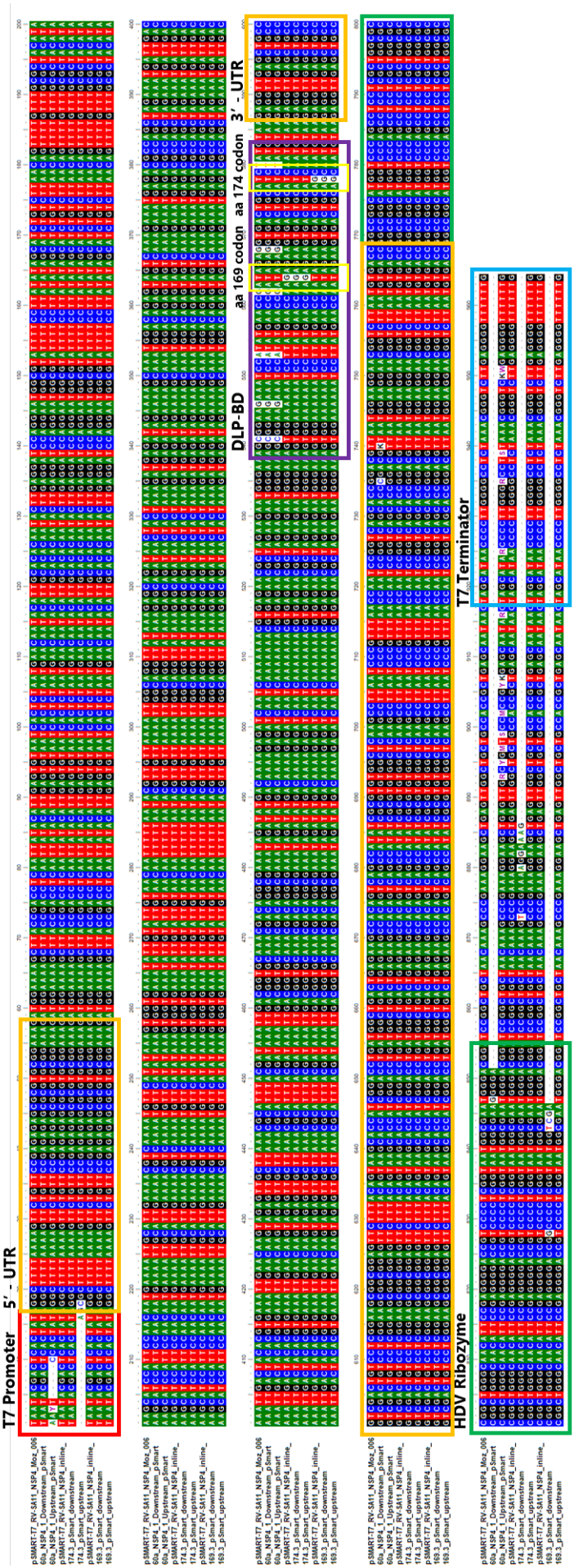


Figure 3.5: Multiple sequence alignment of the forward and reverse Sanger sequences of the SA11_NSP4_0060a_DLPBD, SA11_NSP4_A174S, and SA11_NSP4_R169I constructs. The T7 promoter, 5'-UTR, 3'-UTR, HDV ribozyme, T7 terminator, and DLP binding domain sequences are indicated. The red box indicates the T7 promoter, the gold boxes the 5' and 3'UTRs, the purple box the DLP binding domain, the yellow boxes indicate the codons that code for amino acids 169 and 174, the green box the HDV ribozyme, and the light blue box the T7 terminator.

Figure 3.4 shows that GS6(VP6) the Moz308 and Moz0060a transcription cassettes correctly align with their respective references and do contain the rationally designed modifications. The T7 promoter, terminator, and HDV ribozyme are present in each construct and sequenced correctly. There are multiple differences between the Moz308 and Moz0060a VP6s. The differences are mainly due to amino acid differences throughout the proteins. The three codons that determine the different subgroup epitopes are indicated in the figure. This shows that the sequences for these epitopes are correct.

Figure 3.5 shows the alignment of the transcription cassettes for SA11_NSP4_0060a_DLP-BD, SA11_NSP4_A174S, and SA11_NSP4_R169I. This shows again that the T7 promoter, terminator, and HDV ribozyme are present in each construct and sequenced correctly. The cDNA sequences of the NSP4 DLP binding domain (DLP-BD) are indicated. This shows four 7 single base pair mutations in the DLP binding domain. Mutations at positions 541, 553, 562, 568, and 580 are inherent silent mutations. SA11_NSP4_0060a_DLP-BD has a G546A mutation, as well as T564 which is the in codon that determines the 169 amino acid, and T578 which results in a 174S amino acid at this position. SA11_NSP4_A174S contained the A579T mutation required to generate the A174S mutant. SA11_NSP4_R169I contained the correct G564T mutation, resulting in an R169I mutant.

3.3.3 Assessment of rescue efficiency of different VP6/NSP4 combinations and NSP4 mutants

To assess whether the following six VP6/NSP4 combinations and NSP4 mutants were compatible in an SA11 backbone, the different combinations needed to be tested using plasmid-based rotavirus reverse genetics. The aim was to determine whether certain combinations or mutations were lethal to viral replication, making rescue impossible. This was done using the Kanai *et al.* pT7 SA11-L2 reverse genetics system, Section 3.2.2 and exchanging the plasmids encoding VP6 and NSP4 with the different constructs that test different mutations in VP6 or NSP4. The different combinations that were selected to be tested are listed in Table 3.5. The first combination was Moz308_GS6(VP6) with SA11_GS10(NSP4). The second combination was Moz0060a_GS6(VP6) with SA11_GS10(NSP4). The third, Moz0060a_GS6(VP6) with SA11_NSP4_0060a_DLP-BD. The fourth, SA11_GS6(VP6) with SA11_NSP4_0060a_DLP-BD. The fifth, SA11_GS6(VP6) with SA11_GS10(NSP4)_A174S. The sixth, SA11_GS6(VP6) and SA11_GS10(NSP4)_R169I.

Table 3.5: Plasmids of different combinations of GS6(GS6)/GS10(NSP4) tested for rescue compatibility.

GS6(VP6) construct	GS10(NSP4) construct	Virus designation
pSMART-T7_RV-Moz308_GS6(VP6)	pT7_RV-SA11_GS10(NSP4)	rSA11_Moz308_VP6
pSMART-T7_RV-Moz0060a_GS6(VP6)	pT7_RV-SA11_GS10(NSP4)	rSA11_Moz0060a_VP6
pSMART-T7_RV-Moz0060a_GS6(VP6)	pSMART-T7_RV-SA11_NSP4_0060a_DLP-BD	rSA11_Moz0060a_VP6_DLP-BD
pT7_RV-SA11-L2_GS6(VP6)	pSMART-T7_RV-SA11_NSP4_0060a_DLP-BD	rSA11_NSP4_0060a_DLP-BD
pT7_RV-SA11-L2_GS6(VP6)	pSMART-T7_RV-SA11_GS10(NSP4)_A174S	rSA11_NSP4_A174S
pT7_RV-SA11-L2_GS6(VP6)	pSMART-T7_RV-SA11_GS10(NSP4)_R169I	rSA11_NSP4_R169I

Rescue was performed as described in Section 3.2.2. The Kanai *et al.* GS6(VP6) and GS10(NSP4) plasmids were exchanged with the required plasmids required to test each combination listed in Table 3.5.

Transfection was performed once for each combination due to time constraints. Figure 3.6 shows the dsRNA genomes extracted from the rescue attempts for rSA11_Moz308_VP6, rSA11_NSP4_0060a_DLP-BD, rSA11_NSP4_R169I, and rSA11. Rotavirus genomes can be visualised for each extraction, with GS1(VP1) at 3500 bp, GS2(VP2)/GS3(VP3) at 2800 bp, GS4(VP4) at 2400 bp, GS5(NSP1) at 1600 bp, GS6(VP6) at 1400 bp, GS7(NSP3)/GS8(NSP2)/GS9(VP7) at 1000 bp, GS10(NSP4) at 750 bp, and GS11(NSP5/6) at 650 bp. There is, however, no resolution between GS2 and GS3, and GS7, GS8, GS9. This is typical for a rotavirus genome on an agarose gel. dsRNA for rSA11 had very low signal intensity, due to a lower yield of dsRNA. Differences in signal intensity can be seen between each dsRNA genome. This can be attributed to multiple factors, such as pipetting errors during RNA extraction, not a constant amount of aqueous phase being removed for RNA precipitation, or viruses not growing to the same maximum titre. Rescue attempts of rSA11_Moz0060a_VP6, rSA11_Moz0060a_VP6_DLP-BD, and rSA11_NSP4_A174S did not present CPE, and were not used for RNA extraction. The subsequent passage of viruses that did not rescue at P0 did not result in rescue at P1. The combinations that did not rescue were deemed unrescuable.

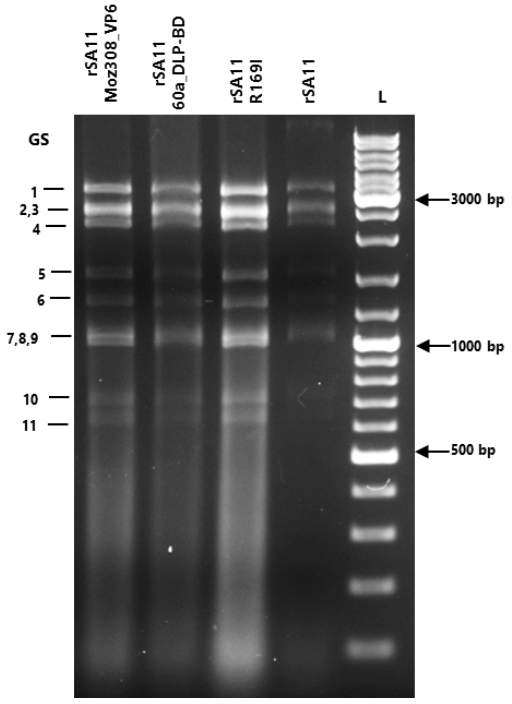


Figure 3.6: 1.5% agarose gel showing dsRNA of rescued viruses. dsRNA genomes extracted from P0 cell pellets. Genomes can be seen for rSA11_Moz308_VP6, rSA11_NSP4_0060a_DLP-BD, rSA11_NSP4_R169I, and rSA11. The other combinations did not present CPE and were not used for RNA extraction.

These results show that only certain combinations of amino acids VP6 and NSP4 are

compatible within an SA11 background. There are three possible explanations for the three combinations that could not be rescued. Firstly, this may be due to an inherent genetic incompatibility. Even though the constructs tested were designed to contain SA11 UTRs it would only have eliminated incompatibility of the (+)ssRNAs of the genome segments, with VP1 during the packaging step of the replication cycle, not at the genome segment selection and assortment step (Borodavka et al., 2017). The selection of (+)ssRNAs of genome segments seems to be determined by intergenome segment contacts, which are often found within the ORFs of the (+)ssRNA themselves. Therefore, since the ORFs are from rotaviruses with different genetic backbone with different codon usages (Moz308_GS6(VP6), Moz0060a_GS6(VP6), SA11_NSP4_0060a_DLP-BD) it may be that this leads to sub-optimal interactions between the (+)ssRNAs of genome segments, especially since genome segment selection is not properly understood. Secondly, an inherent protein-protein incompatibility may prevent rescue. As described in Chapter 1, VP6 contacts VP2 and VP4. It is possible that Moz0060a_VP6 may be incompatible with SA11 VP2 and VP4, which will prevent DLP and TLP formation, especially since its combination with SA11_NSP4_moz0060a_DLP-BD did not result in rescue. Thirdly, it may be that NSP4 mutants, such as the NSP4_A174S mutant results in the DLP/NSP4 interaction being diminished or abrogated and points to certain amino acids in the DLP binding domain of NSP4 being essential for NSP4 transport.

To verify that the rescued viruses still possessed the mutations being investigated in this project, genome segment-specific cDNA synthesis was performed for sequencing of GS6(VP6) and GS10(NSP4), Section 3.2.3. This was done using a one-step cDNA synthesis method and primers that bind to the 5' and 3'-ends of GS6(VP6) and GS10(NSP4). dsRNA was denatured at 95°C by mixing dsRNA with forward and reverse primers in water. This is done to preferentially amplify dsRNA, since the transfected plasmid may still be present after dsRNA extraction and could be amplified by the DNA polymerase. Using this method, amplification from plasmid may still occur.

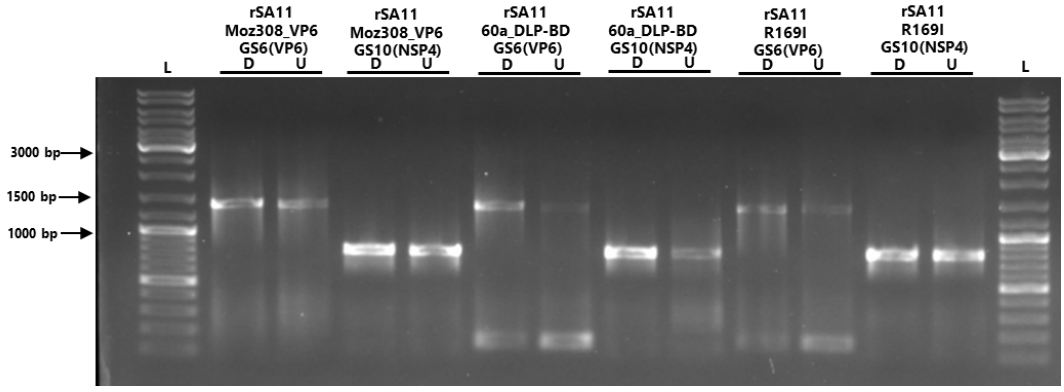


Figure 3.7: 1% agarose gel showing amplicons from one-Step cDNA synthesis of GS6(VP6) and GS10(NSP4) from the extracted dsRNA genomes. D=Denatured, U=Undenatured.

Figure 3.7 shows the denatured and undenatured amplicons of the GS6(VP6) and GS10(NSP4) cDNA synthesis reactions. Each reaction possessed the correct size ampli-

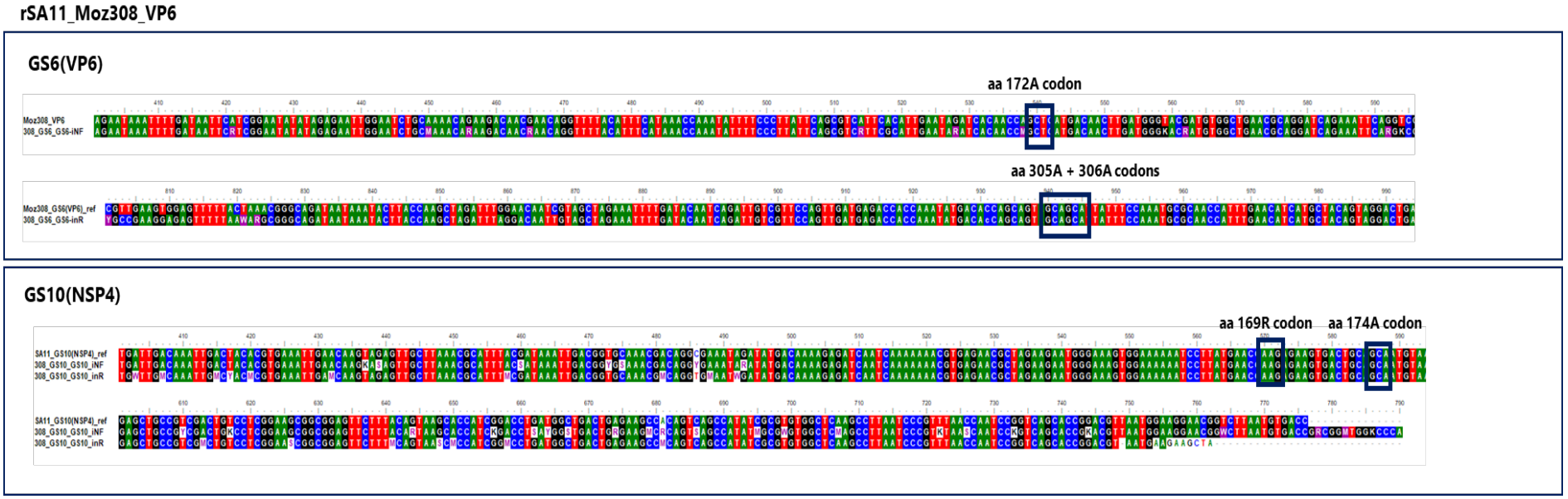
con at 1400 bp for GS6(VP6) reactions and 800 bp for GS10(NSP4) reactions. Some non-specific amplification were seen in each reaction. This is due to the types of primers used, which were originally designed for InFusion cloning, and are not optimal for cDNA synthesis. For GS6(VP6) amplicons, differences in amplification efficiency were seen between denatured and undenatured dsRNA, with lower signal being seen for undenatured templates. No differences were observed between denatured and undenatured GS10(NSP4) dsRNA templates. Differences in GS6 (VP6) amplification efficiency may be due to two reasons. Firstly, denatured dsRNA may have been preferentially amplified, since a higher copy number of dsRNA than plasmid will be present in the dsRNA extracted. This is due to the multiple steps after transfection that allow dilution of the plasmid still present after transfection. Secondly, the GS6(VP6) primers used may anneal less effectively than the GS10(NSP4) primers. Denaturing the dsRNA with primers and allowing the primers to anneal may result in more specific binding of the primers.

To sequence GS6(VP6) and GS10(NSP4) it was decided to use Sanger sequencing, since only two genome segments are of interest to this project. The aim was to determine whether the mutations generated in the plasmids used to rescue the viruses were still present after virus passaging. Prior to being sent for sequencing, each amplicon was purified using a PCR cleanup kit, and aliquots of each cDNA amplicon were sent to Inqaba biotec for Sanger sequencing using the primers that were used to generate the cDNA.

Figure 3.8 shows the subgroup epitope codons of the GS6 (VP6) subgroup and Figure 3.9 shows the aa 169 and 174 codons in GS10(NSP4) (Lopez et al., 1994). Sequencing quality was high for GS10(NSP4), but lower for GS6 (VP6), (data not shown); however, the sequencing data still allowed visualisation of the required locations in GS6(VP6) and GS10(NSP4) to verify that the mutations were still present after viral passaging.

For rSA11_Moz308_VP6 GS6(VP6) the sequence aligned correctly with the reference sequence, with the required 536 GCT (172A) and 934 - 940 GCA GCA (305A, 306A) codons present. For rSA11_Moz308_VP6 GS6(VP6) GS10(NSP4) the expected SA11 GS10(NSP4) reference aligned with the sequenced cDNA, with 545 AGA (169R) and 561 GCA (174A) present. rSA11_NSP4_0060a_DLP-BD GS6(VP6) aligned correctly with SA11 GS6(VP6) and possessed 545 GCT (172A) and 934 - 940 GCA GTA (305A, 306V). rSA11_NSP4_0060a_DLP-BD possessed the 545 ATA (169I) and 561 TCT (174S) mutations. rSA11_NSP4_R169I GS6(VP6) aligned with SA11 GS6(VP6), and the GS10(NSP4) possessed 545 AGA > ATA (R169I) and 561 GCA (174A).

(a) rSA11_Moz308_VP6 cDNA GS6(VP6) and GS10(NSP4) Sanger sequencing.



(b) rSA11_NSP4_0060a_DLP-BD GS6(VP6) and GS10(NSP4) Sanger sequencing

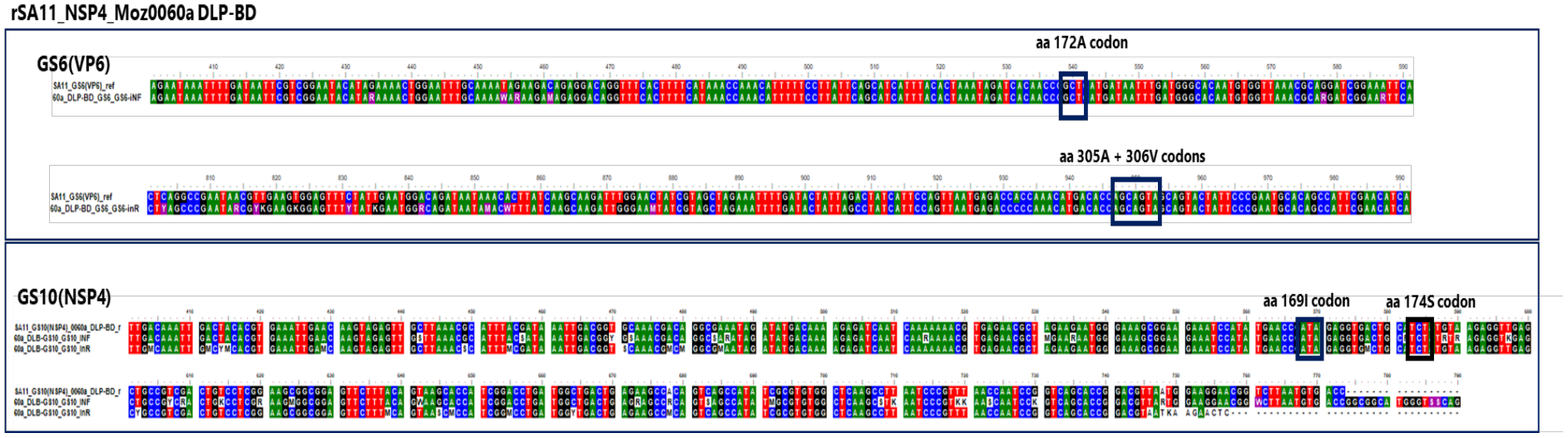


Figure 3.8: (a) Sanger sequencing of rSA11_Moz308_VP6 cDNA and (b) rSA11_NSP4_0060a_DLP-BD cDNA generated from GS6(VP6) and GS10(NSP4). Note that sequencing length does not correspond to the actual length of the construct, since InFusion primers were used for sequencing, resulting in an extra 17 bp being incorporated into each cDNA genome segment. Only the sequences that encode the VP6 subgroup and the sequences for the NSP4 DLP-BD are indicated.

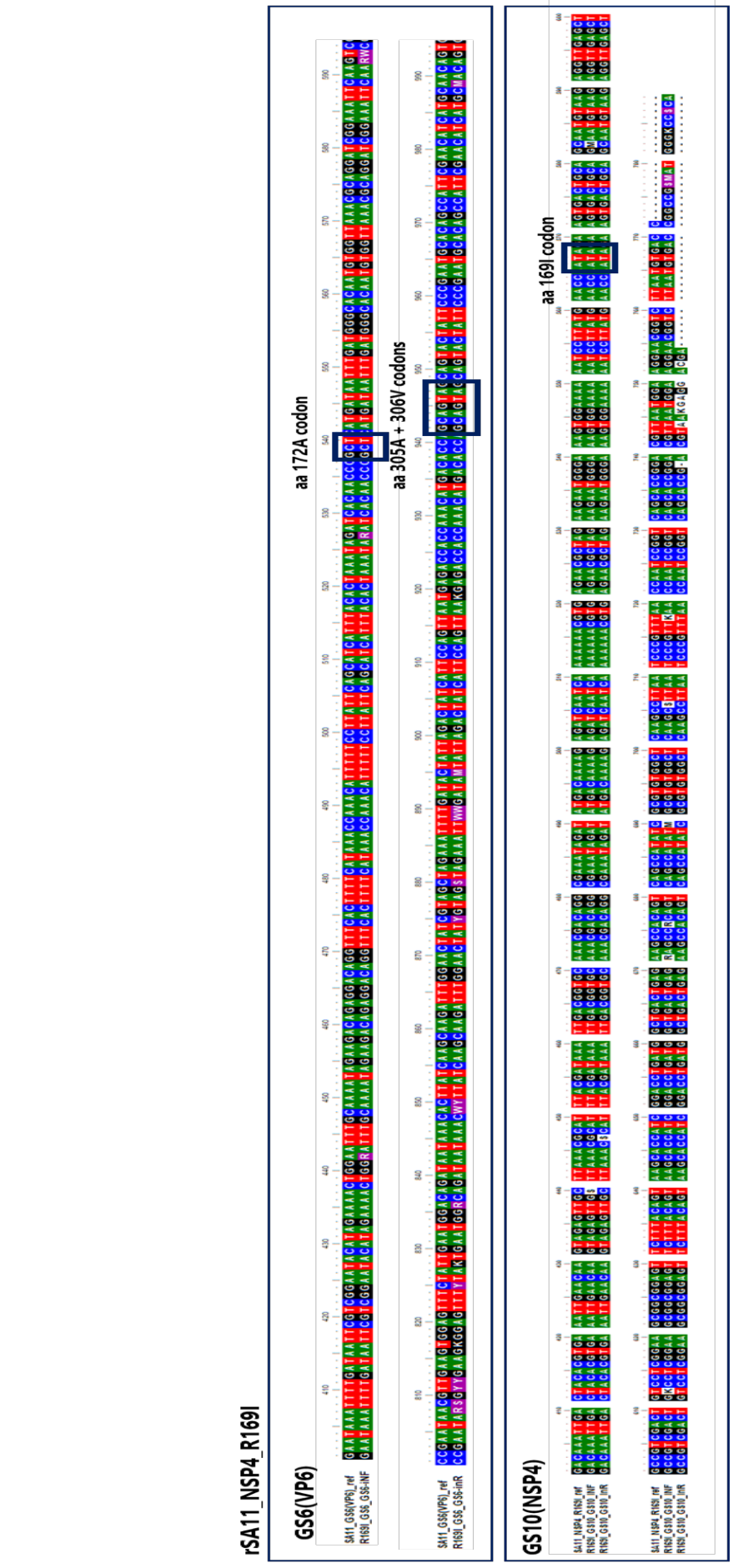


Figure 3.9: Sanger sequencing of rSA11_NSP4_R169I cDNA generated from GS6(VP6) and GS10(NSP4). Only the sequences encoding the VP6 subgroup, as well as the sequences for the NSP4 DLP-BD, are indicated.

The sequencing results for rSA11_Moz308_VP6, rSA11_NSP4_0060a_DLP-BD, and rSA11_NSP4_R169I could be interpreted as follows: Firstly, it is possible to incorporate an I2 VP6 into the SA11 background. Secondly, mutations generated in GS10(NSP4) appeared to be stable after rescue. Thirdly, these results confirmed that only certain GS6(VP6)/GS10(NSP4) combinations could be rescued. The implications of this are more fully discussed in the following section.

3.3.4 Growth kinetics of rescued viruses and implications for GS6(VP6)/GS10 (NSP4) co-reassortment

To determine whether the rescued viruses replicated differently, growth curves were performed as described in Section 3.2.4. Infections of each time point was done in triplicate. Titration was performed in triplicate on three separate days. Three days after each replicate, plaque assays were fixed and stained as described in Section 3.2.4. The data were normalised and a two-way ANOVA with LSD post-hoc was performed to determine whether each virus' growth curve was statistically different compared to SA11, Figures S17 – 21 and Table S.1.

3.3.4.1 VP6/VP2 and VP6/VP4 contacts may have an influence on GS6(VP6) reassortment

The rSA11_Moz308_VP6 growth curve was compared to rSA11, Figure 3.10. At each time point, rSA11_Moz308_VP6 replicated slower than SA11, and it did not reach the same maximum titre as SA11. rSA11_Moz308_VP6 replicated to a final titre of 6.6 x 10^6 PFU/ml. rSA11 replicated to a maximum titre of 7.7 x 10^7 PFU/ml. This titre is what has been previously reported for SA11. This represents an almost two-log reduction in titre for rSA11_Moz308_VP6, which is a large reduction in fitness. The rSA11_Moz308_VP6 virus' growth curve was statistically significant when compared to SA11. Plaque morphology was identical to that of rSA11-L2

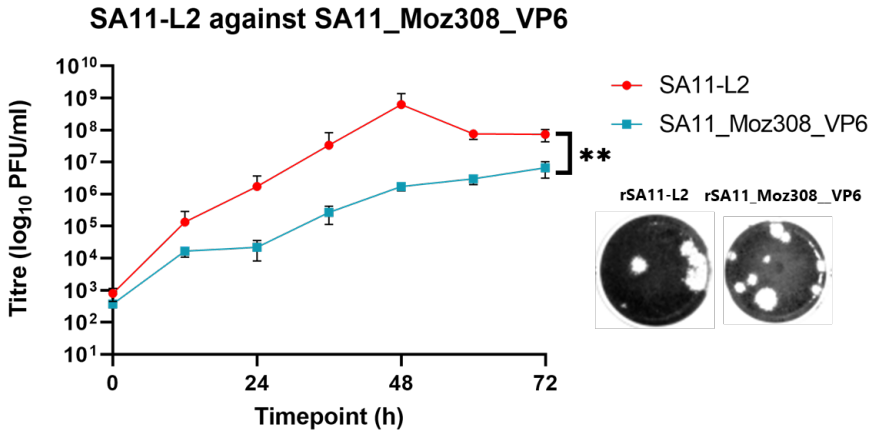


Figure 3.10: rSA11_Moz308_VP6 growth curve and plaque morphology. This shows log_10 PFU/ml against time point in hours. At each time point rSA11_Moz308_VP6 replicated slower than rSA11-L2. ** indicates a significace of $p < 0.001$

The reason for reduced replication may be that the Moz308 VP6 is not totally compatible with SA11. VP6 contacts both the core via VP2, and the TLP via VP4. VP6 amino acids 60–74 contact VP2, with the only difference between SA11 and Moz308 VP6 in this region is a N62D mutation which results in a change from positive aspartic acid to non-charged polar asparagine at this position (Dubois-Dalcq et al., 1984; McClain et al., 2010). Figure 3.11 shows the crystal structure of a Rotavirus UK DLP. This shows residue 62 at the start of the loop that contacts VP2. It is possible that this may result in a less stable DLP, which would affect the infectivity of the virus. VP6 contacts VP4 via 264L, 266N, 270I, and 286D. These contacts are the same in Moz308 and SA11. This may mean in this case that VP6 can restrict reassortment at the protein-protein level, but that there is not an effect with respect to the NSP4 DLP-BD. SA11 and Moz308 possess extremely similar sequences in their DLP-BD, the only variation being 169R for SA11 and 169K for Moz308 NSP4. These amino acids have the same polarity, and it is unlikely that this will have an effect on the VP6/NSP4 interaction.

This may also be true for rSA11_Moz0060a_VP6, for which rescue could not be achieved in this project and where the VP6 may not be compatible with VP2. It is possible that differences in the VP2 or VP6 contacts may make this virus not rescuable. This may also explain why rSA11_Moz0060a_VP6 with SA11_NSP4_0060a_DLP-BD could not be rescued, meaning that the VP6/NSP4 interaction itself may not be incompatible.

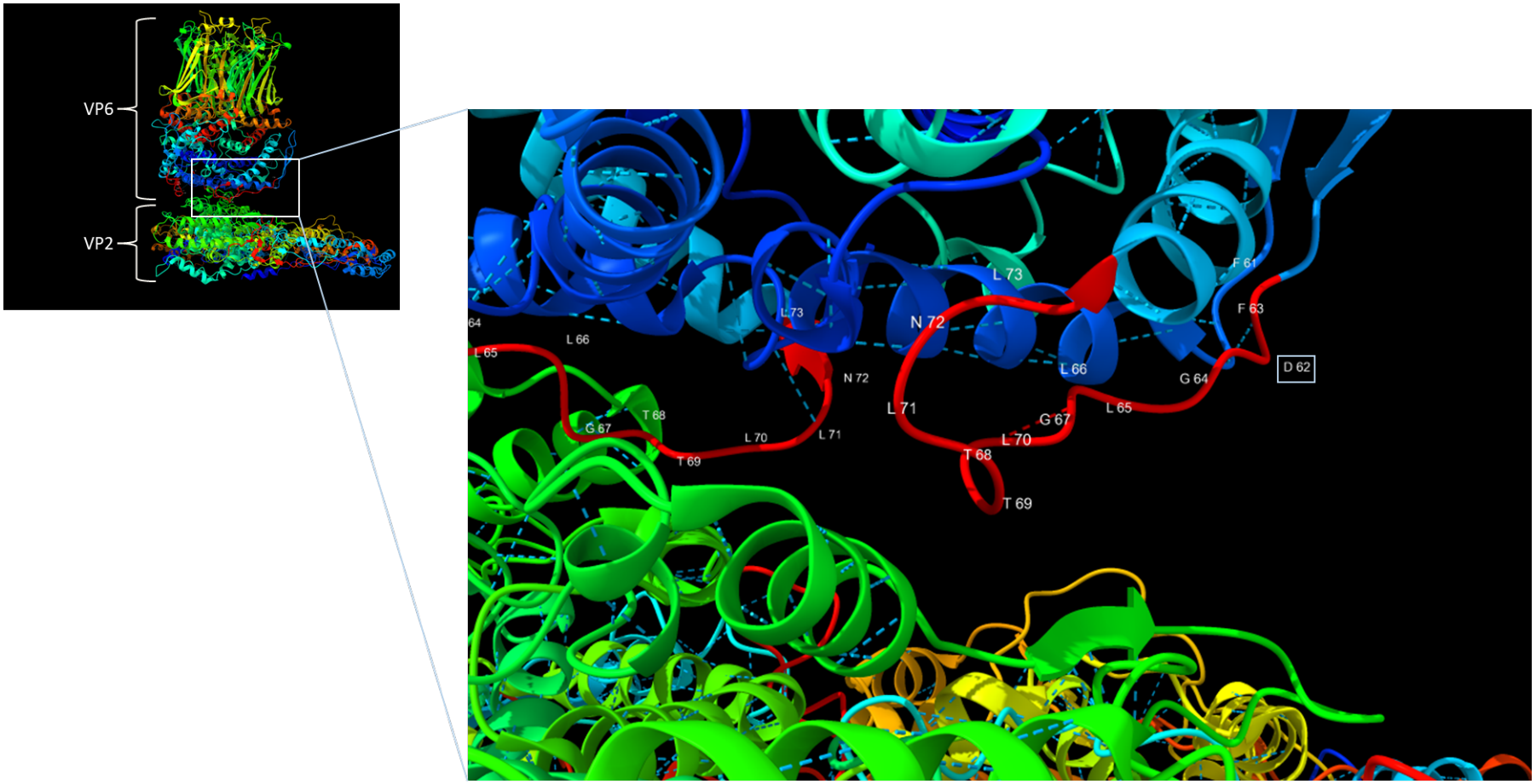


Figure 3.11: VP2 and VP6 contact surfaces. This shows the VP6 aa 61-74 contacts in red. The amino acid residues are labelled from residues 61-74. Note the residue 62, which is an asparagine in SA11 as compared to aspartic acid for rotavirus UK shown here.

3.3.4.2 Differentiating between the role of NSP4 amino acid 169 and 174 with regard to the VP6/NSP4 interaction

The growth curve for rSA11_NSP4_R169I compared to SA11, Figure 3.12. rSA11_NSP4_R169I reached a final titre of 2.4 x 10^8 PFU/ml as opposed to the final SA11 titre of 7.7 x 10^7 PFU/ml. For this, there was no statistical difference when compared to SA11. However, rSA11_NSP4_R169I does seem to grow slower at 24, 36, and 48 hpi when compared to SA11, after which it reaches a titre comparable to SA11.

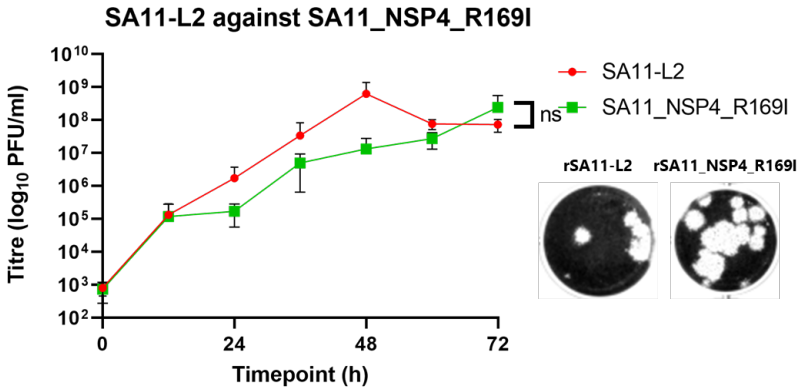


Figure 3.12: rSA11_NSP4_R169I growth curve and plaque morphology. This virus has differences in replication when compare to rSA11, but reached a comparable final titre. ns = not significant. Plaque morphology was similar to SA11.

This result has two possible implications. Firstly, it seems that the amino acid at position 169 is not essential when paired with A174 in a SA11 background. What was notable is the complete absence of rescue of rSA11_NSP4_A174S. This may mean that a single amino acid mutation affects the VP6 / NSP4 interaction, making DLP transport and the final step in the replication cycle impossible, especially since this is the only known function of this amino acid in the DLP-BD (Au et al., 1989; Taylor et al., 1993; Au et al., 1993; Taylor et al., 1996). In Figure 3.3.1 the DLP-BD amino acid sequences are shown. This showed a third possible amino acid at position 169. Serine and threonine, which are polar, are seen at this position in combination 174S. So, from this project, it may point to the fact that a non-polar/polar 169/174 or polar/polar 169/174, but not non-polar/non-polar combination in the DLP-BD may determine the interaction with VP6. This may explain why no field strains with a non-polar/non-polar has been sequenced, since this amino acid set may be lethal to viral replication.

3.3.5 A possible interplay exists between non-polar 169 and polar 174

The growth curve for rSA11_NSP4_0060a_DLP-BD compared to SA11, Figure 3.13. rSA11_NSP4_0060a_DLP-BD reached a final titre of 7.3 x 10^6 PFU/ml whereas SA11 reached a final titre of 7.7 x 10^7 PFU/ml. From this experiment, it appeared that this virus reached its maximum titre one time point earlier (36 h) than SA11 reaches its

maximum titre (48 h). This is then followed by a reduction in growth from 48 hpi. This growth curve is statistically significant when compared to SA11.

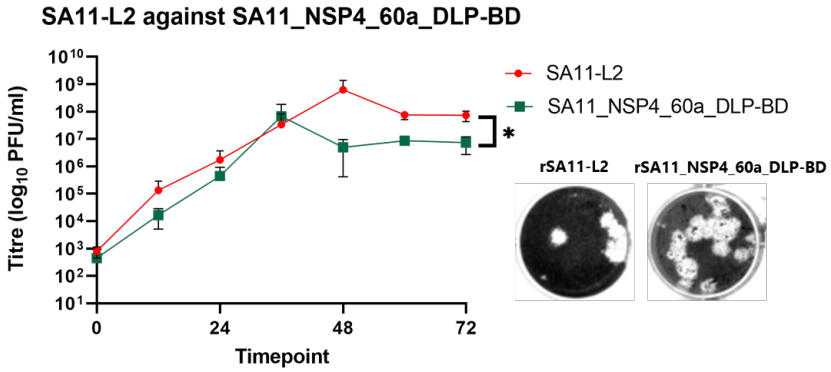


Figure 3.13: rSA11_NSP4_0060a_DLP-BD growth curve and plaque morphology. rSA11_NSP4_0060a_DLP-BD reached its maximum titre at 36 hours, as compared to rSA11 at 48 hours. Plaque morphology was similar to rSA11. * Indicates that the growth curves were significantly different, p = 0.042

When the results for rSA11_NSP4_0060a_DLP-BD are compared to the results for rSA11_NSP4_R169I and rSA11_NSP4_A174S it may mean that a cooperative interplay exists between a nonpolar 169 amino acid and a polar 174 amino acid, for the interaction with VP6 to occur in an SA11 background. This is especially evident since rescue of rSA11_NSP4_R169I rSA11_NSP4_R169I was possible but rescue for rSA11_NSP4_R169I rSA11_NSP4_A174S was not. This may mean that when a polar amino acid is present at 174, a non-polar amino acid is required at position 169. This implies that a non-polar/polar pair (amino acids 169 and 174) is required if amino acid 174 is polar in an SA11 background, especially in the light that these two amino acid positions are the only positions that show variability in the DLP-BD domain. This also has possible implications for co-reassortment in the field, since if the GS10(NSP4) reassorts into a background that requires this amino acid combination, this virus may be able to occupy an ecological niche.

3.4 Summary

Investigation of GS6(VP6)/GS10(NSP4) co-reassortment using the pT7 SA11-L2 reverse genetics system yielded multiple insights. Overall, these results indicate that reassortment may be structurally determined by both VP6 and NSP4, VP6 possibly having to be compatible with the VP2, and a specific amino acid set being required in the DLP binding domain of NSP4. The specific findings were as follows:

1. Amino acid sequence analysis of selected RVA strains showed that for VP6 subgroups, amino acid sequence remains constant between I1 and I2 genotypes.

2. NSP4 amino acid analysis showed that variation only exists at positions 169 and

174, with position 174 appearing to show the strongest selection for a specific amino acid.

3. At NSP4 position 169 amino acids threonine, serine, lysine, and isoleucine were identified in the analysed RVA strains.

4. At NSP4 position 174 amino acids alanine and serine were identified as the only amino acids at this position.

5. A DS-1-like and a Wa-like strain were chosen to test if VP6 subgroup and NSP4 169I, 174S, as well as 169I/174S DLP-BD amino acid mutation effects the replication of SA11.

6. Rescue was only possible for rSA11_Moz308_VP6, rSA11_NSP4_0060a_DLP-BD, rSA11_NSP4_R169I. and not rSA11_NSP4_A174S, rSA11_Moz0060a_VP6_DLP-BD, and rSA11_Moz0060a_VP6. This may show that:

   i rSA11_Moz0060a_VP6 is not compatible with SA11, since rSA11_Moz0060a _VP6_SA11_NSP4_0060a_DLP-BD was also not rescuable.

   ii Non-rescue of rSA11_NSP4_A174S may represent a DLP-BD mutation that is lethal for SA11 replication.

7. Growth kinetics of rSA11_Moz308_VP6 showed a near two-log reduction in final titre. Since this VP6 is of the same genotype as SA11 VP6, this may indicate a structural incompatibility with VP2. Moz308 VP6 has a single point mutation at amino acid 62 when compared to SA11. This may affect contact with VP2.

8. Growth kinetics showed that rSA11_NSP4_R169I replicates similarly to rSA11-L2. This may mean that this mutation in isolation does not affect replication.

9. rS11_SA11_NSP4_0060a_DLP-BD showed that although a lower final titre was observed, a virus with NSP4 R169I and A174S is rescueable. This may point to an interplay of these amino acids when polarity is considered.

Heterocomplexes, such as VP6 and NSP4, are composed of proteins that must exist individually before interaction (Jones & Thornton, 1996). Normally, interacting surfaces are enriched with hydrophobic residues, and most protein-protein interactions occur between hydrophobic surfaces (Wong et al., 2013). However, there is evidence that when the domain that is interacting is intrinsically disordered, polar residues become important in stabilising the interaction (Wong et al., 2013). Rotavirus NSP4 has a disordered C-terminal, in which the DLP-BD resides (Sastri et al., 2014). This may indicate that when VP6 contains a polar subgroup epitope (305N, 306A), such as in the case of Wa-like viruses, the result is that apolar 169I must be paired with polar 174S. Proteins with intrinsically disordered domains can only bind specific partners that have sufficient electrostatic complementary, since the binding of intrinsically disordered segments involves regions that are only partially accessible to solvent (Wong et al., 2013). This may cause high desolvation costs that must be alleviated by a complementary electrostatic interaction. These

results open up a novel area of research in the rotavirus replication cycle. Further work may elucidate a previously unknown reassortment mechanism and elucidate a key step in the rotavirus replication cycle.

Chapter 4

Concluding summary and future prospects

The advent of rotavirus reverse genetics in 2017 represented a very important breakthrough in the field and has significantly broadened the scope of research (Kanai et al., 2017). To date, two overall types of rescued rotaviruses have been generated. Reassorted rotaviruses have been generated that either have the outer capsid proteins, VP4/VP7, from other strains on a SA11 backbone or that have chimeric VP4s that have different head and foot domains (Kawagishi et al., 2020; Falkenhagen et al., 2020, 2021). Further, reverse genetics has been used to investigate rotavirus NSP2 phosphorylation and VP3 function (Criglar et al., 2020; Song et al., 2020). New reverse genetics systems for rhesus rotavirus (RRV) and murine rotavirus have also been developed (Sanchez-Tacuba et al., 2020)

The specific aims of this study were:

1. To improve the stability of the NWU SA11-N5 pSMART reverse genetics system by reorientating the transcription cassette.
2. To investigate the determinants of rotavirus GS6(VP6)/GS10(NSP4) co-reassortment using rotavirus reverse genetics.

4.1 Improving the stability of the NWU SA11-N5 pSMART reverse genetics plasmid set

The SA11-N5 pSMART reverse genetics plasmid set generated in our laboratory was extremely unstable. Most of the eleven plasmids had deletions or mutations when plasmids were transformed and extracted from overnight cultures of colonies on plates or archived glycerol stocks (M.J. Visser, personal communication). The instability could not be alleviated by using any of a whole range of different bacterial host cells.

Due to the instability of the plasmid set, I reanalysed previously generated NGS and Sanger sequencing data from our laboratory. Analysis of the single plasmid NGS using *de novo* assembly in ABySS and alignment in HISAT2 showed that the GS7(NSP3) and GS9(VP7) plasmids did not have a ribozyme. This was then also confirmed by the Sanger sequencing data that was generated from plasmids extracted from archived glycerol stocks,

by myself and M.J. Visser. Since the previous NGS analysis was done using a set of genome segments in a single library, the lack of the ribozyme would not have been detected. The only way in which rescue was previously confirmed for the SA11-N5 pSMART system was genome segment specific amplification of GS4(VP4). The cDNA sequence was then compared to SA11-L2 GS4(VP4). However, SA11-N5 and SA11-N2 have identical GS4(VP4)s, so this would have made differentiation between rescue and wild-type contamination impossible (Mlera et al., 2013). Since we were propagatng SA11-N2 in the laboratory during 2019/2020 as a control virus, the only logical explanation was that M. GJ. Huyzers (2020) most probably never rescued SA11-N5, but had wild-type SA11-N2 contamination that was perceived as rescue.

My survey of the literature into replication of plasmids in bacteria revealed that when using bacterial promoters in plasmids, *E. coli* prefers to have their genes in an orientation where transcription and replication occurs in the same direction (Hamperl & Cimprich, 2016; Brewer, 1988). It is believed that having genes in the opposing orientation results in a clash between the replication fork and transcription machinery, which causes deletions and mutations to alleviate the conflict. The rotavirus reverse genetics systems based on SA11-L2, KU, Odelia, and murine-like D6/2 systems plasmid sets use T7 promoters, that are highly specific and cannot be recognised by bacteria (Kanai et al., 2017; Komoto et al., 2018, 2019; Sanchez-Tacuba et al., 2020). However, the SA11-L2 rotavirus reverse genetics system as well as the reovirus reverse genetics system have their transcription cassettes in the same direction that replication occurs. The SA11-N5 pSMART system does not. Both the plasmid-based AHSV and BTV reverse genetics systems use the pSMART backbone with cassettes in the same orientation as in the SA11-N5 pSMART system. Some instability has been observed for some genome segments (Prof. A.C. Potgieter, personal communication). There is no reported instability in the transcript-based AHSV and BTV systems, and these plasmids do not possess a ribozyme, since it is not required to generate run-off transcripts (van Rijn et al., 2016). It may be possible that the incorrect orientation, coupled with a ribozyme results in instability.

I reorientated the transcription cassettes of the SA11-N5 pSMART system using InFusion and NEBuilder seamless cloning and verified it using Sanger sequencing and NGS. NGS was repeated 12 months later from plasmids that were endotoxin-free purified from archived glycerol stocks. No mutations or deletions were detected. This indicated that the stability of the plasmid set was markedly improved following reorientation of the transcription cassettes.

However, despite several attempts to rescue with the endotoxin-free purified, reorientated SA11-N5 pSMART plasmid set, I did not succeed. Failure to achieve rescue led to the hypothesis that the cell-lines or transfection reagents in use were preventing rescue. Seven different transfection reagents, and five different transfection and infection cell line combinations were tested, with rescue not being achieved in any attempt. Co-transfection with a set of MA104 codon-optimised SA11 expression plasmids expressing VP1, VP2, VP3, VP6, NSP1, NSP2, NSP5, and NSP6 also did not allow rescue. Rescue attempts with

rhesus rotavirus has shown that rescue cannot be achieved without the addition of a 2x ratio of C3P3 plasmid (Sanchez-Tacuba et al., 2020). The C3P3 plasmid contains OPFs encoding Cytoplasmic Capping-Prone Phage Polymerase and contains a T7 polymerase linked to a ASFV capping enzyme, via a glycine-serine-glycine linker. This may mean that extra capping and T7 RNA polymerase might also be required for rescue with the SA11-N5 pSMART system.

After becoming aware of a report in the literature that mycoplasma contamination could prevent rotavirus rescue, PCR testing of transfection and infection cell lines showed that our ST and MA104 cells, that were used for co-seeding and propagating rescued rotaviruses, were heavily contaminated with mycoplasma (Philip et al., 2020). New MA104 and ST cells were obtained, but due to time constraints, rescue with the reorientated SA11-N5 pSMART plasmid set could only be attempted two times. No virus was rescued.

In this project it has been shown that by reorientating the transcription cassette, plasmid stability could be substantially improved. However, what has not been shown is whether the pSMART SA11-N5 reverse genetics system is capable of supporting rescue. In the future, this can be investigated in three ways. Firstly, it can be determined whether a single plasmid prevents rescue by exchanging a single plasmid separately with its corresponding plasmid in the SA11-L2 pT7 system. Secondly, the experiment where different transfection reagents and cell-lines were tested can be repeated using mycoplasma free cells to determine if a specific cell-line and transfection reagent combination is required for rescue. If a successful combination can be found, use of the pSMART SA11-N5 system will be further investigated. Thirdly, use of the system with a higher ratio C3P3 plasmid can be tested to see whether rescue can be achieved. The pSMART SA11-N5 system possesses a plasmid backbone that is 1000 bp smaller than the pT7 SA11-L2 system backbone, which will reduce the plasmid load with 11 000 bp and may result in a more effective rotavirus reverse genetics system.

4.2 Investigating the determinants of rotavirus GS6(VP6)/GS10(NSP4) co-reassortment using rotavirus reverse genetics

Following the lack of success, the SA11-L2 pT7 reverse genetics system was endotoxin-free plasmid extracted, and was shown to be able to support rescue.

From reports in the literature, field strain co-reassorment of rotavirus GS6(VP6)/GS10(NSP4) has been observed. In 2003, it was shown in rotavirus field strains that GS10(NSP4) genotypes cluster with their corresponding GS6(VP6) subgroup (Iturriza-Gomara et al., 2003). Co-reassortment of a DS-1 like GS6(VP6)/GS10(NSP4) pair was observed in 2019 (Tamim et al., 2019). Further, it was identified that a DS-1 like GS6(VP6) or a DS-1 like GS6(VP6)/GS10(NSP4) could reassort into a Wa-like background. No Wa-like GS6(VP6)s were detected that reassorted into a DS-1 like background (Tamim et al., 2019). The only documented interaction between VP6 and NSP4 is the transport of DLPs from the viroplasm to allow maturation of DLPs to TLPs in the endoplasmic reticulum

(Au et al., 1989; Taylor et al., 1993; Au et al., 1993; Taylor et al., 1996).

I analysed another 36 random GS6(VP6) and 38 random GS10(NSP4) whole genome NGS sequences of RVA strains downloaded from Genbank and used the insights gained to formulate a hypothesis. Analysis of the NSP4 DLP binding domain (DLP-BD) showed that only two positions in the amino acid sequence varied, at positions 169 and 174. For Wa - like strains, a 169S or 169I and 174S combination was identified. For DS-1 like strains, 169K, 169S, 174S, and 174A combinations were identified. This generated the hypothesis that NSP4 amino acids 169 and 174 may have an important effect in binding VP6. Sequence analysis of VP6 confirmed that subgroup I is seen in DS-1 like strains and is defined by 172A, 305A, and 306A. Subgroup II VP6 is seen in Wa-like strains, and contained the expected 172M, 305N, and 306N.

Two Mozambican RV strains were selected for the five constructs that were used for this project using the following rationale (Strydom et al., 2019a,b). These were chosen because they are local circulating African strains and since the whole genome NGS clearly showed the GS6(VP6) and GS10(NSP4) combinations of each virus. RVA/Human-wt/MOZ/0308/G2P[4] is a DS-1 like strain with a SGI VP6 and a NSP4 with 169K and 174A. RVA/Human-wt/MOZ/0060a/G12P[8] possesses a SGII VP6 and its NSP4 has 169I and 174S. For the GS6(VP6) constructs, full length Moz308 VP6 and Moz0060a GS6(VP6)s were designed with SA11 UTRs to reduce possible genome packaging issues. The hypothesis was that the Moz308 VP6 may be compatible with an SA11 backbone, but not the Moz0060a VP6. A SA11 GS10(NSP4) with a Moz0060a DLP-BD was used to test whether its combination with a Moz0060a VP6 may result in rescue. Additionally, SA11 NSP4_R169I and SA11 NSP4_A174S constructs were generated using site-directed mutagenesis to test the effect of mutating these amino acids in the SA11 backbone.

Rescue was achieved for rSA11_Moz308_VP6, rSA11_NSP4_0060a_DLP-BD, and rSA11_NSP4_R169I. It was not possible to rescue rSA11_Moz0060a_VP6, rSA11_0060a_VP6 _NSP4_0060a_DLP-BD, and rSA11_NSP4_A174S. The presence of the correct mutations were verified using single genome segment cDNA synthesis and Sanger sequencing. Following sequence verification of rescued viruses, multi-step growth curves were performed to assess the growth kinetics of each virus. rSA11_Moz308_VP6 replicated at a significantly lower rate than SA11. Structure-based analysis implied that a compatibility issue of either VP2 or VP6 resulted in a virus that replicates to a lower titre. rSA11_NSP4_R169I replicated to the same titre as SA11. This showed that the R169I mutation does not have a significant effect on DLP binding, since it does not affect viral growth kinetics. rSA11_NSP4_0060a_DLP-BD replicated significantly slower than SA11. This result was unexpected, especially since rSA11_NSP4_A174S could not be rescued. This result may show that there is a possible cooperative effect between the 169 and 174 amino acids in the NSP4 DLP-BD, where only certain combinations are capable of replication. When linked with the sequencing data analysed it may imply that only a polar/non-polar combination or non - polar/ non - polar combination, but not a polar-polar combination is possible when together with a DS-1 like VP6. This data is supported by what has been

reported for protein-protein interactions. Normally, interactions occur between nonpolar amino acids, but polar residues become important in stabilising the interaction when the domain that is interacting is disordered (Jones & Thornton, 1996; Wong et al., 2013).

In the future there are multiple lines of questioning that need to be pursued. Firstly, the rescue experiments performed in this project must be repeated in triplicate to verify the results obtained. Secondly, reverse genetics can be employed to verify which amino acids in NSP4 partake in the VP6/NSP4 interaction, by mutating every amino acid to its opposite polarity in the NSP4 DLP-BD and attempting to rescue each mutant to see what affect the mutation has on binding. Thirdly, whether the VP6 subgroup epitopes are important in NSP4 binding must also be verified using mutagenesis, since this has only been implicated by sequencing data. Fourthly, where in the cell VP6/NSP4 interactions occur and at which point in the replication cycle, must be verified using immunoprecipation and confocal microscopy.

Bibliography

Aaij, C. & Borst, P. (1972). The gel electrophoresis of DNA. *Biochimica et Biophysica Acta (BBA) - Nucleic Acids and Protein Synthesis*, 269(2), 192–200.

Almazán, F., González, J. M., Pénzes, Z., Izeta, A., Calvo, E., Plana-Durán, J., & Enjuanes, L. (2000). Engineering the largest RNA virus genome as an infectious bacterial artificial chromosome. *Proceedings of the National Academy of Sciences*, 97(10), 5516–5521.

Amarilla, A. A., Sng, J. D. J., Parry, R., Deerain, J. M., Potter, J. R., Setoh, Y. X., Rawle, D. J., Le, T. T., Modhiran, N., Wang, X., Peng, N. Y. G., Torres, F. J., Pyke, A., Harrison, J. J., Freney, M. E., Liang, B., McMillan, C. L. D., Cheung, S. T. M., Guevara, D. J. D. C., Hardy, J. M., Bettington, M., Muller, D. A., Coulibaly, F., Moore, F., Hall, R. A., Young, P. R., Mackenzie, J. M., Hobson-Peters, J., Suhrbier, A., Watterson, D., & Khromykh, A. A. (2021). A versatile reverse genetics platform for SARS-CoV-2 and other positive-strand RNA viruses. *Nature Communications*, 12(1), 3431.

Angel, J., Franco, M. A., & Greenberg, H. B. (2012). Rotavirus immune responses and correlates of protection. *Current Opinion in Virology*, 2(4), 419–425.

Anh, D. D., Van Trang, N., Thiem, V. D., Anh, N. T. H., Mao, N. D., Wang, Y., Jiang, B., Hien, N. D., & Luan, L. T. (2012). A dose-escalation safety and immunogenicity study of a new live attenuated human rotavirus vaccine (Rotavin-M1) in Vietnamese children. *Rotavirus Vaccines for Children in Developing Countries*, 30, A114–A121.

Aoki, S. T., Settembre, E. C., Trask, S. D., Greenberg, H. B., Harrison, S. C., & Dormitzer, P. R. (2009). Structure of Rotavirus Outer-Layer Protein VP7 Bound with a Neutralizing Fab. *Science*, 324(5933), 1444–1447.

Au, K. S., Chan, W. K., Burns, J. W., & Estes, M. K. (1989). Receptor activity of rotavirus nonstructural glycoprotein NS28. *Journal of Virology*, 63(11), 4553–4562.

Au, K.-S., Mattion, N. M., & Estes, M. K. (1993). A Subviral Particle Binding Domain on the Rotavirus Nonstructural Glycoprotein NS28. *Virology*, 194(2), 665–673.

Ayala-Breton, C., Arias, M., Espinosa, R., Romero, P., Arias, C. F., & Lopez, S. (2009). Analysis of the Kinetics of Transcription and Replication of the Rotavirus Genome by RNA Interference. *Journal of Virology*, 83(17), 8819–8831.

Azevedo, M. P., Vlasova, A. N., & Saif, L. J. (2013). Human rotavirus virus-like particle vaccines evaluated in a neonatal gnotobiotic pig model of human rotavirus disease. *Expert Review of Vaccines*, 12(2), 169–181.

Baker, S. F., Nogales, A., Finch, C., Tuffy, K. M., Domm, W., Perez, D. R., Topham, D. J., & Martinez-Sobrido, L. (2014). Influenza A and B Virus Intertypic Reassortment through Compatible Viral Packaging Signals. *Journal of Virology*, 88(18), 10778–10791.

Ball, J. M., Tian, P., Zeng, C. Q.-Y., Morris, A. P., & Estes, M. K. (1996). Age-Dependent Diarrhea Induced by a Rotaviral Nonstructural Glycoprotein. *Science*, 272(5258), 101–104.

Benati, F. J., Maranhão, A. G., Lima, R. S., da Silva, R. C., & Santos, N. (2010). Multiple-gene characterization of rotavirus strains: Evidence of genetic linkage among the VP7-, VP4-, VP6-, and NSP4-encoding genes. *Journal of Medical Virology*, 82(10), 1797–1802.

Bergmann, C. C., Maass, D., Poruchynsky, M. S., Atkinson, P. H., & Bellamy, A. R. (1989). Topology of the non-structural rotavirus receptor glycoprotein NS28 in the rough endoplasmic reticulum. *The EMBO journal*, 8(6), 1695–1703.

Berkova, Z., Crawford, S. E., Trugnan, G., Yoshimori, T., Morris, A. P., & Estes, M. K. (2006). Rotavirus NSP4 induces a novel vesicular compartment regulated by calcium and associated with viroplasms. *Journal of Virology*, 80(12), 6061–71.

Bernstein, D. I., Smith, V. E., Sander, D. S., Pax, K. A., Schiff, G. M., & Ward, R. L. (1990). Evaluation of WC3 Rotavirus Vaccine and Correlates of Protection in Healthy Infants. *The Journal of Infectious Diseases*, 162(5), 1055–1062.

Berois, M., Sapin, C., Erk, I., Poncet, D., & Cohen, J. (2003). Rotavirus nonstructural protein NSP5 interacts with major core protein VP2. *Journal of Virology*, 77(3), 1757–1763.

Bhan, M. K., Lew, J. F., Sazawal, S., Das, B. K., Gentsch, J. R., & Glass, R. I. (1993). Protection Conferred by Neonatal Rotavirus Infection against Subsequent Rotavirus Diarrhea. *The Journal of Infectious Diseases*, 168(2), 282–287.

Bines, J. E., At Thobari, J., Satria, C. D., Handley, A., Watts, E., Cowley, D., Nirwati, H., Ackland, J., Standish, J., Justice, F., Byars, G., Lee, K. J., Barnes, G. L., Bachtiar, N. S., Viska Icanervilia, A., Boniface, K., Bogdanovic-Sakran, N., Pavlic, D., Bishop, R. F., Kirkwood, C. D., Buttery, J. P., & Soenarto, Y. (2018). Human Neonatal Rotavirus Vaccine (RV3-BB) to Target Rotavirus from Birth. *New England Journal of Medicine*, 378(8), 719–730.

Birnboim, H. & Doly, J. (1979). A rapid alkaline extraction procedure for screening recombinant plasmid DNA. *Nucleic Acids Research*, 7(6), 1513–1523.

Bishop, R., Davidson, G. P., Holmes, I. H., & Ruck, B. J. (1973). Virus particles in epithelial cells of duodenal mucosa from children with acute non-bacterial gastroenteritis. *The Lancet*, 302(7841), 1281–1283.

Blazevic, V., Lappalainen, S., Nurminen, K., Huhti, L., & Vesikari, T. (2011). Norovirus VLPs and rotavirus VP6 protein as combined vaccine for childhood gastroenteritis. *Vaccine*, 29(45), 8126–8133.

Block, S. L., Vesikari, T., Goveia, M. G., Rivers, S. B., Adeyi, B. A., Dallas, M. J., Bauder, J., Boslego, J. W., & Heaton, P. M. (2007). Efficacy, Immunogenicity, and Safety of a Pentavalent Human-Bovine (WC3) Reassortant Rotavirus Vaccine at the End of Shelf Life. *Pediatrics*, 119(1), 11–18.

Boehme, K. W., Ikizler, M., Kobayashi, T., & Dermody, T. S. (2011). Reverse genetics for mammalian reovirus. *Methods*, 55(2), 109–113.

Borodavka, A., Desselberger, U., & Patton, J. T. (2018). Genome packaging in multi-segmented dsRNA viruses: distinct mechanisms with similar outcomes. *Current Opinion in Virology*, 33, 106–112.

Borodavka, A., Dykeman, E. C., Schrimpf, W., & Lamb, D. C. (2017). Protein-mediated RNA folding governs sequence-specific interactions between rotavirus genome segments. *Elife*, 6.

Boshuizen, J. A., Rossen, J. W. A., Sitaram, C. K., Kimenai, F. F. P., Simons-Oosterhuis, Y., Laffeber, C., Buller, H. A., & Einerhand, A. W. C. (2004). Rotavirus Enterotoxin NSP4 Binds to the Extracellular Matrix Proteins Laminin- 3 and Fibronectin. *Journal of Virology*, 78(18), 10045–10053.

Boughan, S., Potgieter, A. C., & van Staden, V. (2020). African horse sickness virus NS4 is a nucleocytoplasmic protein that localizes to PML nuclear bodies. *Journal of General Virology*, 101(4), 366–384.

Boyce, M., Celma, C. C., & Roy, P. (2008). Development of reverse genetics systems for bluetongue virus: recovery of infectious virus from synthetic RNA transcripts. *Journal of Virology*, 82(17), 8339–48.

Boyce, M. & Roy, P. (2007). Recovery of infectious bluetongue virus from RNA. *Journal of Virology*, 81(5), 2179–86.

Bravo, J. P. K., Borodavka, A., Barth, A., Calabrese, A. N., Mojzes, P., Cockburn, J. J. B., Lamb, D. C., & Tuma, R. (2018). Stability of local secondary structure determines selectivity of viral RNA chaperones. *Nucleic Acids Research*, 46(15), 7924–7937.

Brewer, B. J. (1988). When polymerases collide: Replication and the transcriptional organization of the E. coli chromosome. *Cell*, 53(5), 679–686.

Bridgen, A. (2012). *Reverse Genetics of RNA Viruses : Applications and Perspectives*. Oxford, United Kingdom: John Wiley & Sons, Incorporated.

Bridgen, A. & Elliott, R. M. (1996). Rescue of a segmented negative-strand RNA virus entirely from clonedcomplementaryDNAs. *Proceedings of the National Academy of Sciences*, 93(26), 15400–15404.

Burke, R. M., Tate, J. E., Kirkwood, C. D., Steele, A. D., & Parashar, U. D. (2019). Current and new rotavirus vaccines. *Current Opinion in Infectious Diseases*, 32(5), 1.

Butash, K. A., Natarajan, P., Young, A., & Fox, D. K. (2000). Reexamination of the Effect of Endotoxin on Cell Proliferation and Transfection Efficiency. *Biotechniques*, 29(3), 610–619.

Castro, C. J. & Ng, T. F. F. (2017). U50: A New Metric for Measuring Assembly Output Based on Non-Overlapping, Target-Specific Contigs. *Journal of Computational Biology*, 24(11), 1071–1080.

Chaimongkol, N., Khamrin, P., Malasao, R., Thongprachum, A., Ushijima, H., & Maneekarn, N. (2012). Genotypic linkages of gene segments of rotaviruses circulating in pediatric patients with acute gastroenteritis in Thailand. *Infection, Genetics and Evolution*, 12(7), 1381–1391.

Chan, J., Nirwati, H., Triasih, R., Bogdanovic-Sakran, N., Soenarto, Y., Hakimi, M., Duke, T., Buttery, J. P., Bines, J. E., Bishop, R. F., Kirkwood, C. D., & Danchin, M. D. (2011). Maternal antibodies to rotavirus: Could they interfere with live rotavirus vaccines in developing countries? *Vaccine*, 29(6), 1242–1247.

Chan, W.-K., Au, K.-S., & Estes, M. K. (1988). Topography of the simian rotavirus nonstructural glycoprotein (NS28) in the endoplasmic reticulum membrane. *Virology*, 164(2), 435–442.

Charpilienne, A., Lepault, J., Rey, F., & Cohen, J. (2002). Identification of Rotavirus VP6 Residues Located at the Interface with VP2 That Are Essential for Capsid Assembly and Transcriptase Activity. *Journal of Virology*, 76(15), 7822–7831.

Chen, J. Z., Settembre, E. C., Aoki, S. T., Zhang, X., Bellamy, A. R., Dormitzer, P. R., Harrison, S. C., & Grigorieff, N. (2009). Molecular interactions in rotavirus assembly and uncoating seen by high-resolution cryo-EM. *Proceedings of the National Academy of Sciences*, 106(26), 10644–10648.

Chen, M.-Y., Kirkwood, C. D., Bines, J., Cowley, D., Pavlic, D., Lee, K. J., Orsini, F., Watts, E., Barnes, G., & Danchin, M. (2017). Rotavirus specific maternal antibodies and immune response to RV3-BB neonatal rotavirus vaccine in New Zealand. *Human Vaccines & Immunotherapeutics*, 13(5), 1126–1135.

Chen Zhongying, Wang Weijia, Zhou Helen, Suguitan Amorsolo L., Shambaugh Cindy, Kim Lomi, Zhao Jackie, Kemble George, & Jin Hong (2010). Generation of Live Attenuated Novel Influenza Virus A/California/7/09 (H1N1) Vaccines with High Yield in Embryonated Chicken Eggs. *Journal of Virology*, 84(1), 44–51. Publisher: American Society for Microbiology.

Cheung, W., Gill, M., Esposito, A., Kaminski, C. F., Courousse, N., Chwetzoff, S., Trugnan, G., Keshavan, N., Lever, A., & Desselberger, U. (2010). Rotaviruses Associate with

Cellular Lipid Droplet Components To Replicate in Viroplasms, and Compounds Disrupting or Blocking Lipid Droplets Inhibit Viroplasm Formation and Viral Replication. *Journal of Virology*, 84(13), 6782–6798.

Ciarlet, M., Conner, M. E., Finegold, M. J., & Estes, M. K. (2002). Group A Rotavirus Infection and Age-Dependent Diarrheal Disease in Rats: a New Animal Model To Study the Pathophysiology of Rotavirus Infection. *Journal of Virology*, 76(1), 41–57.

Ciarlet, M. & Estes, M. K. (1999). Human and most animal rotavirus strains do not require the presence of sialic acid on the cell surface for efficient infectivity. *Journal of General Virology*, 80(4), 943–948.

Conradie, A. M., Stassen, L., Huismans, H., Potgieter, C. A., & Theron, J. (2016). Establishment of different plasmid only-based reverse genetics systems for the recovery of African horse sickness virus. *Virology*, 499, 144–155.

Contin, R., Arnoldi, F., Campagna, M., & Burrone, O. R. (2010). Rotavirus NSP5 orchestrates recruitment of viroplasmic proteins. *Journal of General Virology*, 91(7), 1782–1793.

Coulson, B. S., Londrigan, S. L., & Lee, D. J. (1997). Rotavirus contains integrin ligand sequences and a disintegrin-like domain that are implicated in virus entry into cells. *Proceedings of the National Academy of Sciences*, 94(10), 5389–5394.

Crawford, S. E., Criglar, J. M., Liu, Z., Broughman, J. R., & Estes, M. K. (2019). COPII Vesicle Transport Is Required for Rotavirus NSP4 Interaction with the Autophagy Protein LC3 II and Trafficking to Viroplasms. *Journal of Virology*, 94(1), e01341–19.

Crawford, S. E., Mukherjee, S. K., Estes, M. K., Lawton, J. A., Shaw, A. L., Ramig, R. F., & Prasad, B. V. V. (2001). Trypsin Cleavage Stabilizes the Rotavirus VP4 Spike. *Journal of Virology*, 75(13), 6052–6061.

Criglar, J. M., Crawford, S. E., Zhao, B., Smith, H. G., Stossi, F., & Estes, M. K. (2020). A genetically engineered rotavirus NSP2 phosphorylation mutant impaired in viroplasm formation and replication shows an early interaction between vNSP2 and cellular lipid droplets. *Journal of virology*, 94(15), e00972–20.

Cuadras, M. A., Arias, C. F., & López, S. (1997). Rotaviruses induce an early membrane permeabilization of MA104 cells and do not require a low intracellular Ca2+ concentration to initiate their replication cycle. *Journal of virology*, 71(12), 9065–9074.

Denisova, E., Dowling, W., LaMonica, R., Shaw, R., Scarlata, S., Ruggeri, F., & Mackow, E. R. (1999). Rotavirus Capsid Protein VP5* Permeabilizes Membranes. *Journal of Virology*, 73(4), 3147–3153.

Desheva, J., Lu, X., Rekstin, A., Rudenko, L., Swayne, D., Cox, N., Katz, J., & Klimov, A. (2006). Characterization of an influenza A H5N2 reassortant as a candidate for live-attenuated and inactivated vaccines against highly pathogenic H5N1 viruses with pandemic potential. *Vaccine*, 24(47), 6859–6866.

Desselberger, U. (2014). Rotaviruses. *Virus Research*, 190, 75–96.

Desselberger, U. (2017a). Differences of Rotavirus Vaccine Effectiveness by Country: Likely Causes and Contributing Factors. *Pathogens*, 6(4).

Desselberger, U. (2017b). Reverse genetics of rotavirus. *Proceedings of the National Academy of Sciences*, 114(9), 2106–2108.

Desselberger, U. (2020). What are the limits of the packaging capacity for genomic RNA in the cores of rotaviruses and of other members of the Reoviridae? *Virus Research*, 276, 197822.

Desselberger, U. & Huppertz, H.-I. (2011). Immune Responses to Rotavirus Infection and Vaccination and Associated Correlates of Protection. *The Journal of Infectious Diseases*, 203(2), 188–195.

Desselberger, U., Richards, J., Tchertanov, L., Lepault, J., Lever, A., Burrone, O., & Cohen, J. (2013). Further characterisation of rotavirus cores: Ss(+)RNAs can be packaged in vitro but packaging lacks sequence specificity. *Virus Research*, 178(2), 252–263.

Diaz-Muñoz, S. L., Tenaillon, O., Goldhill, D., Brao, K., Turner, P. E., & Chao, L. (2013). Electrophoretic mobility confirms reassortment bias among geographic isolates of segmented RNA phages. *BMC Evolutionary Biology*, 13(1), 206.

Ding, K., Celma, C. C., Zhang, X., Chang, T., Shen, W., Atanasov, I., Roy, P., & Zhou, Z. H. (2019). In situ structures of rotavirus polymerase in action and mechanism of mRNA transcription and release. *Nature Communications*, 10(1), 2216.

Donato, C. M., Ch'Ng, L. S., Boniface, K. F., Crawford, N. W., Buttery, J. P., Lyon, M., Bishop, R. F., & Kirkwood, C. D. (2012). Identification of Strains of RotaTeq Rotavirus Vaccine in Infants With Gastroenteritis Following Routine Vaccination. *The Journal of Infectious Diseases*, 206(3), 377–383.

Dormitzer, P. R. (2002). The rhesus rotavirus VP4 sialic acid binding domain has a galectin fold with a novel carbohydrate binding site. *EMBO Journal*, 21(5), 885–897.

Dubois-Dalcq, M., Holmes, K. V., & Rentier, B. (1984). Assembly of Rotaviruses. In M. Dubois-Dalcq, K. V. Holmes, & B. Rentier (Eds.), *Assembly of Enveloped RNA Viruses* (pp. 171–182). Vienna: Springer Vienna.

Eaton, H. E., Kobayashi, T., Dermody, T. S., Johnston, R. N., Jais, P. H., & Shmulevitz, M. (2017). African swine fever virus NP868R capping enzyme promotes reovirus rescue during reverse genetics by promoting reovirus protein expression, virion assembly, and RNA incorporation into infectious virions. *Journal of Virology*, 91(11), e02416–16.

Eichwald, C., Rodriguez, J. F., & Burrone, O. R. (2004). Characterization of rotavirus NSP2/NSP5 interactions and the dynamics of viroplasm formation. *Journal of General Virology*, 85(3), 625–634.

Erasmus, B. J. (1972). The Pathogenesis of African Horsesickness. In *1. African Horse Sickness*, Proceedings of the Third International Conference on Equine Infectious Diseases, Paris, July 17-21, 1972. Paris: Karger.

Essere, B., Yver, M., Gavazzi, C., Terrier, O., Isel, C., Fournier, E., Giroux, F., Textoris, J., Julien, T., Socratous, C., Rosa-Calatrava, M., Lina, B., Marquet, R., & Moules, V. (2013). Critical role of segment-specific packaging signals in genetic reassortment of influenza A viruses. *Proceedings of the National Academy of Sciences*, 110(40), E3840–E3848.

Estes, M. K., Graham, D. Y., Gerba, C. P., & Smith, E. M. (1979). Simian rotavirus SA11 replication in cell cultures. *Journal of Virology*, 31(3), 810–815.

Estes, M. K. & Greenberg, H. (2013). Rotaviruses. In D. Knipe & P. Howley (Eds.), *Fields Virology*, volume 2 (pp. 1347–1401). Wolters Kluwer Health, 6 edition.

Falconer, M. M., Gilbert, J. M., Roper, A. M., Greenberg, H. B., & Gavora, J. S. (1995). Rotavirus-induced fusion from without in tissue culture cells. *Journal of virology*, 69(9), 5582–5591.

Falkenhagen, A., Huyzers, M., van Dijk, A. A., & Johne, R. (2021). Rescue of Infectious Rotavirus Reassortants by a Reverse Genetics System Is Restricted by the Receptor-Binding Region of VP4. *Viruses*, 13(3), 363.

Falkenhagen, A., Patzina-Mehling, C., Gadicherla, A. K., Strydom, A., O'Neill, H. G., & Johne, R. (2020). Generation of Simian Rotavirus Reassortants with VP4- and VP7-Encoding Genome Segments from Human Strains Circulating in Africa Using Reverse Genetics. *Viruses*, 12(2), 201.

Falkenhagen, A., Patzina-Mehling, C., Rückner, A., Vahlenkamp, T. W., & Johne, R. (2019). Generation of simian rotavirus reassortants with diverse VP4 genes using reverse genetics. *Journal of General Virology*, 100(12), 1595–1604.

Feenstra, F., Maris-Veldhuis, M., Daus, F. J., Tacken, M. G. J., Moormann, R. J. M., Van Gennip, R. G. P., & Van Rijn, P. A. (2014). VP2-serotyped live-attenuated bluetongue virus without NS3/NS3a expression provides serotype-specific protection and enables DIVA. *Vaccine*, 32(52), 7108–7114.

Feenstra, F., Pap, J. S., & Van Rijn, P. A. (2015). Application of Bluetongue Disabled Infectious Single Animal (DISA) vaccine for different serotypes by VP2 exchange or incorporation of chimeric VP2. *Vaccine*, 33(6), 812–818.

Feinstein, A. (1968). Chapter 6 - Agar gel electrophoresis and immuno-electrophoresis. In I. SMITH (Ed.), *Zone Electrophoresis (Second Edition)* (pp. 194–208). Butterworth-Heinemann.

Flewett, T. H., Bryden, A. S., Davies, H., Woode, G. N., Bridger, J., & Derrick, J. (1974). Relation between viruses from acute gastroenteritis of children and newborn calves. *The Lancet*, 304(7872), 61–63.

Fodor, E., Devenish, L., Engelhardt, O. G., Palese, P., Brownlee, G. G., & García-Sastre, A. (1999). Rescue of Influenza A Virus from Recombinant DNA. *Journal of Virology*, 73(11), 9679–9682.

Fu, C., Wang, M., Liang, J., He, T., Wang, D., & Xu, J. (2007). Effectiveness of Lanzhou lamb rotavirus vaccine against rotavirus gastroenteritis requiring hospitalization: A matched case-control study. *Vaccine*, 25(52), 8756–8761.

Fukui, K. (2010). DNA Mismatch Repair in Eukaryotes and Bacteria. *Journal of Nucleic Acids*, 2010, 1–16.

Garcés Suárez, Y., Martínez, J. L., Torres Hernández, D., Hernández, H. O., Pérez-Delgado, A., Méndez, M., Wood, C. D., Rendon-Mancha, J. M., Silva-Ayala, D., López, S., Guerrero, A., & Arias, C. F. (2019). Nanoscale organization of rotavirus replication machineries. *eLife*, 8.

Gardet, A., Breton, M., Fontanges, P., Trugnan, G., & Chwetzoff, S. (2006). Rotavirus Spike Protein VP4 Binds to and Remodels Actin Bundles of the Epithelial Brush Border into Actin Bodies. *Journal of Virology*, 80(8), 3947–3956.

Geldenhuys, L. (2018). *Generation of a set of SA11 expression plasmids for the development of a T7-RNA polymerase-dependent rotavirus reverse genetic system.* (Dissertation - MSc), North-West University, Potchefstroom.

Gottlieb, P., Qiao, X., Strassman, J., Frilander, M., & Mindich, L. (1994). Identification of the Packaging Regions within the Genomic RNA Segments of Bacteriophage Φ6. *Virology*, 200(1), 42–47.

Greenberg, H., McAuliffe, V., Valdesuso, J., Wyatt, R., Flores, J., Kalica, A., Hoshino, Y., & Singh, N. (1983). Serological analysis of the subgroup protein of rotavirus, using monoclonal antibodies. *Infection and Immunity*, 39(1), 91–99.

Greenberg, H. B. & Estes, M. K. (2009). Rotaviruses: from pathogenesis to vaccination. *Gastroenterology*, 136(6), 1939–51.

Greenberg, H. B., Wyatt, R. G., Kapikian, A. Z., Kalica, A. R., Flores, J., & Jones, R. (1982). Rescue and serotypic characterization of noncultivable human rotavirus by gene reassortment. *Infection and Immunity*, 37(1), 104–109.

Groome, M. J., Koen, A., Fix, A., Page, N., Jose, L., Madhi, S. A., McNeal, M., Dally, L., Cho, I., Power, M., Flores, J., & Cryz, S. (2017). Safety and immunogenicity of a parenteral P2-VP8-P[8] subunit rotavirus vaccine in toddlers and infants in South Africa: a randomised, double-blind, placebo-controlled trial. *The Lancet Infectious Diseases*, 17(8), 843–853.

Groome, M. J., Page, N., Cortese, M. M., Moyes, J., Zar, H. J., Kapongo, C. N., Mulligan, C., Diedericks, R., Cohen, C., Fleming, J. A., Seheri, M., Mphahlele, J., Walaza, S., Kahn, K., Chhagan, M., Steele, A. D., Parashar, U. D., Zell, E. R., & Madhi, S. A.

(2014). Effectiveness of monovalent human rotavirus vaccine against admission to hospital for acute rotavirus diarrhoea in South African children: a case-control study. *The Lancet Infectious Diseases*, 14(11), 1096–1104.

Guerrero, C. A., Mendez, E., Zarate, S., Isa, P., Lopez, S., & Arias, C. F. (2000). Integrin alpha vbeta 3 mediates rotavirus cell entry. *Proceedings of the National Academy of Sciences*, 97(26), 14644–14649.

Hamperl, S. & Cimprich, K. A. (2016). Conflict Resolution in the Genome: How Transcription and Replication Make It Work. *Cell*, 167(6), 1455–1467.

Haselhorst, T., Fleming, F. E., Dyason, J. C., Hartnell, R. D., Yu, X., Holloway, G., Santegoets, K., Kiefel, M. J., Blanchard, H., Coulson, B. S., & von Itzstein, M. (2009). Sialic acid dependence in rotavirus host cell invasion. *Nature Chemical Biology*, 5(2), 91–93.

Heaton, P. M., Goveia, M. G., Miller, J. M., Offit, P., & Clark, H. F. (2005). Development of a Pentavalent Rotavirus Vaccine against Prevalent Serotypes of Rotavirus Gastroenteritis. *The Journal of Infectious Diseases*, 192, S17–S21.

Henschke, N., Bergman, H., Hungerford, D., Cunliffe, N. A., Grais, R. F., Kang, G., Parashar, U. D., Wang, S. A., & Neuzil, K. M. (2022). The efficacy and safety of rotavirus vaccines in countries in Africa and Asia with high child mortality. *Vaccine*, 40(12), 1707–1711.

Hewish, M. J., Takada, Y., & Coulson, B. S. (2000). Integrins alpha 2beta 1 and alpha 4beta 1 Can Mediate SA11 Rotavirus Attachment and Entry into Cells. *Journal of Virology*, 74(1), 228–236.

Himmelreich, R., Plagens, H., Hilbert, H., Reiner, B., & Herrmann, R. (1997). Comparative analysis of the genomes of the bacteria Mycoplasma pneumoniae and Mycoplasma genitalium. *Nucleic acids research*, 25(4), 701–712.

Hoekstra, Dick, S. A. (2001). Cationic lipid-mediated transfection in vitro and in vivo. *Molecular Membrane Biology*, 18(2), 129–143.

Hou, G., Zeng, Q., Matthijnssens, J., Greenberg, H. B., & Ding, S. (2021). Rotavirus NSP1 Contributes to Intestinal Viral Replication, Pathogenesis, and Transmission. *mBio*, 12(6), e03208–21.

Hu, L., Crawford, S. E., Hyser, J. M., Estes, M. K., & Prasad, B. V. (2012). Rotavirus non-structural proteins: structure and function. *Curr Opin Virol*, 2(4), 380–8.

Huyzers, M. (2020). *Local implementation and optimization of rotavirus reverse genetics systems*. Dissertation, North-West University, Potchesfstroom.

Hyser, J. M., Collinson-Pautz, M. R., Utama, B., & Estes, M. K. (2010). Rotavirus disrupts calcium homeostasis by NSP4 viroporin activity. *MBio*, 1(5).

Hyser, J. M., Utama, B., Crawford, S. E., Broughman, J. R., & Estes, M. K. (2013). Activation of the Endoplasmic Reticulum Calcium Sensor STIM1 and Store-Operated Calcium Entry by Rotavirus Requires NSP4 Viroporin Activity. *Journal of Virology*, 87(24), 13579–13588.

Hyser, J. M., Zeng, C. Q. Y., Beharry, Z., Palzkill, T., & Estes, M. K. (2008). Epitope mapping and use of epitope-specific antisera to characterize the VP5∗ binding site in rotavirus SA11 NSP4. *Virology*, 373(1), 211–228.

Iturriza-Gomara, M., Anderton, E., Kang, G., Gallimore, C., Phillips, W., Desselberger, U., & Gray, J. (2003). Evidence for Genetic Linkage between the Gene Segments Encoding NSP4 and VP6 Proteins in Common and Reassortant Human Rotavirus Strains. *Journal of Clinical Microbiology*, 41(8), 3566–3573.

Jackman, S. D., Vandervalk, B. P., Mohamadi, H., Chu, J., Yeo, S., Hammond, S. A., Jahesh, G., Khan, H., Coombe, L., Warren, R. L., & Birol, I. (2017). ABySS 2.0: resource-efficient assembly of large genomes using a Bloom filter. *Genome research*, 27(5), 768–777.

Jamur, M. C. & Oliver, C. (2010a). Cell Fixatives for Immunostaining. In C. Oliver & M. C. Jamur (Eds.), *Immunocytochemical Methods and Protocols* (pp. 55–61). Totowa, NJ: Humana Press.

Jamur, M. C. & Oliver, C. (2010b). Permeabilization of Cell Membranes. In C. Oliver & M. C. Jamur (Eds.), *Immunocytochemical Methods and Protocols* (pp. 63–66). Totowa, NJ: Humana Press.

Jayaram, H., Estes, M. K., & Prasad, B. V. V. (2004). Emerging themes in rotavirus cell entry, genome organization, transcription and replication. *Virus Research*, 101(1), 67–81.

Jayaram, H., Taraporewala, Z., Patton, J. T., & Prasad, B. V. V. (2002). Rotavirus protein involved in genome replication and packaging exhibits a HIT-like fold. *Nature*, 417(6886), 311–315.

Jayashree, S., Bhan, M. K., Kumar, R., Raj, P., Glass, R., & Bhandari, N. (1988). Serum and Salivary Antibodies as Indicators of Rotavirus Infection in Neonates. *The Journal of Infectious Diseases*, 158(5), 1117–1120.

Jere, K. C., Chaguza, C., Bar-Zeev, N., Lowe, J., Peno, C., Kumwenda, B., Nakagomi, O., Tate, J. E., Parashar, U. D., Heyderman, R. S., French, N., Cunliffe, N. A., & Iturriza-Gomara, M. (2018). Emergence of Double- and Triple-Gene Reassortant G1P[8] Rotaviruses Possessing a DS-1-Like Backbone after Rotavirus Vaccine Introduction in Malawi. *Journal of Virology*, 92(3).

Jere, K. C., O'Neill, H. G., Potgieter, A. C., & Van Dijk, A. A. (2014). Chimaeric Virus-Like Particles Derived from Consensus Genome Sequences of Human Rotavirus Strains Co-Circulating in Africa. *PLoS ONE*, 9(9), e105167.

Jiang, X., Jayaram, H., Kumar, M., Ludtke, S. J., Estes, M. K., & Prasad, B. V. V. (2006). Cryoelectron Microscopy Structures of Rotavirus NSP2-NSP5 and NSP2-RNA Complexes: Implications for Genome Replication. *Journal of Virology*, 80(21), 10829–10835.

Jo, W. K., Schadenhofer, A., Habierski, A., Kaiser, F. K., Saletti, G., Ganzenmueller, T., Hage, E., Haid, S., Pietschmann, T., Hansen, G., Schulz, T. F., Rimmelzwaan, G. F., Osterhaus, A. D. M. E., & Ludlow, M. (2021). Reverse genetics systems for contemporary isolates of respiratory syncytial virus enable rapid evaluation of antibody escape mutants. *Proceedings of the National Academy of Sciences*, 118(14), e2026558118.

Jones, S. & Thornton, J. M. (1996). Principles of protein-protein interactions. *Proceedings of the National Academy of Sciences*, 93(1), 13–20.

Juuti, J. T. & Bamford, D. H. (1995). RNA Binding, Packaging and Polymerase Activities of the Different Incomplete Polymerase Complex Particles of dsRNA Bacteriophage φ6. *Journal of Molecular Biology*, 249(3), 545–554.

Kanai, Y., Kawagishi, T., Nouda, R., Onishi, M., Pannacha, P., Nurdin, J. A., Nomura, K., Matsuura, Y., & Kobayashi, T. (2019). Development of Stable Rotavirus Reporter Expression Systems. *Journal of Virology*, 93(4), e01774–18.

Kanai, Y., Komoto, S., Kawagishi, T., Nouda, R., Nagasawa, N., Onishi, M., Matsuura, Y., Taniguchi, K., & Kobayashi, T. (2017). Entirely plasmid-based reverse genetics system for rotaviruses. *Proceedings of the National Academy of Sciences*, 114(9), 2349–2354.

Kanai, Y., Onishi, M., Kawagishi, T., Pannacha, P., Nurdin, J., Nouda, R., Yamasaki, M., Lusiany, T., Khamrin, P., Okitsu, S., Hayakawa, S., Ebina, H., Ushijima, H., & Kobayashi, T. (2020). Reverse genetics approach for developing rotavirus vaccine candidates carrying VP4 and VP7 genes cloned from clinical isolates of human rotavirus. *Journal of Virology*, 95(2), e01374–20.

Kaname, Y., Celma, C. C. P., Kanai, Y., & Roy, P. (2013). Recovery of African horse sickness virus from synthetic RNA. *Journal of General Virology*, 94(10), 2259–2265.

Kawagishi, T., Nurdin, J. A., Onishi, M., Nouda, R., Kanai, Y., Tajima, T., Ushijima, H., & Kobayashi, T. (2020). Reverse Genetics System for a Human Group A Rotavirus. *Journal of Virology*, 94(2).

Khamrin, P., Maneekarn, N., Malasao, R., Nguyen, T. A., Ishida, S., Okitsu, S., & Ushijima, H. (2010). Genotypic linkages of VP4, VP6, VP7, NSP4, NSP5 genes of rotaviruses circulating among children with acute gastroenteritis in Thailand. *Infection, Genetics and Evolution*, 10(4), 467–472.

Kim, D., Paggi, J. M., Park, C., Bennett, C., & Salzberg, S. L. (2019). Graph-based genome alignment and genotyping with HISAT2 and HISAT-genotype. *Nature Biotechnology*, 37(8), 907–915.

Kimelman, A., Levy, A., Sberro, H., Kidron, S., Leavitt, A., Amitai, G., Yoder-Himes, D. R., Wurtzel, O., Zhu, Y., Rubin, E. M., & Sorek, R. (2012). A vast collection of microbial genes that are toxic to bacteria. *Genome research*, 22(4), 802–809.

Kobayashi, T., Antar, A. A. R., Boehme, K. W., Danthi, P., Eby, E. A., Guglielmi, K. M., Holm, G. H., Johnson, E. M., Maginnis, M. S., Naik, S., Skelton, W. B., Wetzel, J. D., Wilson, G. J., Chappell, J. D., & Dermody, T. S. (2007). A Plasmid-Based Reverse Genetics System for Animal Double-Stranded RNA Viruses. *Cell Host Microbe*, 1(2), 147–157.

Kobayashi, T. & Kanai, Y. (2019). Method for producing artificial recombinant rotavirus.

Kobayashi, T., Ooms, L. S., Ikizler, M., Chappell, J. D., & Dermody, T. S. (2010). An improved reverse genetics system for mammalian orthoreoviruses. *Virology*, 398(2), 194–200.

Komoto, S., Fukuda, S., Ide, T., Ito, N., Sugiyama, M., Yoshikawa, T., Murata, T., & Taniguchi, K. (2018). Generation of Recombinant Rotaviruses Expressing Fluorescent Proteins by Using an Optimized Reverse Genetics System. *Journal of Virology*, 92(13).

Komoto, S., Fukuda, S., Kugita, M., Hatazawa, R., Koyama, C., Katayama, K., Murata, T., & Taniguchi, K. (2019). Generation of infectious recombinant human rotaviruses from just 11 cloned cDNAs encoding the rotavirus genome. *Journal of Virology*, 93(8).

Komoto, S., Sasaki, J., & Taniguchi, K. (2006). Reverse genetics system for introduction of site-specific mutations into the double-stranded RNA genome of infectious rotavirus. *Proceedings of the National Academy of Sciences*, 103(12), 4646–4651.

Komoto, S., Tacharoenmuang, R., Guntapong, R., Ide, T., Haga, K., Katayama, K., Kato, T., Ouchi, Y., Kurahashi, H., Tsuji, T., Sangkitporn, S., & Taniguchi, K. (2015). Emergence and Characterization of Unusual DS-1-Like G1P[8] Rotavirus Strains in Children with Diarrhea in Thailand. *PLoS One*, 10(11), e0141739.

Komoto, S., Tacharoenmuang, R., Guntapong, R., Ide, T., Tsuji, T., Yoshikawa, T., Tharmaphornpilas, P., Sangkitporn, S., & Taniguchi, K. (2016). Reassortment of Human and Animal Rotavirus Gene Segments in Emerging DS-1-Like G1P[8] Rotavirus Strains. *PLOS ONE*, 11(2), e0148416.

Kulkarni, P. S., Desai, S., Tewari, T., Kawade, A., Goyal, N., Garg, B. S., Kumar, D., Kanungo, S., Kamat, V., Kang, G., Bavdekar, A., Babji, S., Juvekar, S., Manna, B., Dutta, S., Angurana, R., Dewan, D., Dharmadhikari, A., Zade, J. K., Dhere, R. M., Fix, A., Power, M., Uprety, V., Parulekar, V., Cho, I., Chandola, T. R., Kedia, V. K., Raut, A., Flores, J., & group, S. B.-P. a. (2017). A randomized Phase III clinical trial to assess the efficacy of a bovine-human reassortant pentavalent rotavirus vaccine in Indian infants. *Vaccine*, 35(45), 6228–6237.

Kumar, D., Yu, X., Crawford, S. E., Moreno, R., Jakana, J., Sankaran, B., Anish, R., Kaundal, S., Hu, L., Estes, M. K., Wang, Z., & Prasad, B. V. V. (2020). 2.7 Å cryo-

EM structure of rotavirus core protein VP3, a unique capping machine with a helicase activity. *Science Advances*, 6(16), eaay6410.

Kumar, M., Jayaram, H., Vasquez-Del Carpio, R., Jiang, X., Taraporewala, Z. F., Jacobson, R. H., Patton, J. T., & Prasad, B. V. V. (2007). Crystallographic and Biochemical Analysis of Rotavirus NSP2 with Nucleotides Reveals a Nucleoside Diphosphate Kinase-Like Activity. *Journal of Virology*, 81(22), 12272–12284.

Lawton, J. A., Estes, M. K., & Prasad, B. V. V. (1997). Three-dimensional visualization of mRNA release from actively transcribing rotavirus particles. *Nature Structural Biology*, 4(2), 118–121.

Li, C., Wen, A., Shen, B., Lu, J., Huang, Y., & Chang, Y. (2011). FastCloning: a highly simplified, purification-free, sequence- and ligation-independent PCR cloning method. *BMC Biotechnology*, 11, 92.

Li, H. (2011). A statistical framework for SNP calling, mutation discovery, association mapping and population genetical parameter estimation from sequencing data. *Bioinformatics*, 27(21), 2987–2993.

Lilly, J. & Camps, M. (2015). Mechanisms of Theta Plasmid Replication. *Microbiology Spectrum*, 3(1), PLAS–0029–2014.

Lopez, S., Espinosa, R., Greenberg, H. B., & Arias, C. F. (1994). Mapping the Subgroup Epitopes of Rotavirus Protein VP6. *Virology*, 204(1), 153–162.

Lopez, T., Camacho, M., Zayas, M., Najera, R., Sanchez, R., Arias, C. F., & Lopez, S. (2005). Silencing the Morphogenesis of Rotavirus. *Journal of Virology*, 79(1), 184–192.

Lourenco, S. & Roy, P. (2011). In vitro reconstitution of Bluetongue virus infectious cores. *Proceedings of the National Academy of Sciences*, 108(33), 13746–13751.

Lu, X., McDonald, S. M., Tortorici, M. A., Tao, Y. J., Vasquez-Del Carpio, R., Nibert, M. L., Patton, J. T., & Harrison, S. C. (2008). Mechanism for Coordinated RNA Packaging and Genome Replication by Rotavirus Polymerase VP1. *Structure*, 16(11), 1678–1688.

Ludert, J., Michelangeli, F., Gil, F., Liprandi, F., & Esparza, J. (1987). Penetration and Uncoating of Rotaviruses in Cultured Cells. *Intervirology*, 27(2), 95–101.

Ludert, J. E., Krishnaney, A. A., Burns, J. W., Vo, P. T., & Greenberg, H. B. (1996). Cleavage of rotavirus VP4 in vivo. *Journal of General Virology*, 77(3), 391–395.

Lundgren, O. (2000). Role of the Enteric Nervous System in the Fluid and Electrolyte Secretion of Rotavirus Diarrhea. *Science*, 287(5452), 491–495.

MacLachlan, N. (1994). The pathogenesis and immunology of bluetongue virus infection of ruminants. *Comparative Immunology, Microbiology and Infectious Diseases*, 17(3), 197–206.

Madhi, S. A., Cunliffe, N. A., Steele, D., Witte, D., Kirsten, M., Louw, C., Ngwira, B., Victor, J. C., Gillard, P. H., Cheuvart, B. B., Han, H. H., & Neuzil, K. M. (2010). Effect of Human Rotavirus Vaccine on Severe Diarrhea in African Infants. *New England Journal of Medicine*, 362(4), 289–298.

Malherbe, H. & Harwin, R. (1963). The cytopathic effects of vervet monkey viruses. *South African Medical Journal*, 37(4), 407–11.

Malherbe, H. & Strickland-Cholmley, M. J. A. f. d. g. V. (1967). Simian virus SA11 and the related 0 agent. *Arch Gesamte Virusforsch*, 22(1-2), 235–245.

Marshall, N., Priyamvada, L., Ende, Z., Steel, J., & Lowen, A. C. (2013). Influenza Virus Reassortment Occurs with High Frequency in the Absence of Segment Mismatch. *PLoS Pathogens*, 9(6), e1003421.

Martella, V., Bányai, K., Matthijnssens, J., Buonavoglia, C., & Ciarlet, M. (2010). Zoonotic aspects of rotaviruses. *Veterinary Microbiology*, 140(3-4), 246–255.

Martin, D., Ouldali, M., Ménétrey, J., & Poncet, D. (2011). Structural Organisation of the Rotavirus Nonstructural Protein NSP5. *Journal of Molecular Biology*, 413(1), 209–221.

Masters, M., Colloms, M. D., Oliver, I. R., He, L., Macnaughton, E. J., & Charters, Y. (1993). The pcnB gene of Escherichia coli, which is required for ColE1 copy number maintenance, is dispensable. *Journal of bacteriology*, 175(14), 4405–4413.

Mathieu, M. (2001). Atomic structure of the major capsid protein of rotavirus: implications for the architecture of the virion. *EMBO Journal*, 20(7), 1485–1497.

Matsuno, S., Hasegawa, A., Kalica, A. R., & Kono, R. (1980). Isolation of a Recombinant between Simian and Bovine Rotaviruses. *Journal of General Virology*, 48(1), 253–256.

Matsuo, E., Celma, C. C., & Roy, P. (2010). A reverse genetics system of African horse sickness virus reveals existence of primary replication. *FEBS Letters*, 584(15), 3386–91.

Matsuo, E., Celma, C. C. P., Boyce, M., Viarouge, C., Sailleau, C., Dubois, E., Breard, E., Thiery, R., Zientara, S., & Roy, P. (2011). Generation of Replication-Defective Virus-Based Vaccines That Confer Full Protection in Sheep against Virulent Bluetongue Virus Challenge. *Journal of Virology*, 85(19), 10213–10221.

Matsuo, E. & Roy, P. (2009). Bluetongue Virus VP6 Acts Early in the Replication Cycle and Can Form the Basis of Chimeric Virus Formation. *Journal of Virology*, 83(17), 8842.

Matsuo, E. & Roy, P. (2011). Bluetongue virus VP1 polymerase activity in vitro: template dependency, dinucleotide priming and cap dependency. *PLoS One*, 6(11), e27702.

Matthijnssens, J., Attoui, H., Bányai, K., Brussaard, C. P. D., Danthi, P., del Vas, M., Dermody, T. S., Duncan, R., Fāng, Q., Johne, R., Mertens, P. P. C., Mohd Jaafar, F., Patton, J. T., Sasaya, T., Suzuki, N., & Wei, T. (2022). ICTV Virus Taxonomy Profile: Sedoreoviridae 2022. *Journal of General Virology,*, 103(10).

Matthijnssens, J., Ciarlet, M., Heiman, E., Arijs, I., Delbeke, T., McDonald, S. M., Palombo, E. A., Iturriza-Gomara, M., Maes, P., Patton, J. T., Rahman, M., & Van Ranst, M. (2008). Full Genome-Based Classification of Rotaviruses Reveals a Common Origin between Human Wa-Like and Porcine Rotavirus Strains and Human DS-1-Like and Bovine Rotavirus Strains. *Journal of Virology*, 82(7), 3204–3219.

Matthijnssens, J., Ciarlet, M., McDonald, S. M., Attoui, H., Bányai, K., Brister, J. R., Buesa, J., Esona, M. D., Estes, M. K., Gentsch, J. R., Iturriza-Gómara, M., Johne, R., Kirkwood, C. D., Martella, V., Mertens, P. P. C., Nakagomi, O., Parreño, V., Rahman, M., Ruggeri, F. M., Saif, L. J., Santos, N., Steyer, A., Taniguchi, K., Patton, J. T., Desselberger, U., & Van Ranst, M. (2011). Uniformity of rotavirus strain nomenclature proposed by the Rotavirus Classification Working Group (RCWG). *Archives of Virology*, 156(8), 1397–1413.

Matthijnssens, J. & Van Ranst, M. (2012). Genotype constellation and evolution of group A rotaviruses infecting humans. *Current Opinion in Virology*, 2(4), 426–433.

McClain, B., Settembre, E., Temple, B. R. S., Bellamy, A. R., & Harrison, S. C. (2010). X-ray Crystal Structure of the Rotavirus Inner Capsid Particle at 3.8 Å Resolution. *Journal of Molecular Biology*, 397(2), 587–599.

McDonald, S. M., Nelson, M. I., Turner, P. E., & Patton, J. T. (2016). Reassortment in segmented RNA viruses: mechanisms and outcomes. *Nature Reviews Microbiology*, 14(7), 448.

McDonald, S. M. & Patton, J. T. (2011). Assortment and packaging of the segmented rotavirus genome. *Trends in Microbiology*, 19(3), 136–144.

McNulty, M. S., Curran, W. L., & McFerran, J. B. (1976). The Morphogenesis of a Cytopathic Bovine Rotavirus in Madin-Darby Bovine Kidney Cells. *Journal of General Virology*, 33(3), 503–508.

Milligan, J. F., Groebe, D. R., Witherell, G. W., & Uhlenbeck, O. C. (1987). Oligoribonucleotide synthesis using T7 RNA polymerase and synthetic DNA templates. *Nucleic Acids Research*, 15(21), 8783–8798.

Mingo, R., Zhang, S., Long, C. P., LaConte, L. E. W., & McDonald, S. M. (2017). Genetic determinants restricting the reassortment of heterologous NSP2 genes into the simian rotavirus SA11 genome. *Scientific Reports*, 7(1), 9301.

Mlera, L. (2012). *Preparatory investigations for developing a transcript-based rotavirus reverse genetics system.* (Thesis - PhD), North-West University.

Mlera, L., O'Neill, H. G., Jere, K. C., & van Dijk, A. A. (2013). Whole-genome consensus sequence analysis of a South African rotavirus SA11 sample reveals a mixed infection with two close derivatives of the SA11-H96 strain. *Archives of Virology*, 158(5), 1021–30.

Montier, T., Benvegnu, T., Jaffres, P.-A., Yaouanc, J.-J., & Lehn, P. (2008). Progress in Cationic Lipid-Mediated Gene Transfection: A Series of Bio- Inspired Lipids as an Example. *Current Gene Therapy*, 8(5), 296–312.

Moon, S.-S., Wang, Y., Shane, A. L., Nguyen, T., Ray, P., Dennehy, P., Baek, L. J., Parashar, U., Glass, R. I., & Jiang, B. (2010). Inhibitory Effect of Breast Milk on Infectivity of Live Oral Rotavirus Vaccines. *The Pediatric Infectious Disease Journal*, 29(10).

Mundt, E. & Vakharia, V. N. (1996). Synthetic transcripts of double-stranded Birnavirus genome are infectious. *Proceedings of the National Academy of Sciences*, 93(20), 11131–11136.

Nair, N., Feng, N., Blum, L. K., Sanyal, M., Ding, S., Jiang, B., Sen, A., Morton, J. M., He, X.-S., Robinson, W. H., & Greenberg, H. B. (2017). VP4- and VP7-specific antibodies mediate heterotypic immunity to rotavirus in humans. *Science Translational Medicine*, 9(395), eaam5434.

Nair, N., Newell, E. W., Vollmers, C., Quake, S. R., Morton, J. M., Davis, M. M., He, X. S., & Greenberg, H. B. (2016). High-dimensional immune profiling of total and rotavirus VP6-specific intestinal and circulating B cells by mass cytometry. *Mucosal Immunology*, 9(1), 68–82.

Nair, N. P., Reddy N, S., Giri, S., Mohan, V. R., Parashar, U., Tate, J., Shah, M. P., Arora, R., Gupte, M., Mehendale, S. M., & Kang, G. (2019). Rotavirus vaccine impact assessment surveillance in India: protocol and methods. *BMJ Open*, 9(4), e024840.

Nakagomi, T., Nguyen, M. Q., Gauchan, P., Agbemabiese, C. A., Kaneko, M., Do, L. P., Vu, T. D., & Nakagomi, O. (2017). Evolution of DS-1-like G1P[8] double-gene reassortant rotavirus A strains causing gastroenteritis in children in Vietnam in 2012/2013. *Archives of Virology*, 162(3), 739–748.

Nakasu, S. & Tomizawa, J. (1992). Structure of the ColE1 DNA molecule before segregation to daughter molecules. *Proceedings of the National Academy of Sciences*, 89(21), 10139–10143.

Nibert, M. L., Margraf, R. L., & Coombs, K. M. (1996). Nonrandom segregation of parental alleles in reovirus reassortants. *Journal of virology*, 70(10), 7295–7300.

Nunes, S. F., Hamers, C., Ratinier, M., Shaw, A., Brunet, S., Hudelet, P., & Palmarini, M. (2014). A Synthetic Biology Approach for a Vaccine Platform against Known and Newly Emerging Serotypes of Bluetongue Virus. *Journal of Virology*, 88(21), 12222–12232.

O'Brien, J. A., Taylor, J. A., & Bellamy, A. R. (2000). Probing the Structure of Rotavirus NSP4: a Short Sequence at the Extreme C Terminus Mediates Binding to the Inner Capsid Particle. *Journal of Virology*, 74(11), 5388–5394.

Ogden, K. M., Johne, R., & Patton, J. T. (2012). Rotavirus RNA polymerases resolve into two phylogenetically distinct classes that differ in their mechanism of template recognition. *Virology*, 431(1-2), 50–7.

Olkkonen, V. M., Gottlieb, P., Strassman, J., Qiao, X. Y., Bamford, D. H., & Mindich, L. (1990). In vitro assembly of infectious nucleocapsids of bacteriophage phi 6: formation of a recombinant double-stranded RNA virus. *Proc Natl Acad Sci U S A*, 87(23), 9173–9177.

O'Neal, C. M., Crawford, S. E., Estes, M. K., & Conner, M. E. (1997). Rotavirus virus-like particles administered mucosally induce protective immunity. *Journal of Virology*, 71(11), 8707–8717.

Ousingsawat, J., Mirza, M., Tian, Y., Roussa, E., Schreiber, R., Cook, D. I., & Kunzelmann, K. (2011). Rotavirus toxin NSP4 induces diarrhea by activation of TMEM16A and inhibition of Na+ absorption. *Pflügers Archiv - European Journal of Physiology*, 461(5), 579–589.

O'Neill, E. & Donis, R. O. (2009). Generation and Characterization of Candidate Vaccine Viruses for Prepandemic Influenza Vaccines. In R. W. Compans & W. A. Orenstein (Eds.), *Vaccines for Pandemic Influenza* (pp. 83–108). Berlin, Heidelberg: Springer Berlin Heidelberg.

Page, N. A., Seheri, L. M., Groome, M. J., Moyes, J., Walaza, S., Mphahlele, J., Kahn, K., Kapongo, C. N., Zar, H. J., Tempia, S., Cohen, C., & Madhi, S. A. (2018). Temporal association of rotavirus vaccination and genotype circulation in South Africa: Observations from 2002 to 2014. *Vaccine*, 36(47), 7231–7237.

Panja, S., Aich, P., Jana, B., & Basu, T. (2008). How does plasmid DNA penetrate cell membranes in artificial transformation process of Escherichia coli? *Molecular Membrane Biology*, 25(5), 411–422.

Parr, R. D., Storey, S. M., Mitchell, D. M., McIntosh, A. L., Zhou, M., Mir, K. D., & Ball, J. M. (2006). The Rotavirus Enterotoxin NSP4 Directly Interacts with the Caveolar Structural Protein Caveolin-1. *Journal of Virology*, 80(6), 2842–2854.

Patton J T, Jones M T, Kalbach A N, He Y W, & Xiaobo J (1997). Rotavirus RNA polymerase requires the core shell protein to synthesize the double-stranded RNA genome. *Journal of Virology*, 71(12), 9618–9626. Publisher: American Society for Microbiology.

Phan, T., Ide, T., Komoto, S., Khamrin, P., Okitsu, S., Taniguchi, K., Kikuta, H., Maneekarn, N., Hayakawa, S., & Ushijima, H. (2020). Unusual mono-reassortant of a Wa-like G1P[8] species A rotavirus containing a DS-1-like (genotype 2) NSP4 gene. *Virus Genes*, 56(5), 638–641.

Philip, A. A., Dai, J., Katen, S. P., & Patton, J. T. (2020). Simplified Reverse Genetics Method to Recover Recombinant Rotaviruses Expressing Reporter Proteins. *Journal of Visualised Experiments*, (158), e61039.

Piron, M. (1998). Rotavirus RNA-binding protein NSP3 interacts with eIF4GI and evicts the poly(A) binding protein from eIF4F. *The EMBO Journal*, 17(19), 5811–5821.

Piron, M., Delaunay, T., Grosclaude, J., & Poncet, D. (1999). Identification of the RNA-binding, dimerization, and eIF4GI-binding domains of rotavirus nonstructural protein NSP3. *Journal of virology*, 73(7), 5411–5421.

Pirttimaa, M. J. T. & Bamford, D. H. (2000). RNA secondary structures of the bacteriophage φ6 packaging regions. *RNA*, 6(6), 880–889.

Pollack, J. D., Williams, M. V., & McElhaney, R. N. (1997). The Comparative Metabolism of the Mollicutes (Mycoplasmas): The Utility for Taxonomic Classification and the Relationship of Putative Gene Annotation and Phylogeny to Enzymatic Function in the Smallest Free-Living Cells. *Critical Reviews in Microbiology*, 23(4), 269–354.

Poranen, M. M., Paatero, A. O., Tuma, R., & Bamford, D. H. (2001). Self-Assembly of a Viral Molecular Machine from Purified Protein and RNA Constituents. *Molecular Cell*, 7(4), 845–854.

Potgieter, A. C., Page, N. A., Liebenberg, J., Wright, I. M., Landt, O., & Van Dijk, A. A. (2009). Improved strategies for sequence-independent amplification and sequencing of viral double-stranded RNA genomes. *Journal of General Virology*, 90(6), 1423–1432.

Pretorius, J. M., Huismans, H., & Theron, J. (2015). Establishment of an entirely plasmid-based reverse genetics system for Bluetongue virus. *Virology*, 486, 71–77.

Qiao, X., Qiao, J., Onodera, S., & Mindich, L. (2000). Characterization of Φ13, a Bacteriophage Related to Φ6 and Containing Three dsRNA Genomic Segments. *Virology*, 275(1), 218–224.

Racaniello, V. & Baltimore, D. (1981). Cloned poliovirus complementary DNA is infectious in mammalian cells. *Science*, 214(4523), 916–919.

Ramig, R. F. (1997). Genetics of the rotaviruses. *Annual Review of Microbiology*, 51(1), 225–255.

Ramig, R. F., Garrison, C., Chen, D., & Bell-Robinson, D. (1989). Analysis of Reassortment and Superinfection during Mixed Infection of Vero Cells with Bluetongue Virus Serotypes 10 and 17. *Journal of General Virology*, 70(10), 2595–2603.

Ratinier, M., Shaw, A. E., Barry, G., Gu, Q., Di Gialleonardo, L., Janowicz, A., Varela, M., Randall, R. E., Caporale, M., & Palmarini, M. (2016). Bluetongue Virus NS4 Protein Is an Interferon Antagonist and a Determinant of Virus Virulence. *Journal of virology*, 90(11), 5427–5439.

Reitmeyer, J. C. & Peterson, J. W. (1988). In vitro cytotoxicity of lipopolysaccharides for chinese hamster ovary cells. *FEMS Microbiology Letters*, 49(3), 393–396.

Rice, C. M., Grakoui, A., Galler, R., & Chambers, T. J. (1989). Transcription of infectious yellow fever RNA from full-length cDNA templates produced by in vitro ligation. *The New biologist*, 1(3), 285–296.

Rio, D. C., Ares, M., Hannon, G. J., & Nilsen, T. W. (2010a). Polyacrylamide Gel Electrophoresis of RNA. *Cold Spring Harbor Protocols*, 2010(6), pdb.prot5444.

Rio, D. C., Ares, Jr., M., Hannon, G. J., & Nilsen, T. W. (2010b). Purification of RNA using TRIzol (TRI reagent). *Cold Spring Harbor Protocols*, 2010(6), pdb.prot5439.

Robinson, J. T., Thorvaldsdóttir, H., Winckler, W., Guttman, M., Lander, E. S., Getz, G., & Mesirov, J. P. (2011). Integrative genomics viewer. *Nature Biotechnology*, 29(1), 24–26.

Roner, M. R. & Joklik, W. K. (2001). Reovirus reverse genetics: Incorporation of the CAT gene into the reovirus genome. *Proceedings of the National Academy of Sciences*, 98(14), 8036–8041.

Roner, M. R., Sutphin, L. A., & Joklik, W. K. (1990). Reovirus RNA is infectious. *Virology*, 179(2), 845–852.

Rose, T. L., Marques da Silva, M. F., Goméz, M. M., Resque, H. R., Ichihara, M. Y. T., Volotão, E. d. M., & Leite, J. P. G. (2013). Evidence of Vaccine-related Reassortment of Rotavirus, Brazil, 2008–2010. *Emerging Infectious Disease journal*, 19(11), 1843.

Rottem, S. & Barile, M. F. (1993). Beware of mycoplasmas. *Trends in Biotechnology*, 11(4), 143–151.

Rottem, S. & Naot, Y. (1998). Subversion and exploitation of host cells by mycoplasmas. *Trends in Microbiology*, 6(11), 436–440.

Roy, P. (2017). Bluetongue virus structure and assembly. *Current Opinion in Virology*, 24, 115–123.

Ruiz-Palacios, G. M., Pérez-Schael, I., Velázquez, F. R., Abate, H., Breuer, T., Clemens, S. C., Cheuvart, B., Espinoza, F., Gillard, P., Innis, B. L., Cervantes, Y., Linhares, A. C., López, P., Macías-Parra, M., Ortega-Barría, E., Richardson, V., Rivera-Medina, D. M., Rivera, L., Salinas, B., Pavía-Ruz, N., Salmerón, J., Rüttimann, R., Tinoco, J. C., Rubio, P., Nuñez, E., Guerrero, M. L., Yarzábal, J. P., Damaso, S., Tornieporth, N., Sáez-Llorens, X., Vergara, R. F., Vesikari, T., Bouckenooghe, A., Clemens, R., De Vos, B., & O'Ryan, M. (2006). Safety and Efficacy of an Attenuated Vaccine against Severe Rotavirus Gastroenteritis. *New England Journal of Medicine*, 354(1), 11–22.

Sambrook, J. & Russell, D. (2001). *Molecular Cloning: A Laboratory Manual*. Number v. 2. Cold Spring Harbor Laboratory Press.

Sanchez-Tacuba, L., Feng Ningguo, Meade Nathan J., Mellits Kenneth H., Jaïs Philippe H., Yasukawa Linda L., Resch Theresa K., Jiang Baoming, López Susana, Ding Siyuan, Greenberg Harry B., & Parrish Colin R. (2020). An Optimized Reverse Genetics System

Suitable for Efficient Recovery of Simian, Human, and Murine-Like Rotaviruses. *Journal of Virology*, 94(18), e01294–20.

Sandino, A. M., Jashes, M., Faúndez, G., & Spencer, E. (1986). Role of the inner protein capsid on in vitro human rotavirus transcription. *Journal of Virology*, 60(2), 797–802.

Sastri, N. P., Viskovska, M., Hyser, J. M., Tanner, M. R., Horton, L. B., Sankaran, B., Prasad, B. V. V., & Estes, M. K. (2014). Structural Plasticity of the Coiled-Coil Domain of Rotavirus NSP4. *Journal of Virology*, 88(23), 13602–13612.

Seo, N.-S., Zeng, C. Q. Y., Hyser, J. M., Utama, B., Crawford, S. E., Kim, K. J., Höök, M., & Estes, M. K. (2008). Integrins α1β1 and α2β1 are receptors for the rotavirus enterotoxin. *Proceedings of the National Academy of Sciences*, 105(26), 8811–8818.

Settembre, E. C., Chen, J. Z., Dormitzer, P. R., Grigorieff, N., & Harrison, S. C. (2011). Atomic model of an infectious rotavirus particle. *EMBO Journal*, 30(2), 408–16.

Silvestri, L. S., Tortorici, M. A., Vasquez-Del Carpio, R., & Patton, J. T. (2005). Rotavirus Glycoprotein NSP4 Is a Modulator of Viral Transcription in the Infected Cell. *Journal of Virology*, 79(24), 15165–15174.

Small, C., Barro, M., Brown, T. L., & Patton, J. T. (2007). Genome heterogeneity of SA11 rotavirus due to reassortment with "O" agent. *Virology*, 359(2), 415–24.

Song, Y., Feng, N., Sanchez-Tacuba, L., Yasukawa, L. L., Ren, L., Silverman, R. H., Ding, S., & Greenberg, H. B. (2020). Reverse Genetics Reveals a Role of Rotavirus VP3 Phosphodiesterase Activity in Inhibiting RNase L Signaling and Contributing to Intestinal Viral Replication In Vivo. *Journal of Virology*, 94(9), e01952–19.

Steger, C. L., Boudreaux, C. E., LaConte, L. E., Pease, J. B., & McDonald, S. M. (2019). Group A Rotavirus VP1 Polymerase and VP2 Core Shell Proteins: Intergenotypic Sequence Variation and In Vitro Functional Compatibility. *Journal of Virology*, 93(2).

Strydom, A., João, E. D., Motanyane, L., Nyaga, M. M., Christiaan Potgieter, A., Cuamba, A., Mandomando, I., Cassocera, M., de Deus, N., & O'Neill, H. G. (2019a). Whole genome analyses of DS-1-like Rotavirus A strains detected in children with acute diarrhoea in southern Mozambique suggest several reassortment events. *Infection, Genetics and Evolution*, 69, 68–75.

Strydom, A., Motanyane, L., Nyaga, M. M., João, E. D., Cuamba, A., Mandomando, I., Cassocera, M., de Deus, N., & Neill, H. (2019b). Whole-genome characterization of G12 rotavirus strains detected in Mozambique reveals a co-infection with a GXP[14] strain of possible animal origin. *Journal of General Virology*, 100(6), 932–937.

Sun, Z., Asmann, Y. W., Nair, A., Zhang, Y., Wang, L., Kalari, K. R., Bhagwate, A. V., Baker, T. R., Carr, J. M., Kocher, J.-P. A., Perez, E. A., & Thompson, E. A. (2013). Impact of Library Preparation on Downstream Analysis and Interpretation of RNA-Seq Data: Comparison between Illumina PolyA and NuGEN Ovation Protocol. *PLOS ONE*, 8(8), 1–12.

Sung, P. Y. & Roy, P. (2014). Sequential packaging of RNA genomic segments during the assembly of Bluetongue virus. *Nucleic Acids Research*, 42(22), 13824–13838.

Tamim, S., Matthijnssens, J., Heylen, E., Zeller, M., Van Ranst, M., Salman, M., & Hasan, F. J. A. o. V. (2019). Evidence of zoonotic transmission of VP6 and NSP4 genes into human species A rotaviruses isolated in Pakistan in 2010. *Archives of Virology*, 164(7), 1781–1791.

Taniguchi, K. & Komoto, S. (2012). Genetics and reverse genetics of rotavirus. *Current Opinion in Virology*, 2(4), 399–407.

Tate, J. E., Burton, A. H., Boschi-Pinto, C., & Parashar, U. D. (2016). Global, Regional, and National Estimates of Rotavirus Mortality in Children < 5 Years of Age, 2000–2013. *Clinical Infectious Diseases*, 62(suppl 2), S96–S105.

Tate, J. E., Burton, A. H., Boschi-Pinto, C., Steele, A. D., Duque, J., & Parashar, U. D. (2012). 2008 estimate of worldwide rotavirus-associated mortality in children younger than 5 years before the introduction of universal rotavirus vaccination programmes: a systematic review and meta-analysis. *The Lancet Infectious Diseases*, 12(2), 136–141.

Tatte, V. S. & Chitambar, S. D. (2012). Evidence of discordant genetic linkage in the VP4, VP6, VP7 and NSP4 encoding genes of rotavirus strains from adolescent and adult patients with acute gastroenteritis. *Infection, Genetics and Evolution*, 12(8), 1630–1634.

Tatte, V. S., Rawal, K. N., & Chitambar, S. D. (2010). Sequence and phylogenetic analysis of the VP6 and NSP4 genes of human rotavirus strains: Evidence of discordance in their genetic linkage. *Infection, Genetics and Evolution*, 10(7), 940–949.

Taylor, J. A., Meyer, J. C., Legge, M. A., O'Brien, J. A., Street, J. E., Lord, V. J., Bergmann, C. C., & Bellamy, A. R. (1992). Transient expression and mutational analysis of the rotavirus intracellular receptor: the C-terminal methionine residue is essential for ligand binding. *Journal of Virology*, 66(6), 3566–3572.

Taylor, J. A., O'Brien, J. A., Lord, V. J., Meyer, J. C., & Bellamy, A. R. (1993). The RER-Localized Rotavirus Intracellular Receptor: A Truncated Purified Soluble Form Is Multivalent and Binds Virus Particles. *Virology*, 194(2), 807–814.

Taylor, J. A., O'Brien, J. A., & Yeager, M. (1996). The cytoplasmic tail of NSP4, the endoplasmic reticulum-localized non-structural glycoprotein of rotavirus, contains distinct virus binding and coiled coil domains. *EMBO Journal*, 15(17), 4469–4476.

Thao, T. T. N., Labroussaa, F., Ebert, N., V'kovski, P., Stalder, H., Portmann, J., Kelly, J., Steiner, S., Holwerda, M., Kratzel, A., Gultom, M., Schmied, K., Laloli, L., Hüsser, L., Wider, M., Pfaender, S., Hirt, D., Cippà, V., Crespo-Pomar, S., Schröder, S., Muth, D., Niemeyer, D., Corman, V., Müller, M. A., Drosten, C., Dijkman, R., Jores, J., & Thiel, V. (2020). Rapid reconstruction of SARS-CoV-2 using a synthetic genomics platform. *Nature*, (582), 561–565.

Trask, S. D. & Dormitzer, P. R. (2006). Assembly of Highly Infectious Rotavirus Particles Recoated with Recombinant Outer Capsid Proteins. *Journal of Virology*, 80(22), 11293–11304.

Trask, S. D., McDonald, S. M., & Patton, J. T. (2012). Structural insights into the coupling of virion assembly and rotavirus replication. *Nature Reviews Microbiology*, 10(3), 165–177.

Trask, S. D., Taraporewala, Z. F., Boehme, K. W., Dermody, T. S., & Patton, J. T. (2010). Dual selection mechanisms drive efficient single-gene reverse genetics for rotavirus. *Proceedings of the National Academy of Sciences*, 107(43), 18652–18657.

Troeger, C., Khalil, I. A., Rao, P. C., Cao, S., Blacker, B. F., Ahmed, T., Armah, G., Bines, J. E., Brewer, T. G., Colombara, D. V., Kang, G., Kirkpatrick, B. D., Kirkwood, C. D., Mwenda, J. M., Parashar, U. D., Petri, W. A., Riddle, M. S., Steele, A. D., Thompson, R. L., Walson, J. L., Sanders, J. W., Mokdad, A. H., Murray, C. J. L., Hay, S. I., & Reiner, R. C. (2018). Rotavirus Vaccination and the Global Burden of Rotavirus Diarrhea Among Children Younger Than 5 Years. *JAMA Pediatrics*, 172(10), 958.

Troupin, C., Schnuriger, A., Duponchel, S., Deback, C., Schnepf, N., Dehee, A., & Garbarg-Chenon, A. (2011). Rotavirus Rearranged Genomic RNA Segments Are Preferentially Packaged into Viruses Despite Not Conferring Selective Growth Advantage to Viruses. *PLoS One*, 6(5), e20080.

van de Water, S. G. P., van Gennip, R. G. P., Potgieter, C. A., Wright, I. M., & van Rijn, P. A. (2015). VP2 Exchange and NS3/NS3a Deletion in African Horse Sickness Virus (AHSV) in Development of Disabled Infectious Single Animal Vaccine Candidates for AHSV. *Infection, Genetics and Evolution*, 89(17), 8764–8772.

van Dijk, A. A. & Huismans, H. (1980). The in vitro activation and further characterization of the bluetongue virus-associated transcriptase. *Virology*, 104(2), 347–356.

Van Gennip, R. G. P., Van De Water, S. G. P., Potgieter, C. A., Wright, I. M., Veldman, D., & Van Rijn, P. A. (2012). Rescue of Recent Virulent and Avirulent Field Strains of Bluetongue Virus by Reverse Genetics. *PLoS One*, 7(2), e30540.

van Rijn, P. A. (2019). Prospects of Next-Generation Vaccines for Bluetongue. *Frontiers in Veterinary Science*, 6(407), 407.

Van Rijn, P. A., Daus, F. J., Maris-Veldhuis, M. A., Feenstra, F., & Van Gennip, R. G. P. (2017). Bluetongue Disabled Infectious Single Animal (DISA) vaccine: Studies on the optimal route and dose in sheep. *Vaccine*, 35(2), 231–237.

van Rijn, P. A., Maris-Veldhuis, M. A., Potgieter, C. A., & van Gennip, R. G. P. (2018). African horse sickness virus (AHSV) with a deletion of 77 amino acids in NS3/NS3a protein is not virulent and a safe promising AHS Disabled Infectious Single Animal (DISA) vaccine platform. *Vaccine*, 36(15), 1925–1933.

van Rijn, P. A., van de Water, S. G., Feenstra, F., & van Gennip, R. G. (2016). Requirements and comparative analysis of reverse genetics for bluetongue virus (BTV) and African horse sickness virus (AHSV). *Virology Journal*, 13, 119.

Verwoerd, D. & Huismans, H. (1972). Studies on the in vitro and the in vivo transcription of the bluetongue virus genome. *Onderstepoort Journal of Veterinary Research*, 39(4), 185–192.

Vesikari, T., Karvonen, A., Prymula, R., Schuster, V., Tejedor, J. C., Cohen, R., Meurice, F., Han, H. H., Damaso, S., & Bouckenooghe, A. (2007). Efficacy of human rotavirus vaccine against rotavirus gastroenteritis during the first 2 years of life in European infants: randomised, double-blind controlled study. *The Lancet*, 370(9601), 1757–1763.

Wall, G. V., Wright, I. M., Barnardo, C., Erasmus, B. J., van Staden, V., & Potgieter, A. C. (2021). African horse sickness virus NS4 protein is an important virulence factor and interferes with JAK-STAT signaling during viral infection. *Virus Research*, 298, 198407.

Wang, X. & Quinn, P. J. (2010). Endotoxins: Lipopolysaccharides of Gram-Negative Bacteria. In X. Wang & P. J. Quinn (Eds.), *Endotoxins: Structure, Function and Recognition* (pp. 3–25). Dordrecht: Springer Netherlands.

Ward, R. L., Bernstein, D. I., & Plotkin, S. (2009). Rotarix: A Rotavirus Vaccine for the World. *Clinical Infectious Diseases*, 48(2), 222–228.

Ward, R. L., Mason, B. B., Bernstein, D. I., Sander, D. S., Smith, V. E., Zandle, G. A., & Rappaport, R. S. (1997). Attenuation of a human rotavirus vaccine candidate did not correlate with mutations in the NSP4 protein gene. *Journal of Virology*, 71(8), 6267–6270.

Welter, M. W., Welter, C. J., Chambers, D. M., & Svensson, L. (1991). Adaptation and serial passage of porcine group C rotavirus in ST-cells, an established diploid swine testicular cell line. *Archives of Virology*, 120(3-4), 297–304.

Wentzel, J. (2014). *Investigating the importance of co-expressed rotavirus proteins in the development of a selection-free rotavirus reverse genetics system.* PhD Thesis, North-West University.

Wentzel, J. F., Yuan, L., Rao, S., van Dijk, A. A., & O'Neill, H. G. (2013). Consensus sequence determination and elucidation of the evolutionary history of a rotavirus Wa variant reveal a close relationship to various Wa variants derived from the original Wa strain. *Infection, Genetics and Evolution*, 20, 276–283.

Whitaker, A. M. & Hayward, C. J. (1985). The characterization of three monkey kidney cell lines. *Developments in biological standardization*, 60, 125–131.

Wong, E. T. C., Na, D., & Gsponer, J. (2013). On the Importance of Polar Interactions for Complexes Containing Intrinsically Disordered Proteins. *PLOS Computational Biology*, 9(8), e1003192.

Wu, Y. C. & Liu, S. T. (2010). A Sequence That Affects the Copy Number and Stability of pSW200 and ColE1. *Journal of Bacteriology*, 192(14), 3654–3660.

Young, L., Sung, J., Stacey, G., & Masters, J. R. (2010). Detection of Mycoplasma in cell cultures. *Nature Protocols*, 5(5), 929–934.

Zeng, C. Q. Y., Labbé, M., Cohen, J., Prasad, B. V. V., Chen, D., Ramig, R. F., & Estes, M. K. (1994). Characterization of Rotavirus VP2 Particles. *Virology*, 201(1), 55–65.

Zeng, Y., Zhao, B., Li, T., Zhang, S., Wang, Y., Xu, H., Ge, S., & Xia, N. (2020). Molecular characterization of an uncommon multigene Reassortant G1P[4] rotavirus identified in China. *Infection, Genetics and Evolution*, 85, 104413.

Zhang, X., Kong, W., Ashraf, S., & Curtiss, R. (2009). A One-Plasmid System To Generate Influenza Virus in Cultured Chicken Cells for Potential Use in Influenza Vaccine. *Journal of Virology*, 83(18), 9296–9303. Type: Journal Article.

Zwart, L., Potgieter, C. A., Clift, S. J., & van Staden, V. (2015). Characterising Non-Structural Protein NS4 of African Horse Sickness Virus. *PLOS ONE*, 10(4), e0124281.

[

Appendix]Appendix

A Plasmid maps of pSMART-T7_RV-SA11_inline reverse genetics plasmid set

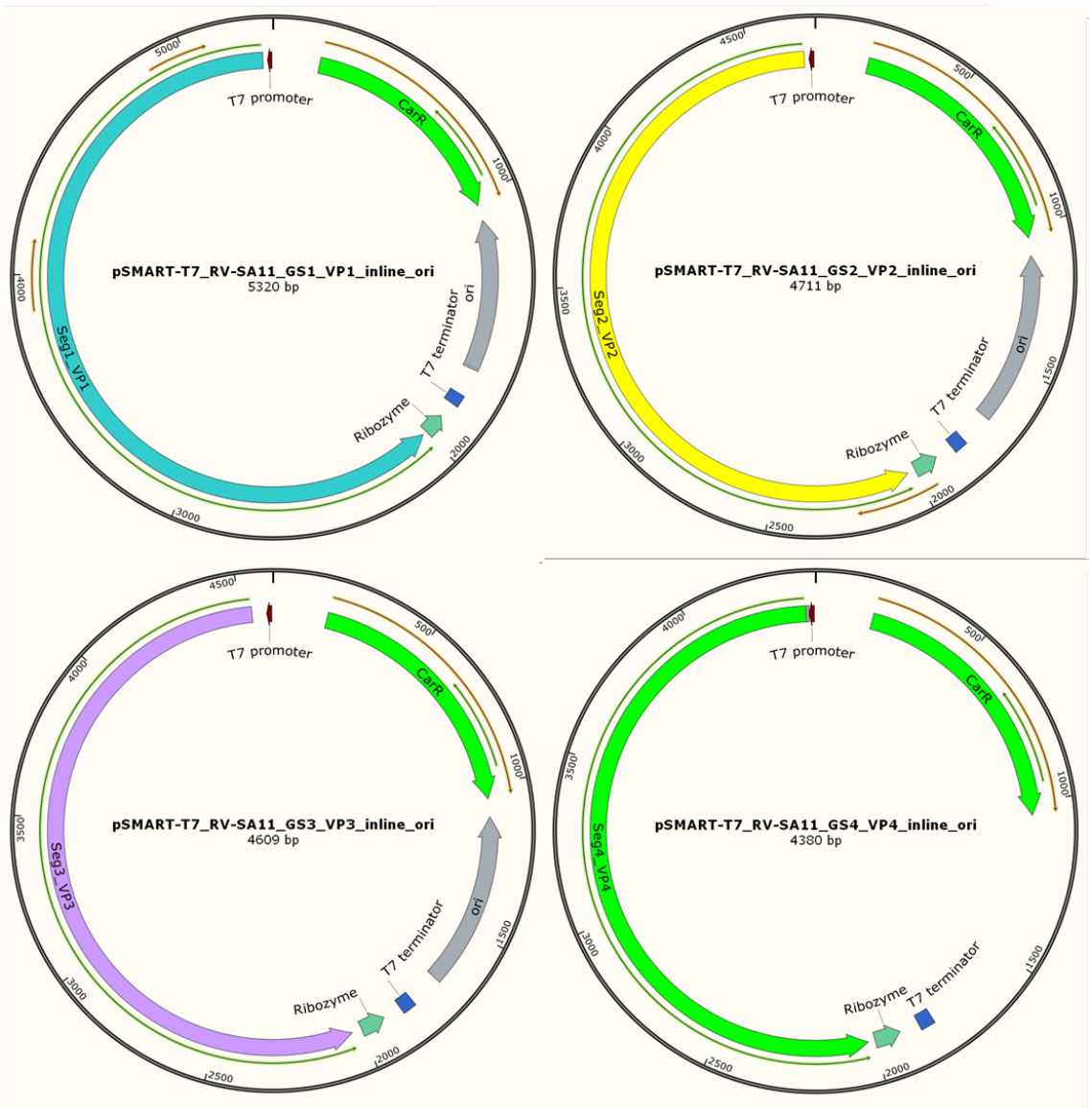


Fig. S1: pSMART-T7_RV-SA11_inline GS1(VP1)-GS4(VP4) reverse genetics plasmid maps

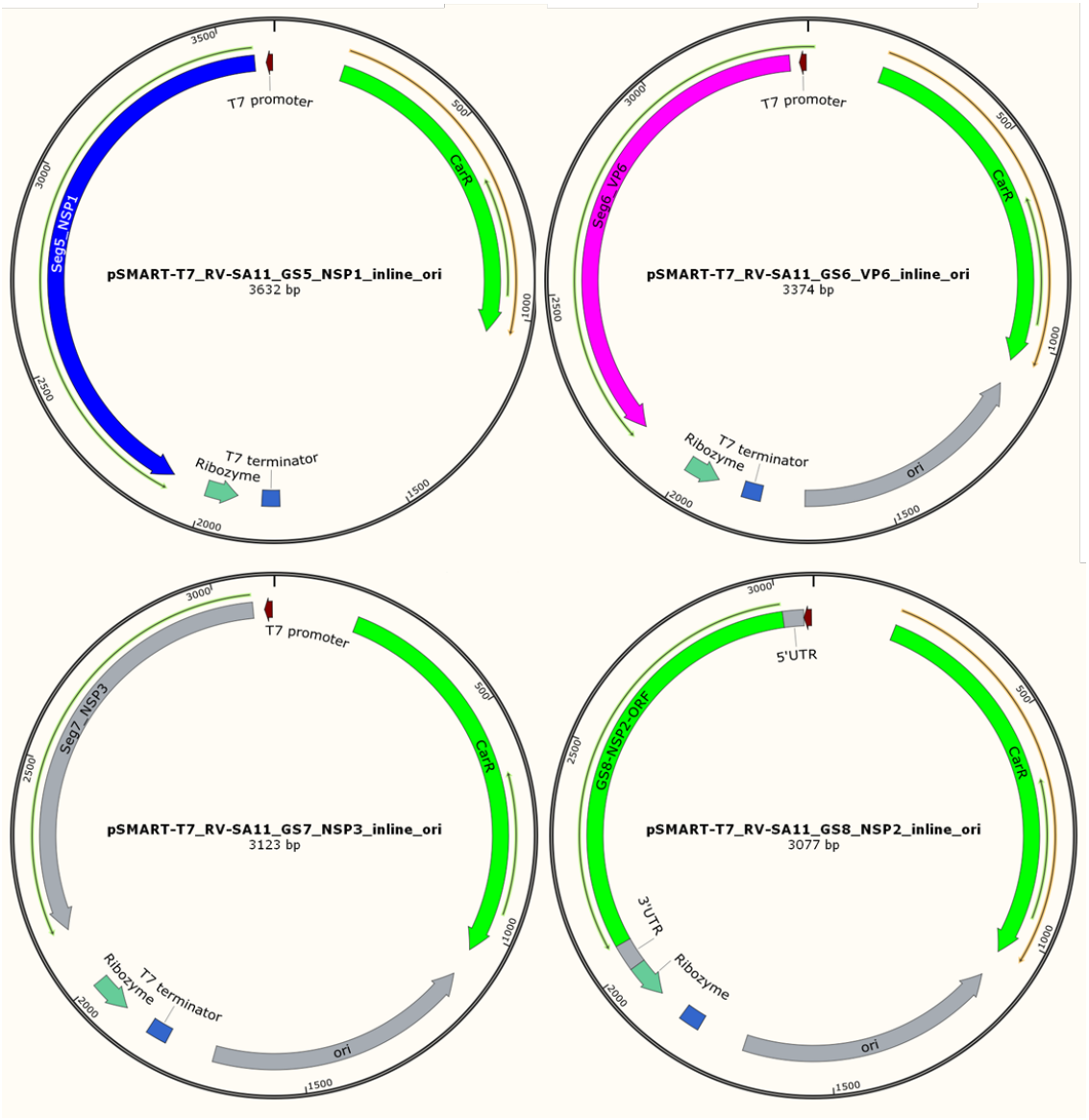


Fig. S2: pSMART-T7_RV-SA11_inline GS5(NSP1)-GS8(NSP2) reverse genetics plasmid maps

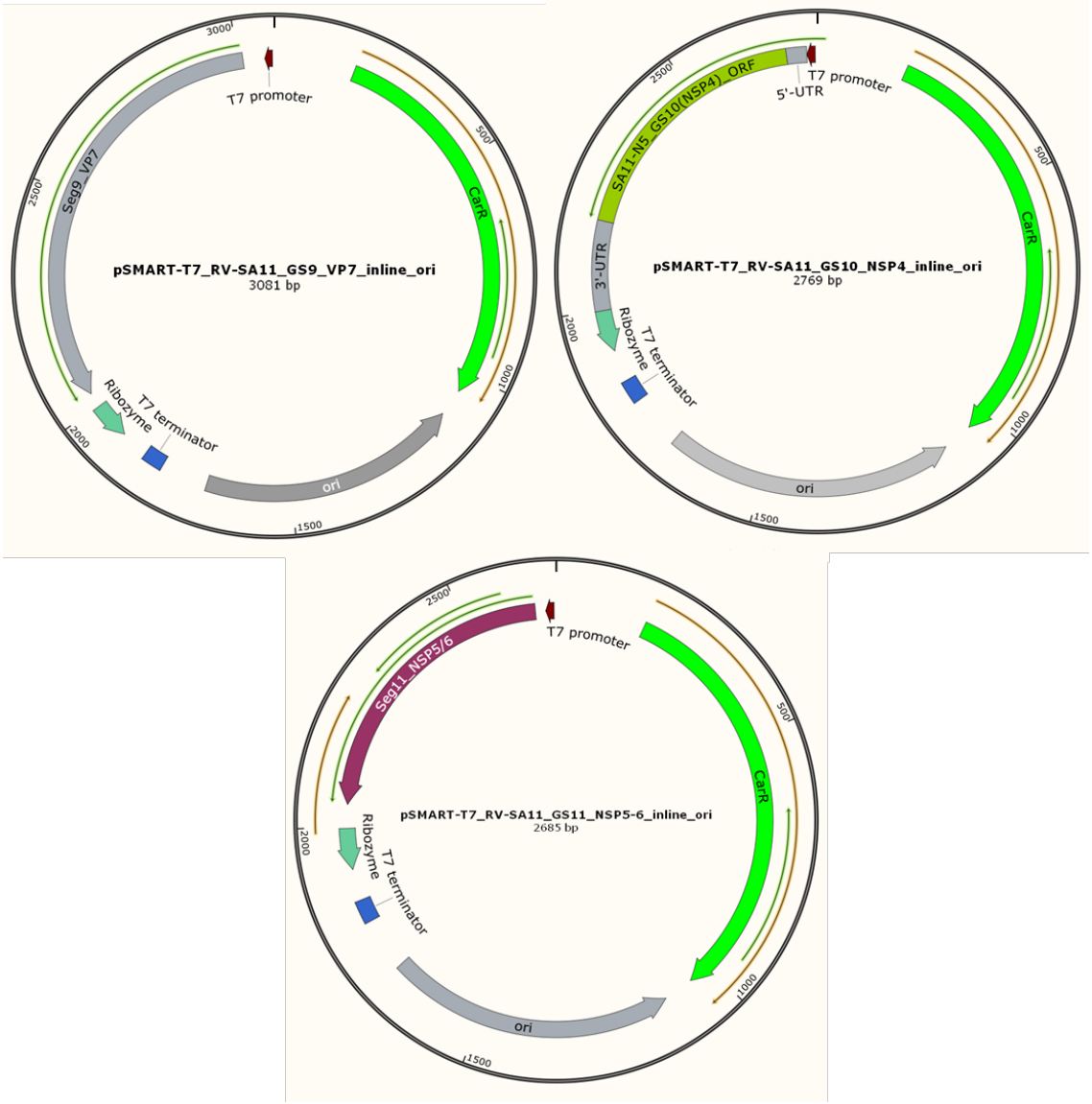


Fig. S3: pSMART-T7_RV-SA11_inline GS9(VP7)-GS11(NSP5/6) reverse genetics plasmid maps

B GS6(VP6)/GS10(NSP4) plasmid maps

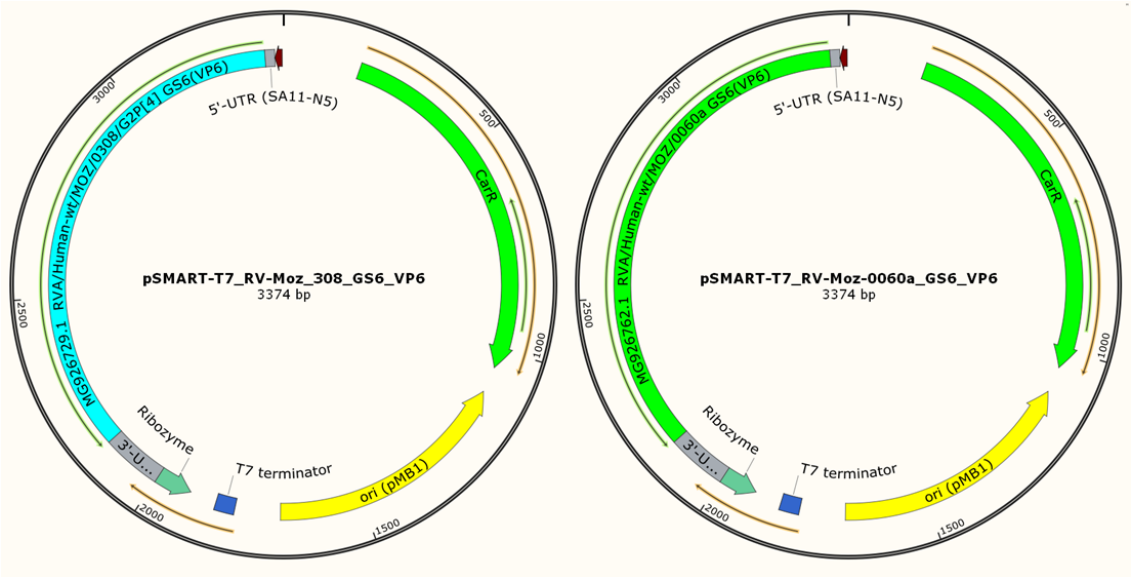


Fig. S4: pSMART-T7_RV-Moz308_VP6 and pSMART-T7_RV-Moz0060a_VP6 plasmid maps

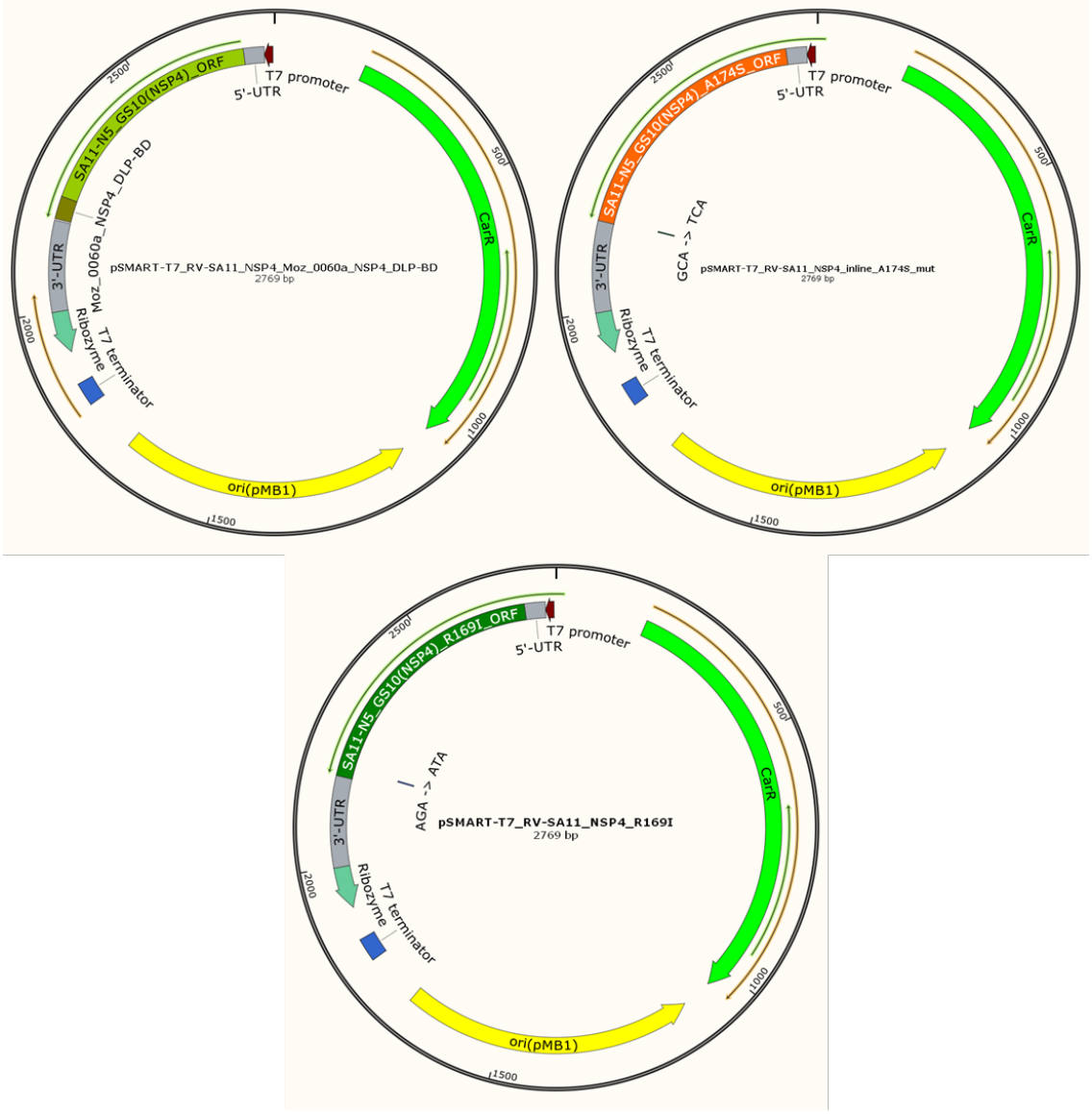


Fig. S5: pSMART-T7_RV-SA11_NSP4_Moz0060a_DLP-BD

C Consensus of NGS of pSMART-T7_RV-SA11_inline plasmid set alignment

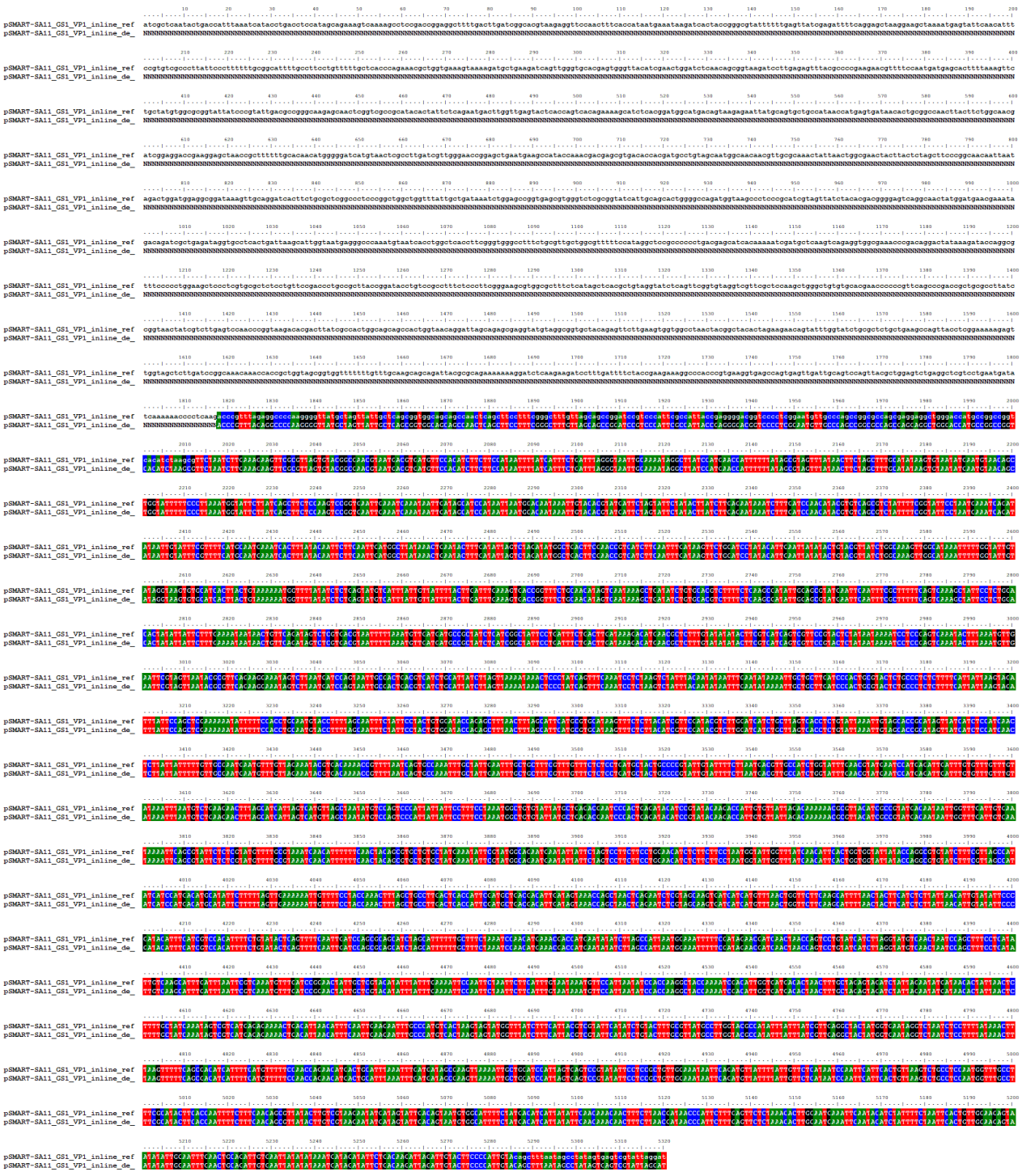


Fig. S6: Alignment of consensus sequence generated from pSMART-T7_RV-SA11_GS1_VP1_inline with reference sequence

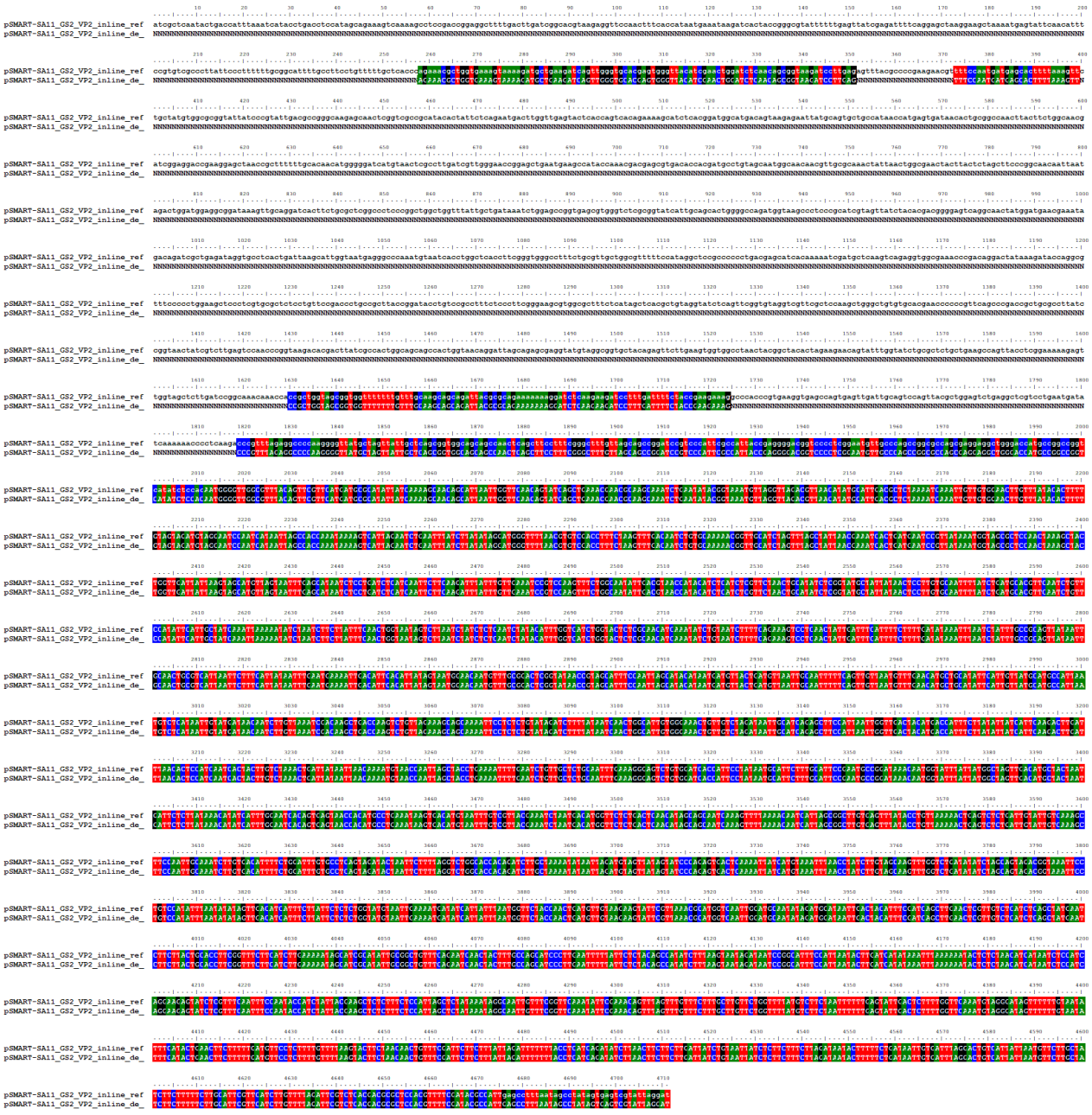


Fig. S7: Alignment of consensus sequence generated from pSMART-T7_RV-SA11_GS2_VP2_inline with reference sequence

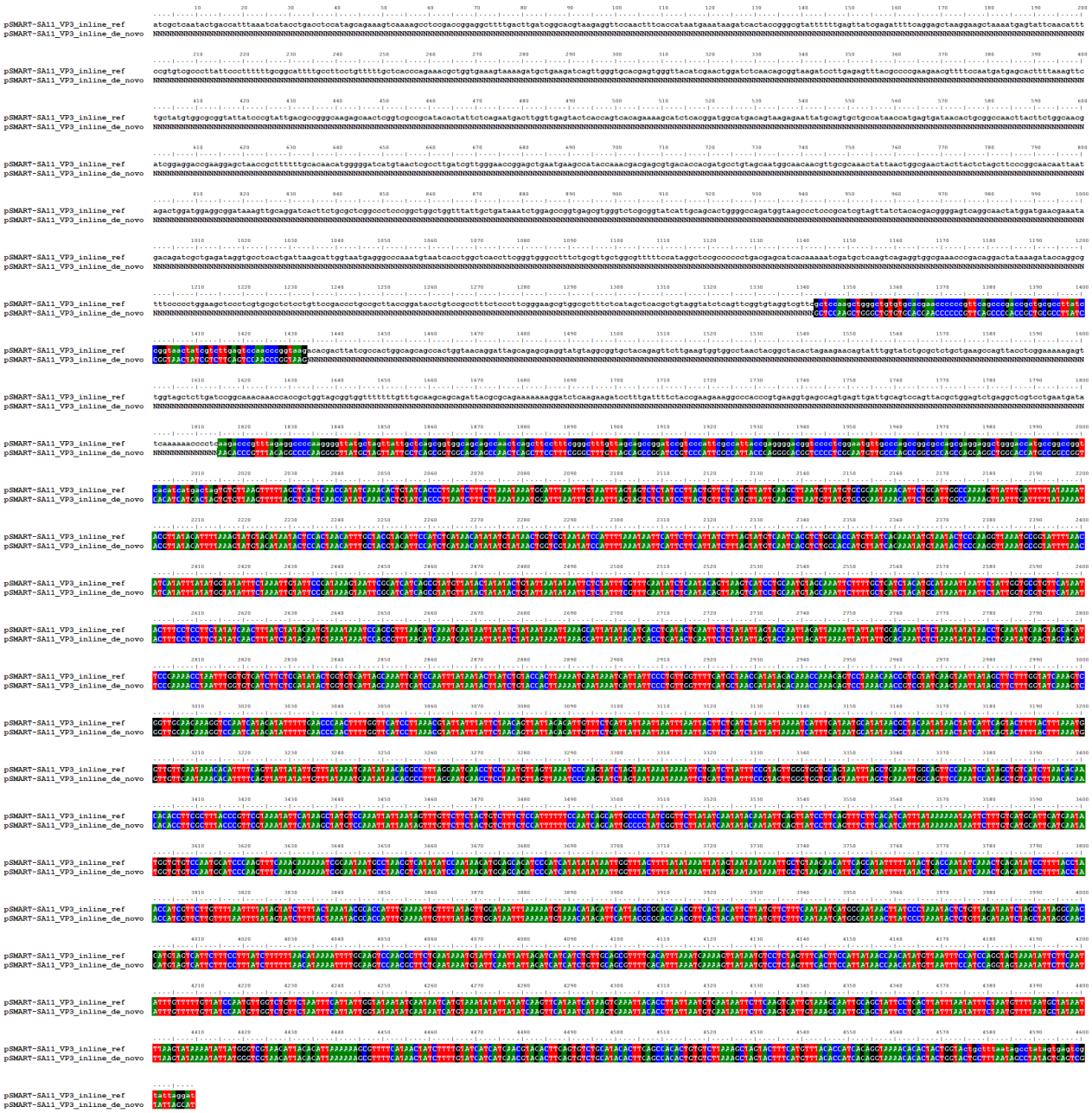


Fig. S8: Alignment of consensus sequence generated from pSMART-T7_RV-SA11_GS3_VP3_inline with reference sequence

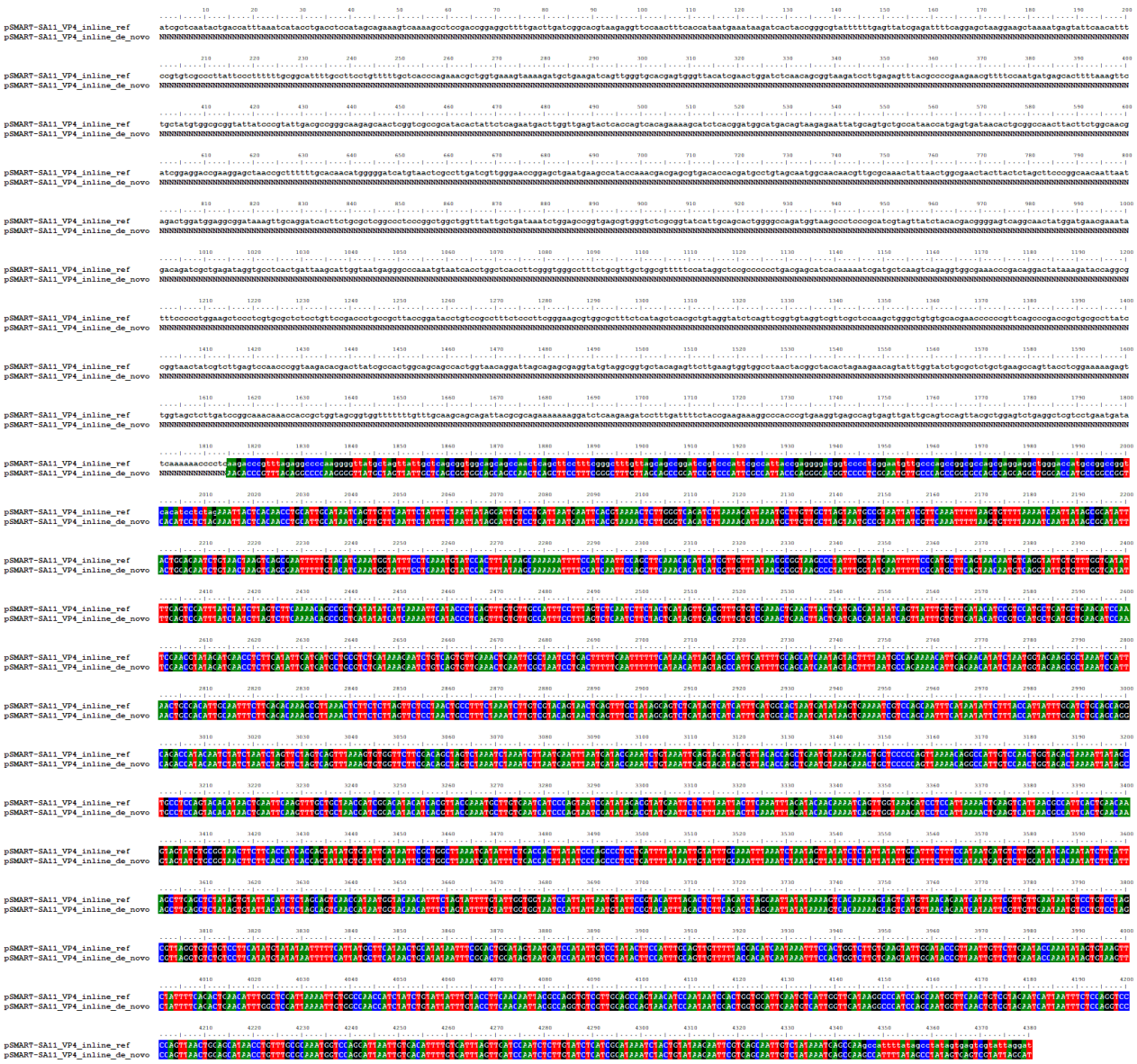


Fig. S9: Alignment of consensus sequence generated from pSMART-T7_RV-SA11_GS4_VP4_inline with reference sequence

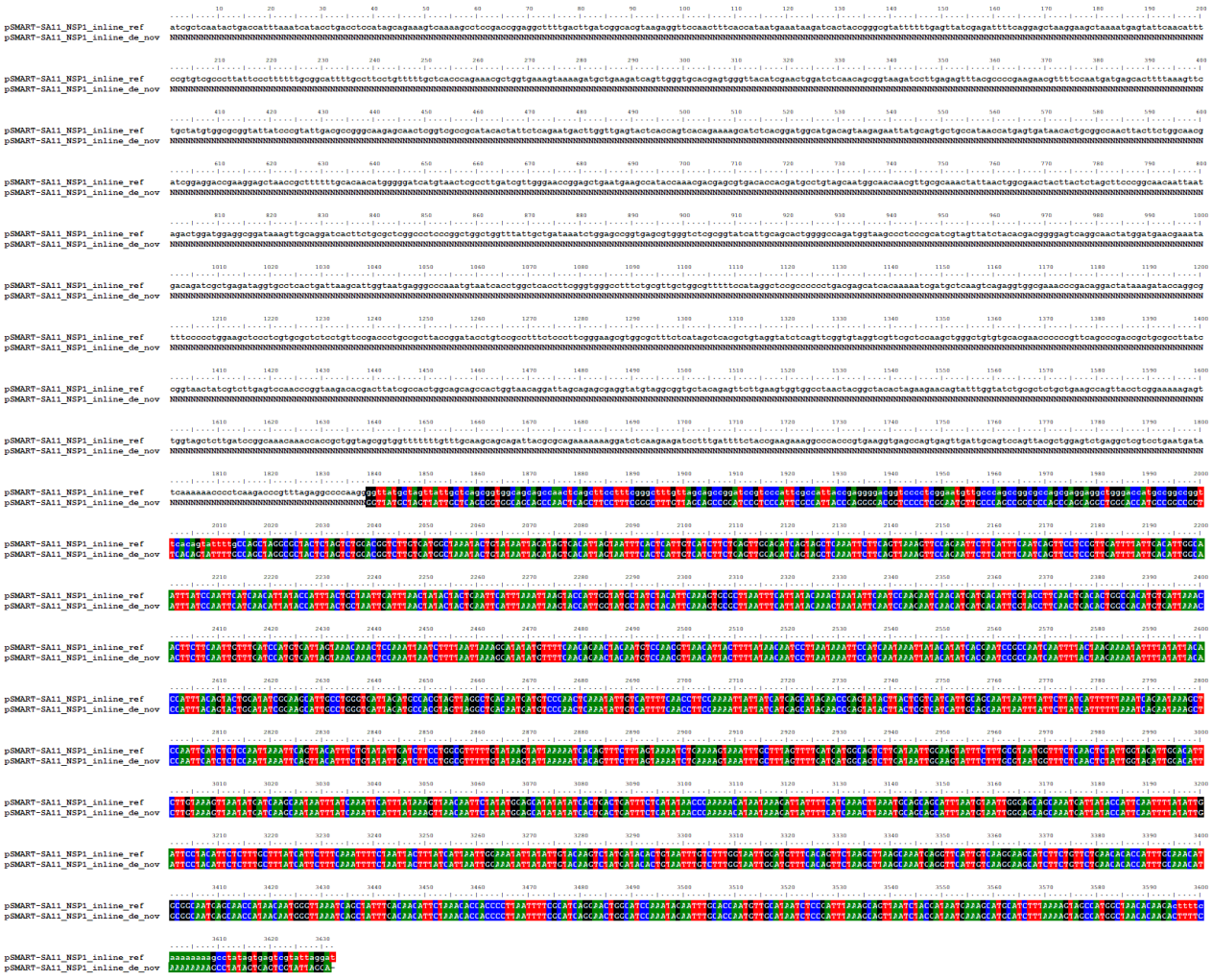


Fig. S10: Alignment of consensus sequence generated from pSMART-T7_RV-SA11_GS5_NSP1_inline with reference sequence

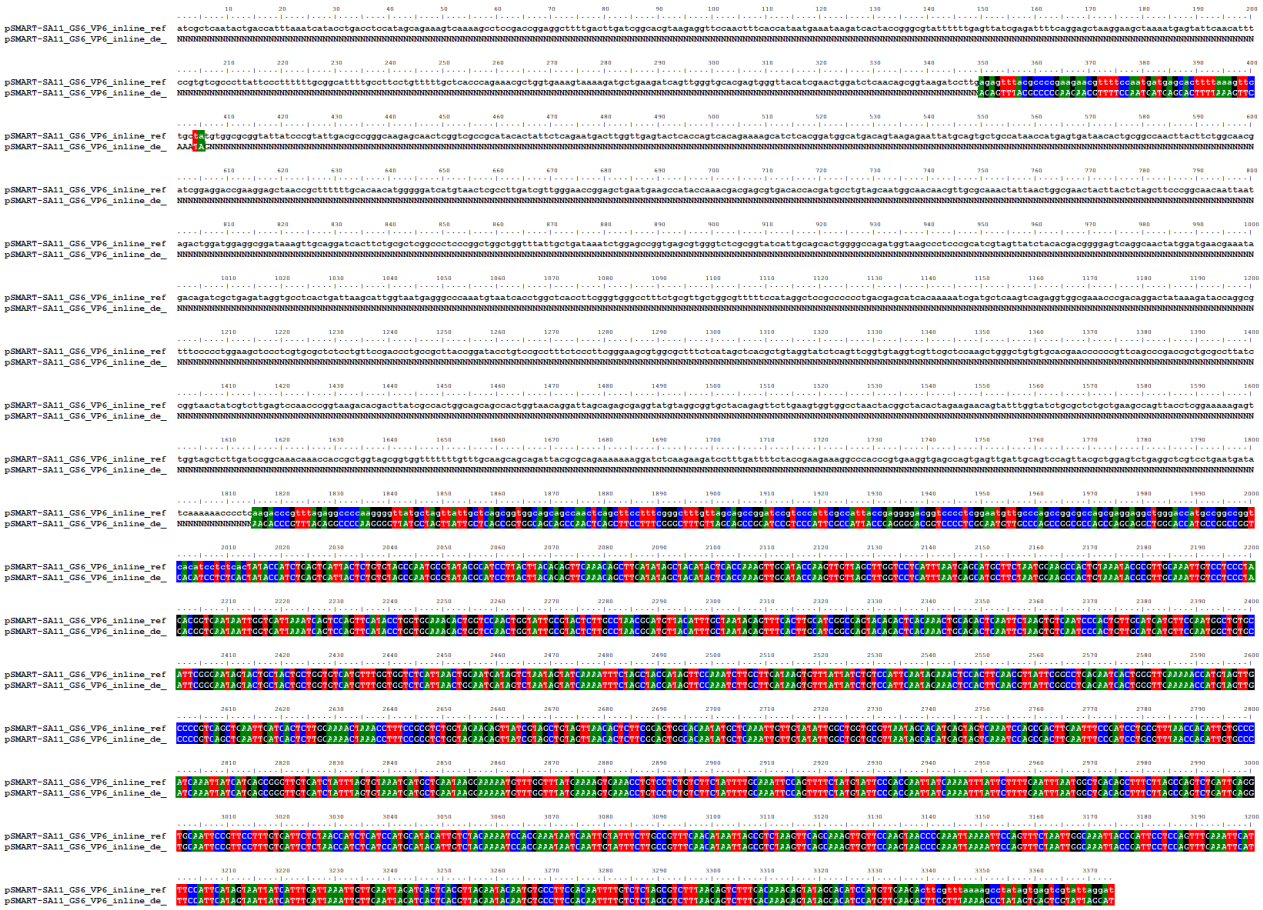


Fig. S11: Alignment of consensus sequence generated from pSMART-T7_RV-SA11_GS6_VP6_inline with reference sequence

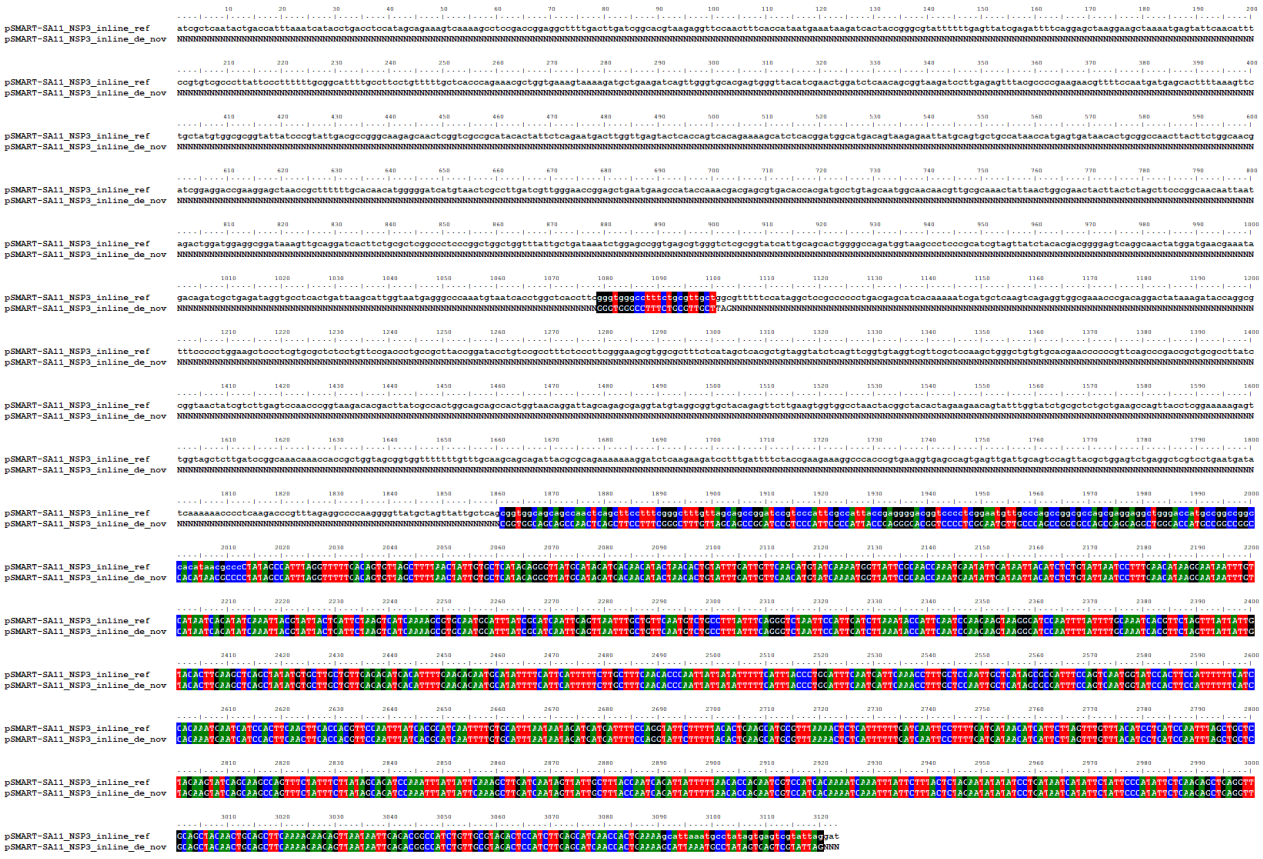


Fig. S12: Alignment of consensus sequence generated from pSMART-T7_RV-SA11_GS7_NSP3_inline with reference sequence

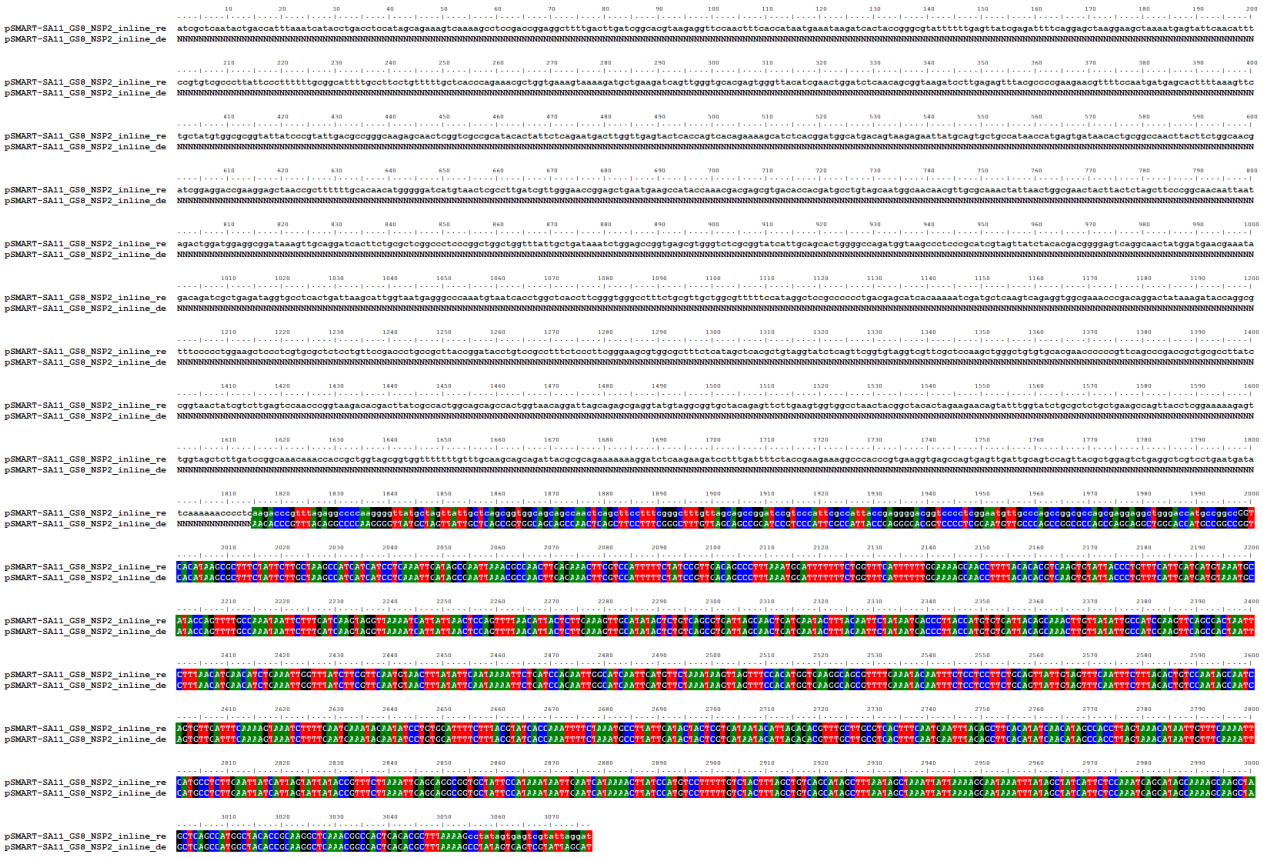


Fig. S13: Alignment of consensus sequence generated from pSMART-T7_RV-SA11_GS8_NSP2_inline with reference sequence

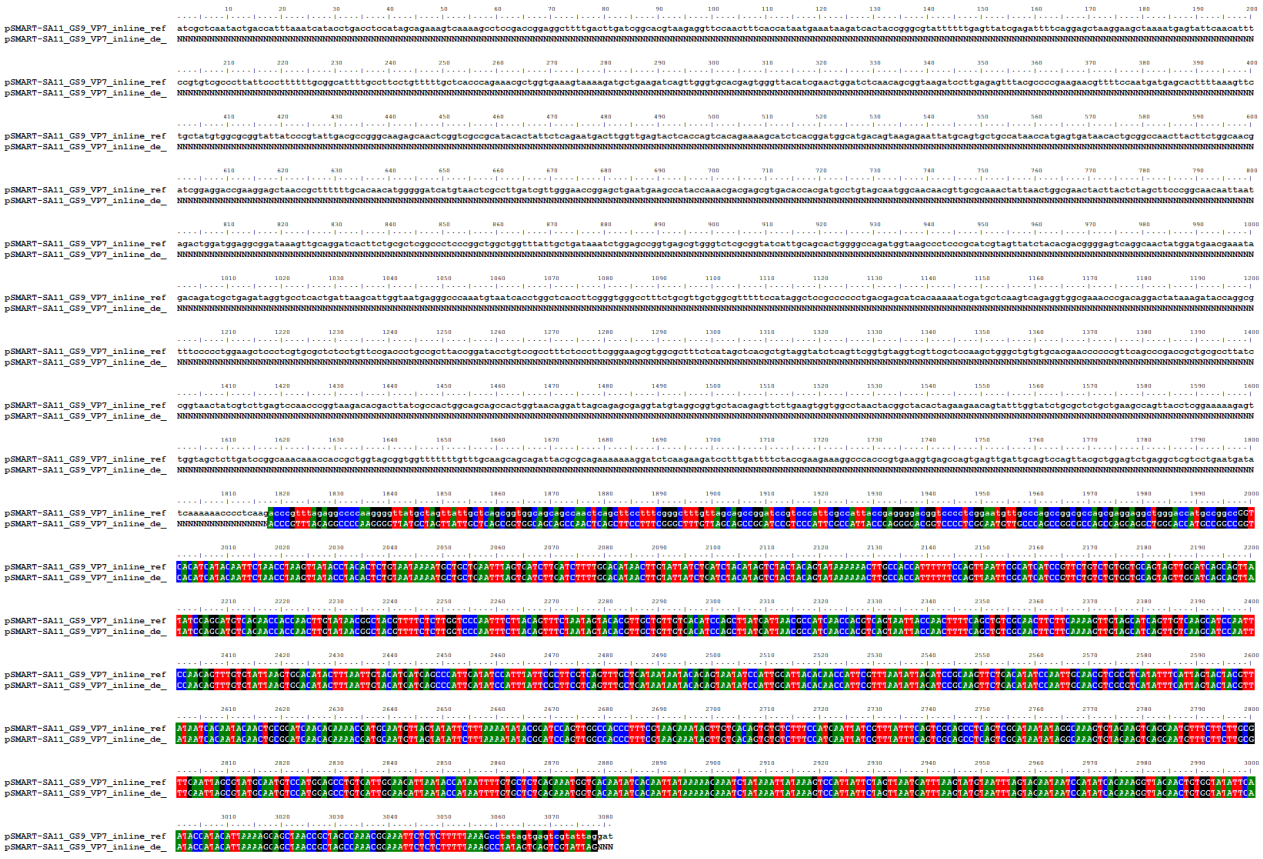


Fig. S14: Alignment of consensus sequence generated from pSMART-T7_RV-SA11_GS9_VP7_inline with reference sequence

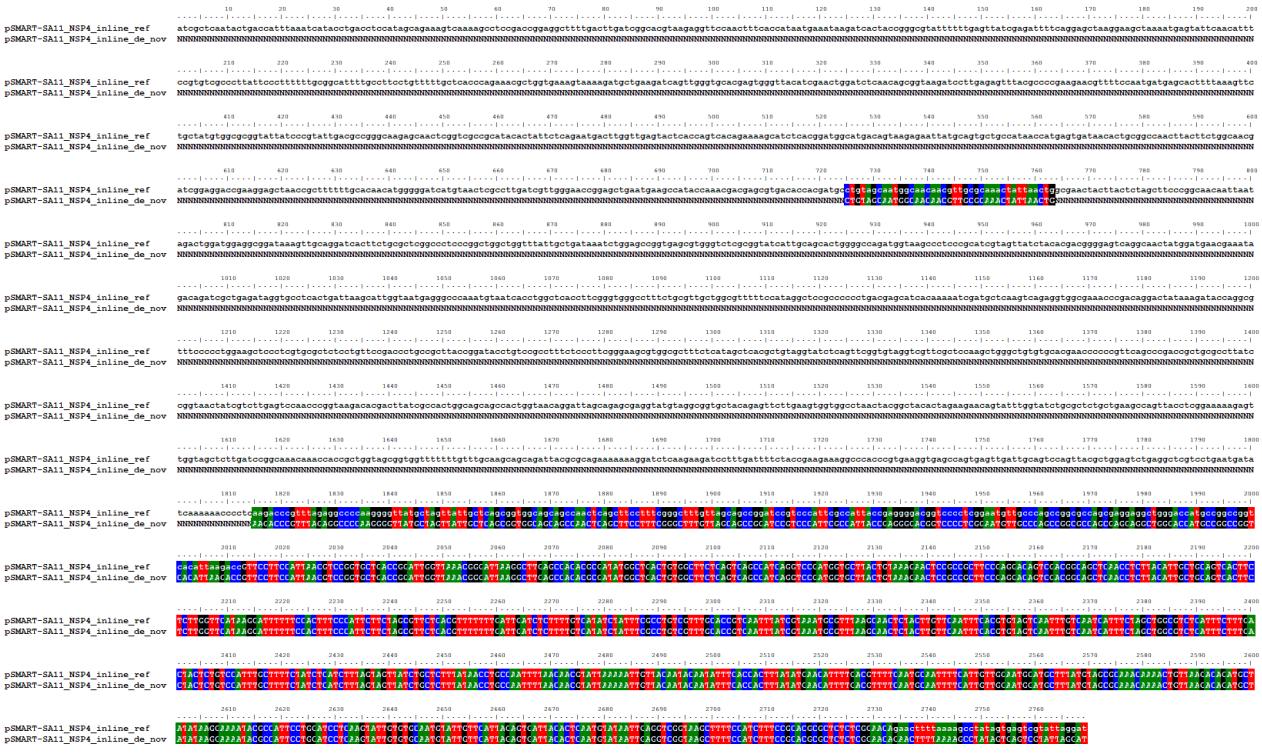


Fig. S15: Alignment of consensus sequence generated from pSMART-T7_RV-SA11_GS10_NSP4_inline with reference sequence

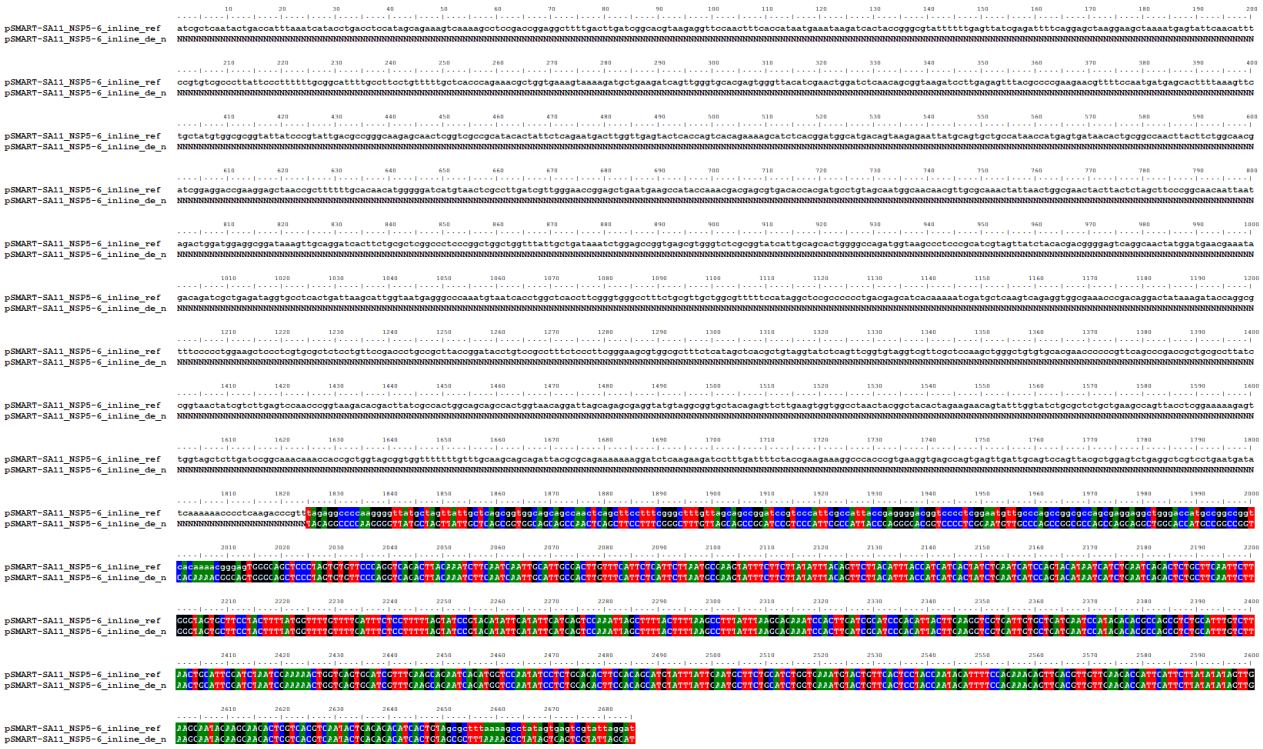


Fig. S16: Alignment of consensus sequence generated from pSMART-T7_RV-SA11_GS11_NSP5/6_inline with reference sequence

D Growth Curve titration raw data

Table S1: PFU/ml raw titration data

SA11-L2	0 hpi	12 hpi	24 hpi	36 hpi	48 hpi	60 hpi	72 hpi	
Repeat 1	1000	1000	1000000	10000000	300000000	100000000	80000000	
Repeat 2	1000	100000	4000000	90000000	70000000	80000000	100000000	
Repeat 3	400	300000	200000	1000000	1500000000	50000000	40000000	
Average	800	133666.66666666666	1733333.3333333333	33666666.666666664	623333333.33333337	76666666.666666672	73333333.333333328	
standard dev	346.41016151377499	152316.55633362164	2003330.5601755625	48993196.806631558	767875858.02220225	25166114.784235824	30550504.633038927	
% standard dev	43.301270189221931	113.95253591044015	115.57676308705169	145.52434695039079	123.18864032441748	32.825367109872808	41.659779045053085	
SA11_NSP4_R169I	0 hpi	12 hpi	24 hpi	36 hpi	48 hpi	60 hpi	72 hpi	
Repeat 1	200	30000	90000	2000000	7000000	12000000	600000000	
Repeat 2	1000	300000	300000	10000000	30000000	30000000	100000000	
Repeat 3	1000	20000	120000	3000000	3000000	40000000	30000000	
Average	733.33333333333337	116666.66666666667	170000	5000000	13333333.333333334	27333333.333333332	243333333.33333334	
standard dev	461.88021535170066	158850.03409925141	113578.16691600547	4358898.9435406737	14571661.99626293	14189197.769195177	310859024.85424697	
% standard dev	62.983665729777357	136.15717208507263	66.810686421179682	87.177978870813476	109.28746497197197	51.911699155592117	127.75028418667685	
SA11_GS6_Moz308	0 hpi	12 hpi	24 hpi	36 hpi	48 hpi	60 hpi	72 hpi	
Repeat 1	100	20000	30000	400000	2000000	4000000	3000000	
Repeat 2	1000	10000	30000	100000	2000000	3000000	10000000	
Repeat 3	20	20000	6000	300000	1200000	2000000	7000000	
Average	373.33333333333331	16666.666666666668	22000	266666.66666666669	1733333.3333333333	3000000	6666666.666666667	
standard dev	544.18134232380055	5773.5026918962558	13856.406460551018	152752.52316519464	461880.21535170026	1000000	3511884.5842842464	
% standard dev	145.76285955101801	34.641016151377528	62.98366572977735	57.282196186947985	26.64693550105963	33.333333333333329	52.678268764263692	
SA11_NSP3_2A-sfGFP	0 hpi	12 hpi	24 hpi	36 hpi	48 hpi	60 hpi	72 hpi	
Repeat 1	40	10000	40000	800000	1000000	1000000	6000000	
Repeat 2	30	1000	10000	300000	100000	300000	4000000	
Repeat 3	10	1000	2000	120000	400000	160000	1000000	
Average	26.666666666666668	4000	17333.333333333332	406666.66666666669	500000	486666.66666666669	3666666.6666666665	
standard dev	15.275252316519465	5196.152422706632	20033.305601755626	352325.60697930166	458257.569495584	450037.03551300452	2516611.4784235829	
% standard dev	266.66666666666669	400	866.66666666666663	338.88888888888886	125	304.16666666666669	366.66666666666663	
SA11_NSP4_60a_DLP-BD	0 hpi	12 hpi	24 hpi	36 hpi	48 hpi	60 hpi	72 hpi	
Repeat 1	300	30000	1000000	200000000	10000000	10000000	10000000	
Repeat 2	1000	10000	200000	1000000	4000000	10000000	10000000	
Repeat 3	50	10000	140000	1000000	1000000	6000000	2000000	
Average	450	16666.666666666668	446666.66666666669	67333333.333333328	5000000	8666666.666666666	7333333.333333333	
standard dev	492.44289008980525	11547.005383792515	480138.86880082235	114892703.56873553	4582575.6949558398	2309401.0767585021	4618802.153517006	
% standard dev	109.43175335329005	69.282032302755084	107.49377659719903	170.63272807237951	91.651513899116793	26.646935501059644	62.983665729777357	

E Statistical analysis using 2-way ANOVA and LSD post-hoc of differences between SA11 and rescued viruses

Tests of Normality

		Kolmogorov-Smirnov[a]			Shapiro-Wilk		
	Virus	Statistic	df	Sig.	Statistic	df	Sig.
Titre	SA11_GS6	.189	7	.200*	.927	7	.525
	SA11_NSp	.254	7	.191	.901	7	.337
	SA11_NSP	.203	14	.121	.895	14	.094
	SA11-L2	.243	7	.200*	.901	7	.338

*. This is a lower bound of the true significance.

a. Lilliefors Significance Correction

Fig. S17: Tests of normality of the normalised log-transformed growth curve data set. Significance values of $p > 0.05$ indicate that the data set has a normal distribution.

Multiple Comparisons

Dependent Variable: Titre

LSD

(I) Virus	(J) Virus	Mean Difference (I-J)	Std. Error	Sig.	95% Confidence Interval	
					Lower Bound	Upper Bound
SA11_GS6_Moz308 (actual)	SA11_NSP3_2A-sfGFP (actual)	-.678181380*	.2502032199	.012	-1.19457545	-.161787314
	SA11_NSp4_60a_DLP-BD (actual)	-.597905601*	.2502032199	.025	-1.11429967	-.081511536
	SA11_NSP4_R169I (actual)	-.664974066*	.2502032199	.014	-1.18136813	-.148580000
	SA11-L2 (actual)	-1.13151745*	.2502032199	.000	-1.64791151	-.615123381
SA11_NSP3_2A-sfGFP (actual)	SA11_GS6_Moz308 (actual)	.678181380*	.2502032199	.012	.1617873143	1.194575445
	SA11_NSp4_60a_DLP-BD (actual)	.0802757785	.2502032199	.751	-.436118287	.5966698441
	SA11_NSP4_R169I (actual)	.0132073143	.2502032199	.958	-.503186751	.5296013799
	SA11-L2 (actual)	-.453336066	.2502032199	.083	-.969730132	.0630579992
SA11_NSp4_60a_DLP-BD (actual)	SA11_GS6_Moz308 (actual)	.597905601*	.2502032199	.025	.0815115358	1.114299667
	SA11_NSP3_2A-sfGFP (actual)	-.080275778	.2502032199	.751	-.596669844	.4361182871
	SA11_NSP4_R169I (actual)	-.067068464	.2502032199	.791	-.583462530	.4493256014
	SA11-L2 (actual)	-.533611845*	.2502032199	.043	-1.05000591	-.017217779
SA11_NSP4_R169I (actual)	SA11_GS6_Moz308 (actual)	.664974066*	.2502032199	.014	.1485800000	1.181368131
	SA11_NSP3_2A-sfGFP (actual)	-.013207314	.2502032199	.958	-.529601380	.5031867513
	SA11_NSp4_60a_DLP-BD (actual)	.0670684642	.2502032199	.791	-.449325601	.5834625298
	SA11-L2 (actual)	-.466543381	.2502032199	.075	-.982937446	.0498506849
SA11-L2 (actual)	SA11_GS6_Moz308 (actual)	1.13151745*	.2502032199	.000	.6151233806	1.647911512
	SA11_NSP3_2A-sfGFP (actual)	.4533360664	.2502032199	.083	-.063057999	.9697301320
	SA11_NSp4_60a_DLP-BD (actual)	.533611845*	.2502032199	.043	.0172177793	1.050005910
	SA11_NSP4_R169I (actual)	.4665433807	.2502032199	.075	-.049850685	.9829374463

Based on observed means.
The error term is Mean Square(Error) = .219.

*. The mean difference is significant at the .05 level.

Fig. S18: Multiple comparison data using a univariate 2-way ANOVA with LSD post-hoc tests. This shows the comaprison of the mean between each virus.

F First replicate plaque assays of viruses rescued in Chapter 3



Fig. S19: Plaque assays of the first replicate of each timepoint for rSA11_Moz308_VP6

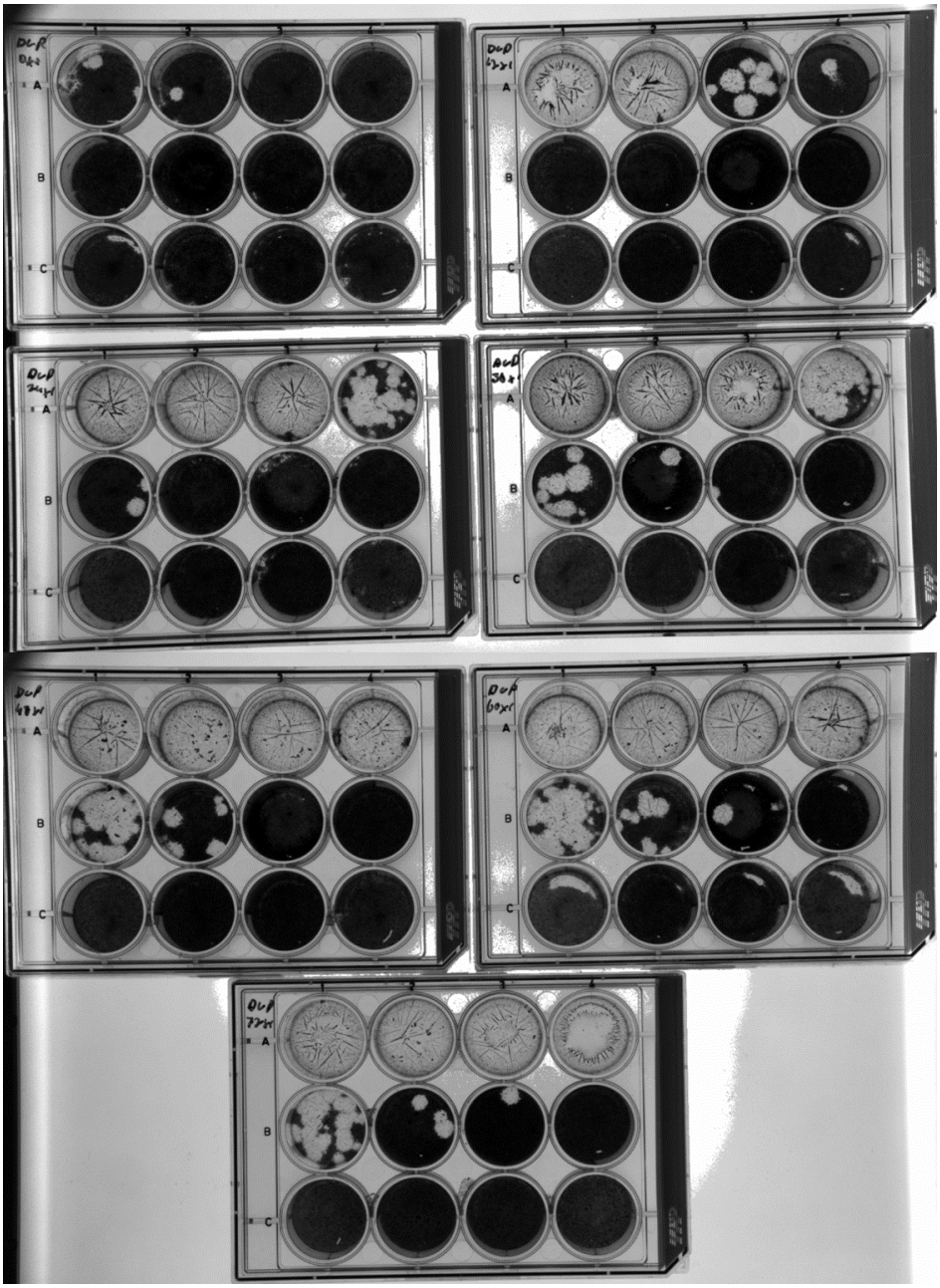


Fig. S20: Plaque assays of the first replicate of each timepoint for rSA11_NSP4_0060a_DLP-BD

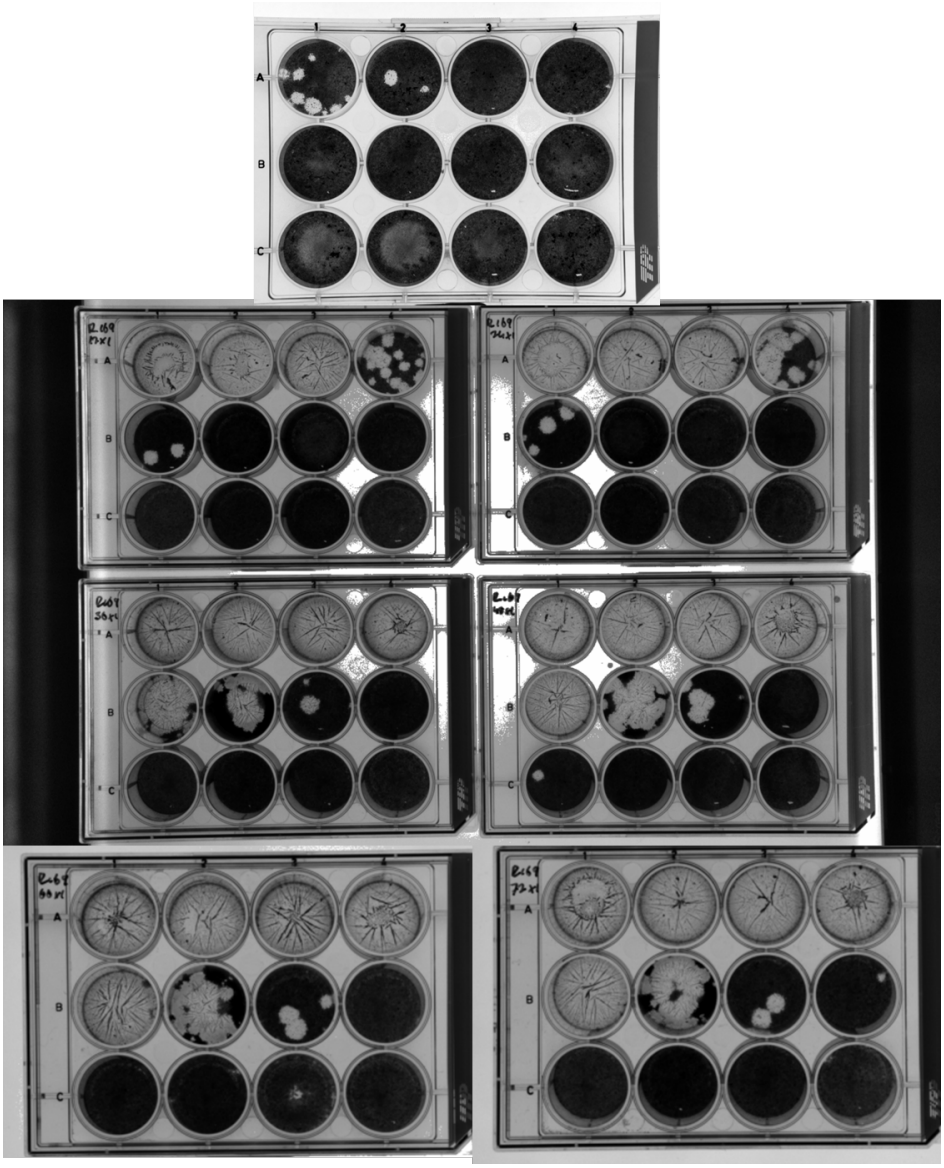


Fig. S21: Plaque assays of the first replicate of each timepoint for rSA11_NSP4_R169I

G Permissions for figures reproduced in this project

Alexander Borodavka, Ulrich Desselberger, John T Patton,

Genome packaging in multi-segmented dsRNA viruses: distinct mechanisms with similar outcomes,

Current Opinion in Virology,

Volume 33,

2018,

Pages 106-112,

ISSN 1879-6257,

https://doi.org/10.1016/j.coviro.2018.08.001.

(https://www.sciencedirect.com/science/article/pii/S1879625718300348)

Abstract: Segmented double-stranded (ds)RNA viruses share remarkable similarities in their replication strategy and capsid structure. During virus replication, positive-sense single-stranded (+)RNAs are packaged into procapsids, where they serve as templates for dsRNA synthesis, forming progeny particles containing a complete equimolar set of genome segments. How the +RNAs are recognized and stoichiometrically packaged remains uncertain. Whereas bacteriophages of the Cystoviridae family rely on specific RNA–protein interactions to select appropriate +RNAs for packaging, viruses of the Reoviridae instead rely on specific inter-molecular interactions between +RNAs that guide multi-segmented genome assembly. While these families use distinct mechanisms to direct +RNA packaging, both yield progeny particles with a complete set of genomic dsRNAs.

Creative Commons

This is an open access article distributed under the terms of the Creative Commons CC-BY license, which permits unrestricted use, distribution, and reproduction in any medium, provided the original work is properly cited.

You are not required to obtain permission to reuse this article.

To request permission for a type of use not listed, please contact Elsevier Global Rights Department.

Are you the author of this Elsevier journal article?

ELSEVIER LICENSE
TERMS AND CONDITIONS

Jan 31, 2022

This Agreement between North-West university -- Jayme Herbert ("You") and Elsevier ("Elsevier") consists of your license details and the terms and conditions provided by Elsevier and Copyright Clearance Center.

License Number	5239290362484
License date	Jan 31, 2022
Licensed Content Publisher	Elsevier
Licensed Content Publication	Virology
Licensed Content Title	Establishment of different plasmid only-based reverse genetics systems for the recovery of African horse sickness virus
Licensed Content Author	Andelé M. Conradie,Liesel Stassen,Henk Huismans,Christiaan A. Potgieter,Jacques Theron
Licensed Content Date	Dec 1, 2016
Licensed Content Volume	499
Licensed Content Issue	n/a
Licensed Content Pages	12
Start Page	144
End Page	155
Type of Use	reuse in a thesis/dissertation

CCC Marketplace™

This is a License Agreement between Jayme Herbert ("User") and Copyright Clearance Zentrum, Inc. ("CCC") on behalf of the Rightsholder identified in the order details below. The license consists of the order details, der Markt Order General Terms and Conditions below, and any Rightsholder Terms and Conditions which are included below.

All payments must be made in full to CCC in accordance with the Marketplace Order General Terms and Conditions below.

Order Date	21-Jul-2022	**Type of Use**	Republish in a thesis/dissertation
Order License ID	1249869-1		
ISSN	0022-538X	**Publisher**	AMERICAN SOCIETY FOR Mikrobiologie.
		Portion	Chart/graph/table/figure

LICENSED CONTENT

Publication Title	Journal of virology	**Rightsholder**	American Society for Microbiology - Journals
Article Title	COPII Vesicle Transport Is Required for Rotavirus NSP4 Interaction with the Autophagy Protein LC3 II and Trafficking to Viroplasms.	**Publication Type**	Journal
		Issue	1
		Volume	94
		URL	https://journals.asm.org/journal/jvi
Author/Editor	AMERICAN SOCIETY FOR MICROBIOLOGY.		
Date	01/01/1967		
Language	English		
Country	United States of America		

REQUEST DETAILS

Portion Type	Chart/graph/table/figure	**Distribution**	Worldwide
Number of charts / graphs / tables / figures requested	1	**Translation**	Original language of publication
		Copies for the disabled?	No
Format (select all that apply)	Print, Electronic	**Minor editing privileges?**	No
Who will republish the content?	Academic institution	**Incidental promotional use?**	No
		Currency	USD
Duration of Use	Life of current edition		
Lifetime Unit Quantity	Up to 499		
Rights Requested	Main product		

NEW WORK DETAILS

Title	Investigating the role of rotavirus GS10(NSP4) and GS6(VP6) in reassortment	**Institution name**	North-West University
		Expected presentation date	2022-09-30
Instructor name	Jayme Herbert		

ADDITIONAL DETAILS

Order reference number	N/A

CCC Marketplace™

This is a License Agreement between Jayme Herbert ("User") and Copyright Clearance Zentrum, Inc. ("CCC") on behalf of the Rightsholder identified in the order details below. The license consists of the order details, der Markt Order General Terms and Conditions below, and any Rightsholder Terms and Conditions which are included below.

All payments must be made in full to CCC in accordance with the Marketplace Order General Terms and Conditions below.

Order Date	21-Jul-2022	**Type of Use**	Republish in a thesis/dissertation
Order License ID	1249869-1		
ISSN	0022-538X	**Publisher**	AMERICAN SOCIETY FOR Mikrobiologie.
		Portion	Chart/graph/table/figure

LICENSED CONTENT

Publication Title	Journal of virology	**Rightsholder**	American Society for Microbiology - Journals
Article Title	COPII Vesicle Transport Is Required for Rotavirus NSP4 Interaction with the Autophagy Protein LC3 II and Trafficking to Viroplasms.	**Publication Type**	Journal
		Issue	1
		Volume	94
		URL	https://journals.asm.org/journal/jvi
Author/Editor	AMERICAN SOCIETY FOR MICROBIOLOGY.		
Date	01/01/1967		
Language	English		
Country	United States of America		

REQUEST DETAILS

Portion Type	Chart/graph/table/figure	**Distribution**	Worldwide
Number of charts / graphs / tables / figures requested	1	**Translation**	Original language of publication
		Copies for the disabled?	No
Format (select all that apply)	Print, Electronic	**Minor editing privileges?**	No
Who will republish the content?	Academic institution	**Incidental promotional use?**	No
		Currency	USD
Duration of Use	Life of current edition		
Lifetime Unit Quantity	Up to 499		
Rights Requested	Main product		

NEW WORK DETAILS

Title	Investigating the role of rotavirus GS10(NSP4) and GS6(VP6) in reassortment	**Institution name**	North-West University
		Expected presentation date	2022-09-30
Instructor name	Jayme Herbert		

ADDITIONAL DETAILS

Order reference number	N/A

ELSEVIER LICENSE
TERMS AND CONDITIONS

Jan 31, 2022

This Agreement between North-West university -- Jayme Herbert ("You") and Elsevier ("Elsevier") consists of your license details and the terms and conditions provided by Elsevier and Copyright Clearance Center.

License Number	5239271057489
License date	Jan 31, 2022
Licensed Content Publisher	Elsevier
Licensed Content Publication	Gastroenterology
Licensed Content Title	Rotaviruses: From Pathogenesis to Vaccination
Licensed Content Author	Harry B. Greenberg,Mary K. Estes
Licensed Content Date	May 1, 2009
Licensed Content Volume	136
Licensed Content Issue	6
Licensed Content Pages	13
Start Page	1939
End Page	1951
Type of Use	reuse in a thesis/dissertation
Portion	figures/tables/illustrations

ELSEVIER LICENSE
TERMS AND CONDITIONS

Jul 16, 2022

This Agreement between North-West university -- Jayme Herbert ("You") and Elsevier ("Elsevier") consists of your license details and the terms and conditions provided by Elsevier and Copyright Clearance Center.

License Number	5350910719722
License date	Jul 16, 2022
Licensed Content Publisher	Elsevier
Licensed Content Publication	Cell
Licensed Content Title	Conflict Resolution in the Genome: How Transcription and Replication Make It Work
Licensed Content Author	Stephan Hamperl,Karlene A. Cimprich
Licensed Content Date	Dec 1, 2016
Licensed Content Volume	167
Licensed Content Issue	6
Licensed Content Pages	13
Start Page	1455
End Page	1467
Type of Use	reuse in a thesis/dissertation
Portion	figures/tables/illustrations

ELSEVIER LICENSE
TERMS AND CONDITIONS

Jan 31, 2022

This Agreement between North-West university -- Jayme Herbert ("You") and Elsevier ("Elsevier") consists of your license details and the terms and conditions provided by Elsevier and Copyright Clearance Center.

License Number	5239270301249
License date	Jan 31, 2022
Licensed Content Publisher	Elsevier
Licensed Content Publication	Current Opinion in Virology
Licensed Content Title	Rotavirus non-structural proteins: structure and function
Licensed Content Author	Liya Hu,Sue E Crawford,Joseph M Hyser,Mary K Estes,BV Venkataram Prasad
Licensed Content Date	Aug 1, 2012
Licensed Content Volume	2
Licensed Content Issue	4
Licensed Content Pages	9
Start Page	380
End Page	388
Type of Use	reuse in a thesis/dissertation
Portion	figures/tables/illustrations

ELSEVIER LICENSE
TERMS AND CONDITIONS

Jan 31, 2022

This Agreement between North-West university -- Jayme Herbert ("You") and Elsevier ("Elsevier") consists of your license details and the terms and conditions provided by Elsevier and Copyright Clearance Center.

License Number	5239270301249
License date	Jan 31, 2022
Licensed Content Publisher	Elsevier
Licensed Content Publication	Current Opinion in Virology
Licensed Content Title	Rotavirus non-structural proteins: structure and function
Licensed Content Author	Liya Hu,Sue E Crawford,Joseph M Hyser,Mary K Estes,BV Venkataram Prasad
Licensed Content Date	Aug 1, 2012
Licensed Content Volume	2
Licensed Content Issue	4
Licensed Content Pages	9
Start Page	380
End Page	388
Type of Use	reuse in a thesis/dissertation
Portion	figures/tables/illustrations

Citation Hyser, J. M., M. Collinson-Pautz, B. Utama, and M. K. Estes. 2010. Rotavirus disrupts calcium homeostasis by NSP4 viroporin activity. mBio 1(5):e00265-10. doi:10.1128/mBio.00265-10.
Editors John Patton, National Institute of Allergy and Infectious Diseases and Terence S. Dermody, Vanderbilt University Medical Center
Copyright © 2010 Hyser et al. This is an open-access article distributed under the terms of the Creative Commons Attribution-Noncommercial-ShareAlike 3.0 Unported license, which permits unrestricted noncommercial use, distribution, and reproduction in any medium, provided the original author and source are credited.

CCC Marketplace™

This is a License Agreement between Jayme Herbert ("User") and Copyright Clearance Zentrum, Inc. ("CCC") on Auftrag of the Rightsholder identified in the order details below. The license consists of the order details, the CCC Terms and Conditions below, and any Rightsholder Terms and Conditions which are included below.

All payments must be made in full to CCC in accordance with the CCC Terms and Bedingungen below.

Order Date	04-Feb-2022	Type of Use	Republish in a thesis/dissertation
Order License ID	1185523-1		
ISSN	0095-1137	Publisher	AMERICAN SOCIETY FOR MICROBIOLOGY.
		Portion	Image/photo/illustration

LICENSED CONTENT

Publication Title	Journal of clinical microbiology	Publication Type	Journal
Article Title	Evidence for genetic linkage between the gene segments encoding NSP4 and VP6 proteins in common and reassortant human rotavirus strains.	Start Page	3566
		End Page	3573
		Issue	8
		Volume	41
		URL	https://journals.asm.org/journal/jcm
Author/Editor	AMERICAN SOCIETY FOR MICROBIOLOGY.		
Date	01/01/1975		
Language	English, English		
Country	United States of America		
Rightsholder	American Society for Microbiology - Journals		

REQUEST DETAILS

Portion Type	Image/photo/illustration	Distribution	Worldwide
Number of images / photos / illustrations	1	Translation	Original language of publication
Format (select all that apply)	Electronic	Copies for the disabled?	No
		Minor editing privileges?	No
Who will republish the content?	Academic institution	Incidental promotional use?	No
Duration of Use	Life of current edition	Currency	USD
Lifetime Unit Quantity	Up to 499		
Rights Requested	Main product		

NEW WORK DETAILS

Title	Investigating the role of rotavirus GS10(NSP4) and GS6(VP6) in reassortment	Institution name	North-West University
		Expected presentation date	2022-06-22
Instructor name	Prof. A.A. van Dijk		

ADDITIONAL DETAILS

Order reference number	N/A

ELSEVIER LICENSE
TERMS AND CONDITIONS

Jul 16, 2022

This Agreement between North-West university -- Jayme Herbert ("You") and Elsevier ("Elsevier") consists of your license details and the terms and conditions provided by Elsevier and Copyright Clearance Center.

License Number	5350870380659
License date	Jul 16, 2022
Licensed Content Publisher	Elsevier
Licensed Content Publication	Virus Research
Licensed Content Title	Emerging themes in rotavirus cell entry, genome organization, transcription and replication
Licensed Content Author	Hariharan Jayaram,M.K Estes,B.V.Venkataram Prasad
Licensed Content Date	Apr 1, 2004
Licensed Content Volume	101
Licensed Content Issue	1
Licensed Content Pages	15
Start Page	67
End Page	81
Type of Use	reuse in a thesis/dissertation
Portion	figures/tables/illustrations

Entirely plasmid-based reverse genetics system for rotaviruses

Y. Kanai, S. Komoto, T. Kawagishi, R. Nouda, N. Nagasawa, M. Onishi, et al.

Proc Natl Acad Sci U S A 2017 Vol. 114 Issue 9 Pages 2349-2354

Accession Number: 28137864 PMCID: PMC5338561 DOI: 10.1073/pnas.1618424114

Permission is not required to use original figures or tables for noncommercial and educational use (i.e., in a review article, in a book that is not for sale) if the article published under the exclusive PNAS License to Publish. Please include a full journal reference and, for articles published in volumes 90–105 (1993–2008), include "Copyright (copyright year) National Academy of Sciences" as a copyright note. Commercial reuse of figures and tables (i.e., in promotional materials, in a textbook for sale) requires permission from PNAS.

ELSEVIER LICENSE
TERMS AND CONDITIONS

Aug 01, 2022

This Agreement between North-West university -- Jayme Herbert ("You") and Elsevier ("Elsevier") consists of your license details and the terms and conditions provided by Elsevier and Copyright Clearance Center.

License Number	5360210832587
License date	Aug 01, 2022
Licensed Content Publisher	Elsevier
Licensed Content Publication	Cell Host & Microbe
Licensed Content Title	A Plasmid-Based Reverse Genetics System for Animal Double-Stranded RNA Viruses
Licensed Content Author	Takeshi Kobayashi,Annukka A.R. Antar,Karl W. Boehme,Pranav Danthi,Elizabeth A. Eby,Kristen M. Guglielmi,Geoffrey H. Holm,Elizabeth M. Johnson,Melissa S. Maginnis,Sam Naik,Wesley B. Skelton,J. Denise Wetzel,Gregory J. Wilson,James D. Chappell et al.
Licensed Content Date	Apr 19, 2007
Licensed Content Volume	1
Licensed Content Issue	2
Licensed Content Pages	11
Start Page	147
End Page	157

Reverse genetics system for introduction of site-specific mutations into the double-stranded RNA genome of infectious rotavirus

S. Komoto, J. Sasaki and K. Taniguchi

Proc Natl Acad Sci U S A 2006 Vol. 103 Issue 12 Pages 4646-4651

DOI: 10.1073/pnas.0509385103

Permission is not required to use original figures or tables for noncommercial and educational use (i.e., in a review article, in a book that is not for sale) if the article published under the exclusive PNAS License to Publish. Please include a full journal reference and, for articles published in volumes 90–105 (1993–2008), include "Copyright (copyright year) National Academy of Sciences" as a copyright note. Commercial reuse of figures and tables (i.e., in promotional materials, in a textbook for sale) requires permission from PNAS.

Marketplace™

This is a License Agreement between Jayme Herbert ("User") and Copyright Clearance Center, Inc. ("CCC") on Auftrag of the Rightsholder identified in the order details below. The license consists of the order details, the CCC Terms and Conditions below, and any Rightsholder Terms and Conditions which are included below.

All payments must be made in full to CCC in accordance with the CCC Terms and Conditions below.

Order Date	04-Feb-2022	Type of Use	Republish in a thesis/dissertation
Order License ID	1185524-1		
ISSN	0022-538X	Publisher	AMERICAN SOCIETY FOR MICROBIOLOGY.
		Portion	Image/photo/illustration

LICENSED CONTENT

Publication Title	Journal of virology	Rightsholder	American Society for Microbiology - Journals
Article Title	Generation of Recombinant Rotaviruses Expressing Fluorescent Proteins by Using an Optimized Reverse Genetics System.	Publication Type	Journal
		Start Page	e00588-18
		Issue	13
		Volume	92
Author/Editor	AMERICAN SOCIETY FOR MICROBIOLOGY.	URL	https://journals.asm.org/journal/jvi
Date	01/01/1967		
Language	English		
Country	United States of America		

REQUEST DETAILS

Portion Type	Image/photo/illustration	Distribution	Worldwide
Number of images / photos / illustrations	1	Translation	Original language of publication
Format (select all that apply)	Electronic	Copies for the disabled?	No
		Minor editing privileges?	No
Who will republish the content?	Academic institution	Incidental promotional use?	No
Duration of Use	Life of current edition	Currency	USD
Lifetime Unit Quantity	Up to 499		
Rights Requested	Main product		

NEW WORK DETAILS

Title	Investigating the role of rotavirus GS10(NSP4) and GS6(VP6) in reassortment	Institution name	North-West University
		Expected presentation date	2022-06-22
Instructor name	Prof A.A. van Dijk		

ADDITIONAL DETAILS

Order reference number	N/A	The requesting person / organization to appear on the license	Jayme Herbert

REUSE CONTENT DETAILS

CCC Marketplace™

Order Number: 1184278
Order Date: 01 Feb 2022

Payment Information

Jayme Herbert
28340485@nwu.ac.za
Payment method: Invoice

Billing Address:
Mrs. Jayme Herbert
North-West university
11 Hoffman street, Buildin g F3, Room 211
Building F3
Potchefstroom, North-Wes t 2520
South Africa

+27 837895767
28340485@nwu.ac.za

Customer Location:
Mrs. Jayme Herbert
North-West university
11 Hoffman street, Buildin g F3, Room 211
Building F3
Potchefstroom, North-Wes t 2520
South Africa

Order Details

1. Journal of virology

Billing Status: Open

Article: Generation of Infectious Recombinant Human Rotaviruses from Just 11 Cloned cDNAs Encoding the Rotavirus Genome.

Order License ID	1184278-1	**Type of use**	Republish in a thesis/dissertation
Order detail status	Completed		
ISSN	0022-538X	**Publisher**	AMERICAN SOCIETY FOR MICROBIOLOGY.
		Portion	Image/photo/illustratio n

0.00 USD
Republication Permission

LICENSED CONTENT

Publication Title	Journal of virology	**Rightsholder**	American Society for Microbiology - Journals
Article Title	Generation of Infectious Recombinant Human Rotaviruses from Just 11 Cloned cDNAs Encoding the Rotavirus Genome.	**Publication Type**	Journal
		Issue	8
		Volume	93
		URL	https://journals.asm.org/journal/jvi
Author/Editor	AMERICAN SOCIETY FOR MICROBIOLOGY.		
Date	01/01/1967		
Language	English		
Country	United States of America		

REQUEST DETAILS

JOHN WILEY AND SONS LICENSE
TERMS AND CONDITIONS

Jan 31, 2022

This Agreement between North-West university -- Jayme Herbert ("You") and John Wiley and Sons ("John Wiley and Sons") consists of your license details and the terms and conditions provided by John Wiley and Sons and Copyright Clearance Center.

License Number	5239250406944
License date	Jan 31, 2022
Licensed Content Publisher	John Wiley and Sons
Licensed Content Publication	The EMBO Journal
Licensed Content Title	Atomic structure of the major capsid protein of rotavirus: implications for the architecture of the virion
Licensed Content Author	Félix A. Rey, Jean Cohen, B.V.Venkataram Prasad, et al
Licensed Content Date	Apr 2, 2001
Licensed Content Volume	20
Licensed Content Issue	7
Licensed Content Pages	13
Type of use	Dissertation/Thesis
Requestor type	University/Academic

CCC | Marketplace™

This is a License Agreement between Jayme Herbert ("User") and Copyright Clearance Center, Inc. ("CCC") on behalf of the Rightsholder identified in the order details below. The license consists of the order details, the Marketplace Order General Terms and Conditions below, and any Rightsholder Terms and Conditions which are included below.

All payments must be made in full to CCC in accordance with the Marketplace Order General Terms and Conditions below.

Order Date	09-Aug-2022	Type of Use	Republish in a thesis/dissertation
Order License ID	1255966-1		
ISSN	0022-538X	Publisher	AMERICAN SOCIETY FOR MICROBIOLOGY.
		Portion	Chart/graph/table/figure

LICENSED CONTENT

Publication Title	Journal of virology	Publication Type	Journal
Article Title	Full genome-based classification of rotaviruses reveals a common origin between human Wa-Like and porcine rotavirus strains and human DS-1-like and bovine rotavirus strains.	Start Page	3204
		End Page	3219
		Issue	7
		Volume	82
		URL	https://journals.asm.org/journal/jvi
Author/Editor	AMERICAN SOCIETY FOR MICROBIOLOGY.		
Date	01/01/1967		
Language	English		
Country	United States of America		
Rightsholder	American Society for Microbiology - Journals		

REQUEST DETAILS

Portion Type	Chart/graph/table/figure	Distribution	Worldwide
Number of charts / graphs / tables / figures requested	1	Translation	Original language of publication
		Copies for the disabled?	No
Format (select all that apply)	Print, Electronic	Minor editing privileges?	No
Who will republish the content?	Academic institution	Incidental promotional use?	No
Duration of Use	Life of current edition	Currency	USD
Lifetime Unit Quantity	Up to 499		

You paused Toucan for 1 hour
Edit the duration Turn Toucan back on

Genetic determinants restricting the reassortment of heterologous NSP2 genes into the simian rotavirus SA11 genome

Rebecca Mingo, Shu Zhang, Courtney P. Long, Leslie E. W. LaConte & Sarah M. McDonald

Scientific Reports volume 7, Article number: 9301 (2017)

Open Access This article is licensed under a Creative Commons Attribution 4.0 International License, which permits use, sharing, adaptation, distribution and reproduction in any medium or format, as long as you give appropriate credit to the original author(s) and the source, provide a link to the Creative Commons license, and indicate if changes were made. The images or other third party material in this article are included in the article's Creative Commons license, unless indicated otherwise in a credit line to the material. If material is not included in the article's Creative Commons license and your intended use is not permitted by statutory regulation or exceeds the permitted use, you will need to obtain permission directly from the copyright holder. To view a copy of this license, visit http://creativecommons.org/licenses/by/4.0/.

ELSEVIER LICENSE
TERMS AND CONDITIONS

Jan 31, 2022

This Agreement between North-West university -- Jayme Herbert ("You") and Elsevier ("Elsevier") consists of your license details and the terms and conditions provided by Elsevier and Copyright Clearance Center.

License Number	5239271250602
License date	Jan 31, 2022
Licensed Content Publisher	Elsevier
Licensed Content Publication	Virology
Licensed Content Title	Rotavirus RNA polymerases resolve into two phylogenetically distinct classes that differ in their mechanism of template recognition
Licensed Content Author	Kristen M. Ogden,Reimar Johne,John T. Patton
Licensed Content Date	15–30 September 2012
Licensed Content Volume	431
Licensed Content Issue	1-2
Licensed Content Pages	8
Start Page	50
End Page	57
Type of Use	reuse in a thesis/dissertation

ELSEVIER LICENSE
TERMS AND CONDITIONS

Jan 31, 2022

This Agreement between North-West university -- Jayme Herbert ("You") and Elsevier ("Elsevier") consists of your license details and the terms and conditions provided by Elsevier and Copyright Clearance Center.

License Number	5239290216949
License date	Jan 31, 2022
Licensed Content Publisher	Elsevier
Licensed Content Publication	Virology
Licensed Content Title	Establishment of an entirely plasmid-based reverse genetics system for Bluetongue virus
Licensed Content Author	Jakobus M. Pretorius,Henk Huismans,Jacques Theron
Licensed Content Date	Dec 1, 2015
Licensed Content Volume	486
Licensed Content Issue	n/a
Licensed Content Pages	7
Start Page	71
End Page	77
Type of Use	reuse in a thesis/dissertation
Portion	figures/tables/illustrations

Reovirus reverse genetics: Incorporation of the *CAT* gene into the reovirus genome

Michael R. Roner and Wolfgang K. Joklik

PNAS July 3, 2001 98 (14) 8036-8041; https://doi.org/10.1073/pnas.131203198

Permission is not required to use original figures or tables for noncommercial and educational use (i.e., in a review article, in a book that is not for sale) if the article published under the exclusive PNAS License to Publish. Please include a full journal reference and, for articles published in volumes 90–105 (1993–2008), include "Copyright (copyright year) National Academy of Sciences" as a copyright note. Commercial reuse of figures and tables (i.e., in promotional materials, in a textbook for sale) requires permission from PNAS



Rotaviruses

Author:
Ulrich Desselberger

Publication:
Virus Research
Publisher:
Elsevier
Date:
22 September 2014

Copyright © 2014 The Authors. Published by Elsevier B.V.

Welcome to RightsLink

Elsevier has partnered with Copyright Clearance Center's RightsLink service to offer a variety of options for reusing this content.

Note: This article is available under the Creative Commons CC-BY-NC-ND license and permits non-commercial use of the work as published, without adaptation or alteration provided the work is fully attributed.

ELSEVIER LICENSE
TERMS AND CONDITIONS

Jan 31, 2022

This Agreement between North-West university -- Jayme Herbert ("You") and Elsevier ("Elsevier") consists of your license details and the terms and conditions provided by Elsevier and Copyright Clearance Center.

License Number	5239261428321
License date	Jan 31, 2022
Licensed Content Publisher	Elsevier
Licensed Content Publication	Current Opinion in Virology
Licensed Content Title	Bluetongue virus structure and assembly
Licensed Content Author	Polly Roy
Licensed Content Date	Jun 1, 2017
Licensed Content Volume	24
Licensed Content Issue	n/a
Licensed Content Pages	9
Start Page	115
End Page	123
Type of Use	reuse in a thesis/dissertation
Portion	figures/tables/illustrations

JOHN WILEY AND SONS LICENSE
TERMS AND CONDITIONS

Jan 31, 2022

This Agreement between North-West university -- Jayme Herbert ("You") and John Wiley and Sons ("John Wiley and Sons") consists of your license details and the terms and conditions provided by John Wiley and Sons and Copyright Clearance Center.

License Number	5239251322623
License date	Jan 31, 2022
Licensed Content Publisher	John Wiley and Sons
Licensed Content Publication	The EMBO Journal
Licensed Content Title	Atomic model of an infectious rotavirus particle
Licensed Content Author	Ethan C Settembre, James Z Chen, Philip R Dormitzer, et al
Licensed Content Date	Dec 14, 2010
Licensed Content Volume	30
Licensed Content Issue	2
Licensed Content Pages	9
Type of use	Dissertation/Thesis
Requestor type	University/Academic
Format	Electronic

CCC Marketplace™

Order Confirmation

Thank you, your order has been placed. An email confirmation has been sent to you. Your order license details and printable licenses will be available within 24 hours. Please access Manage Account for final order details.

This is not an invoice. Please go to manage account to access your order history and invoices.

CUSTOMER INFORMATION

Payment by invoice: You can cancel your order until the invoice is generated by contacting customer service.

Billing Address

Mrs. Jayme Herbert
North-West university
11 Hoffman street, Building F3, Room 211
Building F3
Potchefstroom, North-West 2520
South Africa

+27 837895767
28340485@nwu.ac.za

Customer Location

Mrs. Jayme Herbert
North-West university
11 Hoffman street, Building F3, Room 211
Building F3
Potchefstroom, North-West 2520
South Africa

PO Number (optional)

N/A

Payment options

Invoice

PENDING ORDER CONFIRMATION

Confirmation Number: Pending

Order Date: 21-Jul-2022

1. Journal of virology

0.00 USD

Article: Group A Rotavirus VP1 Polymerase and VP2 Core Shell Proteins: Intergenotypic Sequence Variation and In Vitro Functional Compatibility.

Special Terms Apply

Order License ID	Pending	**Publisher**	AMERICAN SOCIETY FOR MICROBIOLOGY.
ISSN	0022-538X		
Type of Use	Republish in a thesis/dissertation	**Portion**	Chart/graph/table/figure

LICENSED CONTENT

Publication Title	Journal of virology	**Rightsholder**	American Society for Microbiology - Journals

SPRINGER NATURE LICENSE
TERMS AND CONDITIONS

Jul 16, 2022

This Agreement between North-West university -- Jayme Herbert ("You") and Springer Nature ("Springer Nature") consists of your license details and the terms and conditions provided by Springer Nature and Copyright Clearance Center.

License Number	5350901473764
License date	Jul 16, 2022
Licensed Content Publisher	Springer Nature
Licensed Content Publication	Archives of Virology
Licensed Content Title	Evidence of zoonotic transmission of VP6 and NSP4 genes into human species A rotaviruses isolated in Pakistan in 2010
Licensed Content Author	Sana Tamim et al
Licensed Content Date	May 11, 2019
Type of Use	Thesis/Dissertation
Requestor type	academic/university or research institute
Format	print and electronic
Portion	figures/tables/illustrations
Number of figures/tables/illustrations	1
Will you be translating?	no

ELSEVIER LICENSE
TERMS AND CONDITIONS

Aug 01, 2022

This Agreement between North-West university -- Jayme Herbert ("You") and Elsevier ("Elsevier") consists of your license details and the terms and conditions provided by Elsevier and Copyright Clearance Center.

License Number	5360210949358
License date	Aug 01, 2022
Licensed Content Publisher	Elsevier
Licensed Content Publication	Current Opinion in Virology
Licensed Content Title	Genetics and reverse genetics of rotavirus
Licensed Content Author	Koki Taniguchi,Satoshi Komoto
Licensed Content Date	Aug 1, 2012
Licensed Content Volume	2
Licensed Content Issue	4
Licensed Content Pages	9
Start Page	399
End Page	407
Type of Use	reuse in a thesis/dissertation
Portion	figures/tables/illustrations